Quantification of Respiratory Sinus Arrhythmia by Use of Low Order ARX Models

Han Bo
(韩波)

A thesis
submitted in fulfilment of the requirements
for the Degree of
Doctor of Philosophy
in
Physics and Electronic Engineering
at the
University of Waikato

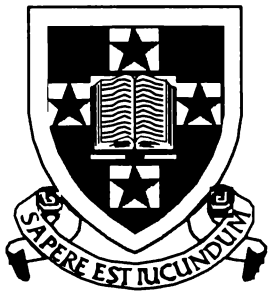

University of Waikato
Hamilton, New Zealand

March 1999

Acknowledgments

During the course of this project, I have received much support, encouragement, advice and assistance from many people, and to this end I am deeply grateful to them all.

My most sincere thanks go to my supervisors Dr John Henderson, Dr Jamie Sleigh and Dr Howell Round for their initiating the project, their unending guidance, encouragement in my research, thesis preparation (the many corrections!) and finding me the funding and the scholarship necessary to undertake this study. I would especially like to recognize the valuable input from them.

I would like to thank all those staff and students who gave assistance and help in my research, and in particular Mrs Heidi Eschmann, Mr Bruce Rhodes and Mr Jason Turuwhenua.

I gratefully acknowledge the receipt of the Waikato University Scholarship and the financial support of the Waikato Medical Research Foundation.

To all other friends inside and outside the university, thanks for showing me that there was more to life than this thesis.

Last, but not least, I would like to thank my wife, Zhang Wei and my son, Han Xu, who encouraged and supported me all the way during my university years.

Abstract

Respiratory Sinus Arrhythmia (RSA) is a change in the heart rate that corresponds to the frequency of respiration, but its causative mechanisms in humans remain only partially determined. In this thesis, models of the human cardiovascular system have been developed to give physiologically reasonable explanations of RSA. In a normally intact system, the cardiovascular system has respiration as input and heart rate as the output, which can be used to evaluate the cardiovascular system dynamics. It is proposed that respiration oscillations play a major role in the generation of RSA in healthy humans through the action of medullary respiratory neurons, which have been shown to both control respiration itself and via a coupling to autonomic centers to modulate heart rate by varying parasympathetic and sympathetic inputs to the sinoatrial node. The Baroreflex does not play an important role in modifying the RSA response in normal conditions but does maintain arterial blood pressure within a fairly narrow range through feedback control. Based on the neural network autoregressive with exogenous input (ARX) model, sensitivity analysis has been employed to demonstrate that instantaneous lung volume (ILV) has a much higher percentage of contribution to heart rate variability (HRV) than systolic blood pressure (SBP) (typically 11.6%, 4.6%) , which agrees well with our cardiovascular system model.

System identification of RSA in random, regular and spontaneous breathing patterns performed well when using an ARX model of low order, typically [4, 2, x]. In order to get a tradeoff between the accuracy of the model and an excessive number of parameters associated with that model, both the false nearest neighbors (FNN) algorithm and visual inspection of the loss function were used for model order determination. Good model qualities were proved by model validations and agreed well with the results of previous research. Studying transfer characteristics from fluctuations of ILV to HRV, the impulse response was obtained from the ARX model and it was then decomposed algebraically into two combinations of exponential decays, i.e., the fast and slow response components. The low order ARX model was tested on data acquired from a range of healthy subjects and patients.

Analysis of the data indicated that the fast response component of the impulse response corresponds to the high frequency power (HF) (0.3-0.5 Hz) of HRV fluctuations, and the slow response component corresponds to the low frequency power (LF) (0.08-0.15 Hz) of HRV fluctuation. The fast component reflects the change of HRV due to parasympathetic input and the slow component is attributed to both sympathetic and parasympathetic input.

Analysis of the model parameters, the amplitude and time constant of impulse response components, showed these can identify differences in the system response due to the shifts in autonomic balance produced by changing posture and in patients with large sympathetic inputs. Compared with HF:LF power ratio, our slow components of impulse response are more informative in quantifying the balance between the sympathetic and parasympathetic response due to respiration.

To our knowledge, this is first attempt to use an ARX model to quantify RSA for patients in uncontrolled situations where the spontaneous breathing pattern can take on a variety of forms. Our study shows that the results of this system identification to patients are reliable quantitative indexes of RSA after the data has been examined to ensure that cardiorespiratory interaction is linear and stationary.

Contents

CHAPTER 3

MODELING HUMAN CARDIOVASCULAR SYSTEM 21

CHAPTER 4

THE LOW ORDER ARX MODEL 31

CHAPTER 5

MULTIVARIATE TIME SERIES PROCESSES 59

List of Figures

List of Tables

Glossary

AIC: Akaike's Information Theoretic Criterion

AF: Ambiguity Function

AMP1: Amplitude 1

AMP2: Amplitude 2

ANS: autonomous nervous systems

AR: Autoregressive

ARX: Autoregressive with Exogenous Input

BEP: Back Error Propagation

bpm: Beat per minute

CNS: Central Nervous System

DV: Dependent Variables

ECG: Electrocardiogram

FNN: False Nearest Neighbors

FPE: Akaike's Final Criterion

HF: High Frequency

HR: Heart Rate

HRV: Heart Rate Variability

IBLI: Iterative Band-Limited Interpolation

ILV: Instantaneous Lung Volume

IPFM: Integral Pulse Frequency Modulation

IV: Independent Variables

LF: Low Frequency

LS: Least Squares

MA: Moving Average

NNARX: Neural Network ARX

ODE: Ordinary Differential Equation

PEMs: Prediction Error Identification Methods

PSA: Power spectral analysis

PSD: Power Spectral Density

RID: Reduced Interference Distributions

RP: Recurrence Plot

R-R: R-R interval

RSA: Respiratory Sinus Arrhythmia

SA: Sino-atrial

SN: Sino-atrial Node

SBP: Systolic Blood Pressure

TC1: Time Constant 1

TC2: Time Constant 2

VILF: Inspection of the Loss Function

VLF: Very Low Frequency

Chapter 1

Introduction

1.1 Background

As is well known, the heart is one of the essential organs since it helps bring oxygen and nutriments to the whole body through the vascular system. Because of the increase in life expectancy and the change in our eating habits, cardiovascular diseases are becoming increasingly common, and are now one of the major causes of human death. However, examination of the physiological interaction and underlying dynamics of human cardiovascular variables has far reaching implications in the understanding of normal physiology as well as cardiovascular disease. These facts have lead to extensive research in the cardiovascular regulatory system.

One of major aspects of the research regarding this topic is the respiration-related variation in the cardiovascular regulatory system [Piepoli *et al.* 1997]. Respiratory Sinus Arrhythmia is used as a noninvasive measure of parasympathetic input to the sinus node, but its causative mechanisms in humans remain unclear.

RSA is a change in the heart rate that corresponds to the frequency of respiration. Typically, the heart rate will increase during inspiration due to stimulation of the sympathetic nervous system during this time, and the heart rate will decrease during expiration due to stimulation of the parasympathetic nervous system. Studies of cardiovascular responses to various perturbations have been used to develop models of RSA in which central processing consisted of various "black boxes". These

models have contributed a great deal to our understanding of the mechanisms by which respiration modulates parasympathetic outflow to the sinus node. But there is still much controversy as to the origin of RSA. Precise details of this mechanism are still debated. Many authors believe that RSA is caused by fluctuations in blood pressure causing a change in heart rate. Others believe that respiration has a more direct link to heart rate through interaction of the central respiratory neurons.

Most of the studies made so far have focused on the experimental laboratory procedures traditionally employed to assess RSA and the baroreflex function. These techniques allowed more understanding of the interaction of cardiovascular variables. However, in these experiments, a more or less artificial stimulation used to investigate RSA may have interfered with the neural control mechanisms under evaluation. The stimulation may have changed the characteristics of the normal RSA. Much effort has been applied to understanding the cardiovascular responses to various perturbations. System identification approaches provide a means to characterize physiologic mechanisms by analysing fluctuations from instantaneous lung volume (ILV) and systolic blood pressure (SBP) to heart rate variability (HRV). The most common technique recently used for system identification is a linear autoregressive with exogenous input (ARX) model which has a highly flexible structure to parameterize the dynamics of the system. However, determination of the model order is much more difficult in terms of " best " ARX model order although high ARX model orders (> 12) have been widely accepted [Triedman *et al.* 1995, Mullen *et al.* 1997, Kim and Khoo 1997]. However, a question remains concerning the number of the model parameters. Does a model with high order describe the 'true system' and can the high order of the model be physiologically interpreted in accordance with *a priori* knowledge of the dynamics? Central to the identification problem is the question of how to obtain a good model fit to the data with as few parameters as possible.

1.2 Layout of Thesis

Following on from the above presentation the goal of this thesis included three aspects: First, we propose a model of a cardiovascular control system which suggests that the respiration oscillations, other than the arterial baroreceptors, is the main contributor to the generation of the natural RSA in the healthy human. Second, to rule out the possibility that cardiac baroreceptor mechanisms of the RSA might be

the most important, we need to quantify the relationship between the change in input signals (ILV and SBP) and output signal (HRV) of the human cardiovascular system. Third, an efficient approach, the low order ARX model, will be developed and applied to healthy subjects and patients to extract as much information as possible. The structure of this thesis will reflect this, with some chapters devoted to more theoretical and others to more applied subjects. More precisely, the outline is the following:

The first part of this thesis provides an overview of physiological factors that are involved in many ways in the structure and function of the human cardiovascular system (Chapter 2). In addition, in an examination of existing assumptions about the origin of RSA in light of recent research literature a review of system identification methods is given in Chapter 3. After addressing the problems of previous research, an alternative hypothesis of the origin of RSA is proposed (Chapter 3).

The second part of this thesis introduces the ARX model and aims at giving an understanding of the ARX model system identification methods especially with low model order, its rationale, properties and use (Chapter 4). It focuses on data filtering and model order determination that is very important for the low order ARX model. In Chapter 5, we pay more attention to the techniques to process the multivariate time series. We look at the relationships describing how the stimulus signals are transformed by the system into response signals and finding the properties of the system before employing parameter system identification. A review of the QRS detection algorithm developed by Pan and Tompkins [1985] and the Berger method [1986] for determining the heart rate signal from the ECG will be given in Chapter 6.

The third and final part of this thesis deals with the application of the ideas and techniques of preceding chapters to healthy subjects and patients. Chapter 7 addresses the sensitivity analysis of HRV to changes in ILV and SBP by using a neural network ARX model. Conclusions can be drawn from the results that a more important role is played by medullary respiratory neurons than the arterial baroreceptors in the origin of normal RSA in the conscious human. Based on our human cardiovascular system model, Chapter 8 demonstrates application of the low order ARX model to RSA identification with a typical example of healthy subjects in order to answer explicitly the question that has not been addressed in previous published work: what is the best order of an ARX model for the cardiovascular system identification? In addition, the influence of prefiltering data is discussed.

In Chapter 9, the low order ILV-HRV ARX model is applied to data obtained from two subject groups: healthy subjects and patient subjects. Model parameter analysis of RSA allows us to evaluate the differences found in the assessment of autonomic control by variations in breathing pattern and in posture from healthy subjects and variations due to sympathetic input in patients.
The thesis then summarizes the main results and conclusions of this work in Chapter 10. Suggestions are made for possible extensions of this research.

1.3 Main Contributions

The main contributions of this research are:

1 A model of the cardiovascular regulatory system is proposed to explain the origin of RSA in the normal physiological condition, that RSA is principally due to central modulation (Chapter 3).

2 Based on the neural network ARX model, sensitivity analysis is employed to identify how much the inputs ILV and SBP contribute to the system response HRV. The results have shown that ILV has a much higher percentage contribution to HRV than SBP has (Chapter 7).

3 The low order ARX model is well designed in order to identify the cardiovascular system. For both random and regular breathing patterns, the quality of the low order ARX model was proved to be good. In addition, because of the low order model, the system impulse response can be decomposed algebraically and become physiological interpretable (Chapter 4, Chapter 8).

4 The cross Reduced Interference Distributions (RID) time-frequency analysis is used to analyze the relation between HRV and ILV. This provides a tool to check any nonlinearity or nonstationarity in the system before setting up the linear ARX model.

5 The applications of the low order ARX model parameter analysis to data obtained from healthy subjects and patients can yield useful results (Chapter 9). It is shown that the model parameter analysis of RSA allows us to evaluate the

differences found in the assessment of autonomic control by variations in breathing patterns and in posture from healthy subjects and variations due to sympathetic input in patients.

1.4 Publication and Presentations

During the period of doctoral study, I have presented following conference papers:

Bo, H., J. D. Henderson and J. W. Sleigh. "A study of relationship between respiration and heart rate based on an autoregressive moving average model". Australian College of Physical Scientists and Engineers in Medicine NZ, Branch Meeting, 1997.

Bo, H., J. D. Henderson and J. W. Sleigh. "System identification of respiratory sinus arrhythmia based on a low order autoregressive with exogenous input model". Annual Australasian conference on Engineering and the Physical Sciences in Medicine, 1998.

The following have been published:

McHugh, G. J., J. W. Sleigh, H, Bo and J. D. Henderson. "Heart rate variability following cardiac surgery fails to predict short-term cardiovascular instability" Anesthesia, and Intensive Care. 25: 621-626,1997

Forester, J., H. Bo, J. W. Sleigh and J. D. Henderson. "Variability of R-R, P-R and R-T Intervals". Am J Physiol 273(Heart Circ Physiol. 42) H2857-H2860, 1997.

It is planned to submit papers on the following:

Henderson, J. D., H Bo, J. P. Meagher, and J. W. Sleigh. "Heart Rate Band-limited Interpolation".

Bo, H., J. D. Henderson and J. W. Sleigh. "System Identification of Respiratory Sinus Arrhythmia Based on a Low Order Autoregressive with Exogenous Input Model"

Bo, H., J. D. Henderson and J. W. Sleigh. "The sensitivity analysis of the cardiovascular system using neural networks ARX model".

Chapter 2

The Human Cardiovascular System

2.1 Overview

The circulatory system is shown diagrammatically in Figure 2-1. It is responsible for supplying the body with blood. It pumps blood from the heart to the lungs to receive oxygen and then back to the heart to be pumped through the body to the brains, kidneys, organs of digestion and reproduction and extremities, returning then to the heart to recommence the cycle.

The cardiovascular system includes the heart and the blood vessels, and the respiratory system contains those organs which are responsible for carrying oxygen from the air to the blood stream and expelling the waste product carbon dioxide. The blood circulates throughout our bodies in veins and arteries. The blood carries oxygen to all cells throughout the body and collects carbon dioxide from it to be expelled through the lungs. We usually think of respiration as the work of the lungs after air is breathed in through the mouth or nose. The lungs do play a very important role, but every living cell in the body is involved in this process. Respiration is the act of burning energy from oxygen. Breathing is an obvious part of the respiratory passages, but these also involve yawning, sneezing, coughing, hiccups, the power of speech, and the sense of smell. The respiratory flow has been utilized by the larynx, or voice box, which uses it to create a multiple range of sounds so that humans can communicate vocally. These systems include organs

which take up space in the head and neck and most of the chest. The cardiovascular and respiratory systems are basic to life and breathing, like the beat of one's heart, and its control is an automatic function which is controlled by the brain.

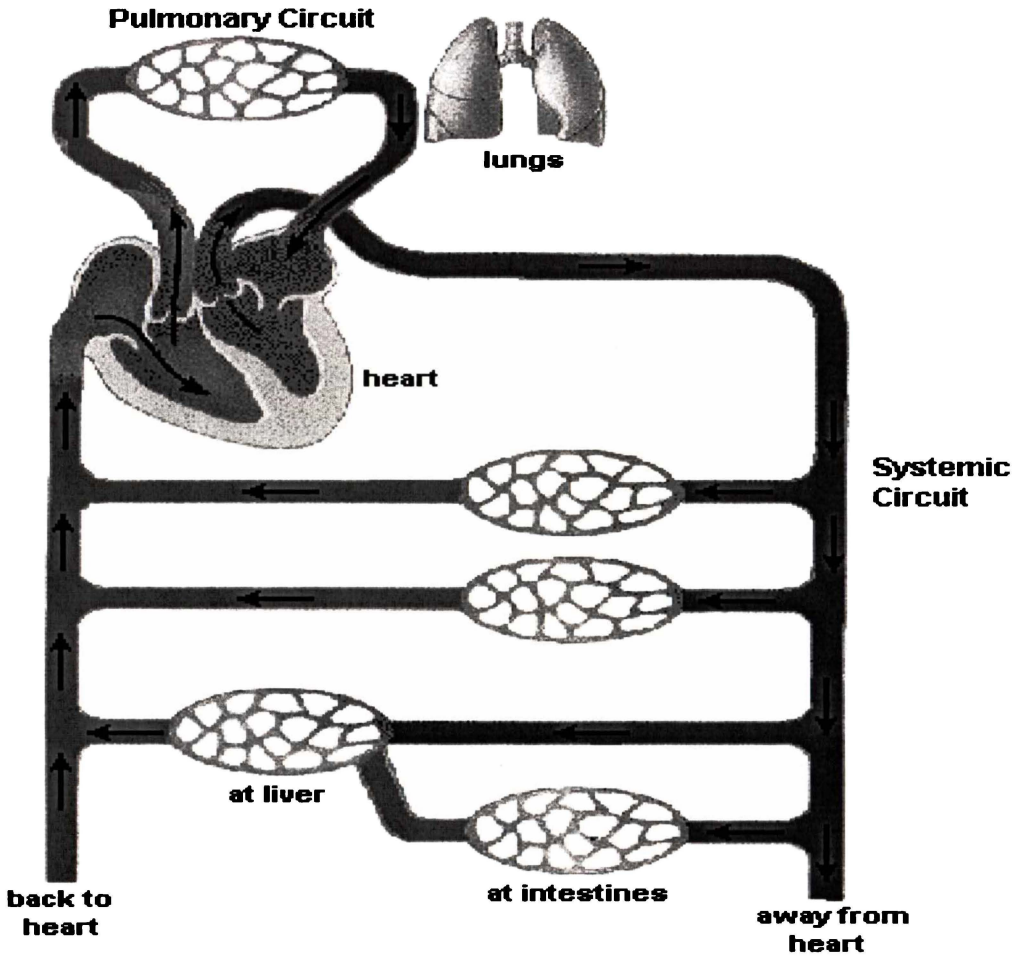

Figure 2- 1 Schematic of the human cardiovascular system [Starr and McMillan 1996]

This chapter contains an overview of physiological factors that are involved in many ways to the structure and function of the human cardiovascular system. Unless otherwise specified, the major sources of information and figures for this chapter are Guyton [1969, 1984], Thibodeau [1992] and Starr and McMillan [1996].

2.2 The Human Heart

The heart is divided into four chambers, forming two distinct pumps. Each pump has an atrium and a ventricle. The atria are thin walled, and serve as expandable

reservoirs that contract to fill the ventricles (just as they do in the snail). The ventricles are thick walled and very muscular. They contract to force the blood into the arteries. The right atrium and ventricle receive blood from the two-vena cavae and deliver it to the lungs via the pulmonary artery. The left atrium and ventricle receive blood from the lungs and deliver it to the aorta, and thence to the rest of the body.

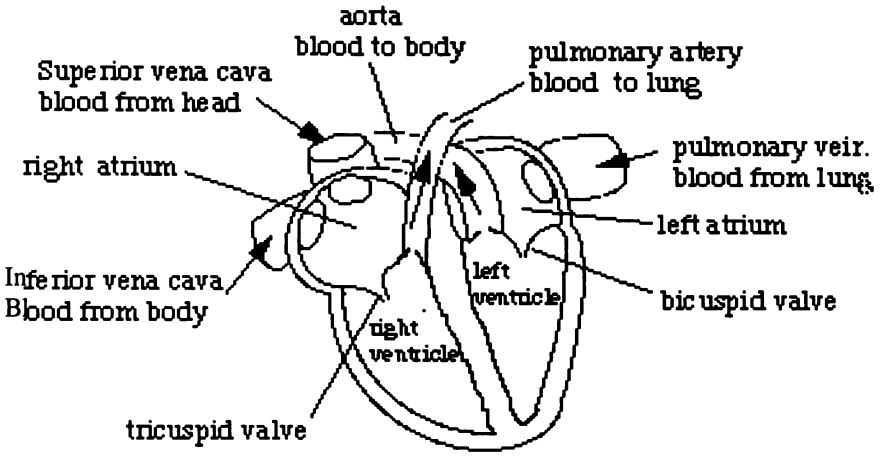

Figure 2- 2 The human heart

2.2.1 Contraction of the heart

Contraction of the heart has several phases that can be roughly divided into diastole, when the muscles relax and systole when they contract. We can start with atrial systole, which is when both atria contract and fill the ventricles (A in figure 2-3). After atrial systole, the bicuspid and tricuspid valves to the ventricles close causing the first heart beat (B in figure 2-3). The ventricles then begin to contract in ventricular systole (B & C in figure 2-3). Initially the valves to the arteries remain closed, but as ventricular pressure exceeds blood pressure in the arteries, they open (C in figure 2-3). Following ventricular systole, the valves to the arteries close causing the second beat (D in figure 2-3). The atria and ventricles then relax and as they do blood flows from the systemic and pulmonary veins into the atria and then into the ventricles, completing diastole (E & F in figure 2-3).

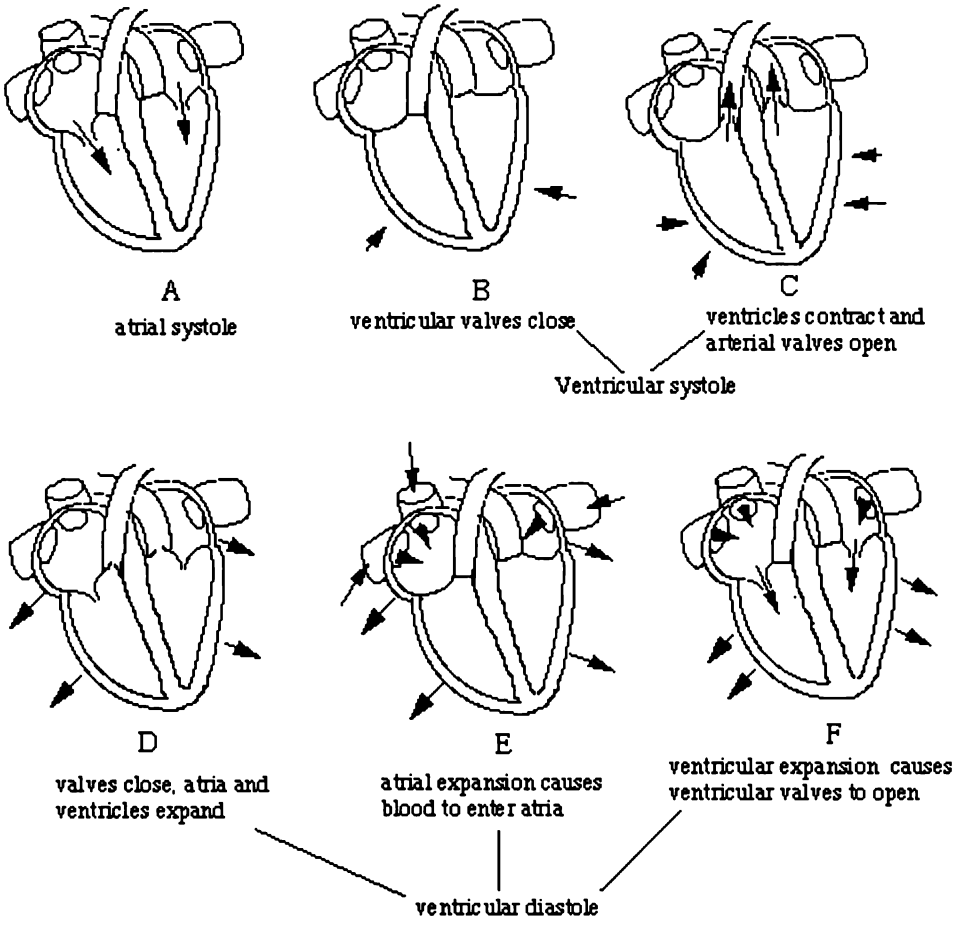

Figure 2- 3 Contraction of the human heart

2.2.2 Pacemakers

The heart has an intrinsic tendency to beat, even isolated cells of a heart will beat in culture. However, the heart has pacemakers to ensure that the heart beats regularly. The pacemakers consist of two groups of cells in the right atrium. These cells produce action potentials endogenously, i.e. without stimulation. One of these lies nears the entrance of the great veins into the right atrium. It sends rhythmical waves of action potentials across the right and then into the left atria that contract together in response. The action potential passes through all of the cells of the atria because they are electrically connected to one another by gap junctions. The action potential of the pacemaker cells is unusual in that they last for 300 ms, whereas an action potential in the nervous system only lasts 2 ms after the action potential, the cells repolarize, and a new action potential is generated. This takes just under 1 second. The heart beats at about 70 times a minute, and this rate reflects timing of these

electrical events in the pacemaker cells. A refractory period, during which a second action potential cannot occur lasts 300 ms and ensures that the heart cannot go into tetanus.

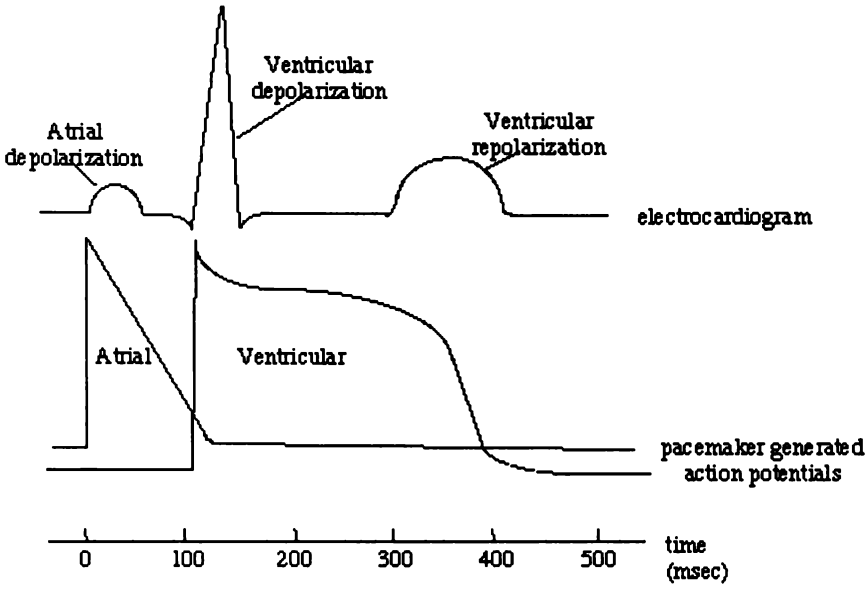

Figure 2- 4 Action potential of pacemaker cells

The wave of excitation passes to the second group of the atrioventricular node cells that are also in the right atrium. These cells are stimulated to produce action potentials which pass down modified muscle fibers (Purkinje fibers) into the ventricles. The ventricles contract in response. It is important that there be a delay of about 0.1 second between the contraction of the atria and ventricles to allow time for filling of the ventricles. This is ensured, firstly, by not having gap junctions between the atrial and ventricular cells. Thus the action potentials spreading through the atrium cannot pass directly into the ventricle. Instead, the second group of pacemaker cells has to be excited before excitation can pass into the ventricles. Secondly, the rate of movement of the action potentials in the Purkinje fibers is relatively slow. Both ventricles contract in concert. The result is that both the right and left atria and ventricles contract almost simultaneously with a 100 msec delay between the atrial and ventricular contractions. The force of the blood coming out of the ventricles is dampened in the aorta and arteries that are elastic and muscular. Elasticity is important as it allows the artery to dampen the force of a pulse of blood

by expanding. The muscles then contract to maintain pressure on the blood as a bolus of blood passes thorough. This ensures that the high pressure of each pulse of blood is moderated to maintain a more even blood pressure. In contrast, the veins are much less muscular.

2.2.3 Nervous control of the heart

Though the heart has its own intrinsic control system and can continue to operate without any nervous influences, the efficacy of heart action can be changed greatly by regulatory impulses from the central nervous system. The nervous system is connected with the heart through two different sets of nerves, the parasympathetic nerves and the sympathetic nerves.

2.2.3.1 Parasympathetic stimulation

Stimulation of the parasympathetic nerves causes the following three important effects on the heart: (1) decreased rate of heart rate, (2) decreased force of contraction of the arterial muscle, and (3) delayed conduction of impulses through the AV node, which lengthens the delay period between atrial and ventricular contraction. All of these effects may be summarized by saying that parasympathetic stimulation decreases all activities of the heart. Usually heart activity is reduced by the parasympathetic nerves during periods of rest. Without such periods of rest, the heart undoubtedly would wear out at a much earlier age than it normally does.

2.2.3.2 Sympathetic stimulation

Stimulation of the sympathetic nerves has essentially the opposite effects on the heart: (1) increased heart rate, (2) increased vigor of cardiac contraction, and (3) increased rapidity of the conduction of the cardiac impulses through the heart. These effects can be summarized by saying that sympathetic stimulation increases the activity of the heart as a pump, sometimes increasing the ability to pump blood as much as 100 percent. This stimulation of the heart is necessary when a person is subjected to stressful situation such as exercise, disease, excessive heat, and other conditions that demand rapid blood flow through the circulatory system. Therefore, the sympathetic effects on the heart are a standby mechanism held in readiness to make the heart beat with extreme vigor when necessary.

2.3 The Systemic Circulation and Its Regulation

Blood circulation other than the heart and the pulmonary circulation is called the systemic circulation. The blood flowing through this part of the circulation provides nutrition to the tissues, cleansing of the blood as it passes through the kidneys, absorption of nutrients from the gastrointestinal tract, and mixing of all the fluids of the body.

2.3.1 Blood flow through the systemic circulation

The heart pumps blood while the blood vessels channel and deliver it throughout the body. Arteries carry blood filled with nutrients away from the heart to all parts of the body. The blood is sometimes compared to a river, but the arteries are more like a river in reverse. Arteries are thick-walled tubes with a circular covering of yellow, elastic fibers, which contain a filling of muscle that absorbs the tremendous pressure wave of a heartbeat and slows the blood down. This pressure can be felt in the arm and wrist - it is the pulse. Eventually arteries divide into smaller arterioles and then into even smaller capillaries, the smallest of all blood vessels. One arteriole can serve a hundred capillaries. Here, in every tissue of every organ, blood's work is done when it gives up what the cells need and takes away the waste products that they do not need. Now the river comparison really does apply. Capillaries join together to form small veins, which flow into larger main veins, and these deliver deoxygenated blood back to the heart. Veins, unlike arteries, have thin, slack walls, because the blood has lost the pressure which forced it out of the heart, so the dark, reddish-blue blood which flows through the veins on its way to the lungs oozes along very slowly on its way to be reoxygenated. After passing back through the heart blood passes into the pulmonary arteries at the right side of the heart. It flows along the pulmonary arteries to the lungs to collect oxygen, then back to the heart's left side to begin its journey around the body again.

2.3.2 Cardiac output

The amount of blood pumped out of the left ventricle to the aorta is the cardiac output. The volume of blood delivered to the tissues, and the blood pressure, are determined by the cardiac output. It is, therefore, important to understand how

output is regulated. Cardiac output is a function of the heart rate and the stroke volume.
Cardiac output = heart rate x stroke volume.

To increase output the heart can increase either the heart rate or the stroke volume, or both. When strenuously exercising the body chooses both. Heart rate can increase to 180 beats/minute and stroke volume can double, resulting in an output of 25 liters/minute, or greater, in trained athletes. However, there are limits to increasing output by increasing heart rate.

2.3.3 Blood pressure

The pressure in a blood vessel is the force that the blood exerts against the walls of the vessel. This force distends the vessel because all blood vessel are distensible, the veins eight times as much as the arteries. Pressure also makes blood attempt to leave a vessel by any available opening, which means that the normally high pressure in the arteries forces blood through the small arteries, then through the capillaries, and finally into the veins. The importance of blood pressure, then, is that it is the force that makes the blood flow through the circulation.

2.3.4 The baroreceptors and blood pressure control

The baroreceptors are stretch receptors found in several of the major blood vessels, including the aorta and the carotid artery. The baroreceptors respond to stretch caused by increased blood pressure, by increasing the rate of nerve discharge. They can respond very quickly to changes in blood pressure - within one heartbeat. The baroreceptor axons travel to the vasomotor center in the medulla oblongata of the brain. The nerves controlling the heart and arterioles come from the vasomotor center. In response to an increase in blood pressure, the vasomotor center decreases sympathetic and increases parasympathetic nerve stimulation of the heart which results in reduction in pacemaker activity and ventricle contractility. It also decreases sympathetic stimulation of the arterioles and veins causing them to dilate. The dilation of the veins causes more blood to accumulate in the veins. The net effect is a decrease in heart rate and stroke volume as well as increased blood flow through tissues and storage of blood in the veins, all of which decreases blood

pressure. Of course, if blood pressure is decreased the opposite reactions would occur, restoring normal blood pressure.

Chemoreceptors associated with the baroreceptors are sensitive to increases in levels of CO_2 and pH, and decreased O_2, which indicate low oxygen levels in the tissues. These chemoreceptors stimulate changes in heart rate.

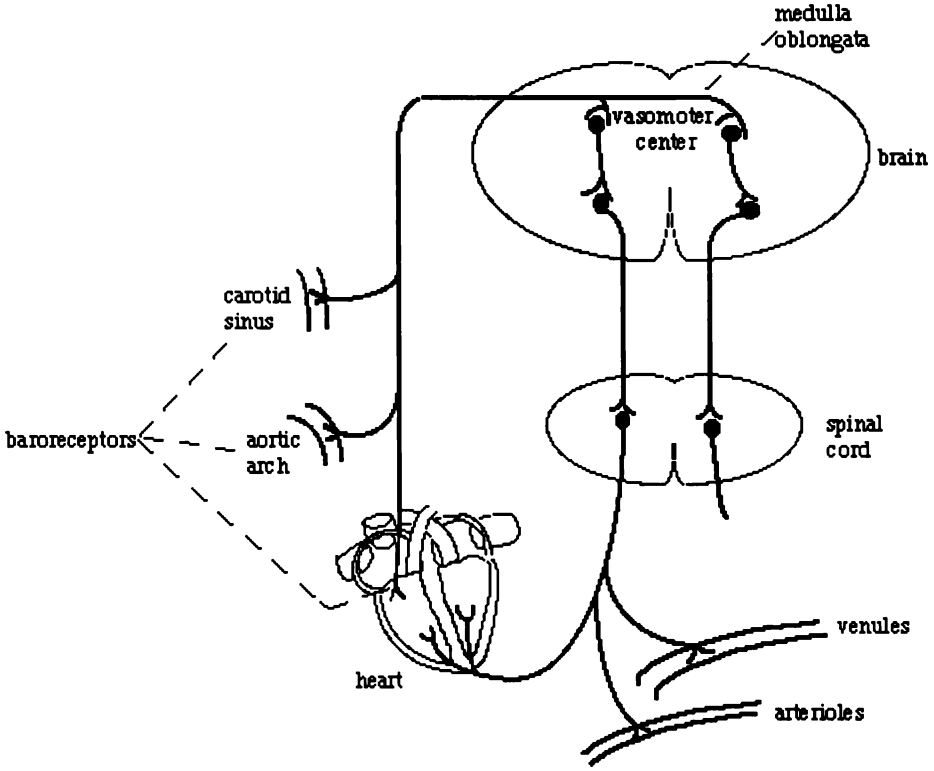

Figure 2- 5 Baroreceptors and the vasomotor center

2.4 Heart Rate Variability

It is well known that heart rate variability (HRV) represents an oscillation at the respiratory frequency. This effect is the central modulation of cardiac vagal and sympathetic efferent activity, a phenomenon referred to as respiratory sinus arrhythmia (RSA). The blood pressure is sensed by the baroreceptors and integrated by sympathetic and parasympathetic activity. This effect creates an oscillation called the Mayer wave (10sec) in both SBP and HRV. So blood pressure and heart rate interact forming a closed loop. The integration of sympathetic and parasympathetic

activity with afferent signals from the baroreceptors produces the beat-to-beat changes in HRV. Figure 2-6 illustrates these relationships in block diagram form. The variability in HRV is due to the synergistic action of the two branches of the autonomic nervous system which acts in balance through neural, mechanical, humoral and other physiological mechanisms, in order to maintain cardiovascular parameters in their optimal ranges and to react optimally to changing external or internal conditions.

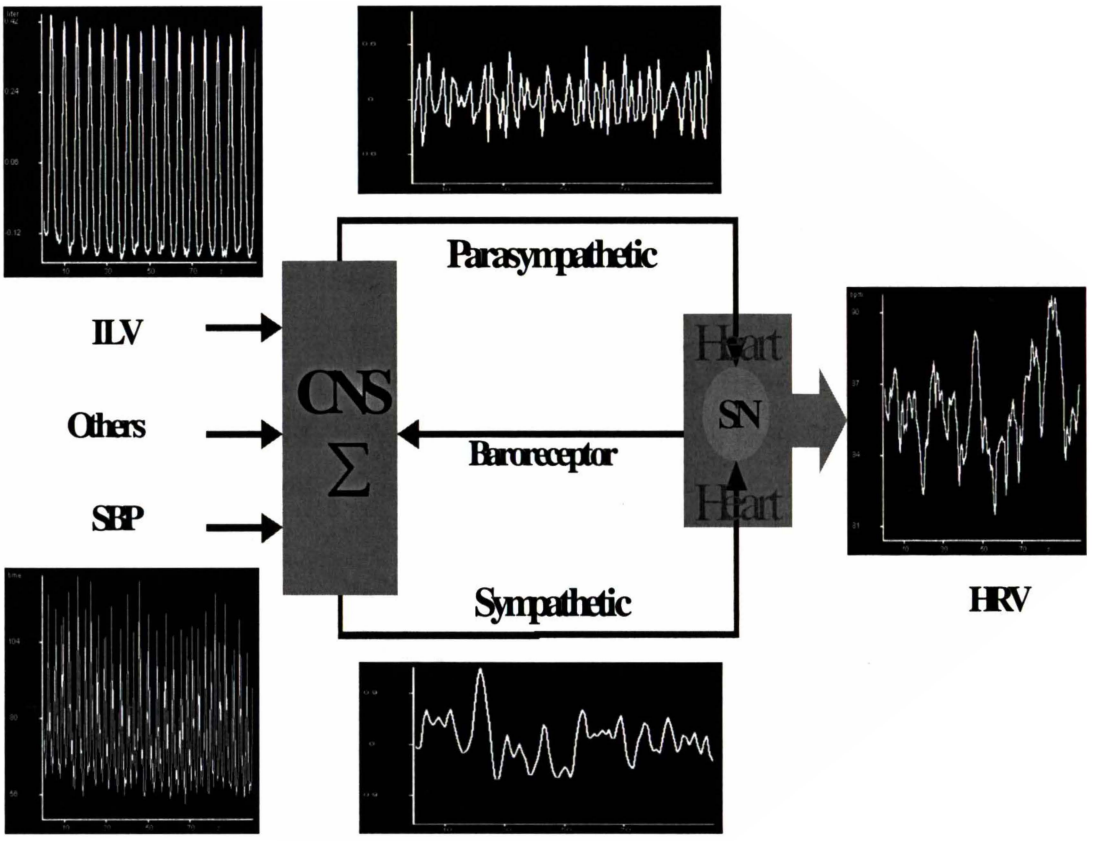

Figure 2- 6 Block diagram of nerves between the heart and brain, the interaction of which is responsible for the generation of HRV

2.4.1 Heart rate variability

The HRV originates in the body's own negative feedback system that control HR via neural, humoral and thermoregulatory effects on the sino-atrial (SA) node. Therefore it contains relevant information about the status of the autonomic nervous system [Hirsch and Bishop 1981]. Over the past 20 years the characteristics of both the

short and long term oscillations in HR have become of great interest from both a physiological and a pathophysiological standpoint. The nature of these oscillations has been investigated with the possibility that HRV analysis might be considered as a measure of the balance in the sympathetic and parasympathetic systems and the state of the autonomous nervous systems (ANS) and cardiac system. In particular, analysis in the frequency domain provides basic information of which the overall variability of the signal is distributed along the frequency spectrum.

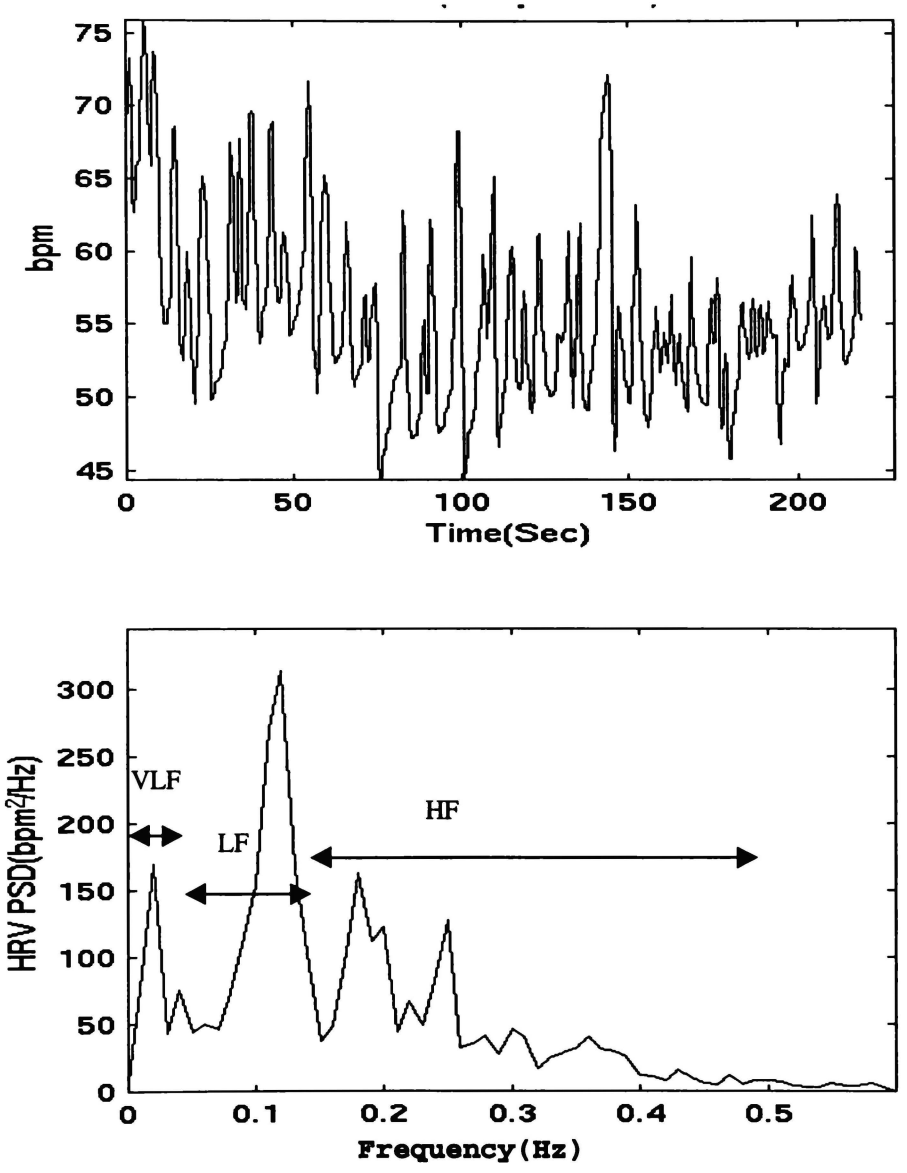

Figure 2- 7 Illustrates a typical HRV signal measured in beat per minute (bpm) and power spectrum for healthy subject. The HRV spectrum is divided into three frequency ranges or bands, VLF (0 to 0.04 Hz), LF (0.04 to 0.15 Hz), and HF (0.15 to 0.5 Hz).

2.4.2 The power spectrum of HRV

There are three primary frequencies of HR oscillations that contain the majority of HR power (Figure 2-7) and these have been related to specific physiological correlates of the cardiovascular system.

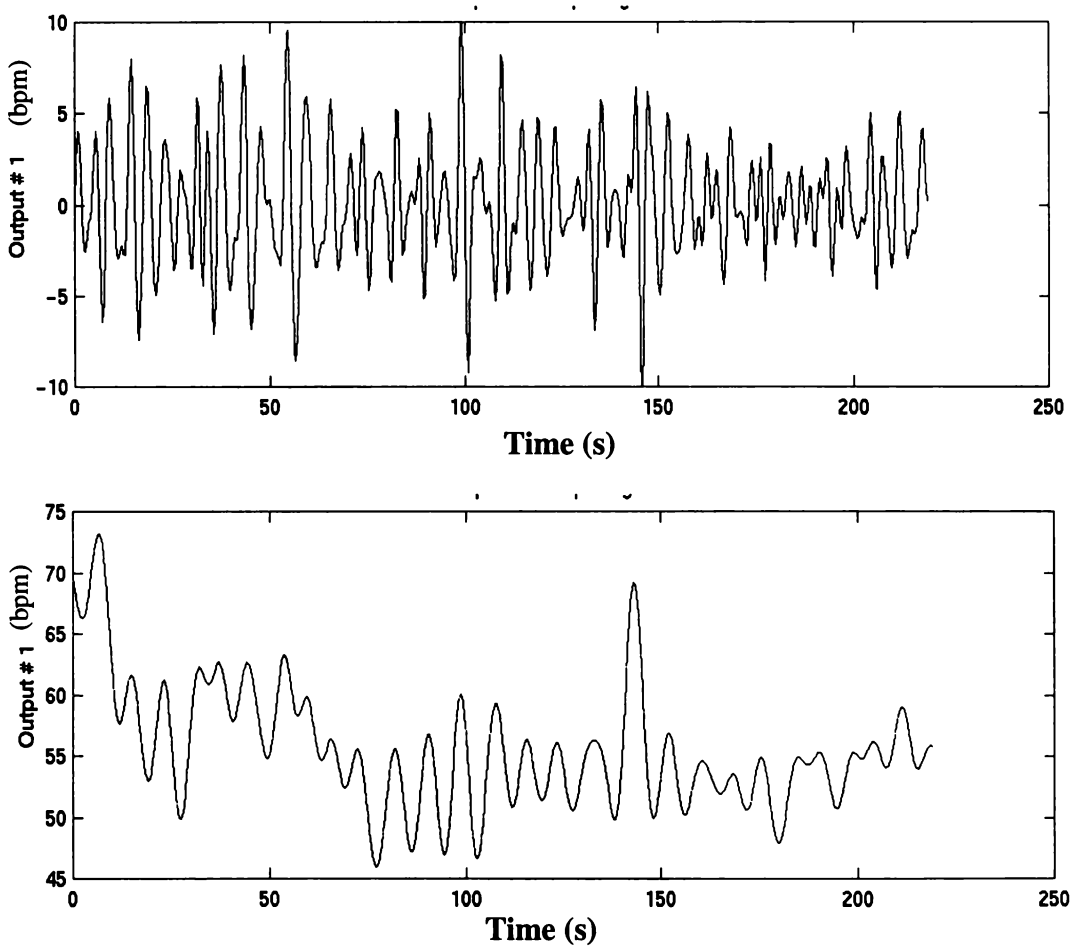

Figure 2- 8 HR signal in Figure 2.7 has been filtered to two frequency components in order to separate the sympathetic and parasympathetic effects on heart rate: top is high frequency part (0.15 - 0.5 Hz) and bottom is low frequency part (0 - 0.15 Hz).

The very low frequency (VLF) component is generally below 0.04 Hz. This component represents many slower frequency peaks (LFP), mainly related to thermoregulation and humoral factors. The low frequency component is centered on 0.1 Hz, ranging between 0.04 and 0.15 Hz. This component seems predominantly due to the sympathetic discharge acting on the cardiac frequency variability. In fact,

a marked increase in its power has always been observed to correspond with sympathetic stimulation, which is a response to blood pressure variations. The high frequency component, at the respiratory frequency, ranging from 0.15 to 0.5 Hz, represents the respiratory sinus arrhythmia, which depends only on the parasympathetic modulation of the HR, and thus is generally considered a marker of parasympathetic activity. The power of the LF and HF components together with the ratio (balance) between the LF and HF have been used as indices of the balance in the sympathetic and vagal systems.

Figure 2-8 shows how filtering techniques can be used to separate the sympathetic and parasympathetic affects on heart rate. In the top trace in Figure 2-8, the low frequency (0 to .15 Hz) has been removed, leaving only the parasympathetic influence. On the other hand, when the high frequency is removed, all that remains (bottom trace) are low frequency (0 to 0.15 Hz) waves which mainly reflect sympathetic activity. In this example, the increase in HR is sympathetically mediated as opposed to parasympathetically inhibited. An increased sympathetic outflow is often accompanied by an inhibition of the parasympathetic system, and increased parasympathetic activity is often accompanied by sympathetic inhibition.

2.5 Summary

The most obvious effect of vagal stimulation is to slow or even stop the heart. The response time of the sinus node is very short and the effect of a single vagal impulse depends on the phase of the cardiac cycle at which it is applied. After cessation of vagal stimulation, HR rapidly returns to its previous level. An increase in HR can also be achieved by reduced vagal activity or vagal block. Thus, any sudden changes in HR are parasympathetically mediated. The slowness of the response to sympathetic stimulation is in direct contrast to vagal stimulation. Short-term regulation of blood pressure is accomplished by a complex network of pressure sensitive "baroreceptors" which are located throughout the heart and in the aortic arch. Since blood pressure regulation is a central role of the cardiovascular system, the factors that alter blood pressure will also govern fluctuations in HR. The afferent impulses (signals travelling to the brain) from the baroreceptor travel via the glossopharyngeal and vagal nerves to the vasomotor centers in the medulla oblongata where they primarily modulate the sympathetic nervous system outflow to the heart and the blood vessels, although there is also some modulation of

parasympathetic outflow to the heart. Thus, the baroreceptor regulates HR, vasoconstriction, venoconstriction and cardiac contractility in order to maintain blood pressure.

The intrinsic heart rate (HR) generated by the sinoatrial node in the absence of any neural or hormonal influence is about 100 to 120 bpm. In a healthy individual, the HR estimated at any given time represents the net effect of the parasympathetic (vagus) nerves, which slow HR and the sympathetic nerves that accelerate it. At rest, both sympathetic and parasympathetic nerves are tonically active with the vagal effect dominant.

Chapter 3

Modeling Human Cardiovascular System

3.1 Introduction

Applications of systems theory to the analysis of fluctuations in heart rate and other hemodynamic variables have provided a means to quantitatively investigate cardiovascular regulatory mechanisms. These studies have been used to develop models of cardiovascular control in which the components of the system consisted of several "black boxes". Such investigations promise to further our understanding of the integrated functioning of cardiovascular regulatory mechanisms in health and disease and offer a potential for new clinical tools that may contribute to diagnosis of a variety of cardiovascular and neuralgic disorders, but as our knowledge of central processing increases, more realistic quantitative models are needed.

This chapter is devoted to the literature dealing with the interaction of heart rate, respiration and blood pressure oscillations. The purpose of this chapter is to examine existing assumptions about the origin of the respiratory sinus arrhythmia (RSA) in light of recent research, and to put forth alternative hypotheses. A literature survey of the two main theories concerning the genesis of RSA provides the basis of our cardiovascular system model which displays a number of physiologically important features and gives a theoretical explanation for results reported in the literature. Our model of the cardiovascular systems suggested a substantial role for a respiratory oscillator in the origin of RSA in humans under natural physiological conditions. This will be explained in the following chapters on cardiovascular system identification.

3.2 Quantification of HRV Due to Respiration and the Baroreflex

In most work on cardiovascular system identification, the methodology has concentrated primarily on measuring the linear system transfer characteristics either by ignoring any nonlinearities and trying to obtain a "best" linear approximation to the transfer function or by searching for a stimulus domain within which the system acts approximately linearly. These linear system descriptions of relationship between heart rate variability (HRV), instantaneous lung volume (ILV) and systolic blood pressure (SBP) have been made using the transfer function in the frequency domain and the impulse response in the time domain. This section is a review of the publications dealing with linear fluctuation analysis of heart rate related to other physiological quantities such as respiration and arterial blood pressure.

3.2.1 Linear system identification techniques

In 1989, Berger *et al.* introduced a novel method that allowed the quantification of transfer characteristics from fluctuations of ILV to HRV over an extended frequency range by broadening the spectrum of the respiratory input. In the experimental protocol, the subject initiated each breath in synchrony with a series of irregularly timed tones, the intervals of which followed a Poisson distribution. The transfer function of the RSA control system was estimated by dividing the cross-power spectrum between ILV and HRV by the power spectrum of ILV [Berger *et al.* 1989, Saul *et al.* 1991]. For a linear dynamic system, the relationship between input and output can be described either by the transfer function in the frequency domain or by the impulse response in the time domain. Impulse response represents the dynamic changes observed at the output when the input is excited by a very short stimulation. Compared with power spectral analysis, impulse response function approach makes use of the phase spectra, and this will provide additional information. Most previous studies of RSA and baroreceptor function have been limited to the frequency domain. Yana *et al.* [1993] proposed a technique for estimating impulse response function from fluctuations of ILV to HRV, which gives various insights into the characteristics of the cardiovascular system. However, it requires a system-theoretical interpretation of the spectrum to estimate time domain parameters, such as delays, amplitudes, or time constants that may underlie the physiological response. It will therefore be useful and important to provide a time domain counterpart to transfer function analysis so as to visualize and quantitatively assess these time domain parameters [Yana *et al.*1993]. This work has been extended

recently to ARX model analysis that yields the impulse responses between HRV and ILV, HRV and SBP and between SBP and ILV [Mullen *et al.* 1997]. In practice, the impulse response function can be obtained from the inverse Fourier transform of the transfer function. Panerai *et al.* [1997] used this technique to analyze the dynamic relationship between HRV and SBP for assessing baroreceptor sensitivity. The authors claim the main potential advantage is to obtain an expression of the dynamic relationship between input and output without the need to preselect segments of data either in time or frequency domain.

Although this Fourier technique and transfer function approach are able to characterize well the overall relation between ILV and HRV, it has been claimed by Triedman *et al.* [1995] that these techniques are insufficient to incorporate explicitly the causal dependence of HRV on respiration because it is mathematically non-casual. In an attempt to overcome the limitations possibly present in earlier techniques, an autoregressive with exogenous input variable (ARX) technique was applied to construct time domain models of heart rate regulation by the autonomic nervous system for analysis of HRV, ILV and SBP signals. Once the model has been analytically defined, the impulse response function and transfer function could be directly obtained from the equations of the model [Mullen *et al.* 1997]. The magnitude of vagal HR modulation was well correlated with that obtained using cross-spectral techniques, as well as to improve the accuracy of the RSA estimates [Triedman *et al.* 1995, Chon. *et al.* 1996]. Also, the measure of early baroreflex gain, the maximal impulse response and the on-beat step response produced by the ARX model, correlate with but are of lower magnitude than gains derived by pharmacological injections [Patton *et al.* 1996].

Kim and Khoo, [1997] similarly used an ARX model to estimate the transfer function and impulse response of HRV/ILV. Their results showed larger errors of transfer function in the frequency range above 0.3 Hz and a considerable error in the estimation of first 4 s of the impulse response. These authors therefore suggested the estimation of RSA impulse response should be interpreted with caution and the peak of impulse response would not be a reliable or accurate quantitative index of RSA unless ILV is broadband with a relatively flat spectrum [Kim and Khoo ibid].

3.2.2 Physiological application of cardiorespiratory transfer function

Saul *et al.*, [1991] completed a series of studies using transfer function analysis to characterize RSA in normal humans. The results of their studies confirm that both cardiac parasympathetic and sympathetic activity are important in modulating HR in response to respiratory activity and that the phase and magnitude characteristics of

the ILV and HRV transfer function can be used to identify the role of each branch of the autonomic nervous system in mediating the response. It was discovered that RSA at frequencies above 0.15 Hz is predominately mediated by vagal activity, which was reduced with standing. Below 0.15 Hz, vagal and sympathetic activity are well balanced but with a 180 degree phase lag. On the whole, the HRV response is determined almost entirely by the response characteristic of the SA node. In addition, there was a small nonautonomic, presumably mechanical, effect of respiration on HR, which had not previously been well characterized in humans.
Respiratory to heart rate impulse response has been obtained by both parametric and non-parametric identification [Yana *et al.* 1993, Triedman *et al.* 1995, Mullen *et al.* 1997]. The authors interpreted the impulse response as a simultaneous withdrawal of vagal and sympathetic nervous activity during inspiration. The difference in time course for the two processes was the explanation of the impulse response peaks. Furthermore, one of the interesting results of their analysis is the noncausal relationship between ILV and HRV. This finding was explained by the hypothesis that both ILV and HRV are in response to a prior common nervous stimulation, with HRV change leading to lung volume changes.

3.2.3 Physiological application of baroreflex control function

As explained in Chapter 2, when the arterial pressure is increased, the baroreflex sensors are stretched and signals are transmitted into the central nervous system. Feedback signals are sent back to reduce arterial pressure downward toward the normal level. This is a process of negative feedback. This nervous control of the arterial pressure is by far the most rapid of all our mechanisms for pressure control. The essential point in evaluating the effects of baroreflex function, which was described in Chapter 2, is the identification of its actual influence on the different components of blood pressure and HRV.
Saul *et al.* [1991] used the transfer function between ABP and HRV to represent the combined effects of the HRV baroreflex and the mechanical feedforward from HRV to ABP. The phases and magnitudes of the transfer function were both consistent with the findings of previous investigators. The phase at most frequencies is neither 0^0 for feedforward from HRV to ABP nor near 180^0 for feedback from ABP to HRV. Therefore the relationship between ABP and HRV is influenced by the interactions between the feedforward and feedback pathways and does not characterize either pathway alone. The R-R interval response is between 8 and 16 ms / mmHg.
Nonparametric and parametric identification were used to get the HRV baroreflex impulse response. Patton *et al.* [1996] claimed that the open–loop baroreflex gain

was obtained by an ARX model during closed-loop conditions and overcame the limitation of the transfer function to separate the effects of SBP on HRV from those of HRV on SBP. The baroreflex gain from the ARX model was linearly correlated with the baroreflex gain obtained using bolus injections of phenylephrine and sodium nitroprussid. The impulse response of SBP to RR interval is characterized by an initial (0-1s) sharp positive peak of 5.5 +/- 4.2 ms / mmHg, reflecting a very rapid increase in RR in response to an increase SBP, following by a negative but lower amplitude oscillation that approaches zero over time [Patton *et al.* 1996].

3.3 The Genesis of the Respiratory Sinus Arrhythmia

RSA is a change in the heart rate that corresponds to the frequency of respiration. Typically, the heart rate will increase during inspiration due to stimulation of the sympathetic nervous system during this time, and the heart rate will decrease during expiration due to stimulation of the parasympathetic nervous system. RSA was first described by Stephen Hales in the horse in 1733. Since then, many studies have confirmed the presence of RSA in a wide variety of species, including humans, and further characterized the causes of normal RSA. The rhythmic change in heart rate can be attributed to varying levels of the neurotransmitter acetylocholine (sympathetic) and norepinephrine (parasympathetic) at nerve endings. However, parasympathetic activity influences heart rate by RSA much more so than sympathetic activity. The noninvasive assessment of parasympathetic influences upon heart rate is of interest to those wishing to better understand the underlying autonomic mechanisms that affect cardiac functioning. RSA is influenced by the following two factors.

A reflexive factor consists of an arteriole response to sympathetic stimulation altering arterial blood pressure via baroreceptors and stretch receptors in the lungs. It alters the heart rate accordingly in a feedback manner. In addition, The atrial reflex (Bainbridge reflex) [Starr and McMillan 1996] plays a major role in the alteration of heart rate as a result of respiration. It accelerates the heart rate when the walls of the right atrium are stretched. Part of the acceleration results from the stretching of the nodal fibers, and part from a sympathetic reflex involving stretch receptors in the atrial wall

The second factor that controls the heart rate with respect to respiration is the central nervous system, which connects the heart and lungs through the cardiac/vagal centre of the medulla. This has been demonstrated experimentally. RSA is the most prominent of the various factors that modulate the beat-to-beat rhythm of the heart

and a consequence rapid fluctuation in parasympathetic neural activity to the sinoatrial node [Eckberg. 1983].

Several theories based on these mechanisms have been proposed for the origin of RSA. One theory concentrates on arterial baroreflex stimulation caused by changes in phase with respiratory induced modulation of arterial blood pressure [DeBoer *et al.* 1987, Baselli, *et al.* 1994]. Another concentrates on the direct influence of medullary respiratory neurons on the vagal motor nucleus [Eckberg and Sleight 1992]. However, these two theories are not mutually exclusive. A further group of researchers claims the feedback originating from the cardiopulmonary baroreceptor may be implicated in the origin of RSA [Taha *et al.* 1995]. Despite many past studies, the precise mechanism of respiration-induced SA is still debated. Two main theories, "medullary respiratory neurons" theory and "arterial baroreflex" theory, are reviewed in this section.

3.3.1 " Medullary respiratory neurons" theory

In 1985, Akselrod *et al.* developed a simple closed loop model of arterial pressure and heart rate which was controlled by looking at the open loop properties of heart rate and atrial blood pressure during breathing in dogs [Akselrod *et al.* 1985]. The authors found that in normal dogs, respiratory variations in ABP were secondary to HRV and are primarily mediated by HRV. The very small residual respiratory frequency variation in ABP is mediated by the mechanical effects of respiration.

Three level resistive breathing producing inspiratory (-) and expiratory (+) pressures of ± 1.6, ±5.4,and ±16.6 cmH_2O, respectively, was used to test the hypothesis that the arterial baroreflex was important in the origin of HRV [Blaber and Hughson 1996]. The phase relationship in a proposed mechanical link from stroke distance (an index of stroke volume derived from Doppler ultrasound) to systolic blood pressure SBP to HRV were not modified during the resistive breathing. Therefore, it was suggested that there is no causal relation between them and both HRV and SBP are modified by common medullary respiratory neurons.

Mullen *et al.* employed both linear and nonlinear system identification approaches to the analysis of fluctuations in heart rate variability, instantaneous lung volume and arterial blood pressure to evaluate closed-loop cardiovascular regulatory dynamics [Mullen *et al.* 1997, Chon *et al.* 1996]. The authors interpreted the impulse response of the HRV/ILV transfer function as simultaneous withdrawal of vagal and sympathetic nervous activity during inspiration. This impulse response is consistent with the observation that on inspiration there is an increasing HRV. However, respiratory influences on HRV have been shown to have a noncausal relationship.

Thus, HRV associated with respiration leads mechanical respiratory activity because the medullary respiration centre controls respiration and via a coupling to autonomic centers, modulates heart rate by varying parasympathetic and sympathetic inputs to the sinoatrial node.

3.3.2 "Arterial baroreflex" theory

DeBoer *et al.*[1987] used phenylephrine to increase peripheral resistance in order to develop a closed loop model. This model incorporated HRV and peripheral resistance control by the baroreflex. The heart rate influences cardiac output, which together with the peripheral resistance determines the value of blood pressure and thus closes the loop. DeBoer's model suggested that respiration first affects the cardiac output causing ABP to fluctuate, resulting in the vagal baroreflex response on HRV. However, the possibility can not be ruled out that both SBP and HRV are independently affected by respiration [DeBoer *et al.* 1987].

Basseli *et al.* [1994] used a closed loop to investigate the origin of RSA. The model suggested that RSA is due to a reflex modulation of the SA node in response to fluctuations in ABP. It was further suggested that the fluctuations in ABP were caused by changes in ventricular filling pressure. Basseli's results are consistent with DeBoer's [Basseli *et al.* 1994].

In 1991, Saul *et al.* broadened the breathing frequency band by having the subjects breathe to a broadened respiratory signal. Propranolol (sympathetic blocker) combined with a supine protocol was used to isolate the vagal influence on heart rate and blood pressure. Atropine (parasympathetic blocker) and upright patients isolated the sympathetic nervous system. This information was used to produce a simple model of vagal and sympathetic modulation of heart rate and blood pressure. Also complete autonomic blockade was used to show that there is mechanical coupling between respiration and the vasculature at frequencies less then 0.25 Hz. Due to the nonparametric nature of their model, the authors could not account for causality and therefore could not differentiate between feedback and feedforward paths between arterial blood pressure and heart rate. The authors did, however, strongly suggest that above 0.25 Hz, the origin of RSA was due to direct cardiopulmonary alteration of RR interval independent of the arterial baroreflex.

More recently, Piepoli and his co-workers [1997] investigated the role played by the arterial baroreceptors in the origin of RSA in conscious humans. Observation of a simple apnea showed that respiration appeared unnecessary for the generation of RSA. Their experimental data indicated that a suitable phase shift between respiration and neck suction might result in either a reduction or a potentiation of RSA. Furthermore, the authors showed that it is possible to separate the effects of

respiration from the baroreceptor input by examination of RR interval when setting the respiration and the neck suction at two close but distinct frequencies. The possible and simple explanation for these results is that arterial baroreceptors play a major role in the generation of RSA. However, one limitation of this study is that RSA can not be described naturally by the RR interval response when baroreflex stimulation is induced during apnea.

3.4 Modeling the Human Cardiovascular System

The following points are generally accepted by both central and peripheral theories:
The HR response is determined almost entirely by the response characteristic of the SA node.

The beat-by-beat variation in heart rate is a consequence of fluctuations in both parasympathetic and sympathetic neural activity to SA node.

Respiration modulates the activity of most sympathetic and parasympathetic efferent nerves both through direct coupling between the medullary respiratory and autonomic centers and through the modulation of central sensitivity to baroreceptor input by changes in baroreceptor input mediated by respiration-reduced changes in SBP.

The phase of the respiration period relative to heart rate determines the strength of vagal influence on the heart.

The main difference in viewpoint between the central and peripheral theories is whether respiratory or baroreceptor modulation of autonomic centers is the main source of the origin of RSA.

Administration of vasoactive drugs or stimulation of the carotid baroreceptors by neck suction was used to stimulate the baroreceptors to enable HRV to be correlated to blood pressure [Piepoli *et al.* 1997]. Although these techniques allowed important insights into the regulatory strategy of the cardiovascular system to be obtained, these pharmacological or mechanical methods assess nonspontaneous phenomena that are slow compared with HR. Consequently, they may be insufficient to appraise the regulatory function under normal conditions. The external stimulation, particular to baroreceptors, and required for the assessment of RSA, may interfere with the neural control mechanisms under evaluation. Strong external stimulation to change either arterial blood pressure or respiration, such as neck suction or the isolated assessments, may not allow characterization of the nature of RSA. For example,

during neck suction, it is suggested that baroreflex pathways other than the medullary respiratory center is a major system for generating RSA.

Berger *et al.* used broadband breathing to characterize cardiovascular rhythms [Berger *et al.* 1989]. The question which should be asked of these techniques is whether voluntary control of breathing affects RSA being measured. Recent studies by Patwardhan *et al.* showed that voluntary control of breathing does not affect cardiovascular rhythms [Patwardhan *et al.* 1995]. More recently, Cooke *et al.* studied the effects of controlled breathing protocols on cardiovascular rhythms and their results showed there is a small influence of voluntary control of breathing on human autonomic activity [Cooke *et al.* 1998]. Therefore, the random breathing protocol can be used to characterize and evaluate the origin of RSA. Hence, we suggest that in normal respiration for a healthy subject, RSA responds to a nervous stimulation which originates mainly from the medullary respiratory center and partly from the modulation of the baroreflex feedback system. Accordingly, we put forward the following model of the cardiovascular system which includes interaction among the three main variables, HRV, ILV and SBP which can be modeled as shown in Fig. 3-1. Respiration acts as an external stimulus centrally on efferent autonomic activity through the central control system and mechanically on the thoracic arteries and veins. Hence, the intact cardiovascular system has respiration as input and heart rate as output, which can be used to evaluate the cardiovascular system dynamics. The system is represented by the autonomically mediated coupling between respiration and heart rate and perturbing noise represented by the fluctuations in HR not contributed by ILV. The structure of the model takes into account all the possible relations among signals, HRV, ILV and SBP. The system therefore can be divided into to three subsystems: (1) direct central modulation of heart rate from respiration, (2) mechanical effects of respiration on blood pressure and (3) baroreflex feedback control system. There are other pathways which are not the subject of this study and which are not shown in the Fig. 3-1, eg, direct mechanical effects between SBP and HRV.

In conclusion, respiratory oscillations play a major role in the generation of RSA in healthy humans through the action of medullary respiratory neurons, which has been shown to both control respiration itself and via a coupling to autonomic centers, to modulate heart rate by varying parasympathetic and sympathetic inputs to the sinoatrial node. Although the baroreflex is involved in the genesis of RSA, it does not play an important role in modifying the RSA response in normal conditions but does maintain arterial blood pressure within a fairly narrow range through feedback control. By modulation of HRV, baroreflex can respond rapidly to the large changes in arterial blood pressure if the baroreflex control system has any external

simulation. In such a particular case, the baroreflex might be the major control system for generating RSA.

The system identification techniques required to evaluate our cardiovascular control modeling will be described in Chapter 7.

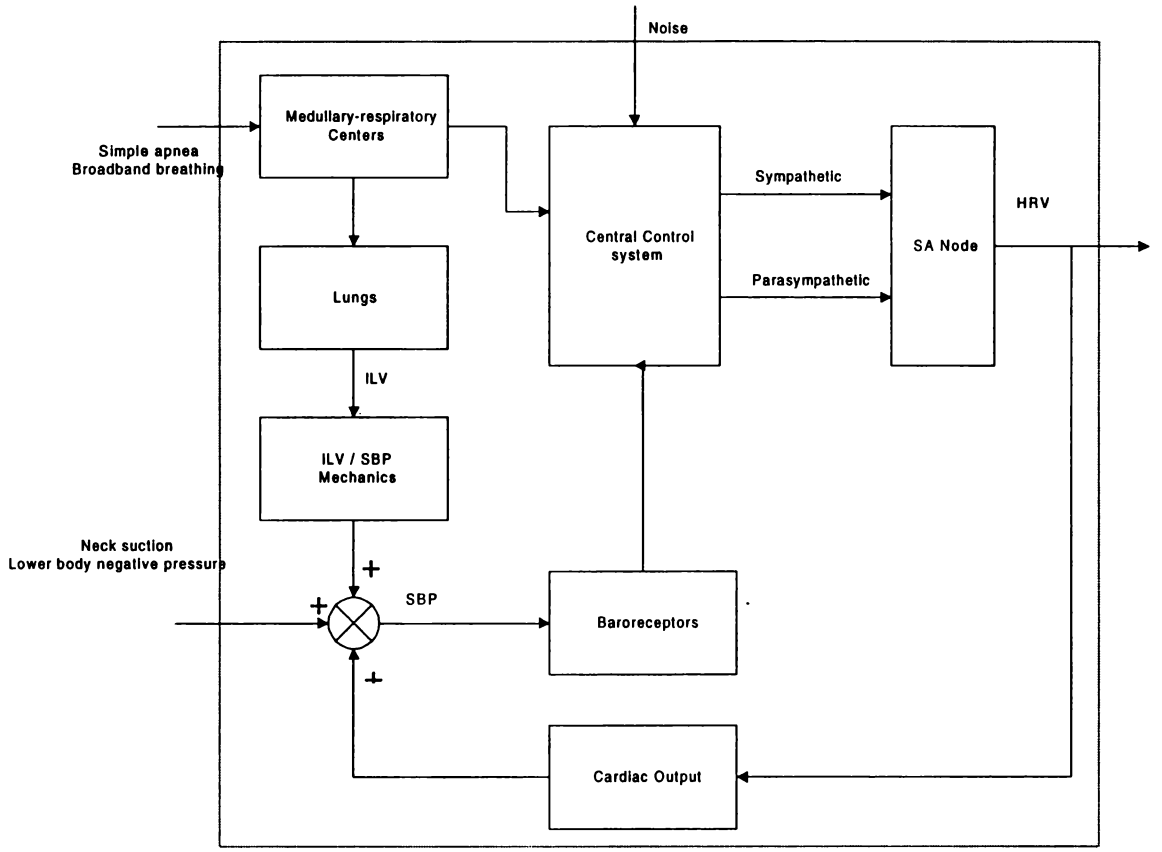

Figure 3- 1 The model of cardiovascular control system used to show heart rate response to autonomic change due to respiration through control of medullary respiratory neurons and modulation of baroreflex feedback system. Other pathways not shown, see text.

Chapter 4

The Low Order ARX Model

4.1 Introduction

Inferring models from observations and studying their properties is really what science is about. The models may be of more or less a formal character, but they all have the basic feature that they attempt to link observations together into some pattern. Ideally, one would model the system with the smallest number of parameters needed to describe the true dynamics of the system, (also known as parsimony). In order to achieve maximum utility, the model must describe the actual system dynamics over the entire range of operating conditions which might be encountered. This process of developing a system model can be performed in two ways: mathematical modeling and system identification. I am indebted for these and many of the following ideas to Lennart Ljung [1987, 1995] who provides much insight into the process of modeling.

The modeling of a system from fundamental laws of physics, such as conservation of mass and energy, or other prior knowledge, is known as mathematical modeling. The fundamental equation describing some simple system is an ordinary or partial differential equation. By using these equations, one can derive a model describing the system. However, since a mathematical model is based only on first principles there are no guarantees that it accurately describes the system dynamics to any degree of accuracy. The mathematical model may be inaccurate because some

dynamics may remain unmodeled or the model parameters are inaccurate. In other cases, the system may be too complex to describe with mathematical modeling techniques. Thus, there is the need to develop system models from input/output data alone (black-box modeling).

System identification deals with the problem of building mathematical models of dynamic systems based on observed data from the systems. The system is regarded as performing a purely mathematical transformation between the inputs and the outputs, and there need not be any direct relationship between the model and the underlying physical processes giving rise to the system properties. System identification can be performed using a number of different approaches. These approaches are divided into two types, parametric and nonparametric. Parametric approaches adopt a relatively specific model of the system; in some cases this may be based on *a priori* knowledge but in other cases the model may be purely mathematical and not based on the underlying physical structure of the system. On the other hand, nonparametric approaches make only very general assumptions regarding system structure (e.g., linearity and stationarity). Nonparametric approaches can reveal potentially unknown system properties and mechanisms, while parametric approaches (while drawing on *a priori* knowledge) have already decided upon structure and determine the best parameters for that model which fit the measured data.

Parametric models are defined by analytic expressions with relatively "few" parameters. For linear systems, parametric identification methods are usually discrete-time and typically involve formulating a regression problem relating the current output to the weighted linear combination of current and past input and/or output samples; the identification procedures determine the weighting coefficients which *best* (i.e., via least-squares or some other error criteria) relate the input signal to the output signal over the time interval of interest. The first step of system identification is to determine the size and type of model. The second step consists of estimating the parameters of the system model from the data. In practice, one must iterate between these two steps to arrive at an accurate low order model of the system.

The choice of the model structure plays the most important role in the success of the resulting model, and is generally parameterized, allowing the mapping it performs to be adapted to fit the data. In attempting to determine empirically the mathematical descriptions associated with linear systems, the autoregressive with exogenous input (ARX) model [Bosch *et al.*. 1994] is a highly flexible structure that can be used to

parameterize the dynamics of such systems. Applied in a system identification context, the ARX model has been used extensively to represent the dynamics of a wide range of physiological systems.
This chapter aims to give an understanding of the ARX model system identification methods especially with a low model order, its rationale, properties and use.

4.2 The ARX Model

The identification of a linear system from input/output data is often done by fitting the data to an ARX type model structure. To illustrate the basic issues associated with ARX modeling, consider a linear system the input of which is u, the output is y and e is a white noise signal. The corresponding ARX model denotes by the parametric linear difference equation format as follows:

$$y(t)+a_1y(t-1) +...+ a_{na}y(t-na) = b_1u(t-nk) +...+ b_{nb}u(t-nk-nb+1) + e(t) \quad (4\text{-}1)$$

which written in matrix form becomes:

$$A\,(q)\,y(t) = B(q)u(t-nk) + e\,(t) \quad (4\text{-}2)$$

Where A and B are polynomials in the delay operator q^{-1}.
Since white noise enters directly into the equation, the model is of the class of equation error models. The equation error is modeled, which is used to represent both modeling errors and measurement noise. In this equation, the $A(q)$ coefficients correspond to the autoregressive (AR) parameters, while the $B(q)$ coefficients are moving average (MA) parameters. The structure is thus entirely defined by the integers na, nb, nk. Na is equal to the number of poles and nb-1 is the number of zeros, which determine the number of previous input and output samples that appear in the model, while nk is the pure time-delay (the dead time) in the system [Ljung 1987,1995]. Hence, the basic input–output configuration in the ARX structure is depicted in Fig.4-1 below.

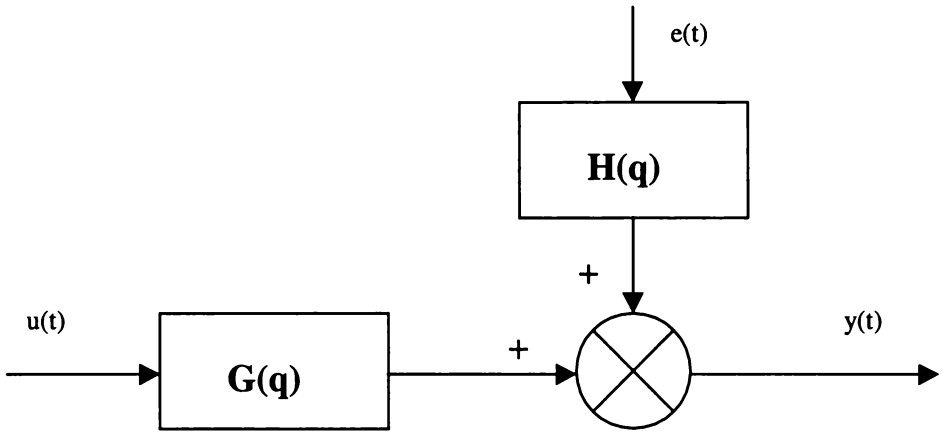

Figure 4- 1 Standard model

Therefore a time domain description of the system is given:

$$y(t) = G(q)u(t) + H(q)e(t) \qquad (4\text{-}3)$$

The function G(q) is called the transfer function of the system and H(q) is a transfer function characterizing the disturbance.

For the ARX model, we see that (4-1) corresponds to (4-3) with

$$G(q) = q^{-nk}\frac{B(q)}{A(q)} \qquad H(q) = \frac{1}{A(q)} \qquad (4\text{-}4)$$

Where B and A are polynomials in the delay operator q^{-1}

$$A(q) = 1 + a_1 q^{-1} + \ldots . + a_{na} q^{-na} \qquad (4\text{-}5)$$
$$B(q) = 1 + b_1 q^{-1} + \ldots . + a_{nb} q^{-nb+1}$$

Determination of an appropriate model order and dead time is one of the major concerns of ARX modeling [Perrott and Cohen 1996]. Hence, in attempting to represent the given system with the ARX model, three fundamental issues arise:

1. Estimation of model order na, nb.
2. Selection of dead time nk.
3. Estimation of the parameter values once the model order and dead time are determined.

4.3 Parameter Estimation

Irrespective of the model structure chosen, it will inevitably contain the parameters which need to be identified from empirical data. In this section, basics of parameter estimation methods based on solving a minimization problem are introduced. The complexity of this minimization is dependent on the chosen model structure. If the output of the model is a linear function which can be minimized by the weights, the loss function is simply a quadratic cost function. A model structure is chosen, and the parameters in the structure are obtained by minimizing the loss function. This leads on to the more important issue of the parameter identification solution method, Least Squares method, which is a standard linear optimization technique to minimize the loss function.

4.3.1 Prediction error approach

We are looking for a test by which the different models' ability to describe the observed data can be evaluated. We have stressed that the essence of the model is its prediction aspect, and we shall judge its performance in this respect. So we can calculate a future output, and compare this with actual output. If the error between measured and predicted output is small enough in some sense, the model can be considered good. The methods based on this principle are called Prediction Error Identification Approach or Prediction Error Identification Methods (PEMs), since the small prediction error when applied to the observed data, is used as a measure of model quality [Bosch. *et al.* 1994].
To formalize the concept, let the prediction error be given by

$$\varepsilon(t+1|t) = y(t+1) - \hat{y}(t+1|t)$$

where y(k) is the measured process output at instant t = k. Suppose that we have complete knowledge of the past at t = k (through measurement), and that we want to predict the process output at t = k +1. The predicted process output is then denoted by $\hat{y}$ (k +1|k), which is called the one-step ahead prediction of y. At time instant k+1 the value of y(k+1) is measured. By comparing the predicted process output $\hat{y}$ (k +1|k) with the measured process output y(k+1), we obtain the prediction error ε(k+1 | k).

A good model, we say, is one that is good at predicting, that is, one that produces small prediction errors when applied to the observed data. Note that there is considerable flexibility in selecting various predictor functions, and this gives a corresponding freedom in defining "good" models in terms of prediction performance resulting in prediction errors. This leads to the question of how we qualify what " small" should mean. The prediction error method is dealing with the measure of the size of ε. However, for the same model, the prediction error can be small at one instant, and large at another. Therefore, a much better measure would be to look at a sequence of prediction errors. To prevent positive and negative prediction errors from canceling each other out, a quadratic prediction error can be taken. Then an appropriate measure for model quality is the following loss function J_N

$$J_N = \frac{1}{N}\sum_{t=1}^{N}\varepsilon^2(t \mid t-1) \tag{4-6}$$

This loss function is referred to as the Mean Square Error (MSE), and is a biased estimate of the variance of the assumed additive noise. A model has good prediction capabilities if the MSE is small enough. The "best" model is thus the model that minimizes (4-6). The identification problem is formulated as a minimization problem.

For the given ARX model structure, the adjustable parameters are collected in vector **w**

$$w = [a_1, \ldots, a_{na}, b_1, \ldots, b_{nb}]^T$$

Based on the one-step ahead prediction of the process output, it can be proved [Bosch. *et al.* 1994] that the prediction error can be written as:

$$\varepsilon(t|t\text{-}1,w) = H^{-1}(q,w)[y(t) - G(q,w)u(t)] \tag{4-7}$$

From (4-2) and (4-7), the ARX prediction model becomes:

$$\hat{y}(t|w) = B(q)u(t) + [1 - A(q)]\, y(t) \tag{4-8}$$

Therefore, the ARX prediction model can be represented as a simple linear regression given by:

$$\hat{y}(t) = x^T(t)w$$

where the parameter vector and regressor are given by:

$$x(t) = [-y(t-1) -y(t-2)....y(t-na),u(t-nk),....,u(t-nb-nk+1)]^T$$

Many variants on this basic structure have been proposed. The reader is referred to [Ljung 1987] for a good survey. These models are attractive as they are simple, to some degree transparent, and the parameters **w** can be estimated by simple linear regression techniques. See section 4.3.2.

Given a data set and a model structure, the aim is to make inferences about the parameter vector **w** so that the model produces a good approximation to the true system. Then the optimal model within the selected model structure will be the model with the parameter vector $\hat{\mathbf{w}}_N$, that minimizes (4-6):

$$\hat{\mathbf{w}}_N = \arg\min_{w \in D_M} J_N(w) \qquad (4\text{-}10)$$

with

$$J_N(w) = \frac{1}{N}\sum_{k=1}^{N}\varepsilon^2(t \mid t-1, w)$$

where "arg min" is the operator that returns the argument that minimizes the loss function. The parameter-dependency in J_N and **w** has been made more explicit. The set $\mathbf{D_M}$ is the set of possible parameter vectors for a chosen model parameterization.

This way of estimating $\hat{\mathbf{w}}_N$ contains many well-known and much used procedures. We shall use the general term prediction-error identification methods (PEM) for the family of approaches that corresponds to (4-3). One such approach is the Least Squares (LS) method [Ljung 1987]

4.3.2 Least squares method

The parametric identification methods that have been considered belong to the family of prediction error methods, which are based on the minimization of the sum of the squared prediction errors. To solve the optimization problem for the linear model structure, ARX, the simple Least Squares method can be employed.

The linear regression model structure is very useful in describing a basic linear system. For the ARX model structure, with (4-8), the criterion (4-10) then becomes

$$J_N(w) = \frac{1}{N}\sum_{k=1}^{N}\left[y(k) - x^T w\right]^2 \tag{4-11}$$

In the optimal solution, the gradient of J_N(w) with respect to w is zero:

$$\frac{\partial}{\partial w} J_N(\hat{w}_N) = 0 \tag{4-12}$$

Then becomes:

$$\frac{\partial}{\partial w} J_N(w) = \frac{1}{N}\sum_{t=1}^{N} 2x(k)\left[y(k) - x^T(k)w\right] = 0 \tag{4-13}$$

Hence, the optimal solution $\hat{w}_N$ can be found by solving the following set of equations, also called the Normal Equations:

$$\left[\frac{1}{N}\sum_{t=1}^{N} x(t)x(t)^T\right] \hat{W}_N = \frac{1}{N}\sum_{k=1}^{N} x(t)y(t) \tag{4-14}$$

so the solution $\hat{W}_N$ is obtained via

$$\hat{W}_N = \left[\frac{1}{N}\sum_{t=1}^{N} x(t)x(t)^T\right]^{-1} \frac{1}{N}\sum_{k=1}^{N} x(t)y(t) \tag{4-15}$$

Provided the indicated inverse exists, it gives the Least Square Method.

4.4 Data Preprocessing

When the data is collected from the system identification experiment and the ARX model is selected, the parameter estimation can still be influenced by the choice of the parameterization, the prefilter and other possible data processing [Ljung 1987, Bosch *et al.* 1994]. In empirical modeling, the resulting model is clearly highly dependent on the quality and availability of the data. This means collected data are not likely to be in a condition for immediate use in system identification. To build models the data set should adequately represent the system being modeled. Apart

from some data processing, such as trend removal, decimation, and removal of spikes done by visual inspection of the data, the quality of the model estimate can be improved considerably by prefiltering the data. Since the dynamics of the system are restricted by the estimate to a limited range of frequencies, we should concentrate on the most interesting frequency region. Prefiltering is suggested to restrict the prediction error to frequency region of interest.

The filter needs to have a number of characteristics to successfully perform. First, the filter must be able to remove non-stationary trends from the time series. Second, the filter should produce a sharp cut-off of the nonstationary and low frequency variation without distorting the frequency components of the interesting region of the signal being studied.

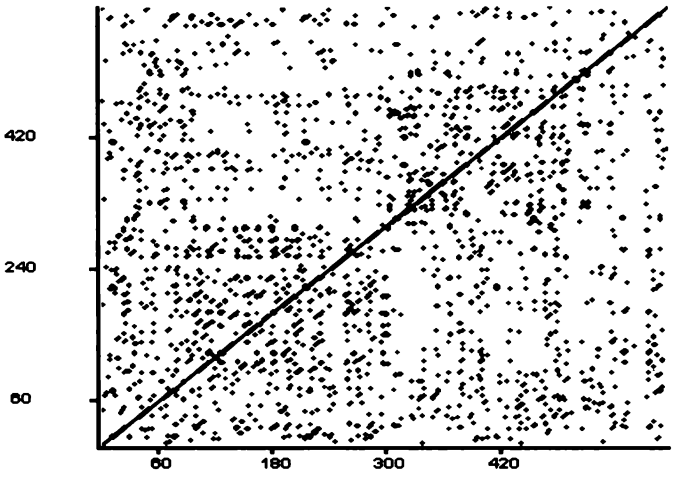

Figure 4- 2 Recurrence plots derived from heart rate variability signal. Computations were performed with following parameter settings: embedding dimension 3, radius 0.01 and the nearest neighbors 10. Both axes are samples numbers

4.4.1 Non-stationarity test of HRV

Recurrence plot (RP) is a relatively simple and straightforward graphical method suitable for both linear and nonlinear signals, which was first described by Eckmann *et al.* in 1987. The RP consists of a dot placed at each position in an embedded distance array (time versus lagged values), which is approximately recurrent, (see below). It is a useful tool for the qualitative assessment of time series which display some features of the distribution of the trajectories of a dynamic system reconstructed from a time series by the method of delays.

In order to obtain the recurrent plot from a (measured) scalar time series which is assumed to be generated by a dynamic system, one has to construct the appropriate series of state vectors $X(t_i)$ of delay coordinators in the n-dimensional phase space according to Takens [1981] theories as:

$$X^n(t_i) = [X(t_i), X(t_i + \tau), ..., X(t_i + (n-1)\ \tau)]^T \qquad (4\text{-}16)$$

Where $t_i = i\delta t$, i=1,....,n and δt is the sampling time. n is called the embedding dimension.

To compute an RP one has to search for the z nearest neighbors of each $X^n(t_i)$. The x-axis of the RP therefore corresponds to $X^n(t_i)$ and the y-axis to the nearest neighbors $X^n(t_{j1})$, ... $X^n(t_{jz})$. A black dot is displayed at coordinate $(X^n(t_i), X^n(t_{jn}))$ whenever the distance between vector $X^n(t_i)$ and vector $X^n(t_{jz})$ is smaller than some threshold radius r. Note that the t_i and t_j are in fact times. Hence, the RP provides natural but subtle time correlation information. For example, a recurrence plot for HRV time series of one health volunteer with embedding dimension 3, radius 0.01 and the nearest neighbors 10, the plot is shown in Fig. 4-2.

It is known that a local feature in the RP gives information on the largest Lyapunov exponent of the system [Middleton, G. V. 1995]. This feature is characterized by to line segments in the plot which are parallel to the main diagonal. The lengths of these line segments are inversely proportional to the largest Lyapunov exponent.

The distribution of the line segment's lengths gives information on the entropy of the time series. It is known that this distribution is exponential, and that the exponent is equal to the entropy.

A global feature in the plot gives information on the stationarity of the time series used. This feature is the density of points as a function of the distance from the main diagonal. When the density decreases as the distance from the diagonal increases (recurrence in phase space gets less frequent as the time difference between two segments corresponding to two reconstruction vectors) one can conclude that the time series is nonstationary on the time scale indicated by the time series.

4.4.2 Linear detrending

Physiological response data often exhibit slow trends such as the heart rate pattern. These trends are usually unrelated to the low frequency components in the stimulus data and therefore must be assumed to be caused by other mechanisms. A common method of detrending is to remove the linear influence. This is done by fitting a linear regression to the data. This method removes the linear trend and transforms the data set into a series with a mean of approximately zero. Linear detrending has little impact on the transfer function of the system and spectrum of data. A spectrum of data with a relatively large proportion of the variance close to 0 Hz is

characteristic of a time series with non-stationary components. If the non-stationarity is caused by a linear trend, linear detrending will remove the non-stationary influence and provide an interpretable spectrum. The removal of trends prior to the computation of system identification is important. If not done properly, it can result in large errors in estimation of a prediction model, especially in the low frequency region.

Unfortunately, the non-stationary influences in a physiological signal can not be removed completely by linear detrending only. In addition, filtering procedures are required for removing non-stationary components.

4.4.3 Prefiltering

The ability to identify a system or to validate a model is determined to a large part by the properties of the input signal. For linear systems, the requirements for using nonparametric methods to identify a system are well known: the input signal must be persistently exciting and must excite all modes of the system. In the frequency domain, this means that the input signal must have power at all frequencies where the system has a significant response. Conversely, the identification will only be valid for the range of frequencies which are identified. By definition, a linear system will have an output bandwidth which is the same or smaller than the input bandwidth (which is defined by the experimentally-determined sampling rate and record length). Parametric methods can estimate system dynamics using less rich (i.e., more restricted range of input amplitudes and frequencies) inputs, provided the model structure is known accurately [Ljung 1987, Bosch *et al.* 1994]. The power component in the VLF band occurring in the spectra of HRV data is generally associated to humoral and temperature regulatory mechanisms [Muzi *et al.* 1993]. Our model intentionally does not incorporate either of these regulatory mechanisms. On the other hand, any system nonstationarities will be reflected as nonstationarities in the system response signal, output signal. In addition, physiological response data often exhibit slow trends which may be caused by other mechanisms. We therefore apply the prefiltering to the output signal to remove these components and cut away the noise or unwanted parts of the output signal. For system identification, the system will have a very weak response in the frequency range when prefiltering is used, since the output signal in this frequency range is much smaller in comparison with the unfiltered input signal.

Given a description (4-3) and having observed the input-output data u, y and formed filtered versions of the output $y_p(t)$, the system can be described as:

$$y_p(t) = G_p(q)u(t) + H_p(q)e(t)$$

$$y_p(t) = L(t) * y(t) \tag{4-17}$$

Consider the description (4.3), the transfer function of filtered system can be given by

$$G_p(t) = L(t) * G(t) \qquad H_p(t) = L(t) * H(t) \tag{4-18}$$

$$y(t) = \frac{G_p(q)}{L_p(q)}u(t) + \frac{H_p(q)}{L_p(q)}e(t) \tag{4-19}$$

Obviously, as result of filtering output data, the transfer function from the system identification is equivalent to a filtered transfer function which is identified from pure input and output. A prefiltering applied to the process output could thus be designed so that the frequency region of interest is emphasized and, more importantly, some nonlinear and nonstationary signals from the system in the low frequency range could be cut out.

4.5 Model Order Determination

We have already seen that an ARX model is easy to estimate because it has an analytical solution. Once a specific parametrization is chosen, we have to select the model order.

The model order should not be selected too low, since an underparameterized model will lack the degrees of freedom necessary to represent the dynamics of the corresponding physical system. It should not be selected too high either, since the higher the model order, the more parameters need to be estimated, and the higher the variance of the estimates is. Moreover, it is difficult to interpret ARX parameters physically if the model is overparameterized. Ideally, for a system we would like a low order model that accurately describes the system dynamics. However, there is often a tradeoff between the accuracy of the model and the simplicity of the model structure. Consequently, we have to look for a compromise: the model must be

accurate enough to reconstruct essential features of the system. On the other hand, it must be simple enough to be useful for conceptualization.

How shall we obtain a good fit to data with few parameters?

A model's ability to predict a given system is described by the bias/variance decomposition, but unfortunately, the resulting error contributions cannot be measured directly. Therefore, model order selection criteria have been derived which are based on limited observed data to match these competing error sources. For system identification used for process analysis and for simulation, it is usually a better idea to visually inspect the fit changing with the number of estimated parameters to get a subjective opinion on whether the improved fit is significant and worthwhile [Ljung 1995]. Another technique, False Nearest Neighbors (FNN) method appears to be a simple, efficient procedure for determining the better ARX model. FNN was developed recently by Rhodes and Morari [1997,1998] and it is an efficient method to determine mathematical relationships between inputs and outputs and is quite helpful as a tool for assisting in system identification. Since the FNN method does not assume that the relationship between the input and output is either linear or nonlinear, it can identify a system that is nonlinear.

4.5.1 Visual inspection of the loss function

A sound way to approach the model order problem is to select the structure that has the smallest loss function for the validation set. Theoretically, for $N \to \infty$, the loss function should tend to a minimum value for increasing model order. So one approach to model order determination is to fit models with an increasing number of parameters to the data and determine the loss function. When the loss function no longer decreases a significant amount for an increased number of parameters, stop fitting parameters. Increasing the model order beyond the true order of the process will not add to the quality of the model. Hence, we would expect that the minimum loss function does not significantly decrease for order higher than a certain value.

However, the loss function will slowly decrease with increasing the model order. The value of loss function decreases since the model picks up more of the relevant features of the data. Even after a model structure has been reached that allows a correct description of the system, the loss function continues to decrease. Because N, the number of data, is finite, the specific noise realization present in the data plays a role. If we select a very high order, it is possible to let the loss function go to zero by the specific noise contribution in the data set. Therefore, for a different data set, with

a different noise realization, the model will not be adequate to model the process dynamics. There is thus a clear trade-off between the loss function and model order and we will be looking for the knee in the curve of loss function versus model order. The effect of the noise realization can be avoided by calculating the value of loss function with the fresh data set other then the ones from which the model is estimated. Certainly, it is good practice to select a model order based on visual inspection to get a subjective opinion on whether the improved fit is significant and worthwhile.

The loss function versus the number of parameters can be plotted. A Matlab routine from the System Identification Toolbox was used to determine the number of parameters used based on visual inspection of the curve. The corner point was looked for in the curve in order to select the structure with the better fit for lower model order [Ljung 1995].

4.5.2 False nearest neighbors (FNN) algorithm

The method of false nearest neighbors (FNN) was proposed by Rhodes and Morari [1997,1998] as a tool for analyzing and determining the proper regressive vector for input/output system identification directly from the time series data. While the algorithm does not determine a specific model form, it does an excellent job of determining what information will be needed by a specific model to represent the dynamics and the smallest regression vector dimension which allows accurate prediction of the output.

For input/output systems, the mathematical form:

$$y(t) = F[y(t-\tau), y(t-2\tau),....., y(t-l\tau), u(t-\tau),....., u(t-m\tau),] \qquad (4\text{-}20)$$

should be found where τ is the sampling time of the system. From this equation, we define two distinct spaces: the prediction space y(t) and the time delay space ($y(t-\tau)$, $y(t-2\tau)$,....., $y(t-l\tau)$, $u(t-\tau)$,....., $u(t-m\tau)$), The knowledge that this relationship between the state-space description and the time delay coordinates exists is not helpful for modeling by itself. The dimension of the state space is unknown directly from input/output data. Therefore we would like to have some tool for equation 4-20 to determine the smallest possible number of delay terms needed to accurately recreate the dynamics directly.

4.5.2.1 False nearest neighbors

FNN algorithms for the input/output systems presented here are an extension of an algorithm developed specifically for autonomous system [Kennel *et al.* 1992]. The concept behind the FNN algorithm is geometric in nature. If the dimension of the time delay space is too small to represent the dynamics of the system, points which are close in the time delay space and far apart in the prediction space can be thought of as false neighbors. However if the dimension of the time delay space is large enough, the points which are close in the time delay space will always remain relatively close in the prediction space.

First embed the time series and form the set of regressors and the related output y(t) from time series data:

$$z_l(k) = [y(k-\tau), \cdots, y(k-l\tau)] \tag{4-21}$$

Choose a point at random on the trajectory, and for each point determine its neighbors. Neighbors, in other words, are points k that are separated in time from the reference point j by some increment τ, but are closer in the embedding space in minimized distance:

$$d = \| z_l(k) - z_l(j) \|_2 \tag{4-22}$$

$z_l(j)$ is known as the nearest neighbor to $z_l(k)$. It should be noted that times k and j themselves are not necessarily close to one another. In fact, if k and j are always close to one another the sampling time may be too small and there may be problem in accurately estimating the embedding dimension.

Determine if the following expression is true or false

$$\frac{|y(k)-y(j)|}{\|z_l(k)-z_l(j)\|_2} \leq R \tag{4-23}$$

where R is a some previously chosen threshold value. If expression 4-23 is true, then the neighbors are recorded as true neighbors. If the expression is false, the neighbors are false neighbors. The number of false neighbors is expected to decrease until a large enough embedding space is reached. At this point the number should be zero, or at least very small. Increasing the embedding dimension further does not produce any further change in the number of neighbors.

4.5.2.2 System dynamics and FNN

For determining the proper embedding dimension, the only change to the original FNN algorithm involves the regression vector itself. For input/output dynamics, the regression vector must contain delayed versions of both the input and the output.

$$\psi_{l,m}(t) = [y(t-\tau),.....y(t-l\tau),u(k-\tau,....u(k-m\tau)]$$

The percentage of false nearest neighbors must be determined for different numbers of delays in both the input and output in order to get the proper embedding dimension. The proposed system dynamics FNN algorithm is detailed below.

With minimized distance $d = [\psi_l(k) - \psi_l(j)]^{1/2}$ find the nearest neighbor $\psi_{l,m}(j)$ for a given regressor $\psi_{l,m}(k)$.

2. If $\frac{|y(k)-y(j)|}{d} \leq R$ is false, the nearest neighbors are false.

3. Continue the algorithm for all times k in the data set. Calculate the percentage of points in the data set which have false nearest neighbors.

4. Continue the algorithm for increasing l and m until the percentage of false nearest neighbors drop to zero or some acceptably small number.

In the above FNN algorithm, the threshold R used in the ratio test is one adjustable parameter. It is quite important to choose the proper threshold since choosing a single threshold which will work well for all data sets, is an impossible task. If R is too small, then the percentage of false nearest neighbors may not drop to zero in the proper embedding dimension. On the other hand, if R is too large it is possible that the FNN algorithm will predict that future outputs are predictable with too small embedding dimension. It has been observed that false nearest neighbors tend to have future outputs which are very different when the embedding dimension is too small. Therefore, the threshold can be safely made fairly large and the algorithm will give small embedding dimensions for accurate prediction. Rhodes and Morari suggested a good choice of the threshold is in the range of 10-15. More detail and the analysis of passing or failing the threshold test is given in [Rhodes and Morari 1997,1998].

4.5.3 Theoretical justification for a low order ARX model

Historically, differential equations have originated in chemistry, physics and engineering. More recently, they have also arisen in models in medicine, biology,

anthropology, and the like. The differential equation is an equation involving an unknown function and one or more of its derivatives. The equation is an ordinary differential equation (ODE) if the unknown function depends on only one independent variable. The order of a differential equation is the order of the highest derivative appearing in the equation.

In the system, its dynamics are captured by a general differential equation of the *m*th order:

$$\frac{d^m y(t)}{dt^m} + A_1 \frac{d^{m-1} y(t)}{dt^{m-1}} + A_2 \frac{d^{m-2} y(t)}{dt^{m-2}} + \cdots + A_m y(t) = u(t) \tag{4-24}$$

y(t) : output *u(t)*: input

It is often either impossible, or extremely difficult, to obtain an exact analytical solution. However, it is sometimes possible to obtain a numerical solution that is close to the true solution in some sense.

4.5.3.1 Numerical differentiation

As one of several techniques, ordinary differential equations can be reduced to the study of a set of m coupled linear combinations of *y(t-jh), j = 1,2,...,m.* The derivatives have the following numerical form:

$$\frac{dy}{dt} \approx k_1(h)\big(y(t) - y(t-h)\big)$$

$$\frac{d^2 y}{dt^2} \approx k_2(h)\big(y(t) - 2y(t-h) + y(t-2h)\big)$$

$$\frac{d^3 y}{dt^3} \approx k_3(h)\big(y(t) - 3(y(t-h) + 3y(t-2h) - y(t-3h)\big)$$

where h is the sample interval.

Therefore

$$\frac{d^j y}{dt^j} \approx k_j(h) \sum_{j=1}^{m} \bar{a}_j y(t - jh)$$

Substituting in Eq. 4-24 and collecting terms:

$$\sum_{j=0}^{m} a_j y(t-jh) = u(t)$$

i.e. the numerical solution (approximation) is the solution of ARX (m,1,0) model.

4.5.3.2 Numerical integration Runge-Kutta method

Alternatively, Eq. 4-24 can be solved using Runge-Kutta method [William *et al.* 1992]. Runge-Kutta methods are designed to approximate Taylor series methods. The basic idea is to use a linear combination of values of *u(t)* to approximate *y(t)*. This linear combination is matched up as closely as possibly with a Taylor series for *y(t)* to obtain methods of the highest possible order.
For first order, difference equation:

$$y(t) = y(t-1) + hu(t-1) + O(h^2)$$

For the fourth-order, Runge-Kutta formula:

$$y(t) = y(t-1) + \frac{h}{6}u(t-h) + \frac{2h}{3}u(t-\frac{h}{2}) + \frac{h}{6}u(t) + O(h^4)$$

i.e. numerical solution (approximation) is the solution of ARX (1,3,0) and therefore m^{th} order difference equation is solution of ARX (1,m,0).

4.5.3.2 Bilinear transform

In addition, a model in the "s" domain can be transformed to the "z" domain using the bilinear transformation [Franklin *et al.* 1988].

$$s \rightarrow \frac{2}{h}\left(\frac{1-z^{-1}}{1+z^{-1}}\right)$$

Hence, the system in eq. 4-24:

$$G(s) = k\frac{1}{s^m + A_1 s^{m-1} + A_2 s^{m-2} + A_m}$$

and

$$G(s) = \bar{K}\frac{(1+z^{-1})^m}{(1+z^{-1})^m + \bar{A}_1(1+z^{-1})^{m-1}(1-z^{-1}) + \bar{A}_2(1+z^{-1})^{m-2}(1-z^{-1}) + \ldots + \bar{A}_m(1-z^{-1})^m}$$

$$= K\frac{1+b_1z^{-1}+b_2z^{-2}+\ldots+b_mz^{-m}}{1+a_1z^{-1}+a_2z^{-2}+\ldots+a_mz^{-m}}$$

Compared with Eq. 4-1, this shows that the solution of m^{th} order ODE is approximated by an ARX model with m inputs and m outputs, i.e. ARX (m, m, 0). ARX (m, m, 0) therefore can be an alternative representation of m^{th} order ODE.

4.5.3.4 Conclusion

Taken together, we have choice of three numerical methods
ARX (m, 1,0), ARX (1, m, 0), ARX(m, m, 0)
where m is order of ODE in Eq. 4-24.
The coefficients of ARX model depend on "h" i.e. a sampling interval. For good modeling, h must be small, i.e. the sampling rate must be high enough. Furthermore the higher "m", the more accurate the approximation $O(h^m)$, because more terms are included in the Taylor series. In our application of ARX model, we have used both FNN and visual inspection of loss function methods to determine model order.

4.6 Estimation of the Dead Time

The selection of the dead time, nk, in the ARX model structure is a very important step in obtaining good identification results. It is possible to get an idea about the dead time in the system by the impulse response. If there is dead time in a process, the process output does not react instantly to the applied input signal.
A dead time d means that first d parameters of the impulse response are zero. In black-box identification, the dead time can be incorporated in two ways. Either the first d coefficients of the B-polynomial are set to zero, or the input sequence is shifted over d samples. Then d must be estimated accurately.
Incorrect dead time is also visible in the parametric models. Underestimated delays (nk too small) show up as small values of leading b_k estimates, compared to their standard deviations. Overestimated dead time (nk too large) is usually visible as a significant correlation between the residuals and the input at the lags corresponding to the missing b_k terms.

Overestimating the dead time will result in too many parameters of the B-polynomial being set to zero. In this case, the identification method must compensate this incorrectness with the other parameters by biased estimates. Whereas, underestimating the dead time will give too few parameters of the B-polynomial being set to zero. Dynamically, this often results in a nonminimum-phase behavior of the model, although the process is minimum phase.

The time between application of the input and reaction of the system output is called dead time. This suggests a lack of correlation between the input and the output for the first nk-1 lags.

Accordingly, both correlation and ARX model stimulated methods can be used to estimate the dead time, which will be discussed in this section.

4.6.1 Correlation analysis method

Assuming the signals are related by a linear system, the relation can be written:

$$y(t) = \frac{1}{N}\sum_{t=1}^{N} g_0(\tau)u(t-\tau) + v(t) \tag{4.25}$$

where $u(t)$; t =1, 2,..N is an input signal

$y(t)$: t = 1,2,...N is an output signal.

Suppose that the input u(t) is white noise and is uncorrelated with the disturbance v

Then, the cross covariance function between the input and the output is

$$R_{yu}(\tau) = \frac{1}{N}\sum_{t=1}^{N} g_0(\tau)R_u(\tau - t) \tag{4.26}$$

where $R_u(\tau - t)$ is the auto covariance function of input u. If u is white noise with variance σ_u^2, this become

$$R_{yu}(\tau) = g_0(\tau)\sigma_u^2$$

Consequently, if the dead time is d, $R_{yu}(\tau)$ is zero for $\tau <= d-1$. So the dead time can be estimated by applying a white noise signal to the input, and determining the cross-covariance function of y and u. If the input is not white noise in practice, a prewhitening filter L(q) are used for it, so

$$u_F(t) = L(q)u(t) \tag{4.27}$$

is approximately white. By filtering the output sequence through the same filter and computing Eq. 4-26 based on the filtered data, a natural estimate of the dead time is obtained as the cross-covariance function will be zero for the first d-1 lags if the process has a dead time of d samples.

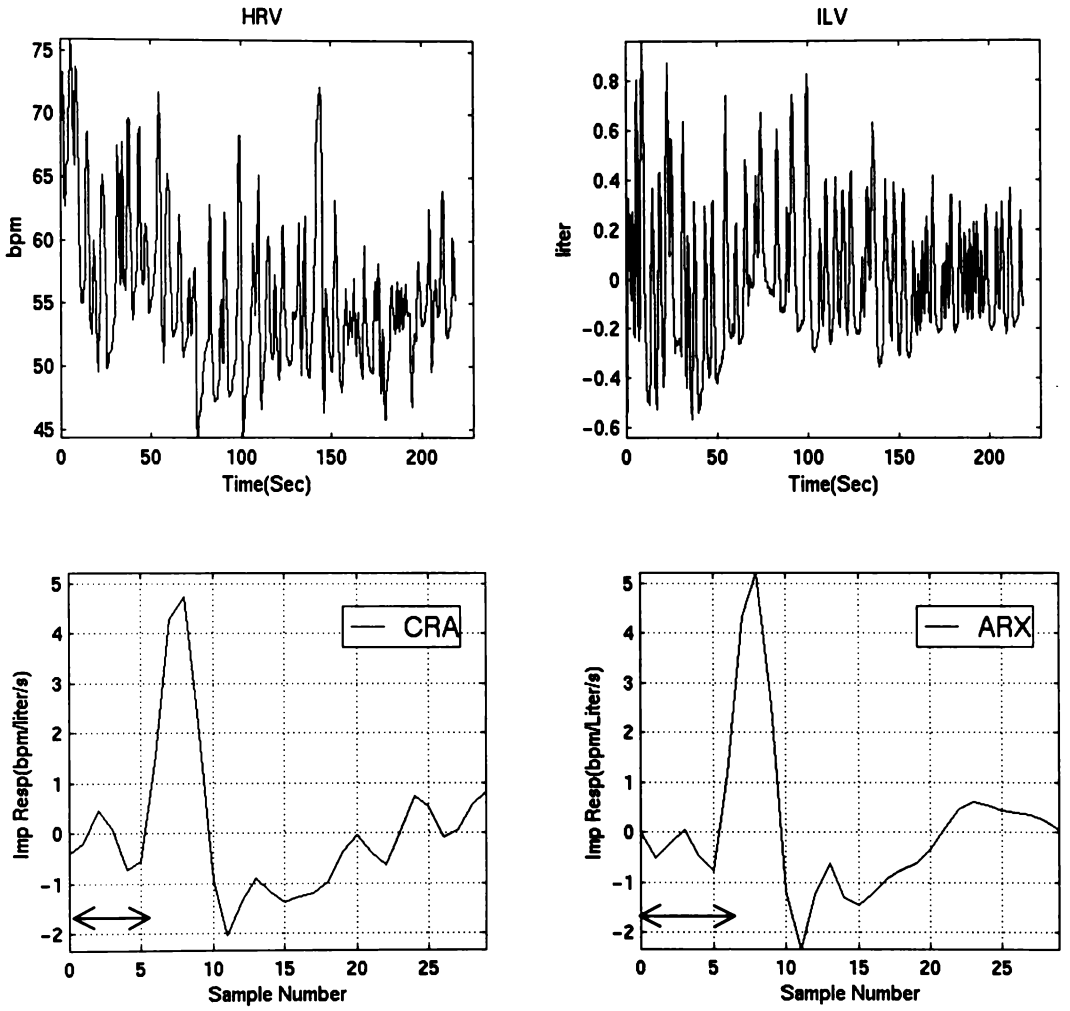

Figure 4- 3 HRV and ILV time series (upper) during random breathing in a healthy subject and the dead time estimation by the correlation and The ARX model method (lower). Sample frequency =2.56 Hz.

4.6.2 ARX model stimulated method

We use order nn = [4 10 1] to setup an ARX model with high moving average order to inspect the largest reaction of the output to an input in the 10 point input set. We can get the output of the model when the input is an impulse. Because the input order is set as 10, hence the output reflects the impulse response of the process of

input from ILV (t+1) to ILV (t+10). Uncorrelated or less correlated points will be checked easily if the system has a delay.

4.6.3 An example: estimation of dead time

Both the correlation analysis and the ARX model stimulation method are illustrated by the following practical example.
In cases with random breathing for one healthy volunteer, the ARX model was used to study transfer characteristics from fluctuations of instantaneous lung volume to heart rate variability. To build up the ARX model, the dead time was estimated by both the correlation analysis method and the ARX method. In a close agreement, both methods suggested the dead time to be 6 samples, 2.34s, which can be seen in Fig. 4-3. The upper plots show HRV and ILV time series signal. The lower plots show the dead time estimated by both methods.

4.7 Model Validation

The parameter estimation procedure picks out the "best" model within the chosen model structure. The crucial question then is whether it makes sense or not. Therefore we need a means to evaluate the correctness, the validity, of the model. The process of establishing the adequacy of a given mathematical model includes several aspects:
Does the model agree sufficiently well with the observed data?
Is the model good enough for the required purpose?
Does the model describe the " true system"?

4.7.1 Residual analysis

One way to evaluate a model once the best model coefficients have been determined is to apply it to newly produced data and look at the residuals. If the model parameters have been estimated correctly then we expect the residuals to be "random" and "close to zero". Therefore, the residuals should have three properties: the residual is white noise, the residual is independent of past input and has small variance. Hence residual analysis comes down to investigating if both the auto

correlation of a residual and the cross correlation function between a residual and input go significantly outside the 95% confidence intervals.

The residuals are those parts of the data that are not explained by the model. For a nonrecursive, Prediction Error Method, the residual equals the prediction error ε(t, w):

$$\varepsilon(t,w) = H^{-1}(q,w)[y(t) - G(q,w)u(t)]$$

So residuals ε (t)= ε(t, w) will be (near) white if the model is in good agreement with a true system, where w is the real parameter value.

Hence, the residual analysis now comes down to an examination of the whiteness of the residual if it is sufficiently uncorrelated with the input and within 95% confidence intervals.

4.7.1.1 Whiteness test of the residuals

The residuals (prediction error) $\varepsilon(t)$ is white noise and its autocovariance function has a specific form. The typical test for whiteness of residuals is to estimate the autocovariance estimate:

$$R_\varepsilon(\tau) = \frac{1}{N}\sum_{t=1}^{N-\tau}\varepsilon(t)\varepsilon(t+\tau)$$

Where $\varepsilon(t) = \varepsilon(k, w)$, if $\varepsilon(t)$ indeed is a white-noise sequence, then $R_\varepsilon(\tau)$ would be asymptotically χ^2(M) distributed:

$$\sqrt{N}\,\frac{R_\varepsilon(\tau)}{R_0(0)} \in As\mathcal{N}(0,1)$$

where As$\mathcal{N}$ (0,1) means that the given quantity asymptotically converges in distribution to the normal distribution, with mean 0 and variance 1. Independence between the residuals can thus be tested by checking if $\sqrt{N}R_\varepsilon(\tau)/R_\varepsilon(0)$ χ^2(M) in the certain confidence intervals. For more detail, refer pages 428-429 in [Ljung 1987].

To use this test for model validation, we compute the residuals, calculate the normalized autocovariance function, and plot them together with confidence levels (see Fig. 4-4A). If the autocovariance function goes significantly outside these confidence intervals, do not accept the corresponding model as a good description of the system.

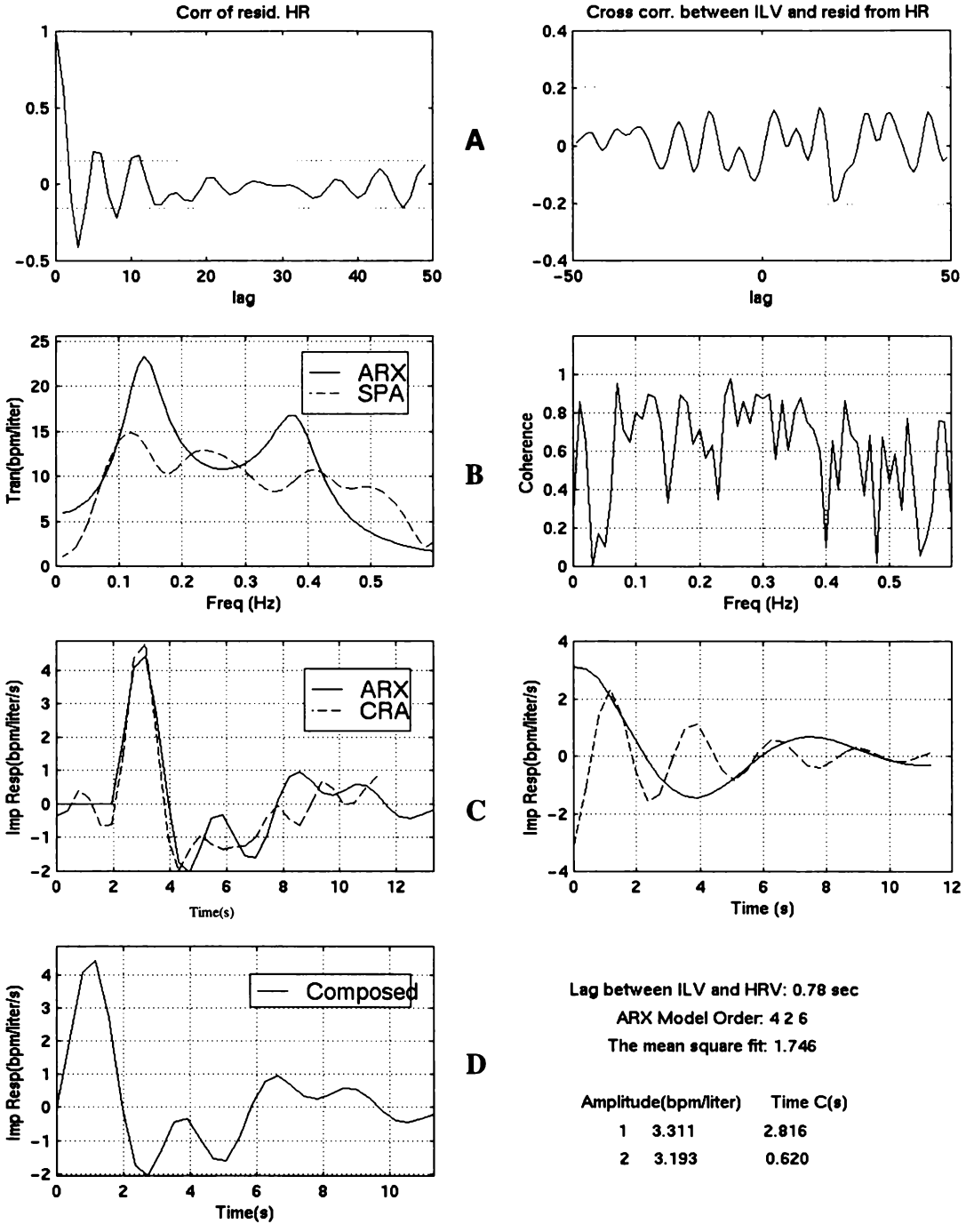

Figure 4- 4 The ARX model during random breathing, residual analysis (A), transfer function characteristics (B), impulse response and its low and high frequency components (C). The impulse response synthesized from high and low frequency components determined by the model parameters. (D). (All data from the subject presented in Fig. 8-1).

4.7.1.2 Independence between residuals and input

Independence between the residuals and the input implies that all parts of the output due to the input have been explained by the process model • . Often it is more

important that the dynamic part • describes G well than that the entire model be correct. This is obviously true when a prediction error method has been used. Therefore, testing the independence of input and residuals provides a basis for the decision whether or not to accept the model •

Independence of input u and residuals ε is usually tested using the cross-covariance function:

$$R_{\varepsilon u}(\tau) = \frac{1}{N}\sum_{k=1}^{N} u(t)\varepsilon(t-\tau)$$

Now if u and ε are independent, we have that

$$\sqrt{N}R_{\varepsilon}(\tau) \in As\mathcal{N}(0,1)$$

and

$$P = \sum_{k=-\infty}^{\infty} R_{\varepsilon}(k)R_{u}(k)$$

If N_a denotes the a level of $\mathcal{N}(0,1)$ distribution, we could check if

$$\left|R_{\varepsilon u}(t)\right| \leq \sqrt{\frac{P}{N}}\, N_a$$

To evaluate a model, the cross-covariance function of input and residuals is plotted, together with the confidence intervals. In this way it can easily be seen, in Fig. 4-4A, whether or not the model is invalid (Ljung 1987).

4.7.2 Cross validation

A more straightforward method of validation is to compare the real and simulated output to check whether a model is capable of reproducing the observed output when driven by the actual input. If they differ too much, we conclude that the model is invalid.

Obviously, it is a much more rigorous and revealing test to perform this simulation, as well as the residual test, on a fresh data set [y u] that was not used for the model estimation. Often, the observed data set is spilt into two disjoint sets, one for identifying the model and one for the model validation. In addition, the separate

validation data set can guide model selection to fit its own identification and ideally, a new independent validation set is required for each test.

As an additional validation of the ARX model, it is informative to compare the impulse response of the ARX model with the one that is estimated using correlation analysis. If there is a good agreement between the two, it can be concluded with some confidence that some essentially correct features have been picked up by the model, since the nonparametric identification does not impose any assumption regarding system structure.

4.8 Decomposed Impulse Response

Good and simple insight into a model's dynamic properties is obtained by looking at its impulse response. The low order ARX model employed in this study not only provides a useful and quantitative means for evaluating the transfer characteristics from fluctuations of ILV to HRV, but also makes it possible for the impulse response to be analytically decomposed to components from the model parameters.

In Eq. 4-4 and Eq. 4-5, if the delay from input to output nk =0, the transfer function corresponding to the ARX model has the polynomial representation:

$$G(q) = \frac{B(q)}{A(q)} = \frac{b_1 + b_2 q^{-1} + b_3 q^{-2} + \cdots\cdots + b_{nb} q^{-nb+1}}{1 + a_1 q^{-1} + a_2 q^{-2} + \cdots\cdots + a_{na} q^{-na}} \tag{4-28}$$

Replace the forward shift operator q with z-transform in (4-28), then

$$G(z) = \frac{r(1)}{1 - p(1)z^{-1}} + \frac{r(2)}{1 - p(2)z^{-1}} + \cdots\cdots + \frac{r(na)}{1 - p(na)z^{-1}} \tag{4-29}$$

Where the transfer function is expressed in corresponding partial fraction expansion or residue representation (nb < na).

Therefore, from the ARX parameters, A and B, we use partial fraction techniques to find column vector r which contains the residues and column vector p which contains the pole location [Krauss *et al.* 1994].

Thus *g(m)* impulse response:

$$g(m) = r_1 e^{-l_1 m} + r_2 e^{-l_2 m} + \cdots\cdots + r_n e^{-l_n m}$$

where

$$p_n = e^{-l_n} \qquad l_n = \ln\left(\frac{1}{p_n}\right)$$

Thus each residue gives a damped exponential, which may in certain cases be oscillatory.

Amplitude $AMP_n = r_n$

Time constant: $TC_n = T_s / \ln\left(\frac{1}{\mathrm{Re}\{p_n\}}\right) \qquad m = \frac{t}{T_s}$

M file, [A, B] = th2arx (th) in system identification toolbox [Liung 1995] and [r, p, k]= residuez (B, A) in signal processing toolbox [Krauss *et al.* 1994] are used for above calculation.

Overall, we can use the ARX parameters to get the impulse response and decompose the components of an impulse response.

Chapter 5

Multivariate Time Series Processes

Thus far in the last two chapters, we have been concerned with linear system identification using the ARX modelling, which can provide a comprehensive view of characterising fluctuations in HRV, ILV and SBP signals. However, for healthy adults, there are non-linear couplings between these signals and HRV below 0.05 Hz has a substantial component attributable to non-linear coupling from ILV and SBP [Chon *et al.* 1996]. We thereby need to test data for non-linear effects before we start to build up an ARX model. That is, is it likely that data can not be explained by a linear ARX model? We now turn our attention to the situation where we have observations on a multivariate time series and more interested in the relationship that describe how the stimulus signals are transformed by the system into response signals and in find the properties of the system before practising parameter system identification.

These stimulus-response relationships can be expressed either in the time domain or the frequency domain. There are two basic characterisation functions that summarise cross correlation structures between signals: the cross-correlation function in the time domain, cross-spectrum in the frequency domain, both with certain distinct features that complement each other. Recently, a new method has been proposed for characterising the correlation properties of a multivariate time series in a time-frequency plant based upon time-frequency analysis, called cross time-frequency distributions. The cross time-frequency analysis can be employed to supplement traditional time/frequency domain characterisation techniques.

5.1 Cross Correlation Analysis

Suppose we have N observation on two variables, y(t) and u(t) , at unit time intervals over the same period. The observations may be regarded as a finite realisation of the discrete-time stochastic process, and therefore y(t) and u(t) are discrete-time stochastic signals.

$$C_{uy}(\tau) = E\{u(t)-m_u)(y^*(t-\tau)-m_y)\} \tag{5-1}$$

In order to describe a bivariate process it is useful to know the moments up to the second order. For a univariate process, the moments up to the second order are the mean and the autocovariance function. For a bivariate process, the moments up to second order consist of the mean and autocovariance function for each of the two signals plus a new function, called the cross-covariance function, which is given by where m_u and m_y are the mean values of the two sequences.

Obviously, this is a measure of how "correlated" are values of y(t), τ sec before the present values of u(t). However, the size of cross-coefficients depends on the units in which y and u are measured. Thus for interpretation, it is useful to standardise the cross-covariance function to produce a related quantity, which is the cross-correlation given by

$$R_{uy}(\tau) = E\{u(t)y^*(t-\tau)\} \tag{5-2}$$

There exists a relation between the cross-covariance function and the cross-correlation function:

If one of the signals, y(t) or u(t) has a zero mean, the cross-covariance and the cross-correlation function are equal.

The cross-correlation function exhibits the following properties:

$$R_{uy}(\tau) = R_{uy}(-\tau)$$

$$|R_{uy}(\tau)|^2 <= R_{uu}(0)\, R_{yy}(0)$$

$$|R_{uy}(\tau)| <= [R_{uu}(0)\, R_{yy}(0)]^{1/2}$$

The cross-correlation can be used to find system dynamic characteristics, that is, an estimate of the impulse response of a system can be obtained by correlation analysis. The basic idea is to suppress the noise term by correlation of the data with appropriate signals [Bosch *et al.* 1994].

Let us assume the following linear relation between signals y(t) and u(t)

$$y(t) = g_0(\ell)u(k-\ell) + v(t) \qquad (5\text{-}3)$$

where u(t); t =1, 2,..N is an input signal and y(t): t = 1,2,...N is an output signal. Suppose that the input u(t) is white noise and is uncorrelated with the disturbance v Then, the cross covariance function between the input and the output is

$$R_{yu}(\tau) = \frac{1}{N}\sum_{k=1}^{N} g_0(\ell)R_u(\tau - \ell) \qquad (5\text{-}4)$$

5.2 Cross Spectral Analysis

The cross-correlation function is the natural tool for examining the relationship between two time series in the time domain. In this section we introduce a complementary function, called the cross spectral density function or cross-spectrum and coherence function, which is the natural tool in the frequency domain. Given data on two time series, or input and output of a system, cross spectrum and coherence function may all be estimated. As they stand, they provide a description of the relationship between the two signals in the frequency domain. There need be no assumption that the two signals are linked by any kind of linear relationship. Indeed, one of the attractions of cross-spectral analysis is that it may permit the characterisation of cyclical relationships which are difficult to model in the time domain. Unless otherwise specified, the major sources of information for this section are Bosch *et al.* [1994], Marmarelis and Marmarelis [1978] and Ljung [1987].

5.2.1 Cross spectrum

The cross spectrum contains all the information concerning the relationship between two series in the frequency domain. The relationship between two series is normally characterised by the cross-amplitude spectrum, $| P_{yu}(\omega) |$ and the phase spectrum, the argument arg. $P_{yu}(\omega)$. These two quantities are derived from the cross-spectrum, but they are real rather than complex.

We define the cross-spectrum of a discrete bivariate process measured at unit intervals of time as the Fourier transform of the cross-correlation function, namely

$$P_{uy}(\omega) = \sum_{-\infty}^{\infty} R_{uy}(\tau) e^{-j\omega\tau} \tag{5-5}$$

Alternatively, the transfer function of the system can be found by utilising the following relation:

$$H(\omega) = \frac{P_{yu}(\omega)}{P_{uu}(\omega)} \tag{5-6}$$

It should be noted that H(ω) is a complex quantity whose phase is the same as that of P_{yu} (ω), which indicates what portion of the period corresponding to the frequency of the output signal is delayed with respect to the input. Whereas the transfer magnitude reflects the degree to which input signal content at a discrete frequency f becomes manifest in output energy.

5.2.2 Coherence function

If noise is additive for both the input u(t) and output y(t), then the measured input and output signals $u_m(t)$ and $y_m(t)$ are, respectively:

$$u_m(t) = x(t) + e_1(t)$$
$$y_m(t) = y(t) + e_2(t)$$

The measure power spectra, such as $Pm_{yy}(\omega)$ and $Pm_{uu}(\omega)$, are also contaminated by noise. Therefore, the system equation:

$$P_{yu}(\omega) = H(\omega) P_{uu}(\omega) \tag{5-7}$$

given such assumption as $P_{ue1}(\omega) = 0$, becomes

$$Pm_{yu}(\omega) = H(\omega)\,[Pm_{uu}(\omega) - P_{e1e1}(\omega)] \tag{5-8}$$

In addition, the system may be somewhat nonlinear, further invalidating Eq.(5-8). It is desirable to have a measure (an index) of the extent to which the response is due to the stimulus (is "coherent" with the stimulus) and not to extraneous sources of

noise. To achieve this, we define the following quantity, which is called the coherence function:

$$coh(\omega) = \frac{|Pm_{uy}(\omega)|^2}{Pm_{uu}(\omega)Pm_{yy}(\omega)} \tag{5-9}$$

where y(t) and u(t) are the measured signals, We note that this quantity, $coh(\omega)$, is real. If the system is linear and noise is absent,

$$\text{coh}(\omega) = 1$$

However, if the stimulus (input) and response signal (output) are contaminated by measured noise, e1 and e2, respectively, then measured spectra are as following:

Cross spectrum: $P_{yu}(\omega) = Pm_{yu}(\omega)$

Response spectrum: $P_{yy}(\omega) + P_{e2e2}(\omega) = Pm_{yy}(\omega)$

Stimulus spectrum: $P_{uu}(\omega) + P_{e1e1}(\omega) = Pm_{uu}(\omega)$

Therefore, in this case:

$$coh(\omega) = \frac{|P_{uy}(\omega)|^2}{[P_{uu}(\omega)+P_{e1}e1(\omega)][P_{yy}(\omega)+P_{e2e2}(\omega)]} \tag{5-10}$$

a quantity clearly less than unity since the power spectrum is a positive definite function. Therefore, in the presence of contamination noise the coherence function becomes less then unity. Also from Eq.5-9, the coherence function is a positive quantity, and is always less than or equal to unity.

From Eq. 5-10 we also have, assuming $P_{e1} = 0$,

$$coh(\omega) = \frac{P_{uy}(\omega)|H(\omega)|^2}{|H(\omega)|^2 P_{uu}(\omega)+P_{e2e2}(\omega)} \tag{5-11}$$

Therefore, at any frequency f, the coherence function gives the fraction of power at the response that is due to the input. In any case, whenever coherence is less than unity, either the system is non-linear, the signals do not have a completely causal relationship (ie., the signal are contaminated by noise), or both. The deviation of coherence from unity is a quantitative measure of these conditions. In addition, when the coherence is small, the estimated gain, phase and coherence may all be unreliable [Marmarelis and Marmarelis 1978]. This may not be surprising once it is realised that the sample coherence can be interpreted as a measure of the 'correlation' between the input and the output at different frequencies.

5.3 Cross Time-Frequency Analysis

The standard approach is to compute cross spectral and coherence estimates from windowed Fourier transforms. Although Fourier transform carries complete information about the signal (assuming one deals with a deterministic signal) in frequency range, the information on where these frequencies are localised in time is contained in the phase spectrum of the Fourier transform of a signal. This method makes sense only if the signal is stationary. If not, the signal should be considered locally, which means the signal should be revealed explicitly in the frequency spectrum at a particular time. Clearly, the frequency content of many natural and man-made signals changes drastically with time, and standard Fourier analysis does not fully describe such nonstationary signals. Among such signals are speech, sonar and radar, optical images, and biological and geophysical signals. Similarly, frequency or time description of linear coupling between signals alone is not sufficient in such problems of nonlinear or nonstationary coupling. Conventional spectral analysis is not able to get full insight into the mutual relationships between the input and output. An example in our research is the problem of nonlinear coupling between ILV and HRV in patient data which is not fully reflected by coherence function. The change of linear coupling between ILV and HRV with time is important to set up linear ARX modelling for patient data. In order to study the spectral changes or cross spectral change of the signals with time, this need for local analysis has led to the development of an approach that combines the information of the time and frequency domain into a time-frequency representation. By mapping a one-dimensional function of time or frequency into a two-dimensional function of time and frequency, the mixed time-frequency representation (TFR) localises the signal energy in both the time and frequency directions. This gives the frequency content at each instant of time and hence describes how the spectrum is changing in time.

5.3.1 Time-Frequency Distribution

In a time-frequency representation, the localisation of the energy of a signal is considered as a joint function of time and frequency. The question of how to represent a signal by a joint function of time and frequency has been addressed by many researchers [Gabor 1946; Ville 1948; Rihaczeck 1968;]. Most derivations of a fundamental time-frequency representation start with the definition of a set of

desirable properties that a time-frequency representation should have. This set of properties is then the starting point for the derivation of a representation that satisfies those properties. In many cases the derivation results in a different representation, depending on the properties one chooses to be satisfied with. An important breakthrough came with the recognition that many of the previously derived representations all belong to the same class: the class of quadratic shift-invariant representation, also known as Cohen's class [Cohen 1966]. One of the best known time-frequency representations within the Cohen's class is the Wigner distribution. The Wigner distribution is considered to be representative for the Cohen's class. In that quantity, it is the time-frequency representation that has been studied most extensively, apart from the sliding-window Fourier transformation. The Wigner distribution has many important and interesting properties [Classen and Mecklenbrauker 1980]. In addition, the Wigner distribution has the important property of satisfying the time and frequency marginal in terms of the instantaneous power in time, and the energy spectrum in frequency.

A distribution $P(t,\omega)$ from Cohen's class can be interpreted as the two-dimensional Fourier transform of a weighted version of the ambiguity function (AF) of the signal

$$P(t,\omega) = \frac{1}{2\pi}\int_{-\infty}^{\infty}\int_{-\infty}^{\infty} A(\theta,\tau)\Phi(\theta,\tau)\times e^{-j\theta t - j\tau\omega}\,d\theta\,d\tau \tag{5-12}$$

where $A(\theta,\tau)$ is the AF of the signal s(t), given by

$$A(\theta,\tau) = \int_{-\infty}^{\infty} s^*\left(t-\frac{\tau}{2}\right)s\left(t+\frac{\tau}{2}\right)e^{j\theta t}\,dt \tag{5-13}$$

The weight function $\Phi(\theta,\tau)$ is called the kernel; it determines the specific properties of the distribution. The product $A(\theta,\tau)\Phi(\theta,\tau)$ is known as the characteristic function. Indeed, $\Phi(\theta,\tau)$ tries to let the signal term remain unchanged, and to reject the interference terms. Actually, the change from the term, the time-frequency plane to the ambiguity plane allows a precise characterisation of the weighting function $\Phi(\theta,\tau)$ the smoothing function [Auger *et al.* 1995]. The kernel for the Wigner distribution is unity, so the generalised ambiguity function is identical to the ambiguity function and its t-f representation preserves both the auto-terms and the cross-term.

Let $R_s(t,\tau)$ be the instantaneous autocorrelation of a complex signal s(t). It can be obtained by considering the symmetric auto-correlation of a signal around fixed time t, i.e.

$$R_s(t,\tau) = s\left(t+\frac{\tau}{2}\right)s^*\left(t-\frac{\tau}{2}\right) \tag{5-14}$$

A Wigner distribution $W(t,\omega)$ of a function s(t) is defined as the non-stationary power spectrum that is associated with the instantaneous auto-correlation function:

$$W(t,\omega) = \frac{1}{2\pi}\int_{-\infty}^{\infty} R_s(t,\tau)e^{-j\omega\tau}dt \tag{5-15}$$

It is the Fourier transformation of the instantaneous auto-correlation over the time shift variable τ.

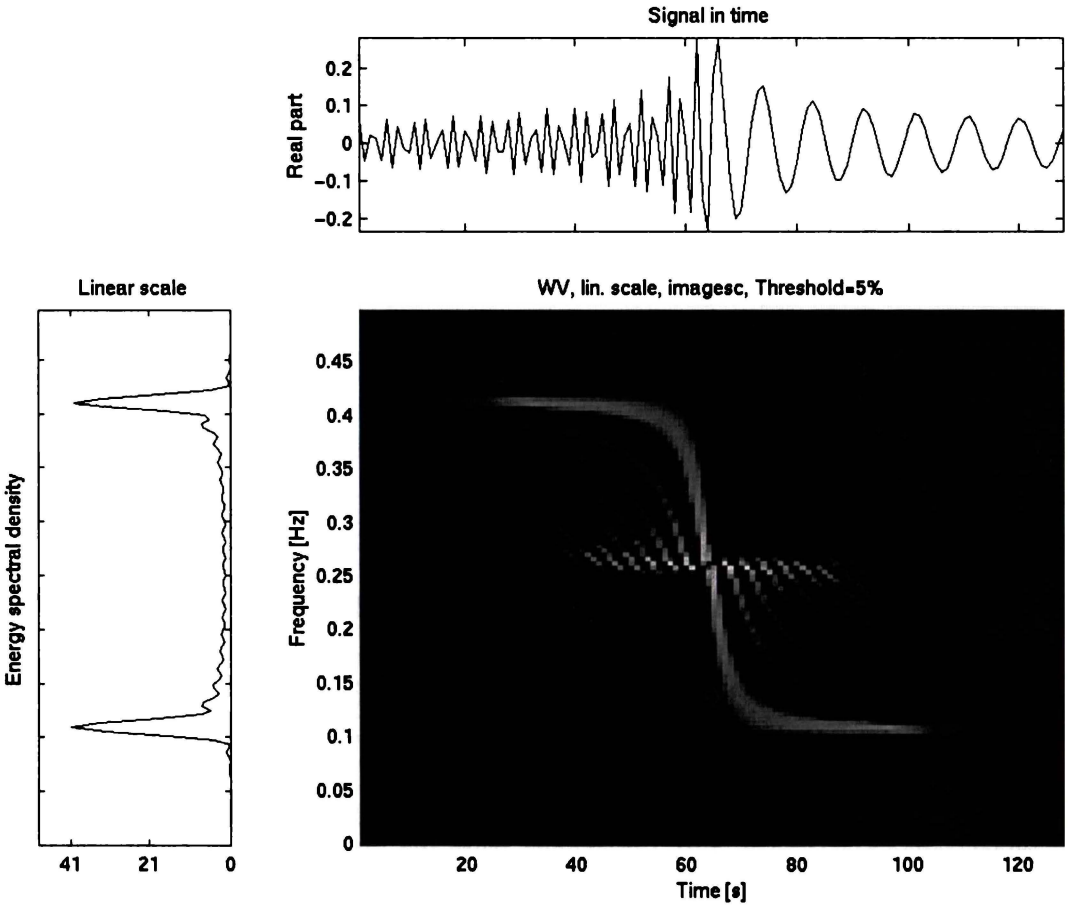

Figure 5- 1 Wigner distribution of a doppler signal: many interference terms are present, due to the biliearity of the distribution (produced by Time-Frequency Toolbox, Auger *et al.*.1995)

The major drawback of the Wigner distribution is that it produces cross terms (i.e., interference) between signal components located in different regions in the time-

frequency plane because the AF is a bilinear functional of the signal. These phenomena may cause difficulties in interpreting the Wigner distribution as an energy distribution over time and frequency. Therefore, the kernel is often selected to weight the AF such that the auto-components, which are centred at the origin of the (θ,τ) ambiguity plane, are passed, while the cross-components, which are located away from the origin, are suppressed [Jeong and Williams 1992]. The Wigner distributions of the example signal are shown in Fig 5-1: we notice that the energy is not the distribution that we could expect for this signal. Although the signal term is well localised in the time-frequency plane, numerous other terms (the interference terms, due to the bilinearity of the Wigner distribution) are present at positions in time and frequency where the energy should be null.

In summary, the Wigner distributions satisfy many desirable properties, but since it is quadratic, the Wigner distributions introduce cross-terms in the time-frequency plane which can disturb the readability of the representation. One way to attenuate this interference is to smooth the distribution in time and in frequency, according to their structure.

5.3.2 Reduced interference distributions

The limitation of the Wigner distribution described motivates new time-frequency representation that overcomes the drawback. The Choi-Williams distribution is an attempt to improve on Wigner distribution [Choi and Williams 1989]. It has an exponential-type kernel:

$$\Phi(\theta,\pi) = e^{-\theta^2\tau^2/\sigma} \tag{5-16}$$

where the parameter σ trades off autoterm resolution for cross-term suppression or vice versa. In fact, as σ becomes very large the kernel approaches the Wigner distribution kernel. Inversely, the smaller σ, the better reduction of the interference. This choice provides the best resolution by which the cross-terms become large and approach Wigner distribution cross-term in size. In a strict sense, the Choi-Williams distribution violates the support properties.

The Choi-Williams distribution kernel is used to smooth the distribution in time and in frequency, but the consequence of this is a decrease of the time and frequency resolutions, and more generally a loss of theoretical properties. However, the performance of the Choi-Williams has pointed the way to the design of desirable

time-frequency distributions and the ambiguity domain interpretation of its performance suggests a new methodology for obtaining such distributions.

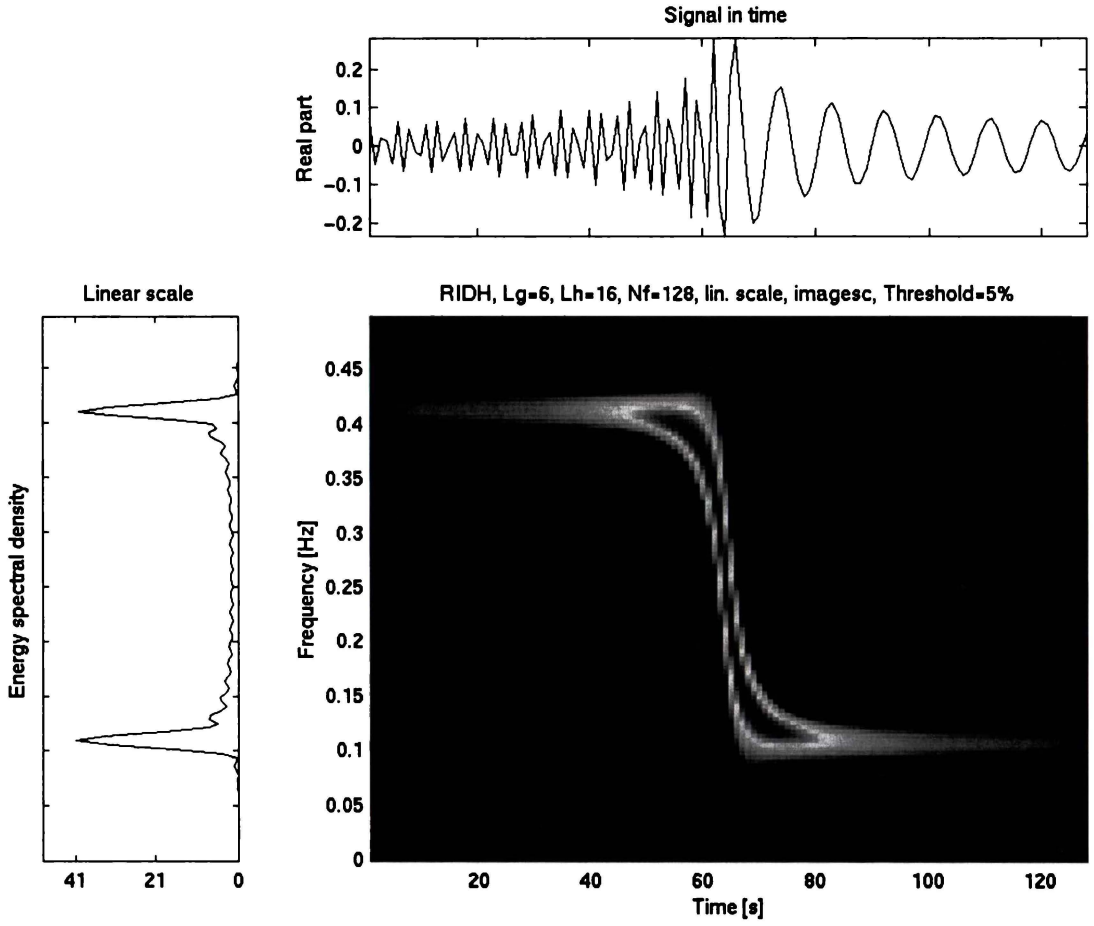

Figure 5- 2 Reduced Interference distribution of a doppler signal, much fewer interference terms are present compared with Wigner distribution produced by Time-Frequency Toolbox [Auger *et al.* 1995]

A new class of time-frequency distribution, called the reduced interference distributions (RID), has been introduced by Williams and Jeong [1989] to incorporate the idea of interference reduction in the Choi-Williams distribution. The RID provides high resolution in time and frequency, and easy-to-interpret localisation of the signal energy spectrum in the time-frequency plane, although one can find signals that will not be effectively handled by the RID. It's kernel has many desirable properties but does not satisfy the distribution property of nonnegativity.

To meet the time support and frequency support properties which the Wigner distribution have, the RID kernel should be a cross-shaped low-pass filter, to satisfy [Jeong and Williams 1992,Williams *et al.* 1995]:

$$|\Phi(\theta,\tau)| << 1 \qquad for\ |\theta\tau| >> 0.$$

In 1992, Jeong and William proposed the following procedure to design a RID kernel.

Step 1. A primitive real-valued function $h(t)$ is designed to satisfy the following:

H1: $h(t)$ has unit area, i.e., $\int h(t)dt = 1$.

H2: $h(t)$ is a symmerical function of time, i.e., $h(-t) = h(t)$.

H4: $h(t)$ is time-limited on [-1/2,1/2], i.e., $h(t) = 0$ for $|t| > ½$.

H4: $h(t)$ tapers smoothly towards both ends so that its frequency response has little high frequency content, that is, $|H(q)| < 1$ *for* $|q| > 0$, where $H(q)$ is the Fourier transfer of $h(t)$.

Step 2. Take the Fourier transfer of h(t),i.e.,

$$\Phi(\theta,\tau) = H(\theta\tau) = \int h(t)e^{-j\theta\pi}dt$$

The kernel design procedure described is sufficient to guarantee RID properties. There is a great deal of flexibility in choosing the primitive $h(t)$ so that desirable features of the signal are enhanced and cross-terms and noise can be diminished.

One easy way to design a primitive function $h(t)$ is to use well-known windows, e.g., the Hanning window, and their frequency characteristics. $H(\theta\tau)$ should be interpreted as a filter rather than as a convolution operator which is the interpretation it is given by most spectral analysis methods. However, $H(\theta\tau)$ expands into a two-dimensional filter in θ *and* τ. We need to consider the 2-D characteristics of $H(\theta\tau)$, which has a cross shape.

There is a trade-off between the autoterm resolution and the cross-term reduction of the distribution. If $h(t)$ is a smooth function with little high frequency content, the resultant distribution effectively suppresses the interference terms at the expense of the autoterm resolution. On the other hand, if $h(t)$ is an impulse-like function, then the resultant distribution suffers from strong interference to maintain high auto-term resolution.

Compared with the performances of Wigner distribution, the RID (Fig. 5-2) provides a clear display of the t-f structure of the signal resolving individual features without any loss of definition due to smearing and cross-terms. The Wigner distribution resolves the signal component, the significant cross-terms however being greater than ones in the RID distribution. The RID reduces the cross terms fairly effectively, showing only small hints of the cross terms. It still has a very good resolution in

time and frequency, offering excellent interpretability as a time-varying frequency spectrum.

5.3.3 Cross time-frequency distributions

As the Wigner distribution is a bilinear function of the signal s(t), the quadratic superposition principle applies. Consider the signal s(t) that is the sum of two signals: s(t) = u(t)+y(t). The instantaneous auto-correlation function is given by

$$R_{u+y}(t,\tau) = u\left(t+\frac{\tau}{2}\right)u^*\left(t-\frac{\tau}{2}\right) + y\left(t+\frac{\tau}{2}\right)y^*\left(t-\frac{\pi}{2}\right) + u\left(t+\frac{\tau}{2}\right)y^*\left(t-\frac{\tau}{2}\right) + y\left(t+\frac{\tau}{2}\right)u^*\left(t-\frac{\tau}{2}\right)$$

It can be written as

$$R_{u+y}(t,\tau) = R_u(t,\tau) + R_y(t,\tau) + R_{uy}(t,\tau) + R_{yu}(t,\tau)$$

We now find the Wigner distribution of the sum of two signals:

$$W_{u+y}(t,f) = W_u(t,f) + W_y(t,f) + 2\,\mathrm{Re}\{W_{uy}(t,f)\}$$

where

$$W_{uy}(t,f) = \int_{\infty}^{\infty} u\left(t+\frac{\tau}{2}\right)y^*\left(t-\frac{\tau}{2}\right)e^{-j2\pi f\tau}\,d\tau$$

is the cross Wigner distribution of x(t) and y(t). It can be considered as a bivariate version of the Wigner distribution and the instantaneous cross-energy of two signals. The Wigner distribution interference terms of signal s(t) that is the sum of two signals, u(t) and y(t), will be non-zero regardless of the time-frequency distance between the two signals. These interference terms are troublesome since they may overlap with auto-terms (signal terms) and thus make it difficult to visually interpret the Wigner distribution image (Fig. 5-1). On the other hand, the cross time-frequency distributions of two signals u(t) and y(t) evaluate the common energy between signals of the t-f plane. These representations can be used to determine if time-frequency components in one signal are related to time-frequency components in another signal.

As for cross-term suppression in the RID, the cross terms are, in general, reduced in height but spread over a larger time-frequency area. The cross terms in the RID are

the 2-D convolution between the cross terms in the Wigner distribution and the time-frequency domain kernel of the RID. Williams *et al.* [1995] demonstrated by comparatively evaluating the cross Wigner distribution and cross-RID that the cross-RID is more useful than the cross Wigner distribution and allows a significantly better interpretation of common energy over the t-f plane.

Cross-RID for heart rate signal and respiratory signal in regular breathing is presented in Fig. 5-3 and Fig. 5-4. These figures have shown that cross-RID is able to give an instantaneous correlation between HRV and ILV in the time-frequency domain as expected and in particular provide a tool to analyse phase shift between HRV, ILV. We will discuss its physiological meaning in Chapter 8.

Cross Time-Frequency Analysis can be used to analyse relations between HRV, ILV in their t-f representation thereby providing a better level of signal comprehension. It is extremely advantageous to determine if HRV and ILV can be modelled by the ARX model by use of cross t-f coherence. It is possible in the case of nonstationary or nonlinear coupling between HRV and ILV for cross t-f coherence to be lower in some parts of a time series while the coherence function is high. It shows coherence changes as a function of time and frequency.

In addition, while the phase spectrum P_{yu} (ω), indicates what portion of the period corresponding to the frequency of the output signal is delayed with respect to the input, the cross phase distribution shows us how this delay changes with time, which is important for the ARX model set up.

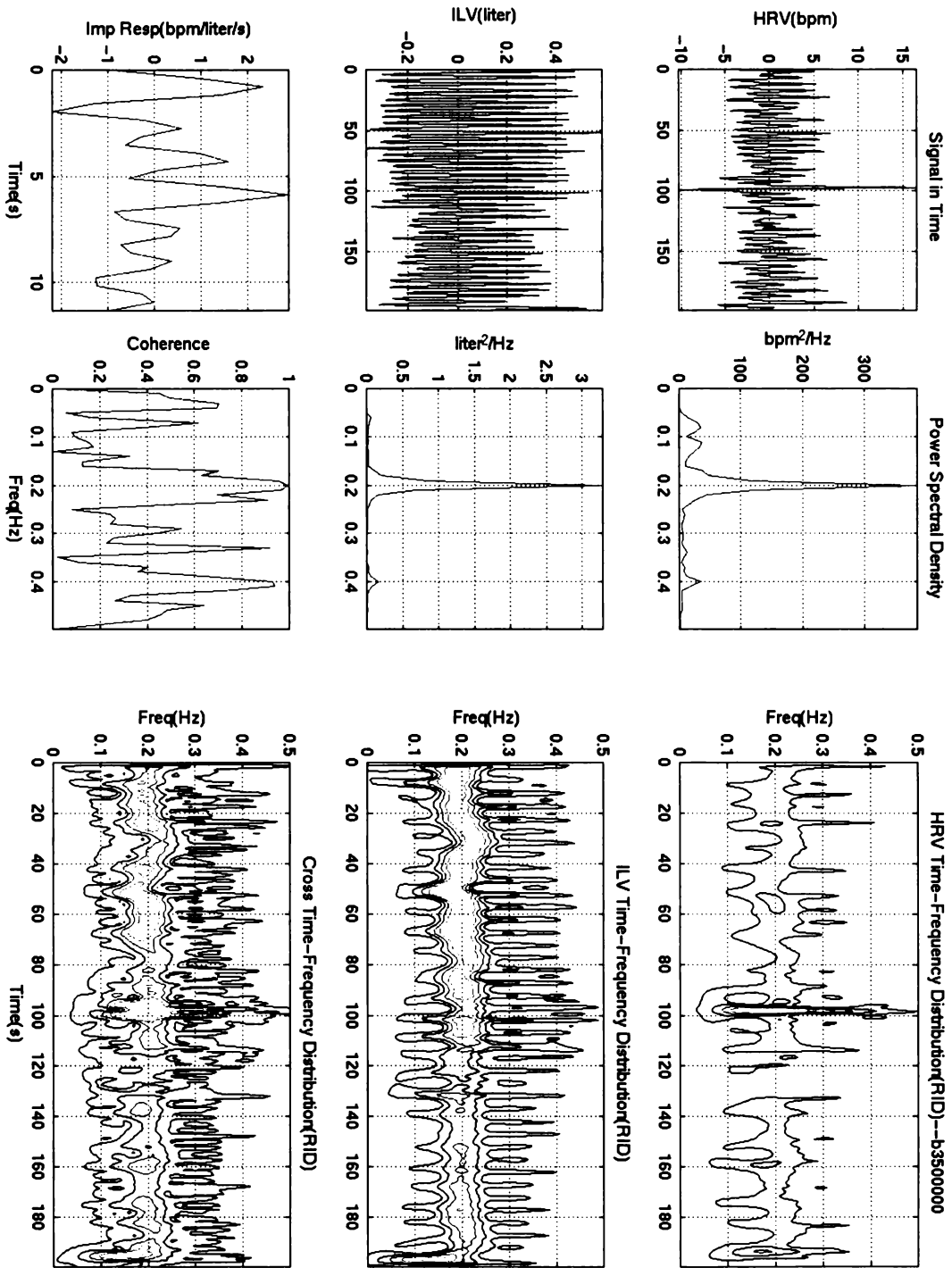

Figure 5- 3 Comparison of the RID of HRV and ILV with their Cross-RID. A: HRV, the power spectral density of HRV and the RID of HRV. B: ILV, the power spectral density of ILV and the RID of ILV. C: Impulse Response from ILV to HRV, coherence of HRV and ILV and the Cross-RID of HRV and ILV.

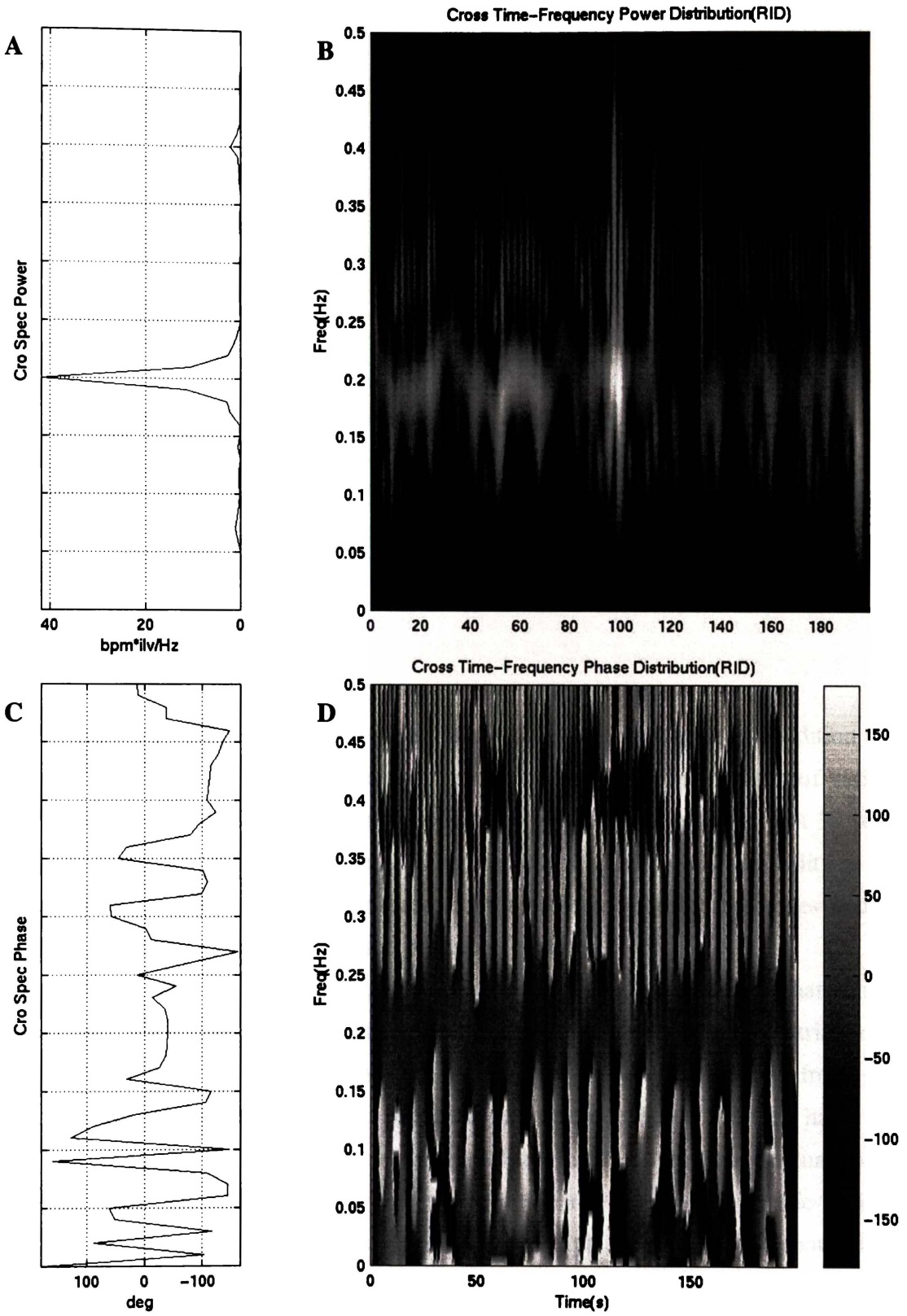

Figure 5- 4 The Cross RID of HRV and ILV. A: cross-amplitude spectrum of HRV and ILV. B: cross-amplitude RID of HRV and ILV. C: phase spectrum of HRV and ILV. D: phase RID of HRV and ILV

Chapter 6

Measurement and Interpolation of Heart Rate

6.1 Introduction

The heart rate (HR) is a signal of great interest for assessing the heart condition of a patient, and can be helpful in diagnosis, since it reflects the interactions of various physiological systems on the heart. The HR has been studied over the past 30 years as a measure of physical well being. The amount of spontaneous variability in the heart rate has been shown to decrease with various pathological states and to gradually improve during regression of disease process.

The HR signal originates in the body's own negative feedback systems that control heart rate via neural, humoral, and thermoregulatory effects on the sino-atrial node. The most precise measure of the heart rate is its extraction from the electrocardiogram (ECG). The practical extraction process should have the following characteristics: it needs a high-pass filter that removes slow fluctuations of the baseline, as well as a low-pass filter that removes the myographic activity (electrical activity of the muscles, located in the high frequencies). It should then amplify the QRS complex with respect to the other waves, in order to facilitate its extraction. Finally, an efficient algorithm for the derivation of heart rate converts ECG to an event process and calculates the rate of occurrence of the derived event.

A review of the QRS detection algorithm developed by Pan and Tompkins [1985] will be given in the first part of this chapter. We briefly describe the Berger method

[Berger *et al* 1986] and our Iterative Band-Limited Interpolation (IBLI) method for recovering heart rate. Full reports of this research and IBLI method can be referenced in Appendix A of this thesis [Henderson *et al.* 1995].

6.2 Electrocardiogram

The electrocardiogram is a very important tool for assessing the ability of the heart to transmit the cardiac impulse. When the impulse travels through the heart, electrical current generated by the action potential of the heart muscle spreads into the fluids surrounding the heart, and a minute portion of the current actually flows as far as the surface of the body. By placing electrodes on body surface, such as on the two arms, and connecting these to an appropriate recording instrument, the electrical voltages generated during each heartbeat can be recorded.

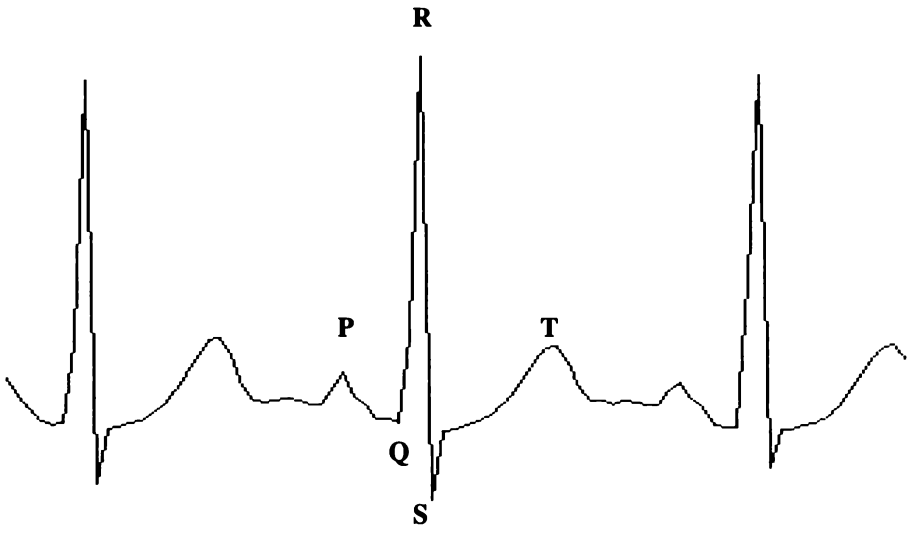

Figure 6- 1 The normal electrocardiogram

The normal electrocardiogram (ECG) illustrated in Figure 6-1 gives a view of the global activity of the heart. A classical ECG sequence consists of the repetition of a pattern containing five characteristic waves (respectively named P, Q, R, S, and T). The small hump in the recording labeled P is caused by electrical voltage generated by passage of the impulse through the atria. The spikes marked Q, R and S are caused by passage of the impulse through the ventricles, and the hump T is caused

by return of the membrane potential in the ventricular muscle fibers to its normal resting level at the end of contraction.

6.3 QRS Detection Algorithm

6.3.1 Introduction

QRS detection is complicated by the physiological variability of the QRS complexes and by the various types of noise that can be present in the ECG signal. Noise sources include muscle noise, artifacts due to electrode motion, power-line interference, baseline wander, and T waves with high-frequency characteristics similar to QRS complexes.

In Pan and Tompkins [1985], digital filters reduce the influence of these noise sources, and thereby improve the signal-to-noise ratio. Software QRS detectors typically include one or more of three different types of processing steps [Pahlm and Sornmo 1984]:

- Linear digital filtering
- Nonlinear transformation
- Decision rule algorithms

Pan and Tompkins [1985] use all three types. Linear processes include a bandpass filter, a deviate and a moving window integrator. The nonlinear transformation which is employed is signal amplitude squaring. Adaptive thresholds and T-wave discrimination techniques provide part of the decision rule algorithm.
The slope of the R wave is a popular signal feature used to locate the QRS complex in many QRS detectors [Ahlstrom and Tompkins 1983]. An analog circuit or a real-time derivative algorithm that provides slope information is straightforward to implement. However, by its very nature, a derivative amplifies the undesirable higher frequency noise components. Also, many abnormal QRS complexes with large amplitudes and long duration are missed in the purely derivative approach because of their relatively low R-wave slopes. Thus, R-wave slope alone is insufficient for proper QRS detection. To achieve reliable performance we must

extract other parameters from the signal such as amplitude, width, and QRS energy [Nygards and Sornmo 1981, Ligtenberg and Kunt 1983].

6.3.2 Algorithm overview

The QRS detection algorithm that was implemented is a modification of an algorithm proposed by Pan and Tompkins [1985]. This algorithm reliably detects QRS complexes using slope, amplitude, and width information. We used this algorithm and implemented it in the C language, which run on 386 and 486 computers. All the processing is done with integer arithmetic so that the algorithm can operate in real time without requiring excessive computing power. In this section, we give brief introduction of Pan's QRS [1985] detection algorithm.

First, in order to attenuate noise, the signal passes through a digital bandpass filter composed of cascaded high-pass and low-pass filters. The next process after filtering is differentiation, followed by squaring, and then moving window integration. Information about the slope of the QRS is obtained in the derivative stage. The squaring process intensifies the slope of the frequency response curve of the derivative and helps restrict false positives caused by T waves with higher than usual spectral energies. The moving window integrator produces a signal that includes information about the slope and the width of the QRS complex.

The algorithm is divided into three processes: learning phase 1, learning phase 2, and detection. Learning phase 1 requires about 2 s to initialize detection thresholds based upon signal and noise peaks detected during the learning process. Learning phase 2 requires two heartbeats to initialize RR-interval average and RR-interval limit values. The subsequent detection phase carries out the recognition process and produces a pulse for each QRS complex. The threshold and other parameters of the algorithm are adjusted periodically to adapt to changing characteristics of the signal.

Pan and Tompkins [1985] use two sets of thresholds to detect QRS complexes. One set comprises thresholds of the filtered ECG, and the other thresholds of the signal produced by the moving window integration. Our implementation uses only a single moving window integration threshold. Preprocessing of the ECG with the digital bandpass filter improves the signal-to-noise ratio and permits the use of a lower threshold than would be possible on the un-filtered ECG. This increases the overall detection sensitivity. The detection threshold floats over the noise that is sensed by the algorithm. This approach reduces the number of false positives caused by types of noise that mimic the characteristics of the QRS complex.

Once a valid QRS complex is recognized, there is a 200 ms refractory period before the next one can be detected since QRS complexes cannot occur closer than this physiologically. This refractory period eliminates the possibility of a false detection such as multiple triggering on the same QRS complex during this time interval.
To be realizable, a QRS detection algorithm must adapt each of its parameters with time so it can operate properly for the ECG's of different patients, as well as for ECG morphology changes in a single patient. In the algorithm, the threshold automatically adapts periodically based upon signal peak values.

6.3.3 Methods

Bandpass Filter The bandpass filter reduces the influence of muscle noise, 50Hz interference, baseline wander, and T-wave interference. The desirable passband to maximize the QRS energy is approximately 5-15 Hz [Goovaerts *et al.* 1976, Thankor *et al.* 1983]. The filter is a fast, real-time recursive filter, in which poles are located to cancel zeros on the unit circle of the z plane [Lynn 1977]. This approach results in a filter design with integer coefficients. Since only integer arithmetic is necessary, 386 and 486 personal computers have the available computing power to implemented a real-time filter and to do the QRS recognition task as well.
This class of filters having poles and zeros only on the unit circle permits limited passband design flexibility. For sampling rate of 200 Hz, it is not possible to design a bandpass filter directly for the desired passband of 5-15 Hz, using this together to achieve a 3dB passband from about 5-12 Hz, reasonably close to the desired region.

Low-Pass Filter The transfer function of the second-order low-pass filter is

$$H(z) = \frac{(1-z^{-6})^2}{(1-z^{-1})^2}$$

The amplitude response is

$$|H(\omega T| = \frac{\sin^2(3\omega T)}{\sin^2(\omega T/2)}$$

where T is the sampling period. The difference equation of the filter is

$$y(nT) = 2y(nT-T) - y(nT-2T) + x(nT) - 2x(nt-6T) + x(nT-12T)$$

extract other parameters from the signal such as amplitude, width, and QRS energy [Nygards and Sornmo 1981, Ligtenberg and Kunt 1983].

6.3.2 Algorithm overview

The QRS detection algorithm that was implemented is a modification of an algorithm proposed by Pan and Tompkins [1985]. This algorithm reliably detects QRS complexes using slope, amplitude, and width information. We used this algorithm and implemented it in the C language, which run on 386 and 486 computers. All the processing is done with integer arithmetic so that the algorithm can operate in real time without requiring excessive computing power. In this section, we give brief introduction of Pan's QRS [1985] detection algorithm.

First, in order to attenuate noise, the signal passes through a digital bandpass filter composed of cascaded high-pass and low-pass filters. The next process after filtering is differentiation, followed by squaring, and then moving window integration. Information about the slope of the QRS is obtained in the derivative stage. The squaring process intensifies the slope of the frequency response curve of the derivative and helps restrict false positives caused by T waves with higher than usual spectral energies. The moving window integrator produces a signal that includes information about the slope and the width of the QRS complex.

The algorithm is divided into three processes: learning phase 1, learning phase 2, and detection. Learning phase 1 requires about 2 s to initialize detection thresholds based upon signal and noise peaks detected during the learning process. Learning phase 2 requires two heartbeats to initialize RR-interval average and RR-interval limit values. The subsequent detection phase carries out the recognition process and produces a pulse for each QRS complex. The threshold and other parameters of the algorithm are adjusted periodically to adapt to changing characteristics of the signal.

Pan and Tompkins [1985] use two sets of thresholds to detect QRS complexes. One set comprises thresholds of the filtered ECG, and the other thresholds of the signal produced by the moving window integration. Our implementation uses only a single moving window integration threshold. Preprocessing of the ECG with the digital bandpass filter improves the signal-to-noise ratio and permits the use of a lower threshold than would be possible on the un-filtered ECG. This increases the overall detection sensitivity. The detection threshold floats over the noise that is sensed by the algorithm. This approach reduces the number of false positives caused by types of noise that mimic the characteristics of the QRS complex.

The high-pass filter has a delay of 15 ½ T.

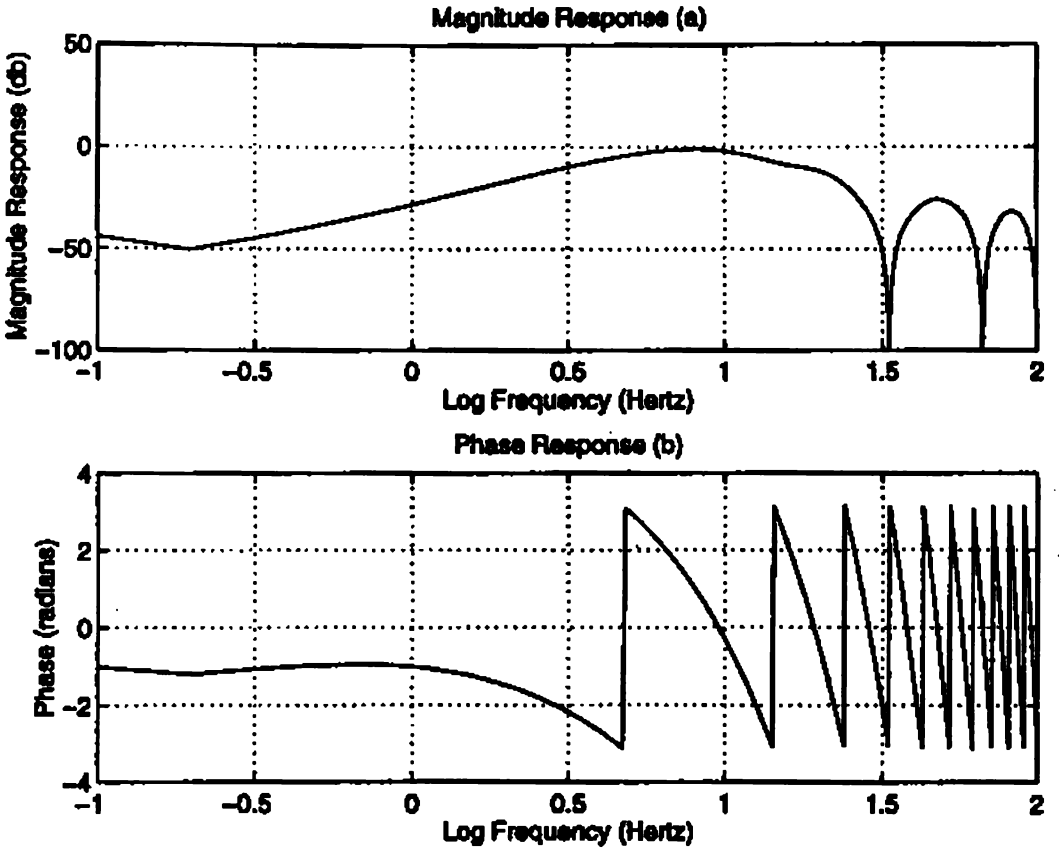

Figure 6- 2 Amplitude and phase response of the digital bandpass filter

Derivative After filtering, the signal is differentiated to provide the QRS complex slope information. A five-point derivative is used with the transfer function:

$$H(z) = (1/8T)(-z^{-2} - 2z^{-1} + 2z^{1} + z^{2})$$

The amplitude response is

$$|H(\omega T)| = (1/4T)[\sin(2\omega T) + 2\sin(wT)]$$

The difference equation is [Ligtenberg and Kunt 1983]

$$y(nT) = (1/8T)[-x(nT - 2T) - 2x(nT - T) + 2x(nT + T) + x(nT + 2T)]$$

Figure 6-3 shows that the frequency response of this derivative is nearly linear between D.C. and 30 Hz (i.e., it approximates an ideal derivative over this range). Its delay is two samples, and a maximum gain of $\frac{3\sqrt{3}}{8T}$

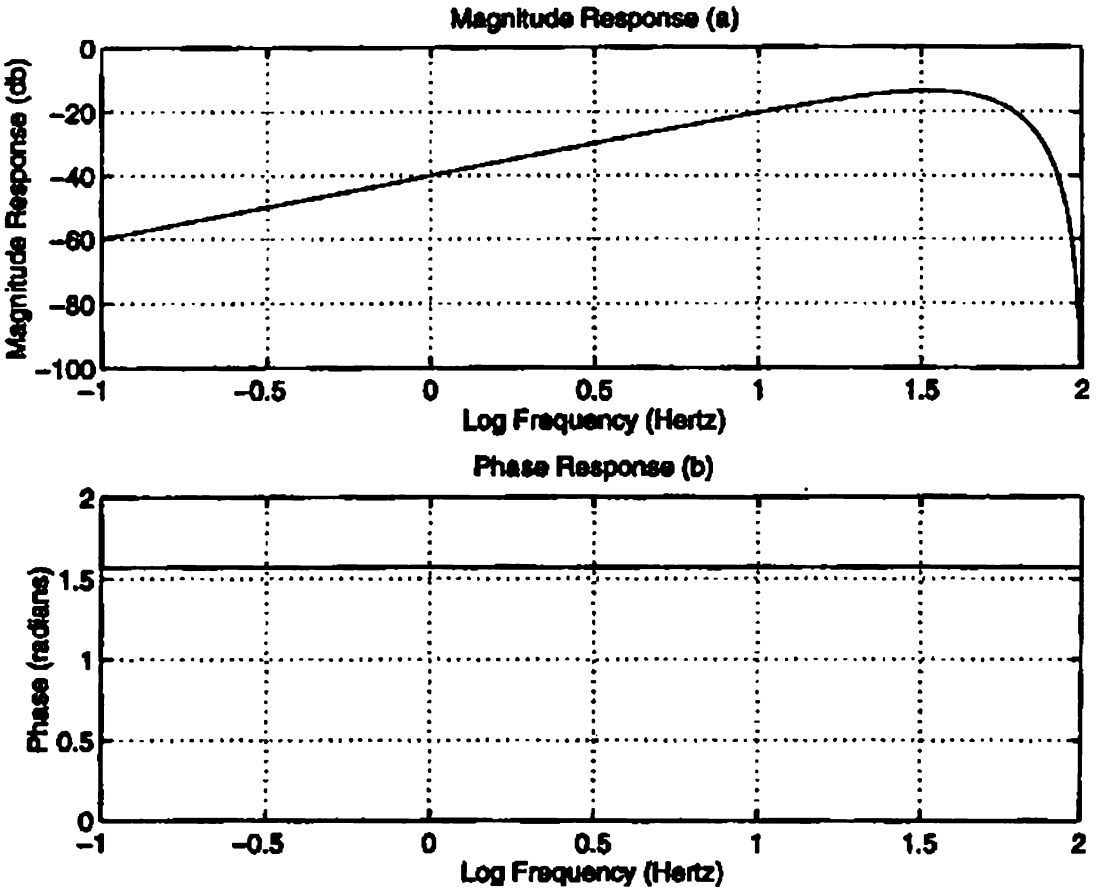

Figure 6- 3 Amplitude and phase response of the digital derivative filter

Squaring Function After differentiation, the signal is squared point by point. The equation of this operator is

$$y(nT) = [x(nT)]^2$$

This makes all data points positive and performs nonlinear amplification of the output derivative emphasizing the higher frequencies (i.e., predominantly the ECG frequencies).

Moving – Window Integration The purpose of the moving-window integration is to obtain waveform feature information in addition to the slope of the R wave. It is calculated from:

$$y(nT) = (\frac{1}{N}[x(nT-(N-1)T) + x(nT-(N-2)T) + \ldots + x(nT)]$$

where N is the number of samples in the width of the integration window.
The number of samples N in the moving window is important. Generally, the width of the window should be approximately the same as the widest possible QRS complex. If the window is too wide, the integration waveform will merge the QRS and T complexes together. If it is too narrow, some QRS complexes will produce several peaks in the integration waveform. These can cause difficulty in subsequent QRS detection processes. For our sample rate of 200 samples/s, the window is 30 samples wide (150 ms).

Fiducial Mark The QRS complex corresponds to the rising edge of the integration waveform. The time duration of the rising edge is equal to the width of the QRS complex. A fiducial mark for the temporal location of the QRS complex can be determined from the rising edge according to the desired waveform feature to be marked such as the maximal slope or the peak of the R wave.

Adjusting the Threshold The threshold is automatically adjusted to float over the noise. A low threshold is possible because of the improvement of the signal-to noise ratio by the bandpass filter. The threshold is initially calculated as

$$thrsh = (maxb[0] + maxb[1] + maxb[2]) / 6$$

which is half the average of the last 3 peaks, where maxb[0 – 2] are the first 3 peaks over the first 8 seconds. Subsequently, the threshold is calculated as half the median of the last 3 peaks

$$thrsh = (maxb[k]) / 2$$

where maxb [k] is the median of the last 3 peaks maxb [0 – 2].

6.3.4 Quadratic interpolation

Quadratic splines interpolate the range between data points by a 2nd order polynomial (quadratic). Quadratic spline curve fitting ensures that each spline is equal to the data points, and that the first derivative of the spline is continuous. When an R wave is detected, quadratic interpolation is used to resolve the R wave's

time location to an accuracy of one millisecond, rather than five milliseconds without the used of interpolation, which has been proved experimentally.

6.4 Heart Rate Interpolation

The QRS detection is achieved using Pan's method to converts ECG to series of point events, heart rate. Several authors have used the integral pulse frequency modulation (IPFM) model to recover the properties of the assumed input signal from the observed event series [Berger *et al.* 1986, DeBoer *et al.* 1987, Hyndman and Mohn 1975, Rempelman *et al.* 1977].

Thus, before any HRV signal processing, the array of irregularly spaced RR intervals must be interpolated to form an evenly spaced heart rate signal, see Fig 6-4. Then the RR intervals are interpolated by the Berger method, with a sampling frequency of 20Hz, to produce an evenly sampled heart rate signal.

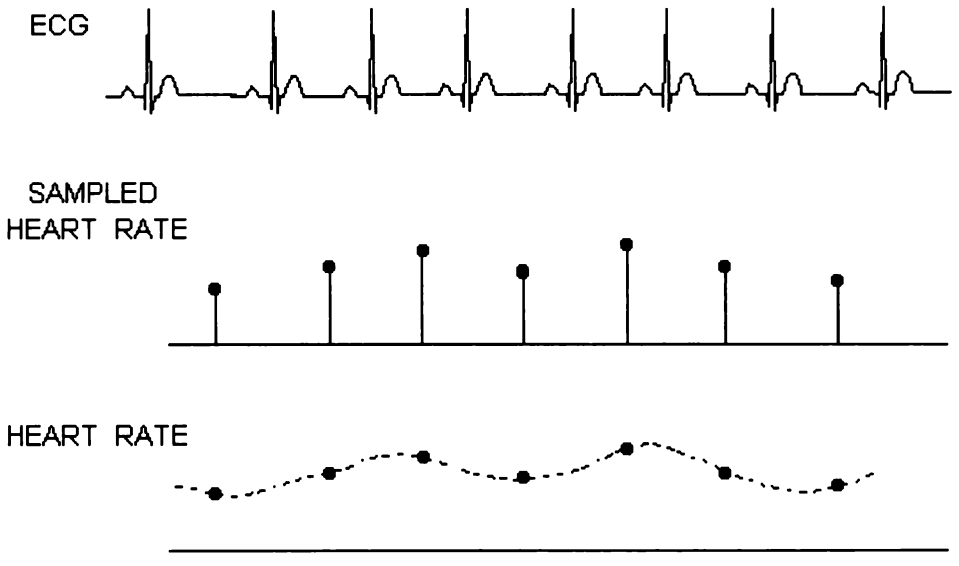

Figure 6- 4 The Heart Rate Signal. The heart rate samples equal the inverse R-R intervals of the ECG. The dotted heart rate signal signifies that values in between samples are unknown [Appendix A]

In an IPFM model, the input signal is integrated until the integral reaches a fixed reference value. Then a pulse is emitted and the integrator is reset a zero, whereupon the cycle starts again. The IPFM model that generated the simulated RR intervals is

shown in Fig. A-2 of Appendix A. The output pulse train simulates the R-R interval sequence of the ECG and each RR interval is a measure of the average input during that interval. Thus it can be seen that the input signal controls the frequency of the oscillator and it may therefore be considered the continuous heart rate signal.

Berger et al presented a simple algorithm to derive a heart rate signal from the ECG signal in [Berger *et al.* 1986]. The procedure involved is as follows. The ECG is sampled at a sufficiently high rate and then a "local window" is defined at each heart rate sample point as the time interval extending from the previous sample to the next. The value of the heart rate at each sample point is taken to be the number of intervals that fall within the local window centered at that point divided by the width of the window. Finally, heart rate can be used for further signal processing.

Convolution of the heart rate signal with the rectangular window has the effect on the power spectrum of multiplication by a low-pass filter. The shape of the filter W(f) is

$$W(f) = \left[\frac{\sin\left(\frac{2\pi f}{f_r}\right)}{\frac{2\pi f}{f_r}} \right]^2$$

where f_r is the sampling frequency of the heart rate signal, and $2/f_r$ is the width of the rectangular window in the time domain. The filter passes very little power beyond the Nyquist rate. Based on this, a new method for estimating a set of uniform samples from the non-uniformly sampled heart rate data, Iterative Band Limited Interpolation (IBLI), has been developed by Henderson *et al.*, see Appendix A.

The value of the signal at any time t can be recovered by the Band-limited interpolation [Jerri 1977]:

$$f_{(t)} = \sum f_n \frac{\sin(\pi(t - t_n / \Delta T)}{(\pi(t - t_n)\Delta T)}$$

if heart rate signal frequency is not higher than W and uniquely specified by samples f_n which uniformly spaced in time by $\Delta T = (1/2W)$ – the Nyquist sampling rate.

Then in principle it is possible to recover the unknowns, i.e., the uniformly sampled set $\{f_n\}$, by solving the 2TW equation:

$$f_p = \sum f_n \frac{\sin(\pi(t - t_n / \Delta T)}{(\pi(t - t_n)\Delta T)}, \qquad p = 1....2TW$$

Compared with the Berger method, IBIL can accurately estimate the power spectra of heart rate and does not generate harmonic and intermodulation products. However, the Berger method is particularly simple to implement and is very fast. It is for this reason, we decided to continue its use retaining the possibility of using IBLT at a later stage.

For more detail discussion on IBLI method, please refer Appendix A.

Chapter 7

Sensitivity Analysis of the Cardiovascular System

7.1 Introduction

Central to the problem for the origin of RSA is quantifying the relationship between the change in input signals (ILV and SBP) and output signals (HRV) of the human cardiovascular system. Several mathematical methods have been used in both time and frequency domain (refer Chapter 4). However, to our knowledge, none of them specially reported on the relative proportion of HRV related to ILV and to SBP.

This chapter addresses the sensitivity analysis of HRV to changes in ILV and SBP and demonstrates the more important role played by medullary respiratory neurons than the arterial baroreceptors in the origin of RSA in the conscious human. A dual-input ARX model has been used for cardiovascular system identification by Mullen *et al.* [1997] and Barbieri *et al.* [1997]. Based on the dual-input ARX, we firstly posed the use of a Back Error Propagation (BEP) neural network for identifying human cardiovascular system and then quantifying the influence of ILV and SBP on HRV. The results of this study are consistent with our human cardiovascular system model that respiration oscillations play the major role in the generation of RSA in healthy humans through the action of the medullary respiratory neurons (see Chapter 4).

Unless otherwise specified, the major sources of information about neural networks in this section are Murray [1996] and a shareware neural network application Neural Fusion [1997].

7.2 The Dual-input ARX model

Blood pressure is modulated both by the direct physical effects of respiration and by heart rate. In turn, it has feedback influences of its own on RSA, which can be seen in our cardiovascular system model in section 3-4. For this reason, the ARX model with input ILV only might be insufficient to characterize RSA and to investigate any influence from SBP on RSA. Hence, a dual-input ARX model is used to investigate RSA with specific attention to the role that input SBP plays in the origin of RSA.
The main difficulty with the human baroreflex control system is to identify the open loop transfer function under closed loop conditions because the presence of feedback significantly complicates the task of separately identifying the properties of the open loop and feedback elements of the system. As it is not possible to insert a disturbance signal within the loop, attempts to identify the system from input-output measurement will only yield estimates of overall closed loop transfer function [Ljung 1987]. To compare the changes of HRV due to ILV and SBP, we need to investigate the overall closed loop baroreflex control system other than open loop and feedback of the system separately. Moreover, from the point of view of the whole cardiovascular system, the overall closed loop baroreflex is the local control system, which is shown in our cardiovascular system model in section 3-4.
For the whole cardiovascular system with single input ILV and output HRV, we have the ARX model:

$$HRV(t)+ a1_1HRV(t-1)+...+ a1_{na\,1}HRV(t-na1) = b1_1ILV(t-nk1)+ ...+ b1_{nb}1LV(t-nk1-nb1)+ e1(t)$$

If in addition to input ILV, SBP is considered as another input variable of the system, we then have the dual-input ARX mode as:

$$HRV(t)+ a1_1HRV(t-1)+... + a1_{na\,1}HRV(t-na1) = b1_1ILV(t-nk1)+ ... + b1_{nb1}ILV(t-nk1-nb) + b2_1SBP(t-nk2)+ ... + b2_{nb2}SBP(t-nk2-nb2)+ e2(t)$$

We use both ARX models to study the variations in heart rate that occur with respiratory activity to study RSA. Although the dual-input ARX model offers

theoretical advantages, it will be useful to compare the model parameters from a single input ARX model and a dual input ARX model by using each to evaluate the same data, since it will give us a general idea what kind of role SBP plays in the origin of RSA.

7.3 A Back Error Propagation Neural Network

Neural networks originated in attempts at mathematical modeling of the way that the human brain works, but have since been applied to a wide variety of problems. Some of these applications have been very successful and the topic has become a rapidly expanding research area.

A neural network can be thought of as a system connecting a set of inputs to a set of outputs in a possibly non-linear way. The connections between inputs and outputs are typically made via one or more hidden layer of neurons. Figure 7-1 shows an example of neural networks with three layers. The arrows indicate the direction of each relationship and the neural network illustrated is typical in that there is no feedback. The neural network is therefore of a type called a feedforward neural network.

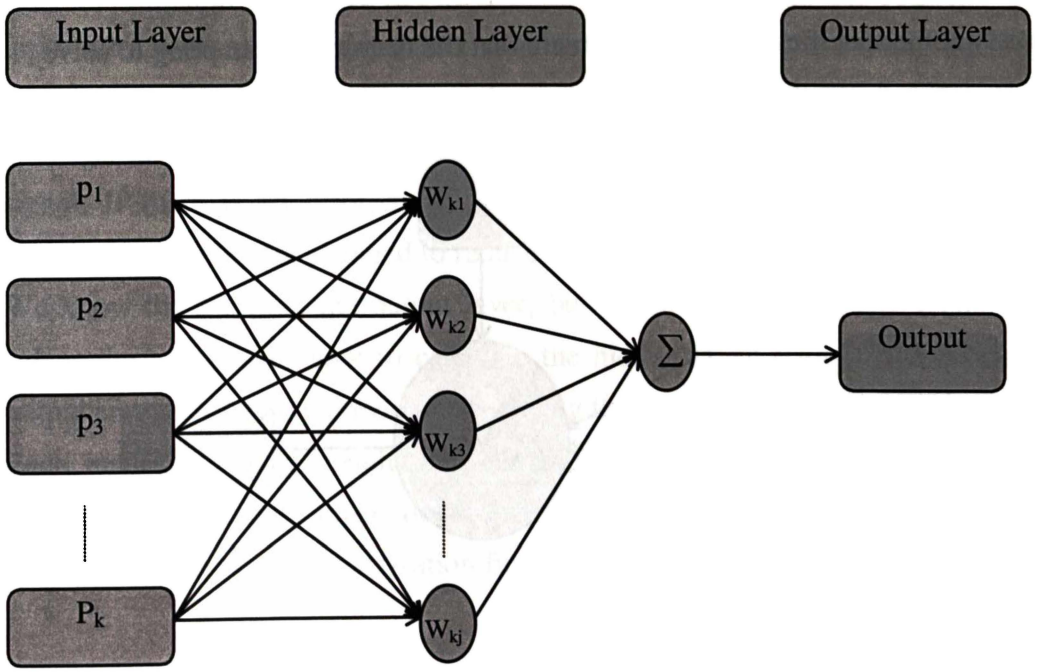

Figure 7- 1 A three-layered feedforward neural network

A Back Error Propagation (BEP) neural network is one of the most important and widely used network models, and is constructed of many inner-connected processing elements (neurons) each executing a simple nonlinear equation. It provides a way of using examples of a target function to find the coefficients that make a certain mapping function approximate the target function as closely as possible. The mapping function used in BEP is complex. The easiest way to understand it is to visualize it as the computation carried out by a neural network. More specifically, it is the computation carried out by a fully connected three-layer feedforward network. The neurons are partitioned into layers, with each neuron in a layer fully connected to all neurons in the next higher layer. Hence, as demonstrated by Fig. 7-1, all input layer neurons are connected to every hidden layer neuron and every hidden layer neuron is connected to the output neuron. Each connection has a strength or weight associated with it, and a network learns or is trained by modifying these weights. This results in the mapping of inputs to outputs via an abstract hidden layer.

The network is feedforward. When using or testing a trained network, the input values set the values of elements in the first hidden layer, which influence the next layer, and so on until it sets values for the output layer elements.

Each neuron has one activation function, given by f(.) in the hidden layer, which is typically a nonlinear function. The activation function tends to limit the amplitude of the output of the neuron. A typical hidden layer neuron from the preceding network has k+1 weights (k-inputs, 1-activation function). An activation function is chosen to satisfy some specification of the problem that the neuron is attempting to solve.

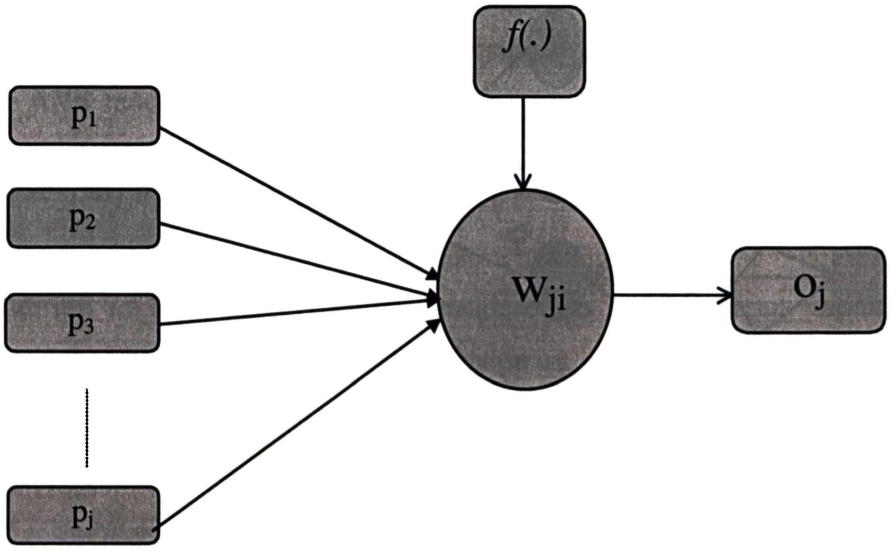

Figure 7- 2 Details of a hidden layer neuron.

What if a known input pattern produces a wildly incorrect output signal? Then we need to train the network through a learning process. Learning in neural networks is done by changing the weighting factors (weights) at each element to reduce output errors.

After training on a statistically designed experiment, a network can be used to predict the behavior of multivariate experimental data. Inputs or Independent Variables (IV) from the experimental database enter the network at the input layer, and outputs or Dependent Variables (DV) exit at the output layer. The input neurons contain simple scaling activation functions that translate the range of the independent variable from real world numbers to the most linear part (See Figure 7-2) of the neural equation (i.e. $0.2 < IV < 0.8$, centered at 0.5). The hidden and output layer neurons are nonlinear activation functions of the form:

$$o_j = \frac{1}{1+e^{-\sum_i w_{ji} o_i + w_j \Theta}}$$

Where, w_{ji} denote connection weights, o_i denotes output of a previous layer's neuron, $w_j\Theta$ denotes the adjustable threshold for the neuron, i denotes the number of inputs to the neuron from the previous layer and j denotes the current neuron.

Training the network involves first initializing the connection weights to small random numbers. Then row by row the independent variables are presented to the input layer neurons and a dependent variable is presented to the training input of the output layer. The network first calculates its own output value and then compares this with the target value presented to the output neuron. This difference is the error signal. If there is no error, then no learning takes place. Otherwise, the inner-connecting weights are changed to reduce the error.

We know the errors at the output layer, but not at the hidden layer elements. BP solves the problem of how to calculate the hidden layer errors. It propagates the output errors back to the previous layer using the output element weights.

Each inner-connecting weight between the output layer and the hidden layer is changed by an amount proportional to the product of an error signal and the first derivative of the nonlinear activation function as given by:

$$\frac{\partial o_j}{\partial net_j} = o_j(1-o_j)$$

Where: net_j denotes the total network error, o_j denotes the output of the current neuron and j denotes the current neuron. The error signal for the hidden layer to input layer, for which there is no target value, is calculated recursively in terms of the error signals of the neurons to which it directly connects and the weights of those connections.

The presentation of the experimental data is repeated until the network is adequately trained. Adequacy can be measured as: all predictions within a tolerance band, an R square value, a time limit, the number of presentations of the experimental data or a minimum total error. Generally, if the data is from a well-designed experiment the network can be trained aggressively (i.e. 2000-10000 presentations of the data). However, if the data is highly variable or from a poorly designed experiment a more cautious training session is in order (i.e. stop training at an R square or limit the training to 500-2000 presentations).

7.4 Neural Network ARX model

In general, a nonlinear model is required to represent the physiological system accurately. More recently, the use of the neural network has been applied to the field of the system identification. Unfortunately, this issue is much more difficult in the nonlinear case than the linear case. Not only is it necessary to choose a set of regressors but also a network architecture is required. Nørgaard *et al.* [1996] have provided a neural network based system identification matlab toolbox on the internet (http://kalman.iau.dtu.dk/research/control/nnsysid.html), which mainly focuses on the neural networks as a generic model structure for the identification of nonlinear dynamic systems.

The idea for building the neural network model is to select the same regressors used for linear system identification and then determine the best possible network architecture with the given regressors as inputs.

One of neural network model structures is Neural Network ARX model (NNARX) with the same regressor structure as that of an ARX model, which is given by:

$$\varphi(t) = \left[y(t-1) \ldots y(t-n_a) \ldots u(t-n_b) \ldots u(t-n_b-n_k+1)\right]^T$$

Predictor:

$$\tilde{y}(t|\theta) = \tilde{y}(t|t\text{-}1,\theta) = g(\varphi(t),\ \theta)$$

Where $\varphi(t)$ is a vector containing the regressors, θ is a vector containing the weights and g is the function realized by the neural network. The parameters na nb and nk represent the model order of the moving average (linear and nonlinear), autoregressive (linear and nonlinear) and dead time terms respectively, determing the structure of the regressor vector.

This three–layer NNARX model is shown in fig. 7-3. In the hidden layer, the neural networks use a polynomial representation of the activation function. Because it is commonly used, we have applied the back error propagation algorithm to train neural networks.

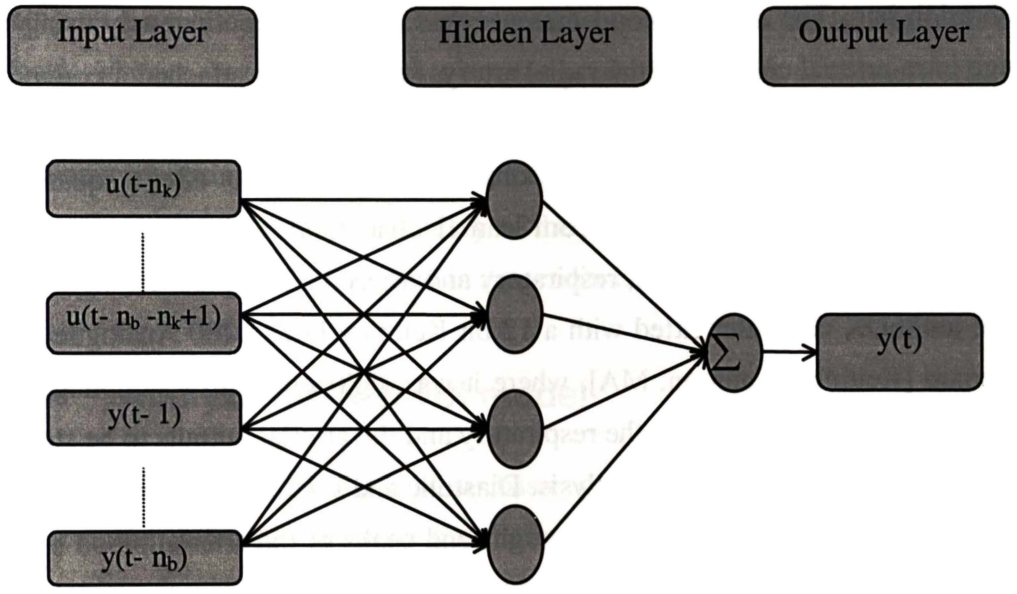

Figure 7- 3 Neural Network ARX model

7.5 Methods

A study was performed with HRV, ILV and SBP recorded from a group of health volunteers to do the sensitivity analysis of HRV to changes in ILV and SBP.

7.5.1 Experimental study

The study was approved by the Waikato Regional Ethics Committee and full informed consent was obtained from all participants. Eight male (aged 25-40) healthy subjects participated in the study. No subject had a history of

cardiopulmonary disease. All the experiments were done in a room with dimmed lighting between 9 A.M. and 3 P.M. with subjects in a supine position. The subjects had fasted for a minimum of two hours and were not on any vasoactive medication, and had not had any caffeine containing drink for 10 hours previously.

7.5.2 Data collection

Respiratory data was collected using a respiratory inductance plethysmograph [Respitrace 150 Studley Data Systems, Oxford]. The output was in DC mode with no autoreset. It was calibrated by having each subject fully empty and fill an 800-ml calibration bag. The arterial blood pressure was measured continuously using a 20 gauge intra-arterial catheter in the radial artery, to which was attached a commercial pressure monitoring system (Baxter Health Care, Irvine, CA, USA). Optimal damping of the system was checked by observing the overshoot after a square-wave input pulse. The ECG was taken from lead II of a standard ECG monitor [Nihon Kohden Lifescope 9]. The ECG, respiratory and arterial blood pressure signals were fed to a 486DX computer fitted with a 12 bit Keithley DAS-1200 Analogue/Digital I/O board [Keithley, Taunton, MA], where it was digitized using a sampling rate of 200 Hz for ECG and 20 Hz for the respiratory and the arterial outputs to be stored on a personal computer for further analysis. Diastolic and systolic blood pressure values were determined respectively as the troughs and peaks of the arterial blood pressure signal.

The C program for above data collection has been through a number of upgrades and modification over the years it has been in used at the Waikato Hospital. A number of studies have utilized it for an analysis of HRV, three trials have used it for heart rate, respiratory and arterial signal acquisition. The latest version of this C program can be referred to in the block diagram in Appendix C.

7.5.3 Training the NNARX model

The NNARX model was trained by presenting the training set data in a random order to the model.

The BEP algorithm makes use of the gradient calculations in training NNARX. Generally, all the weights in the network are initialized to have a small, random value. This should mean that the net activation value for the output layer is almost zero and the Multi-Layer Perceptron will output a value of approximately 0.5 when

an output activate function is being used and 0 when the output transfer function is simply an identity, linear mapping.

The weight training process then continues by identifying which patterns occur in the current training epoch and calculating the network's output for each pattern. Training ceases when the performance of the network falls beneath some pre-specified error tolerance or the number of learning steps exceeds some maximum value (BEP can be extremely slow, requiring tens of thousands of learning iterations). In order to calculate the current performance of a network, the complete data set is used to query the network and the MSE value is calculated, without updating the weights. The data is split into a training and a testing set, where the training set is used to calculate the weight update gradients and the testing set is used to decide when to stop learning and to test the predictive quality of the network.

Before training the model, one should select training parameters, such as, number of hidden neurons, maximum presentations of the training matrix, type of training used, and termination parameters. A summary of the parameters used in BEP networks to control the training behavior is listed in Appendix D.

7.5.4 Analyze the NNARX model

The statistical method calculates some basic statistics on the residual value. The residual is the difference between the measured output and the model prediction. Good models should have a residual mean near zero with a tight normal distribution, hence, the standard deviation, minimum, maximum and sum squares values should also approach zero. The R square statistic can be used to indicate overall how good is the model. As the model performance increases the R square statistic will approach one.

Residual Mean The residual is the difference between the measured and predicted values. The closer the mean is to zero the better the model is predicting.

Residual Std Dev The better the model predicts the closer the standard deviation will be to zero.

Residual Minimum This is the worst case under estimated prediction. The closer this value is to zero the better.

Residual Maximum This is the worst case over estimated prediction. The closer this value is to zero the better.

Residual Sum Sq This value is the total sum squares of all the residuals. The lower this number the better.

R Square The closer this number is to 1.0 the better.

Apart from a numerical or statistical method, the graphical method can also be used for analyzing a model's performance by plotting output and predicted output. This graph simply overlays the measured values on top of the predicted values. The better the model predicts the harder it is to discriminate between the measured and predicted plots

7.5.5 The sensitivity analysis using neural network

NNMODEL is an effective modeling tool that discovers relationships from a database of examples. It then generates a compact module that captures from simple linear to complex, non-linear relationships in a form that is readily executable. It excels at modeling systems such as fuzzy estimation, probabilities, expert experience and judgment, process sensor measurements and control strategies.

The NNMODEL combines a back-error propagation neural network with an advanced statistical based hidden neuron growth heuristic to outperform established methodologies on a wide range of problems while remaining statistically conservative. Unlike standard statistical regression, NNMODEL automatically develops an excellent functional model.

Use a BEP neural network to generate a sensitivity report showing the sensitivity of the output variables to changes in the input variables. The sensitivity is calculated by summing the changes in the output variables caused by moving the input variables by a small amount over the entire sensitivity calculation data set.

7.6 Results

7.6.1 The sensitivity analysis

For NNARX model analysis in an example subject, the input and output data pair was divided sequentially into two data segments. The 388 point data segment was

used to train the network, and the 389 point data segment was used as a part of the current data matrix in order to test the predictive quality of the neural network.

To train the NNARX model, the maximum number of hidden neurons is 4, Learning Rate is 0.75, Error Tolerance is 0.001 and Good R Square is 0.9.

To make sensitivity analysis more simple and sensible, the NNARX model was applied for the training data segment with the simplest model order, na = 1, nb =1. Note that the accuracy of the NNARX model identification is dependent on the selection of the model order. However, if the R square statistic for the NNARX model is reasonably good, the simplest model order will give us more straight forward way to look at the response of HRV to changes in ILV and SBP.

The NNARX model was created and trained using the initial settings in NNMODEL software for the training parameters. After training, the following model statistics were reported and are shown in the table 7-1.

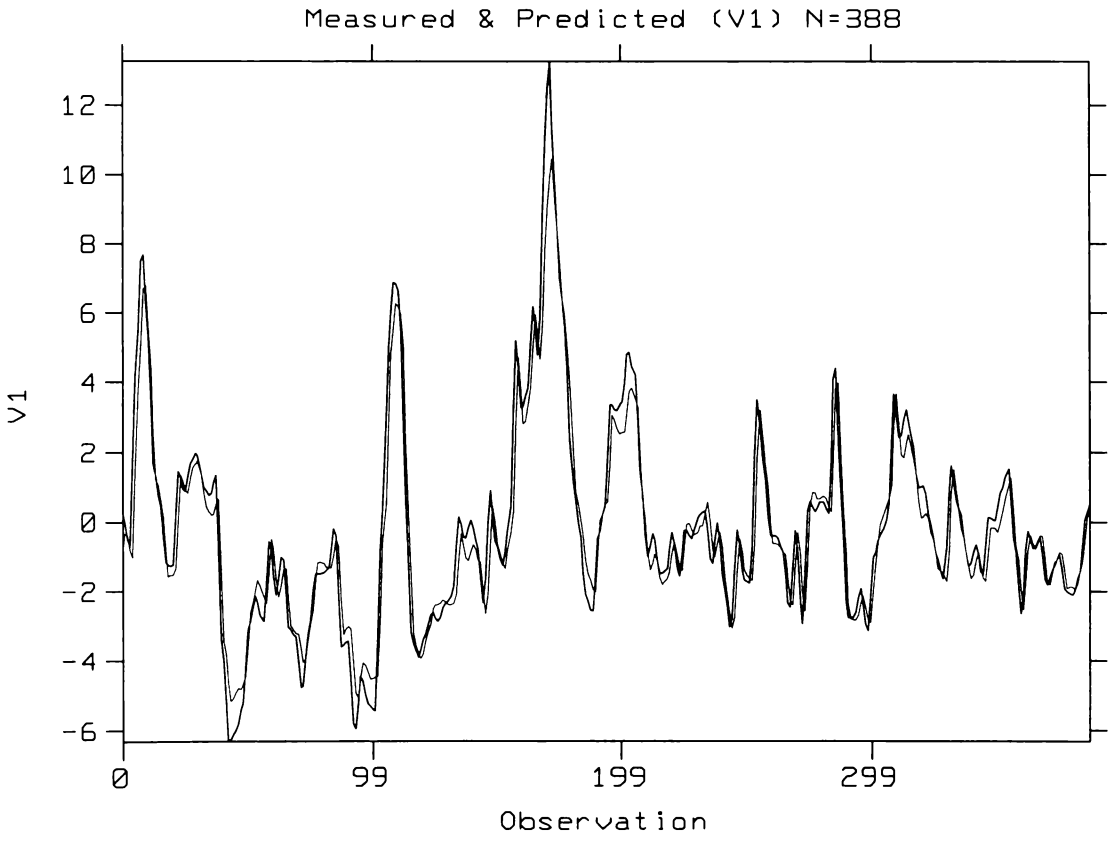

Figure 7- 4 A measured HRV and predicted HRV from NNARX (1 1 1) for subject No 5.

Variables		Mean	Std Dev	Minimum	Maximum	Sum Sq
Input	ILV(t)	-0.005203	0.467785	-0.769000	2.616000	84.903130
	SBP(t)	-0.104234	3.258409	-8.955000	9.241999	4119.4857
	HRV(t-1)	0.151846	2.142594	-4.449000	9.162999	1781.1942
Output HRV(t)	Measured	0.150787	2.142679	-4.448000	9.163999	1781.3361
	Predicted	-0.036284	1.944361	-4.052832	8.011460	1466.8497
	Residual	0.187070	0.773232	-2.261617	3.456700	231.98057
	R Square	0.915821				

Table 7- 1 Model statistics report for the subject in figure 7-4

A measured and predicted graph was generated for the test data segment to view how the model performed. This graph demonstrates that the model seems to capture much of HRV and the model with the simplest order seems to predict HRV fairly well.

A sensitivity analysis was run to see which variables account for most of the variability of HRV. The results are presented on the table 7-2. To compare the performance of the two variables, ILV and SBP, in attribution to the change of HRV, ILV has much higher percentage than SBP has.

Variable Name	Average of the absolute values of HRV (t) sensitivity	Peak sensitivity	Peak Row
HRV(t-1)	0.83785	+0.01011	105
ILV(t)	0.11632	+0.00177	24
SBP(t)	0.04583	+0.00080	372

Table 7- 2The sensitivity analysis of HRV to changes in ILV and SBP for the subject in figure 7-4

NNARX model sensitivity analysis was run for each of the eight healthy subjects. Table 7-3 shows the results. T-test for Dependent Samples was performed for

Average of the absolute values of the change in HRV (t) sensitivity to evaluate the differences between ILV and SBP. The results in Table 7-4 showed that the sensitivity of HRV to changes in ILV is significantly larger than that due to SBP.

Subjects	Average of the absolute values of HRV (t) sensitivity (%)			
	HRV(t-1)	ILV(t)	SBP(t)	R Square
1	0.70970	0.22702	0.06328	0.869336
2	0.60336	0.25349	0.14315	0.913573
3	0.81673	0.12577	0.05750	0.892461
4	0.76847	0.17507	0.05646	0.891095
5	0.83785	0.11632	0.04583	0.915821
6	0.83232	0.11900	0.04869	0.878280
7	0.93798	0.04077	0.02126	0.942506
8	0.77459	0.19729	0.02812	0.879234

Table 7- 3 The sensitivity analysis of HRV to changes in ILV and SBP in 8 healthy subjects

Valid Number of subject = 8	ILV (8)		SBP(8)		T- test	
	Mean	Std.Dv	Mean	Std.Dv	t	p
sensitivity (%)	.156841	.069433	.058036	.37337	5.432152	.00097

Marked differences are significant at $P < 0.05$

Table 7- 4 Result of T-test for Independent Samples to compare difference between the sensitivity of HRV to changes in ILV and one in SBP

7.7 Discussion

As we mentioned in Chapter 3, though the effects of respiration on heart rate in humans have been known for many years, a full explanation of these fluctuations is still unclear. We have proposed a model of a cardiovascular control system which suggests respiration oscillations, other than the arterial baroreceptors is the main contributor to the generation of RSA in healthy humans. In addition, this model can be applied to a patient without requiring any external stimulation. Moreover, we think that any artificial stimulation required for the assessment of RSA and any

approaches which may interfere with the neural control mechanism do not allow an adequate characterization of the dynamic features of RSA.

The most practical approach to assess the nature of RSA is based on system identification of the cardiovascular control system, which can provide the evaluation of RSA through a study of the relationship between input and output without an external stimulation of the patient. In this case, output HRV and two inputs, ILV and SBP are used to identify the parameters of a preselected mathematical model of RSA. Once the model has been analytically defined, sensitivity analysis of HRV to changes in ILV and SBP can be directly obtained from the model if the model is simple enough. It then offers the possibility of addressing important aspects of natural RSA that can only with extreme difficulty be investigated through experimental laboratory procedures involving humans. This is thanks to the neural network ARX model which is well suited for analyzing sensitivity of HRV to changes in ILV and SBP.

As a means of system identification techniques, NNARX has been popular recently in the area of the cardiovascular system [Chon and Cohen 1997. Hiroyuki. *et al.* 1994]. Their results have shown that the neural networks can provide accurate NNARX parameter estimation. In dealing with model HRV and ILV, Chon and Cohen [1997] reported that a slightly better model prediction is obtained by the neural networks than the least-squares method. However, in the physiological system modeling, one is often interested in determining separate input contributions to the system response. By using the NNARX model sensitivity analysis, different input contributions to the system response can be separately identified.

The results of the sensitivity analysis have shown that ILV has a much higher percentage of contribution to change of HRV than SBP has. The simplest explanation for this result is that the respiration oscillations play a major role in the generation of RSA in healthy humans. It therefore provides strong support for our model that the origin of RSA in the normal physiological condition is principally the central and not peripheral modulation of the baroreceptor.

Chapter 8

System Identification of Respiratory Sinus Arrhythmia

8.1 Overview

Through the interaction of the sympathetic and parasympathetic nervous system on the sinoatrial node, respiration-entrained oscillations cause the beat-by-beat variation in heart rate at the same frequency as respiration, which is known as respiratory sinus arrhythmia. Evaluation of RSA and its transfer function are of great interest from both a physiological and pathophysiological standpoint and it is believed to be a useful tool in examining the balance between autonomic parasympathetic and sympathetic modulation of the cardiovascular system [Piepoli *et al.* 1997, Muzi and Ebert 1993, Saul *et al.* 1991,1989]. For this part of the literature review, please refer Chapter 3.

In the previous chapter, our study suggested a substantial role for respiration oscillator in the origin of RSA in humans under natural physiological conditions. The model of the cardiovascular system is developed to give physiologically reasonable explanations of RSA. The results of the sensitivity analysis of HRV to changes in ILV and SBP using neural networks agreed well with our hypothesis. The dynamic behavior of RSA therefore can be investigated on the basis of the relationship between the fluctuations in ILV and HRV without taking into account the role that the variability of SBP plays in the phenomenon. The baroreflex does not

have an important influence on the generation of RSA, but acts as a local feedback control network of the cardiovascular system which tends to stabilize arterial pressure.

Accordingly, the application of system identification methods to the analysis of the fluctuations in ILV and HRV, based on the ARX model should provide useful information about the dynamic behavior of the autonomic nervous system. While ARX models with high model order selected by the model validity criterion, Akaike's Final Criterion (FPE) and his Information Theoretic Criterion (AIC) [Ljung 1987,1995], agree well with the observed data in random breathing, a question remains concerning the number of the model parameters. Does the model with high order describe the 'true system' and can the high order of the model be physiologically interpreted in accordance with *a priori* knowledge of the dynamic relationship between ILV and HRV? Central to the identification problem is the question of how to obtain a good model fit to the data with as few parameters as possible.

In this paper, we attempt to build a mathematical model which can capture the essential features of the dynamics while remaining simple enough to be useful for interpretation. Therefore, we have proposed an ARX model of low order to study the time domain transfer characteristics of fluctuations from ILV to HRV. Both the False Nearest Neighbors (FNN) algorithm [Rhodes and Morari 1997] and Visual Inspection of the Loss Function (VILF) [Ljung 1987, Bosch and Klauw 1994] have been used to determine the ARX model order. Regardless of what goes on inside the 'black box' if we ignore *a priori* knowledge of the dynamic relationship between ILV and HRV, both the FNN and VILF suggest that there is a little to be gained by high input order after proper selection of dead time. Furthermore, cardiac acceleration and deceleration is synchronous with respiration if proper delay has been inserted in HRV [Jennings *et al.* 1996]. The acceleration of heart rate can scarcely be affected by breathing 4 to 5 seconds earlier, again suggesting a low model order. Because the low order model contains few parameters, its impulse response, including its two exponential decay components, can be obtained directly from the model parameters.

The quality of the model estimate can be improved considerably by prefiltering the data with in addition proper selection of dead time to insure the system output reacts instantly to the applied input signal.

In this study, we aim to explicitly answer the question that has not been addressed in previous published work: What is the best order of an ARX model for the

cardiovascular system identification? In addition, we explore the influence of prefiltering data and the choice of the dead time.

8.2 Methods

8.2.1 Study subjects

The study was approved by the Waikato Regional Ethics Committee and full informed consent was obtained from all participants. Fourteen healthy volunteers aged between 19 to 39 years participated in the study. A three lead ECG and a respiratory trace were recorded from the subjects. The subjects had fasted for a minimum of two hours and were not on any vasoactive medication, and had not had any drink containing caffeine for 10 hours previously.

8.2.2 Measurement

Respiratory data was collected using a respiratory inductance plethysmograph [Respitrace 150 Studley Data Systems, Oxford]. The output was in DC mode with no autoreset. It was calibrated by having each subject fully empty and fill an 800-ml calibration bag. The ECG was taken from lead II of a standard ECG monitor [Nihon Kohden Lifescope 9]. This ECG and respiratory data were fed to a 386DX computer fitted with a 12 bit Keithley DAS-1200 Analogue/Digital I/O board [Keithley, Taunton, MA], where it was digitized using a sampling rate of 200 Hz for ECG and 20 Hz for the respiratory output to be stored on a personal computer for further analysis.

8.2.3 Experimental protocol

Heart rate and respiratory data were collected from each subject for runs of 300 beats. They were in a random order, in either regular or random breathing. In the random breathing pattern, subjects breathed irregularly according to the random modified Poisson distribution, as proposed by Berger *et al.*[1989], to produce a broad band respiratory signal. In both regular and random breathing, the timing of each breath was determined by a bleep produced by a computer, according to a

simple program. In the random breathing pattern runs, the computer warned the subject of the duration of each forthcoming breath by displaying the time (seconds) on the screen. Therefore, if it was a long duration breath, the subject was able to take a somewhat bigger tidal volume commensurate with the anticipated apnoeic period.

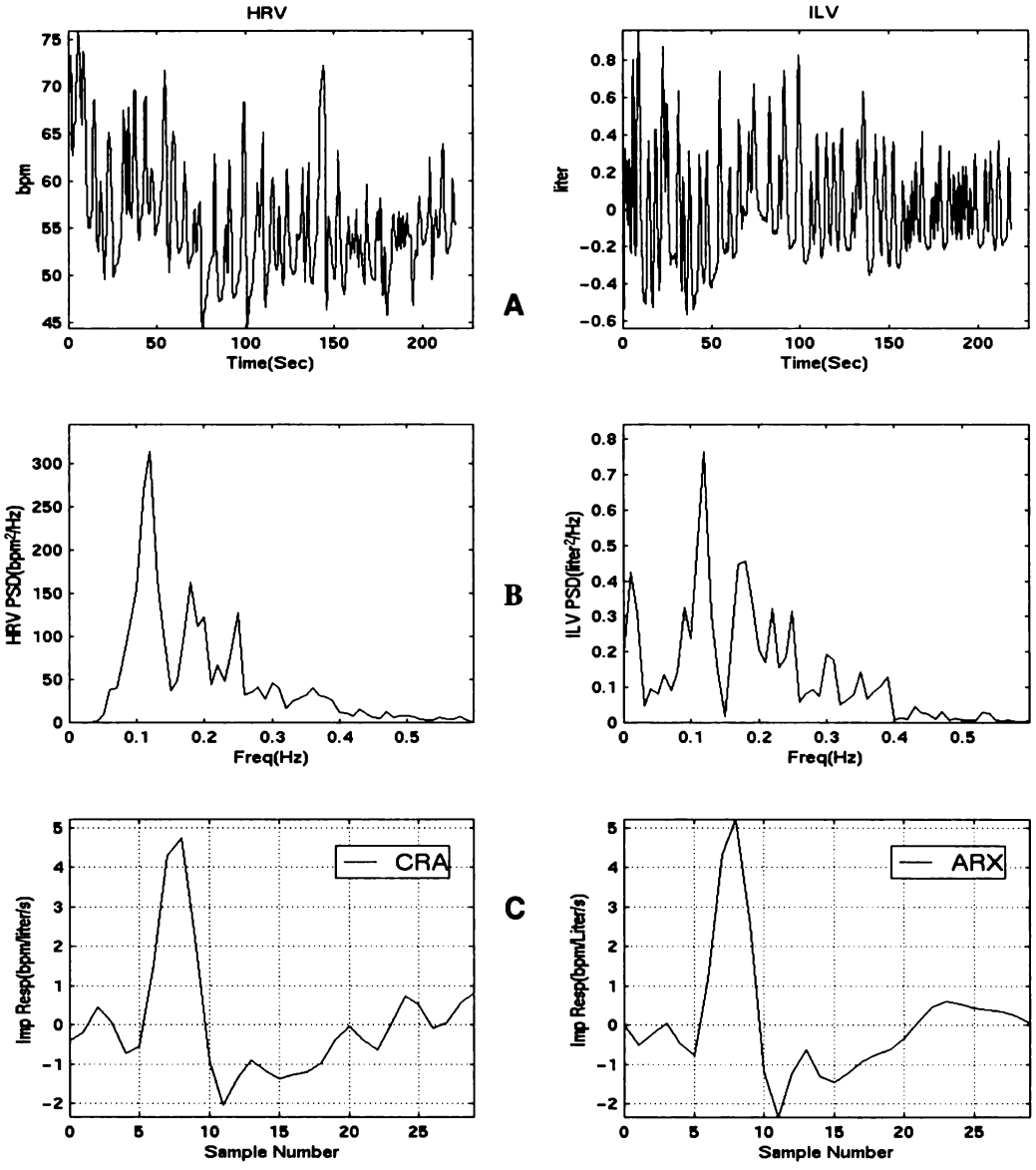

Figure 8- 1 HRV and ILV time series during random breathing (A), their power spectral density (B) in a heathy subject and the dead time estimation by the correlation and ARX model method (C).

8.2.4 Data analysis

The data was acquired and pre-processed on-line using purpose written programs in C++ language. The QRS complex of ECG was detected and the peak of R wave located to within +/- 1ms using quadratic interpolation. All the R-R intervals and ILV were edited automatically, and then by visual inspection, to exclude all the

undesirable peaks, which accounted for <1% in every subject. A smoothed instantaneous HRV time series was constructed at 2.56 Hz. The ILV records were calibrated and then decimated to 2.56 Hz.

We used Welch's averages periodogram algorithm for computing the power spectrum, cross spectrum, coherence and transfer function. The HRV and ILV data were detrended, Hanning windowed and fast Fourier transformed, using common MATLAB routines [Krauss *et al.* 1994]. The RID is computed by using Matlab Time-Frequency Toolbox [Auger *et al.* 1996].

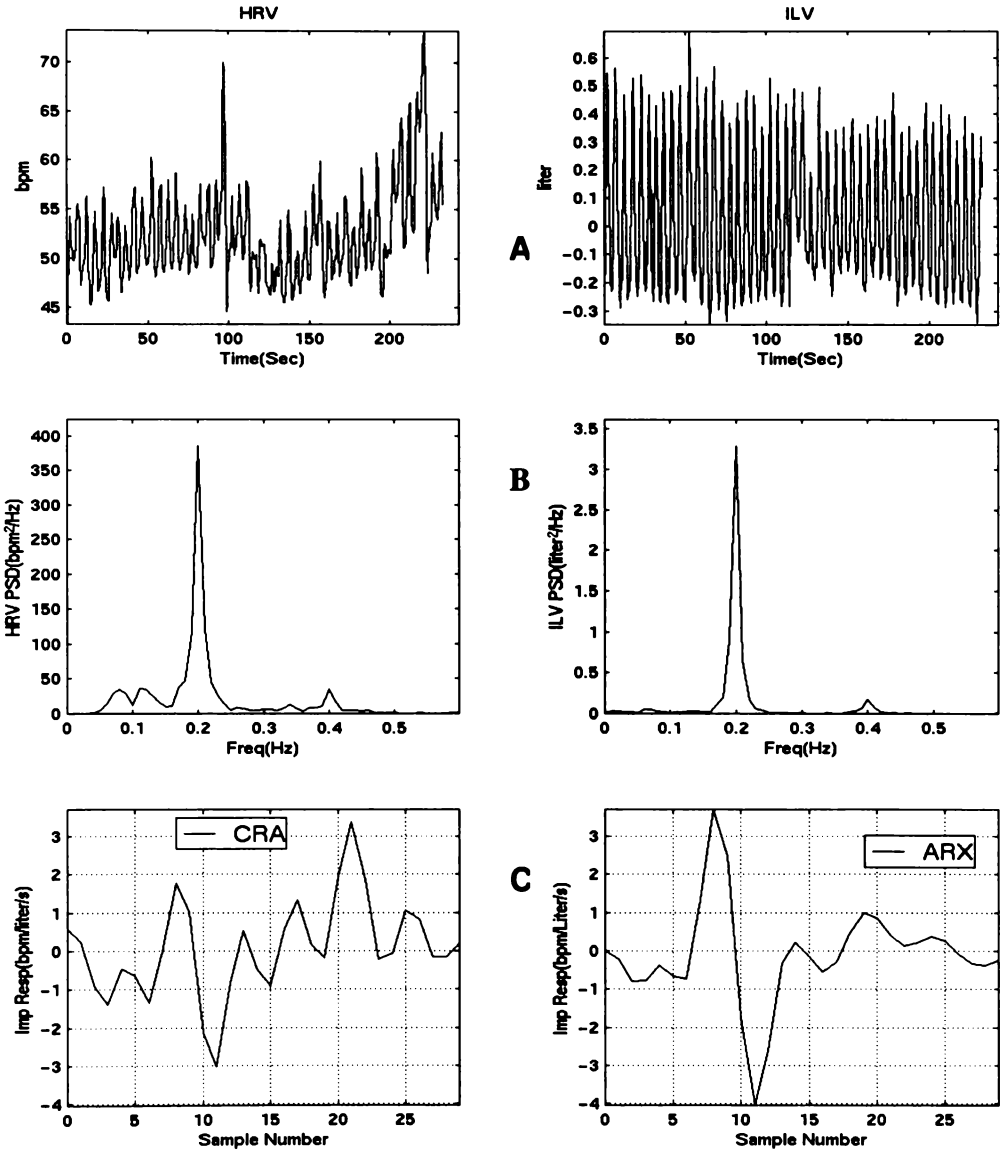

Figure 8- 2 HRV and ILV time series during regular breathing (A), their power spectral density (D) in the subject presented in Fig.8-1 and the dead time estimation by the correlation and ARX model method (C).

8.3 Results

To better explain how the lower order ARX model identifies the system and estimation of the impulse response of HRV to ILV, the typical results for one of 14 subjects will be used as an example and are shown in this section, which provide a quantitative representation of the cardiovascular regulatory state of the individual while related and supine quietly. Our findings for all subjects will be summarized in the next chapter.

8.3.1 The ARX model determination

Fig. 8-1 (A, B) shows a typical example of the fluctuations of HRV and ILV when the subject was in a random breathing pattern together with their power spectral density. In addition, Fig. 8-2 (A, B) shows an example of the fluctuations of HRV and ILV together with their power spectral density in a regular breathing pattern with the same subject.

The effects of different filters on the stationarity of the HRV signal in random breathing were explored by use of the recurrence plot, which is shown in Fig. 8-3. It is obvious that most of the non-stationarity of HRV is concentrated in frequencies below 0.04 Hz. Hence, we used a fifth order zero phase shift Butterworth bandpass filter with passband 0.04 to 0.5Hz.

In cases with random breathing, the dead time was estimated by both the correlation analysis method and the ARX method. In agreement, both methods suggested the dead time to be 6 samples, 2.34s, which can be seen in Fig. 8-1 (C). For regular breathing in the same subject, the dead time, six samples, were obtained by the ARX method as shown in Fig. 8-2 (C).

To get the model order, FNN analysis was performed for all the random and regular breathing pattern data. The threshold for False Nearest Neighbor (FNN) Analysis was 17.3, and the number of Data Points was 561. Obviously, the percentage of false nearest neighbors (FNN%) goes to zero when there are enough input and output lags to make a good model. Referring to Table 8-1 for one example, the FNN suggests that both ARX model order nn = [4 2] and nn= [3 3] is a possible selection. Visual inspection of the loss function was also performed for the same data, as shown in Fig. 8-4. Order nn = [4 2] was a reasonable selection for the ARX model. Hence, the order selected was: $n_a = 4$, $n_b = 2$.

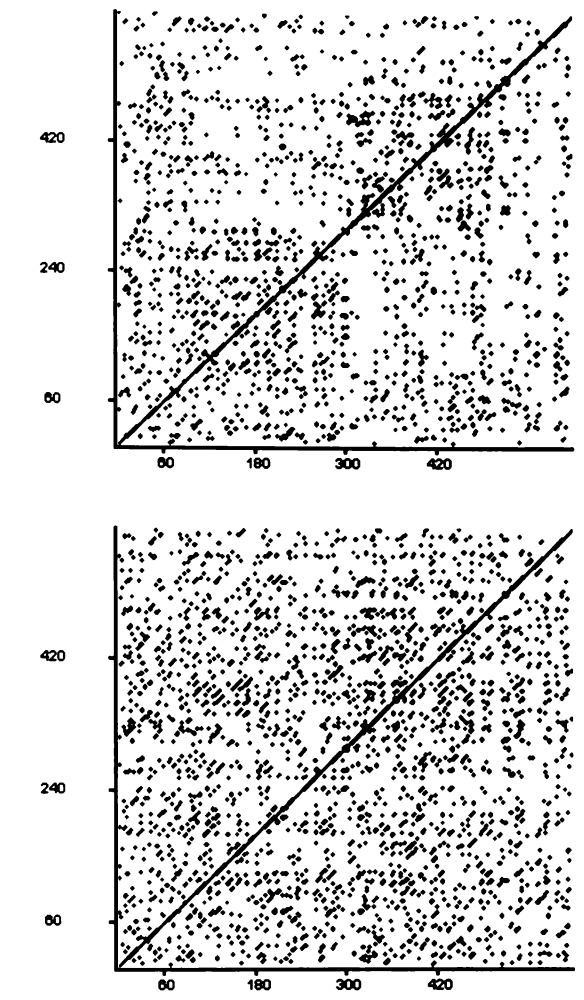

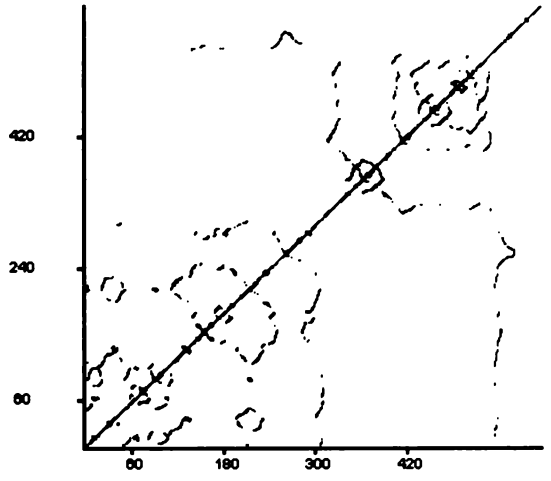

Figure 8- 3 Recurrence plots for different frequency range for non-stationary analysis in the subject presented in Fig. 8-1. A. Original HRV data. B. HRV data with high pass filter 0.04 Hz. C. HRV data with low pass filter 0.05Hz. Both axes are sample numbers

Input ILV / Output HRV Order

$n_b \backslash n_a$	0	1	2	3	4	5
0	100.00	96.786	51.341	15.950	6.284	2.878
1	52.679	55.179	9.302	1.971	0.718	0
2	84.417	27.013	2.683	0.358	0	0
3	67.742	13.441	0.896	0	0	0
4	50.100	4.847	0.539	0	0	0
5	35.791	2.158	0.540	0	0	0

Table 8- 1 False Nearest Neighbor Percentage Table Entries are % of False Nearest Neighbors in the subject presented in Fig.8-1.

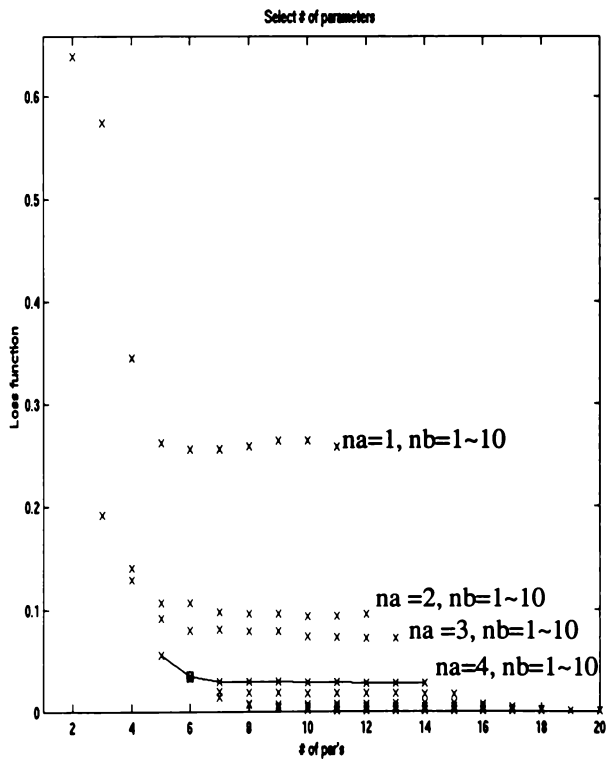

Figure 8- 4 Visual inspection of the Loss Function to see how the fit changes with the umber of estimated parameters in the subject presented in Fig. 8-1.

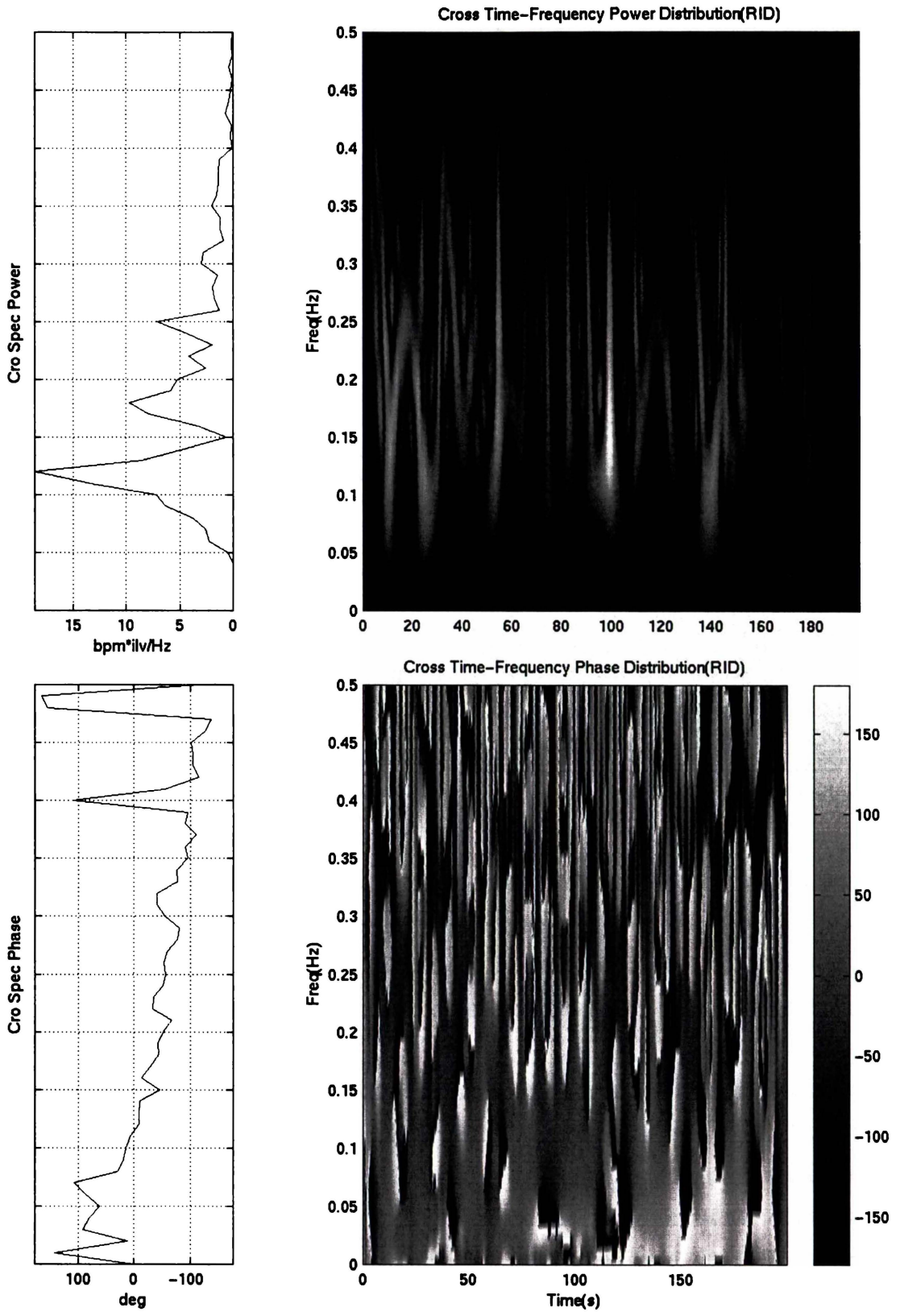

Figure 8- 5 The cross spectrum and cross time-frequency distribution (RID) during random breathing. Upper is cross-amplitude spectrum and cross-energy time-frequency. Lower is phase spectrum and cross phase distribution (All data from the subject presented in Fig. 8-1).

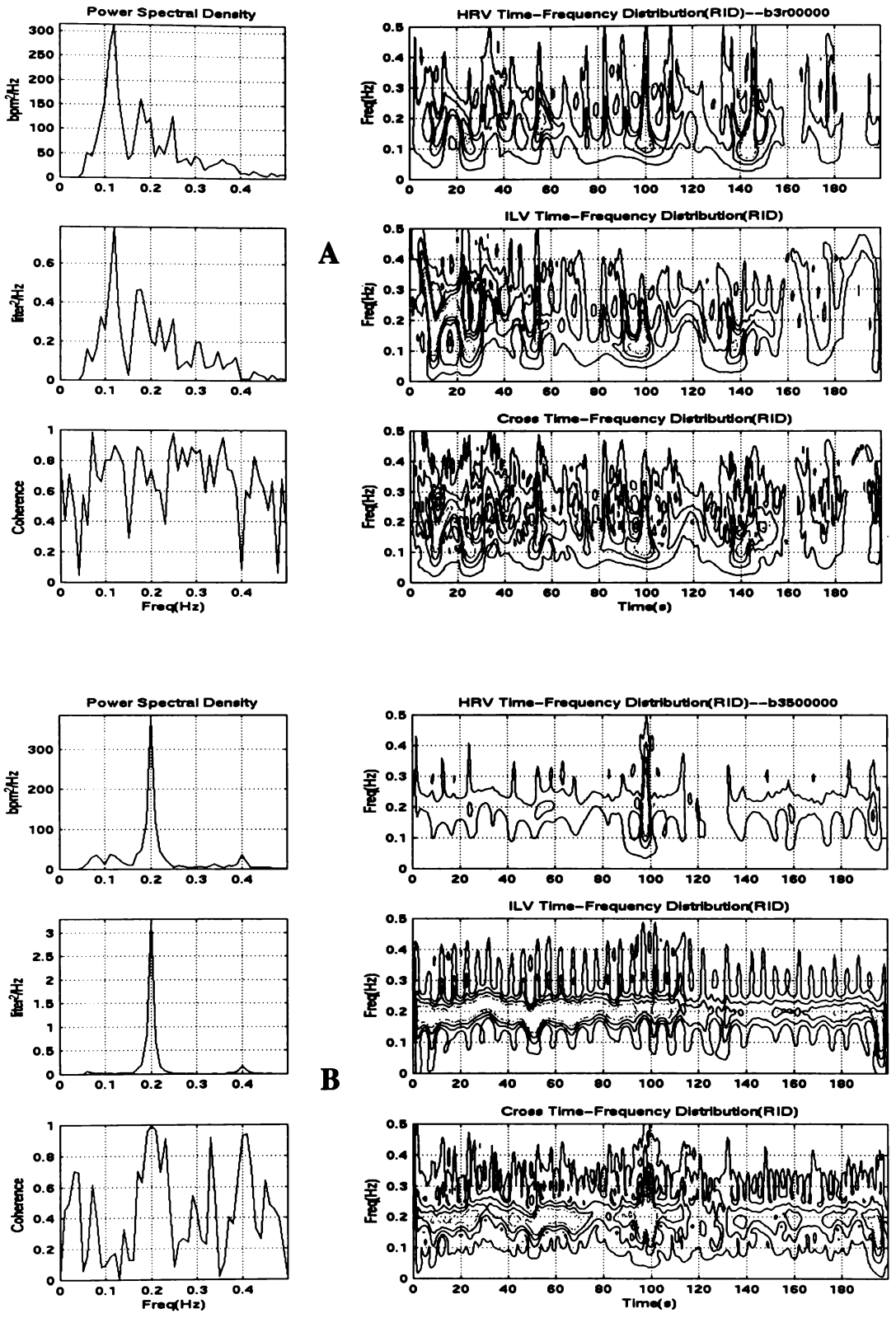

Figure 8- 6 A. The spectrum of HRV and ILV, their auto-RID, coherence and cross RID during random breathing. B. The spectrum of HRV and ILV, auto RID, coherence and cross RID during regular breathing (All data from the subject presented in Fig. 8-1).

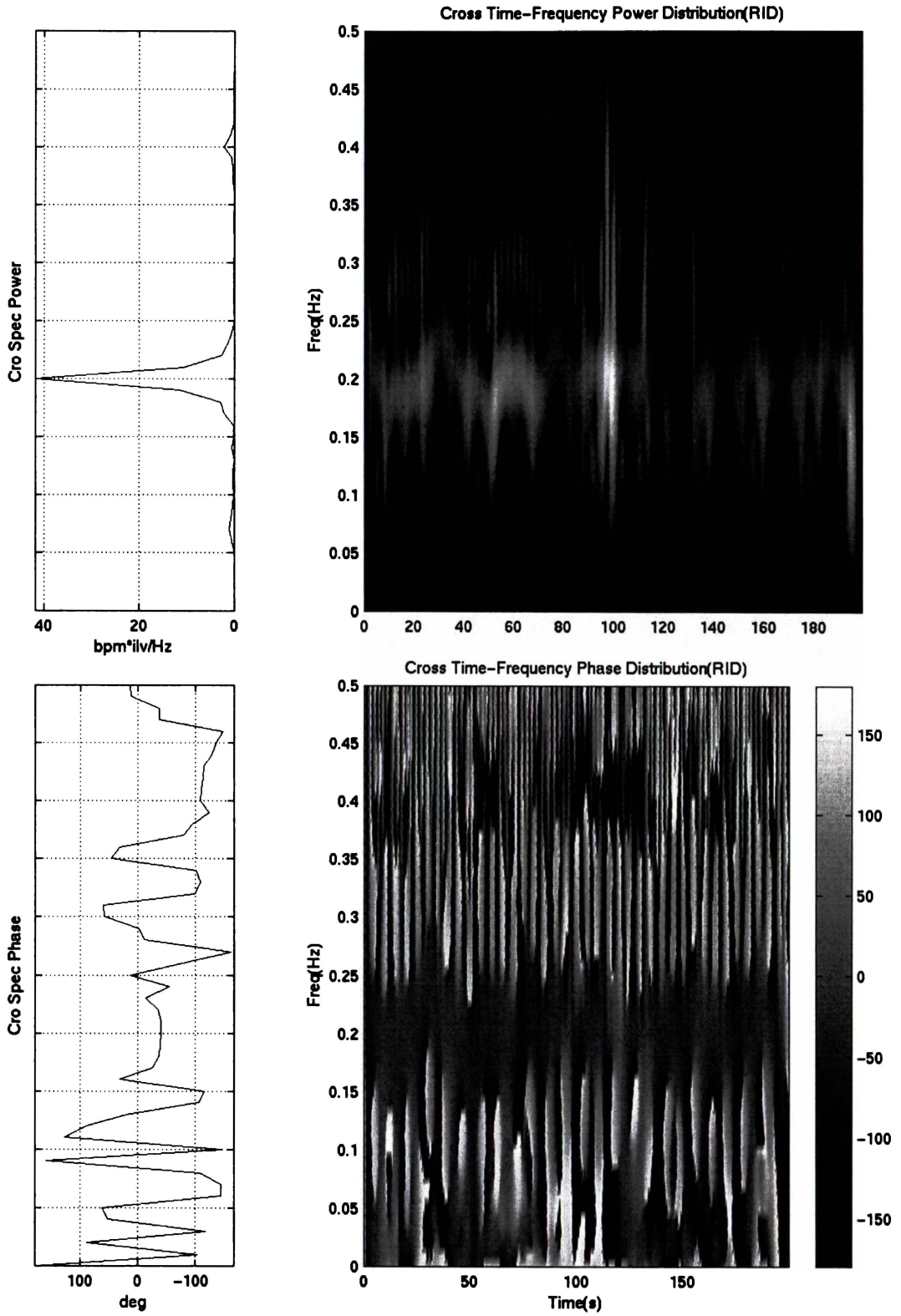

Figure 8- 7 The cross spectrum and cross time-frequency distribution (RID) during regular breathing (0.2Hz). Upper is cross-amplitude spectrum and cross-energy time-frequency. Lower is phase spectrum and cross phase distribution (All data from the subject presented in Fig. 8-2).

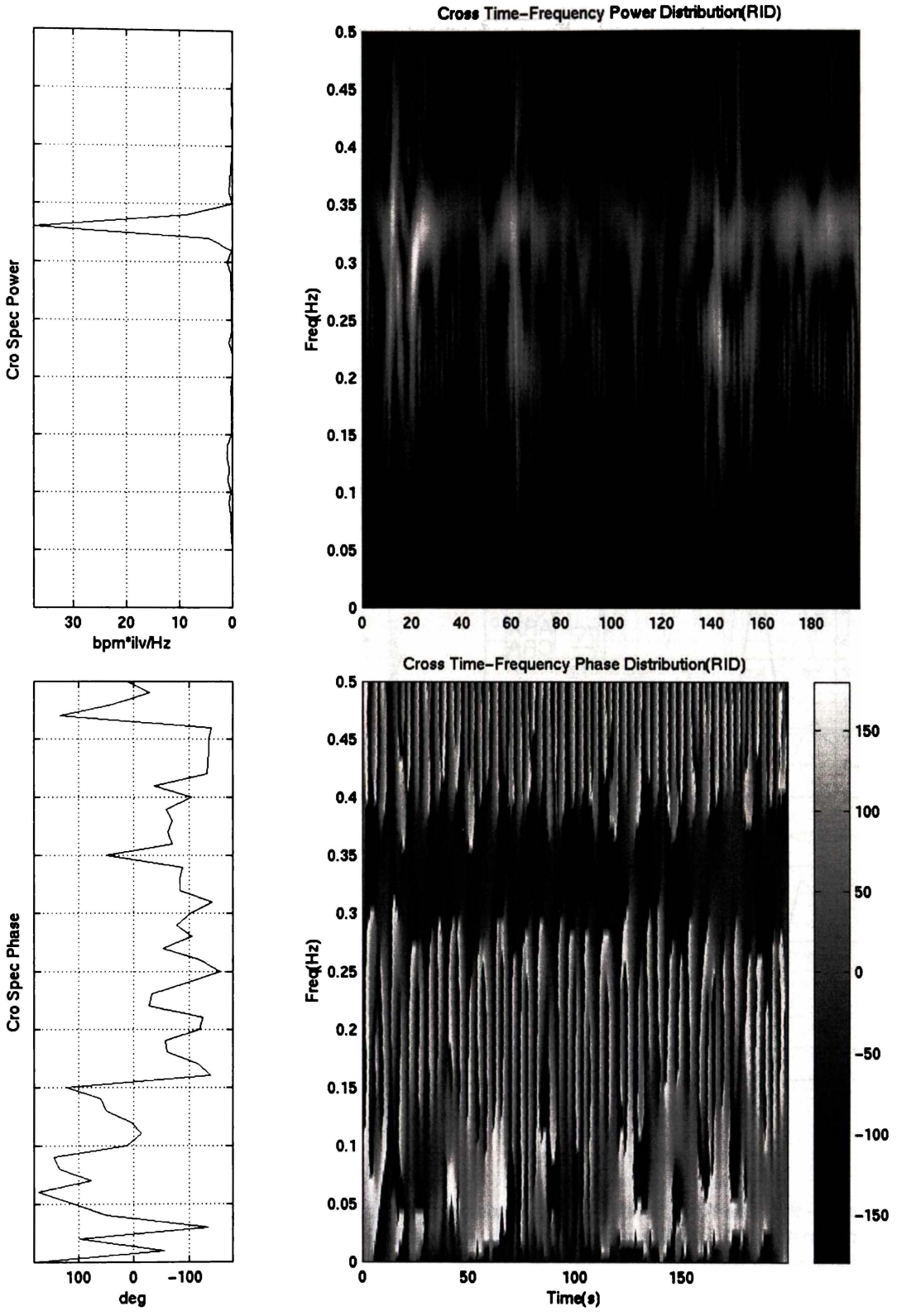

Figure 8- 8 The cross spectrum and cross time-frequency distribution (RID) during regular breathing (0.35Hz). Upper is cross-amplitude spectrum and cross-energy time-frequency. Lower is phase spectrum and cross phase distribution (All data from the same subject presented in Fig. 8-2).

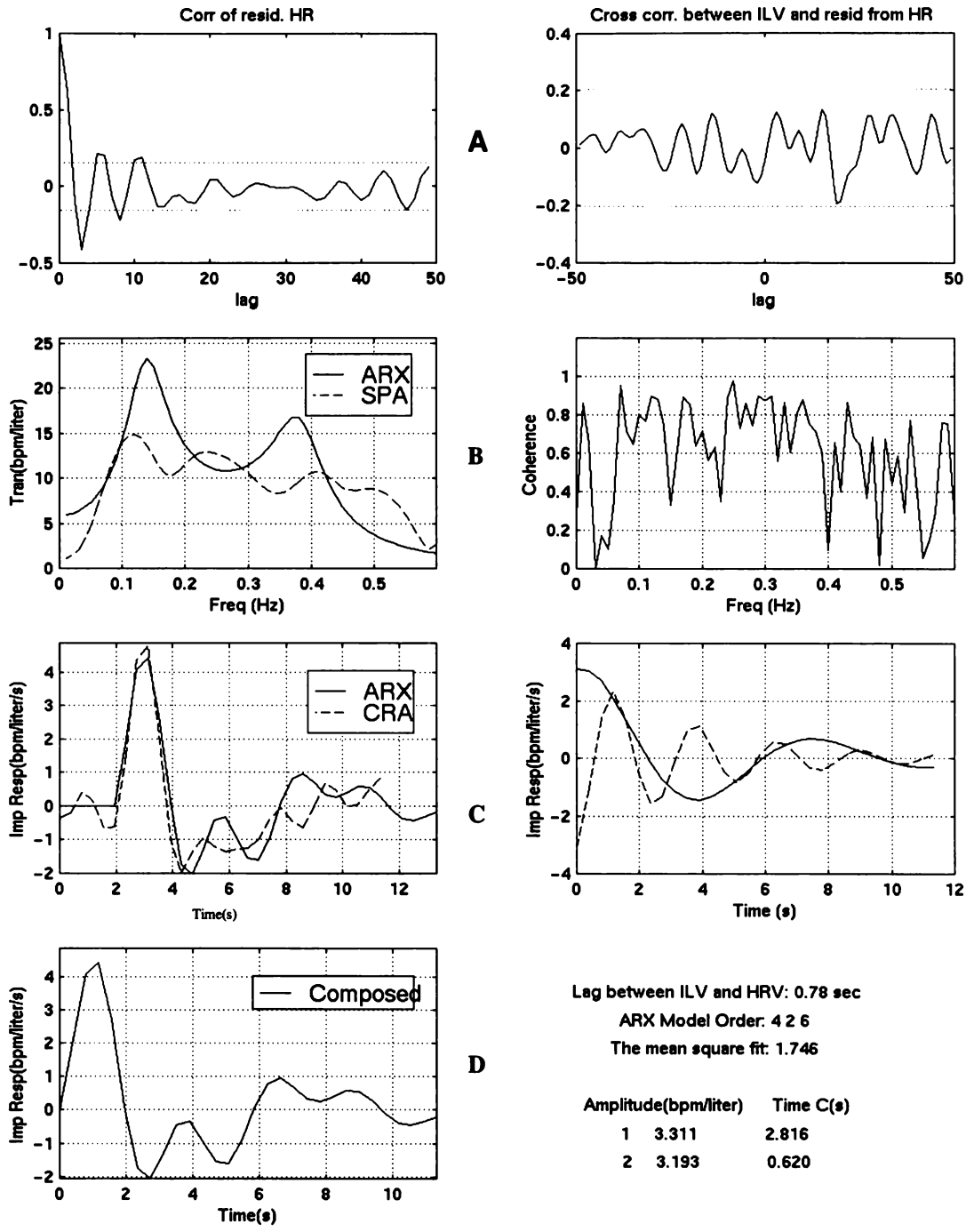

Figure 8- 9 The ARX model during random breathing, residual analysis (A), transfer function characteristics (B), impulse response and its low and high frequency components (C). The impulse response synthesized from high and low frequency components determined by the model parameters. (D). (All data from the subject presented in Fig. 8-1).

The auto RID of HRV and ILV, the cross spectrum, and cross RID of HRV and ILV in the random breathing pattern and regular breathing pattern are presented in Fig. 8-5, 8-6, 8-7, and 8-8. For random breathing, cross-RID extract the instantaneous energy components of HRV due to the respiration in the broad frequencies region

while for regular breathing, in very narrow frequencies regions, which are not available by cross spectrum analysis. Further more, the delay between HRV and ILV is obviously shown in the phase distribution.

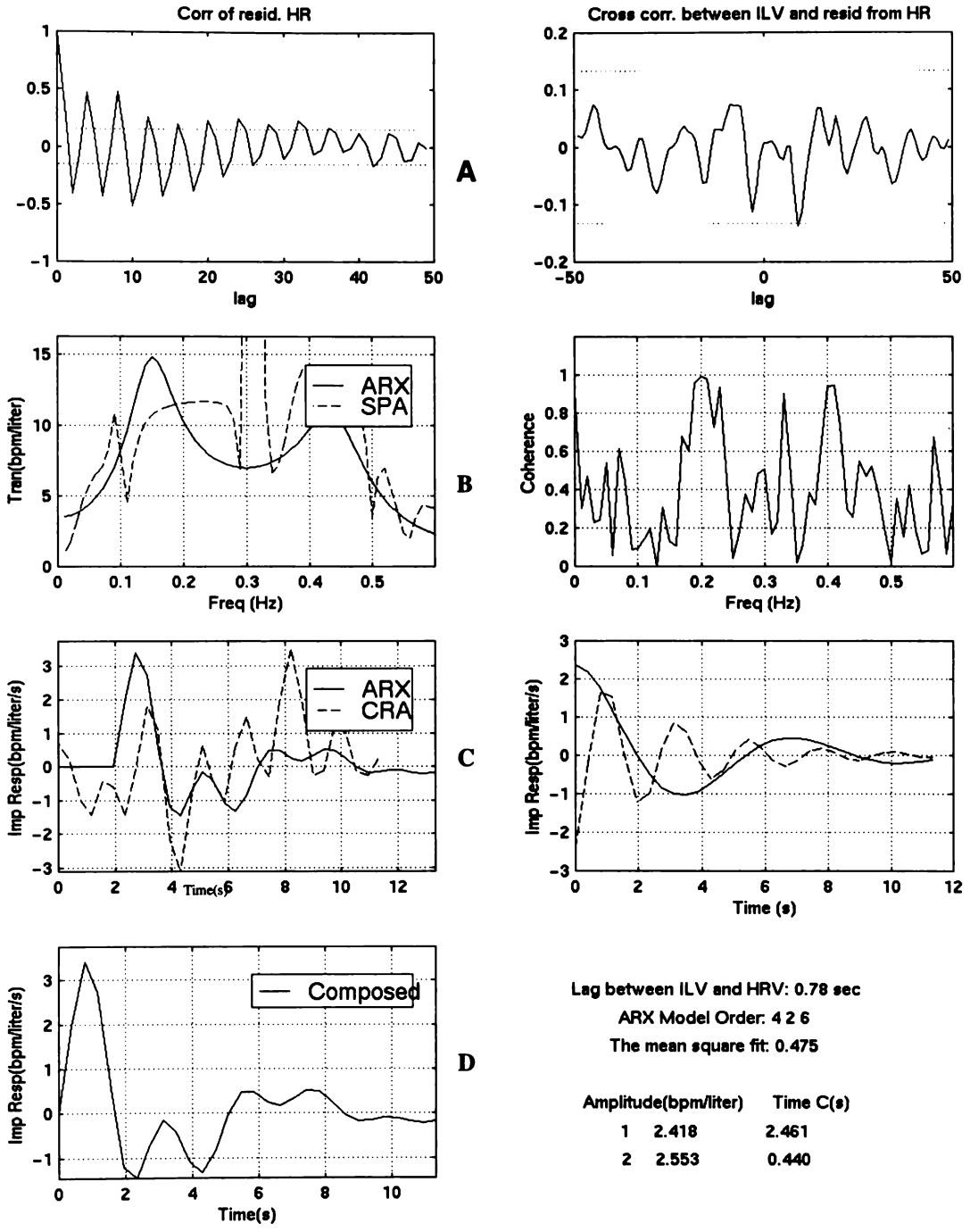

Figure 8- 10 The ARX model during regular breathing, models residual analysis (A) transfer function characteristics (B), impulse response and its low and high frequency components (C). The impulse response synthesised from high and low frequency components determined by the model parameters. (D). (All data from the subject presented in Fig. 8-1).

8.3.2 The ARX model validation

Model validations based on residual analysis (Figs. 8-9A, 8-10A) and on cross validation were performed. For the latter a simulation of the ARX model derived from random breathing data was run with input from regular breathing (Fig. 8-11). Both methods demonstrated that the ARX model of low order is an adequate model. Fig. 8-10 summaries the results of the ARX model with the regular breathing pattern input. Its impulse response and transfer function is very similar to those for the random breathing pattern (Fig. 8-9). Fig. 8-11 (B, C) presents the results of the comparison of the measured HRV and its power spectral density (in regular breathing pattern) with the simulated HRV and its spectrum estimated by the ARX model (in random breathing pattern). A significant linear relationship was noted in both time and frequency range. Moreover, residual analyses of the random breathing ARX model using regular breathing data were performed to evaluate model qualities (Fig. 8-11 (A)).

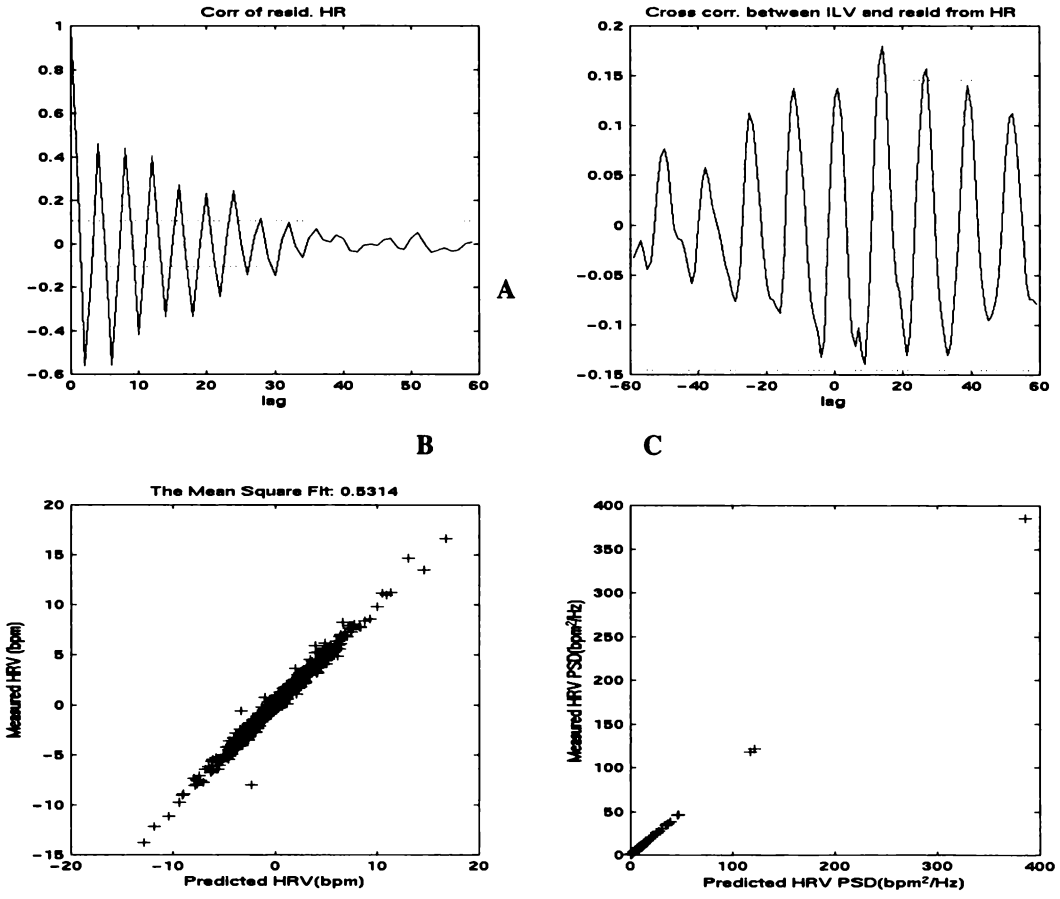

Figure 8- 11 Residual analysis (A) and comparison of HRV as estimated by ARX model build up by random breathing and measured regular breathing HRV in the subject presented in Fig. 8-1. B. Measured HRV vs. predicted HRV. C. Power spectral density of measured HRV vs. power spectral density of predicted HRV.

Fig. 8-9 and Fig. 8-10 shows the impulse response of an ARX model, order (4 2 6), identified from both random and regular breathing data and by the correlation method (labeled CRA in Fig. 8-9 (C) and 8-10 (C)), which represents the response of the HRV with a 1-liter impulse applied to ILV. Good agreement is seen in the random breathing and less agreement in regular breathing.

Furthermore, as illustrated in Fig. 8-12, the impulse responses from the ARX model in low order is remarkably similar to one from ARX model of the high order, which was calculated by Akaike information criterion (AIC).

8.3.3 Parameters of the Impulse response

The impulse response was decomposed into 2 exponential decays, the fast and the slow response components, which are shown in Fig. 8-9 for random breathing and in Fig. 8-10 for regular breathing. Each component has two parameters: amplitude and time constant, which are estimated and listed in Fig. 8-9, 8-10. Corresponding to these components in the time domain, we can find two related peaks in transfer function, one is around 0.12 Hz and other is around 0.4 Hz (See Fig. 8-9,8-10).

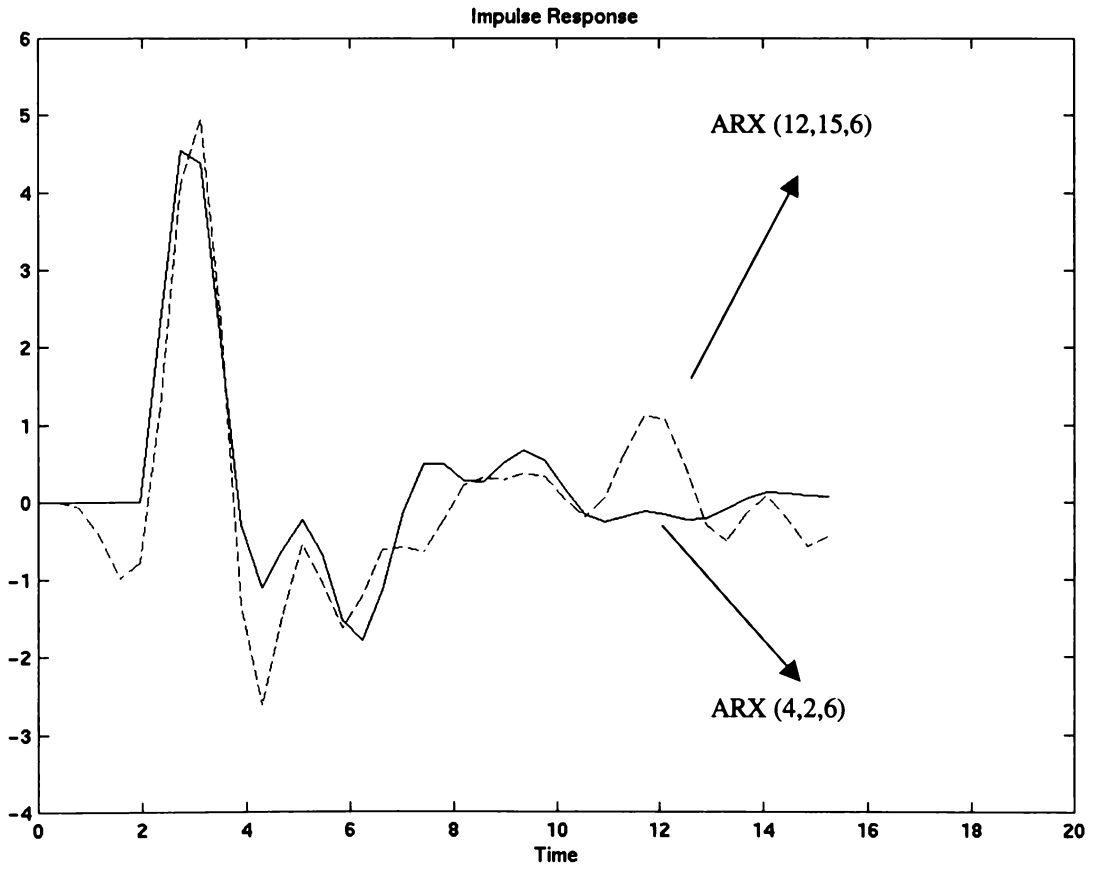

Figure 8- 12 Compare the impulse response from ARX (4,2,6) and ARX (12,15,6) in the subject presented in Fig.8-1.

Although the above is only one example taken from 14 healthy subjects, the observations and results described in this chapter are consistent with data for all 14 subjects. As well, we evaluated the low order ARX model for these 14 subjects during random and regular breathing during altered autonomic states. The quantitative significance of these results are reported statistically in the next chapter.

8.4 Discussion

The results presented above confirm the work of previous investigators [Chon. *et al.*, 1996,1997, Saul. *et al.* 1989, 1991, Triedman *et al.* 1995, Kim and Khoo 1997, Yana. *et al.* 1993] showing ARX techniques can be used to construct a time domain model of HRV regulation by the autonomic nervous system. Unlike previous investigators, we have explicitly addressed the problem of the dead time, filtering, ... etc. We have also been able to get equivalent results with a low order ARX in 14 healthy subjects – much more physiologically meaningful. We have demonstrated in this chapter that the ARX model with a low order and single delay is a simple and efficient tool for handling HRV in the cardiorespiratory system when random breathing or regular breathing occurs.

8.4.1 Selection of ARX model order

Determination of an appropriate model order is a major concern when using the ARX model to represent the system's dynamics. Selection of the structure that has the smallest loss function for the fresh data set is a good way to approach the model selection problem. Theoretically, the loss function should tend to a minimum value with increasing model order. Increasing the model order beyond the true order of the process will not add to the quality of the model. In addition, the more parameters which need to be estimated the higher is the variance of the estimates and the impulse response will be too sensitive to corruption by noise. Moreover, it is difficult to interpret the physiological meaning of the ARX parameters if the model is overparameterized. Conversely, the model order should not be selected too low, since an underparameterized model will lack the degrees of freedom necessary to describe the dynamics of the corresponding physical system. Ideally, for a system we would like a low order model that accurately describes the system dynamics. There is a tradeoff between the accuracy of the model and the simplicity of model

structure. The FNN method appears to be a simple, efficient procedure for determining the best ARX model order. Our experience illustrates the success of the FNN in determining the smallest regression vector allowing adequate prediction of the output.

8.4.2 Effects of prefiltering

Filtering strongly influences ARX modeling and identification results. Frequencies above 0.5 Hz were filtered out, because they are above the range of HRV output. Oscillatory frequencies below 0.05 Hz have been attributed to a thermoregulatory feedback mechanism [Muzi and Ebert 1993]. For our healthy subjects, in a random breathing mode, HRV output has much more low frequency content than in regular breathing. Therefore, the thermoregulatory feedback mechanism can not be considered the only factor. Model prediction was affected seviouly by these slow oscillations. Most of the nonlinear contribution to HRV is concentrated at frequencies below 0.05 Hz [Chon *et al.* 1996] and the nonlinear dynamics in heart rate variability do not arise as a consequence of nonlinear input from the respiration to the cardiovascular oscillator [Kanters *et al.* 1997]. Moreover, most of the non-stationarity of HRV is concentrated in the frequencies below 0.05 Hz according to results of our recurrence plots of HRV. As is to be expected, the residual error produced by the ARX model estimated from random breathing data increases when input data from regular breathing is used for validation. Hence, prefiltering for removal of low frequencies is necessary and is a complement to detrending. Not surprisingly, filtering the data before estimation, through a bandpass filter improves the fit in our region of interest.

8.4.3 Cross distribution

For random breathing, the cross-RID of the HRV and ILV in Fig. 8-6A contain significant energy in the region of the t-f plane, where components in the HRV and ILV are similar. Components in frequencies 0.04-0.5 Hz have similar t-f structure in the auto-RID evaluation. This cross RID presented here indicates that the seizure signal components in the frequency band 0.04-0.5 Hz are common to HRV and ILV signals. The system identification based on the linear ARX model assumed the relation between ILV and HRV to be linear in the analysis by the coherence function which is sufficiently large in our modeling frequency range of 0.05-0.5 Hz.

However, in addition the RID evaluation for HRV, ILV and cross HRV and ILV indicates the high coherence in t-f plant. The regular breathing data also show the same feature, but with a narrower frequency band.

The cross time-frequency distribution provides a tool to analyze phase shift between HRV and ILV. Its phase shift distributions for regular breathing at different rate shows that a phase shift between HRV and ILV depends on the respiratory frequency in agreement with the findings in the literature [Zhang *et al.* 1997], which suggested that phase changes of HRV in response to ILV stimulation is frequency-dependent. In random breathing (Fig. 8-5), the phase change with time in all frequency ranges is presented. Whereas, in regular breathing (Fig. 8-7 and 8-8), the phase keeps relatively constant in respiratory frequency. Furthermore, comparing regular breathing at 0.2 and 0.35 Hz respiratory rate, a different delay between HRV and ILV is shown in the cross-RID. Therefore, change of time delay between HRV and ILV in random breathing for different individual subjects can be explained by phase shift.

8.4.4 The low order ARX model

One of the major findings of this study is that for both random and regular breathing patterns, the quality of the low order ARX model, for the relationship between respiration and heart rate, was proved to be good in the following respects. Firstly, residual analysis showed that the correlation function lies significantly inside the 95% confidence intervals. Next, there is a very good agreement between the impulse response of our ARX model and one that was estimated using correlation analysis for a random breathing pattern. Thirdly, employing ARX model structures should offer good capabilities of describing different possible input patterns. It is not surprising that the model will perform well when evaluated by its performance for the same input breathing pattern. For our healthy subjects, the ARX model of the relation between random breathing and heart rate successfully predicted the heart rate output with fresh random breathing data sets. The real test is whether it is also capable of also predicting heart rate from fresh regular breathing data sets. Fig.8-7 shows the excellent performance for this cross validation. Hence, the system characteristics with a different breathing pattern input were reflected in the same ARX model. When we used the ARX model with order nn = [4 2 6] to model the same healthy subject in both random breathing pattern and regular breathing pattern, our study demonstrated another important point. It was observed that model transfer

processes was the explanation of the impulse response. Actually, the component associated with the sympathetic system is different from the one in Yana's model. The enhancement of the HRV at low frequency could originate from the decrease of the mean vagal as well as sympathetic tones [Berger *et al.* 1989], it is therefore difficult to directly relate the specific spectral peaks to the sympathetic or parasympathetic tones. In addition, it is hard to divide an impulse response into sympathetic and parasympathetic components mathematically because they have common frequency responses in the low frequency range of HRV spectrum. In Triedman's model, sympathetic components include the oscillatory component which was indicated by Yana's model. The overshoot in the impulse response is attributed to this low damping in the system.

It is known that the autonomic control of heart is the result of opposing sympathetic (stimulatory) and parasympathetic (inhibitory) influences, and these two systems work together to elicit a response [Tortora 1987]. Therefore, HRV response for sympathetic input should be simultaneous, other than with in a series of pure delay of 1.7 seconds as suggested in Yana's model.

In our model, the impulse response decomposed to a fast increase in HRV and slow decrease in HRV, which corresponds to the two peaks each in the transfer function of the frequency domain. These two components of impulse response of HRV reflect autonomic nervous modulation of cardiorespiratory interaction, where the fast component reflects the change of HRV due to parasympathetic input and the slow component is attributed to both sympathetic and parasympathetic input.

In this chapter, we have proposed a low order ARX model for the study of the time domain transfer characteristics of fluctuations from ILV to HRV in healthy subjects. In addition, system identification using the lower order ARX model was evaluated with a view to its capability to differentiate between altered autonomic states induced by breathing patterns and posture in healthy subjects. This is because an important consideration in assessing the success of the system identification procedure is to determine whether the results are consistent with accepted physiological findings. Results of a study based on data from 14 subjects will be discussed in detail in the following chapter.

characteristics estimated from the ARX model coefficients, such as impulse response and transfer function were quite similar as is shown in Fig. 8-9, 8-10. Moreover, we have compared impulse responses from the low order ARX model with one from the high order ARX model as shown in Fig. 8-12. The similarity between the impulse responses strongly supports the ARX model with low order. All the above indicate that this ARX model in low order has captured the essential features of the dynamics. Therefore, the simplicity of our ARX model is well suited to contribute to the explanation of the qualitative properties of respiratory sinus arrhythmia.

8.4.5 Components of the impulse response

A model is used to describe the salient features and behavior of the system under study. Accordingly, we note the ARX model of low order employed in this study not only provides a useful and quantitative means for evaluating the transfer characteristics from fluctuations of ILV to HRV, but also makes it possible for the impulse response to be analytically decomposed to two components from the model parameters. In Yana's analysis, the impulse response was first estimated and then modeled again as the sum of two exponentials with a variable delay. These were presented as three components: the fast positive, the delayed slow negative, and the oscillatory components. [Yana *et al.* 1993]. Whereas in our method the components of the impulse response can be obtained directly from parameters of the low order model, which correspond to the two corners in the transfer function in the frequency domain. Obviously, the physiological meaning of these components has the potential to provide insights into the cardiovascular system.

The interpretation of the components is different from Yana's. The physiological meaning of these components in Yana's model is suggested by a previous study in the frequency domain [Saul *et al.* 1989]. Associated with vagal efferent activity, the fast positive component model acted as a single pole low-pass filter in series with an inverter. The slow negative component represents sympathetic efferent activity as a second order low-pass filter in series with a pure delay of 1.7 seconds.

Triedman *et al.* [1995] produced a similar impulse curve using an ARX model which included an immediate and brief increase in HRV and a simultaneous but slow and low magnitude decrease in HRV. The authors associated the two components with a simultaneous withdrawal of sympathetic and vagal nervous control of the heart during inspiration. The difference in time course for the two

Chapter 9

Model Parameter Analysis of RSA Applied to Experimental Subject Groups

9.1 Introduction

Application of the low order ARX model can quantify specific parameters leading to a new insight into the physiological regulation of Heart Rate. Model parameter analysis of the respiratory sinus arrhythmia provides information in addition to that obtained by means of the well-known spectral and cross-spectral analyses of variability signals. This approach could improve knowledge of the respiratory sinus arrhythmia mechanisms involved in heart rate and respiration relationship in both physiological and clinical conditions.

By using a low order ARX model with its simplicity, model parameter analysis of the respiratory sinus arrhythmia can process signals to characterize quantitatively the system and evaluate how the respiratory sinus arrhythmia adapts in response to varying physiopathological conditions.

In this chapter, we apply the low order ILV-HRV ARX model developed in Chapter 8 for determination of RSA to data obtained from two subject groups: healthy subjects and patients. Model parameter analysis of RSA allows us to evaluate the differences found in the assessment of autonomic control brought about by variations in breathing pattern and in posture in healthy subjects and by variation of sympathetic tone in patients.

9.2 Methods

In this study, we used data obtained from the same healthy subjects group as selected from in Chapter 8. Therefore for measurement, experiment protocol and data analysis used for the healthy subject group in this chapter, please refer to section 8.2.2 and 8.2.3. In this section, we focus on methods used for the patient subject group.

9.2.1 Subjects

All subjects gave their consent, and the study was approved by the Waikato Regional Ethics Committee.
We had two main groups of subjects participating in the study. In group one, 14 healthy subjects were included, i.e. the same subject group as described in Chapter 8. In group two, 49 general patient subjects joined in the test. A three lead ECG and a respiratory trace were recorded from the subjects. The subjects had fasted for a minimum of two hours and were not on any vasoactive medication, and had not had any drink containing caffeine for 10 hours previously.

9.2.2 Measurement

Data collecting for both healthy and patient subject groups was the same as is described in Chapter 8. Please refer section 8.2.2 for more detail.

9.2.3 Experimental protocol

All heart rate and respiratory data for the present study were collected from patients in the supine position in runs of about 300 beats. After instrumentation and supine rest of 30 min, data were collected during spontaneous breathing. Some of the patients had a history of vascular disease or thyroid disease or heavy smoking and some had minor operations.

9.2.4 Data analysis

We used Welch's averaged periodogram algorithm for computing the power spectrum, cross-spectrum, coherence and transfer functions [Krauss *et al* 1994].

Epochs of 512 samples of interpolated HRV and ILV were divided into nine overlapping segments of 128 samples each. The reduced interference distribution was used for the time-frequency distribution analysis.

Prefiltering was used to remove the trends in output data which reflect the non-stationarity of the system. In addition, data examination was employed by using the coherence function and time-frequency distribution analysis to ensure the system is linear.

For comparison between groups, statistical analyses were carried out by means of T-test for Independent Samples whereas T-test for Dependent Samples was performed for within-group variation in change of posture and breathing pattern. $P< 0.05$ was considered significant.

9.3 Results

The healthy subjects and patients have been classified into 5 groups:

1. Healthy subjects (14) with good modeling (GH1). The data in this group can be well modeled by the linear ARX model in both random and regular breathing patterns. All subjects were tested in random breathing. 9 subjects were tested in regular breathing, but among these, only 5 were tested in a standing posture.
2. Patient subjects (24) with good modeling (GP1). The data in this group can be modeled by the linear ARX model.
3. Patient subjects (8) with good modeling (GP2). The data in this group can be modeled by linear ARX model and is characterized by a large sympathetic input.
4. Patient subjects (8) with poor modeling (GP3). The data in this group can not be modeled by linear ARX model because of a very low coherence function (<0.3).
5. Patient subjects (9) with poor modeling (GP4)). The data in this group can not be modeled by linear ARX model although they have average coherence function around 0.5.

In GP1, there are 22 patients whose medical history record is known. 11 subjects are female and their mean age is 53 years old (range: 29-84), 6 had minor operations, 4 patients have a history of vascular disease, thyroid disease or heavy smoking.

In GP 3 and GP4, there are 14 patients whose medical history record is known. 4 subjects are female and their mean age is 49 years old (range:20-68), 2 had minor operations, 10 patients have a history of vascular disease, or thyroid disease, or heavy smoking.

Using the low order ARX model for data obtained from these five groups, results of model parameter analysis for respiratory sinus arrhythmia are given in this section.

9.3.1 Examining the data

A typical example of a test for non-stationarity from healthy subject GH1 is provided by HRV data shown in Fig. 8-3. Having identified non-stationarity in the data, we need to deal with it. The prefiltering for each subject is used to remove the trends in output data which reflect the non-stationarity of the system. The effect of prefiltering is given in Fig. 8-3 of Chapter 8.

Figs. 9-1 and 9-2 present one example of the detection of nonlinearity of cardiorespiratory coupling from the group of patients in GP4.

First of all, this subject yields a significant relationship (>0.5 coherence) between HRV and ILV over most of the low and high frequency ranges (0.15-0.5 Hz) shown in Fig. 9-2.

Secondly, compared with cross-spectrum analysis, the cross-time frequency distribution presents a different energy distribution with frequency. In cross-spectrum, most spectral power was present around 0.32 Hz with which respiratory oscillation coincided. Whereas the cross-time frequency distribution shows the cross spectral power not only distributed around 0.32 Hz, but also around 0.2 Hz. Note that the cross-spectrum phase, which shows the most erratic behavior, is correctly recognized in this frequency ranges.

Finally, comparing the time–frequency distribution of HRV with one in ILV, output signal HRV (Fig.9-2) did not respond well to the change of input signal ILV in some parts of the data. In addition, the cross time-frequency distributions were computed to show common frequency contents between respiration and heart rate.

Taken together, these checks determine if nonlinear coupling exists between HRV and ILV.

9.3.2 The effect of breathing pattern in healthy subjects

The impulse response and its parameters of decomposition were calculated for 9 subjects and conditions in GH1 groups (see Chapter 8). Fig. 9-3 and Fig 9-4 show the sensitivity of the parameters of the low order ARX model to a change in breathing pattern, by comparison of the results obtained from an individual healthy subject in random breathing and regular breathing. Similar results of the system

identification for each individual in healthy subject group GH1 were obtained. Table 9-1 shows the parameters of the decomposed impulse response for each subject in this group.

The T-test for Dependent Samples was performed in group GH1 for parameters of the decomposed impulse response to evaluate the differences between random breathing and regular breathing pattern and these statistical comparisons are given in Table 9-2.

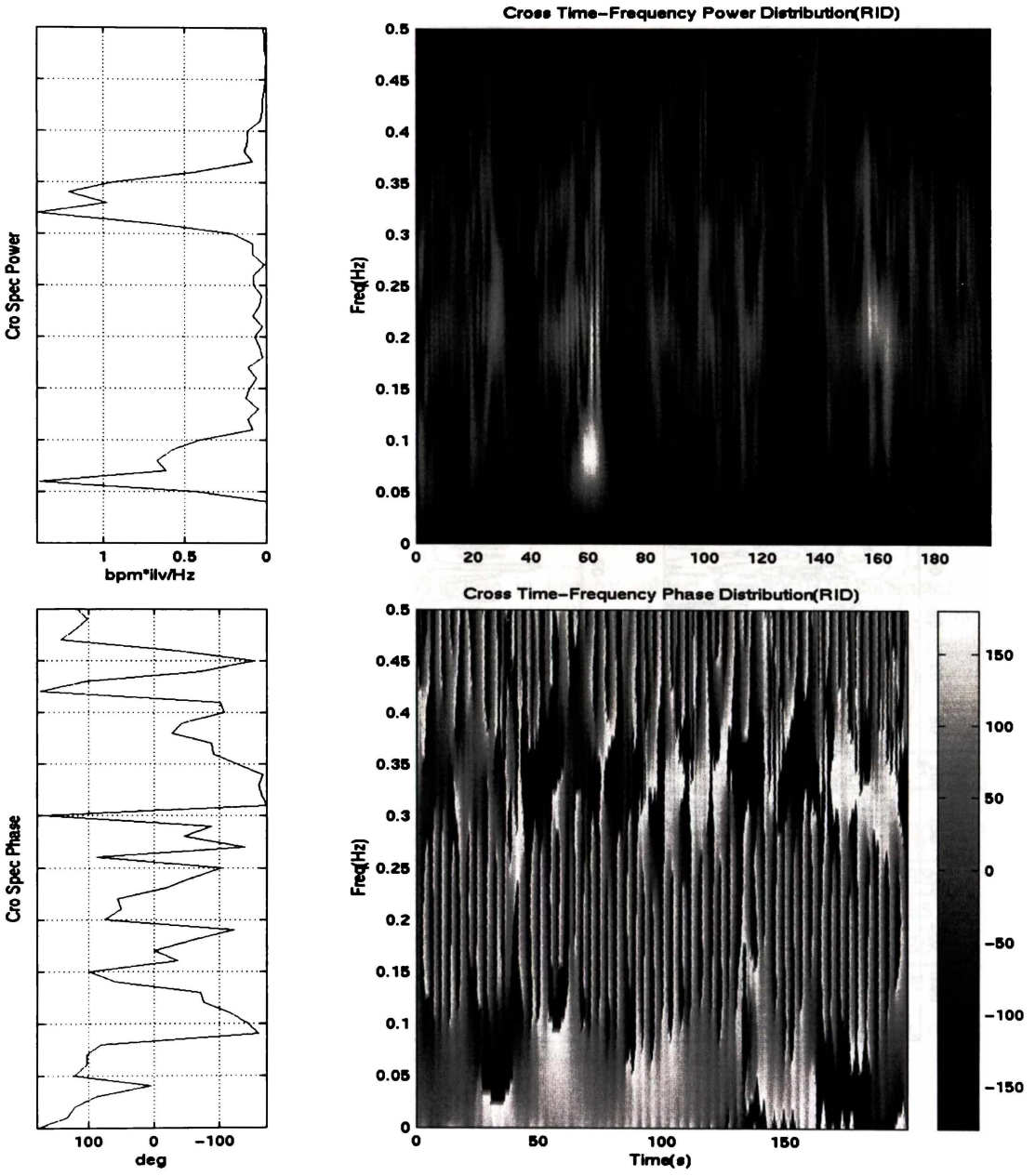

Figure 9- 1 The cross spectrum and cross time-frequency distribution (RID) during spontaneous breathing for an example patient subject in group GP4. Upper is cross-amplitude spectrum and cross-energy time-frequency. Lower is phase spectrum and cross phase distribution.

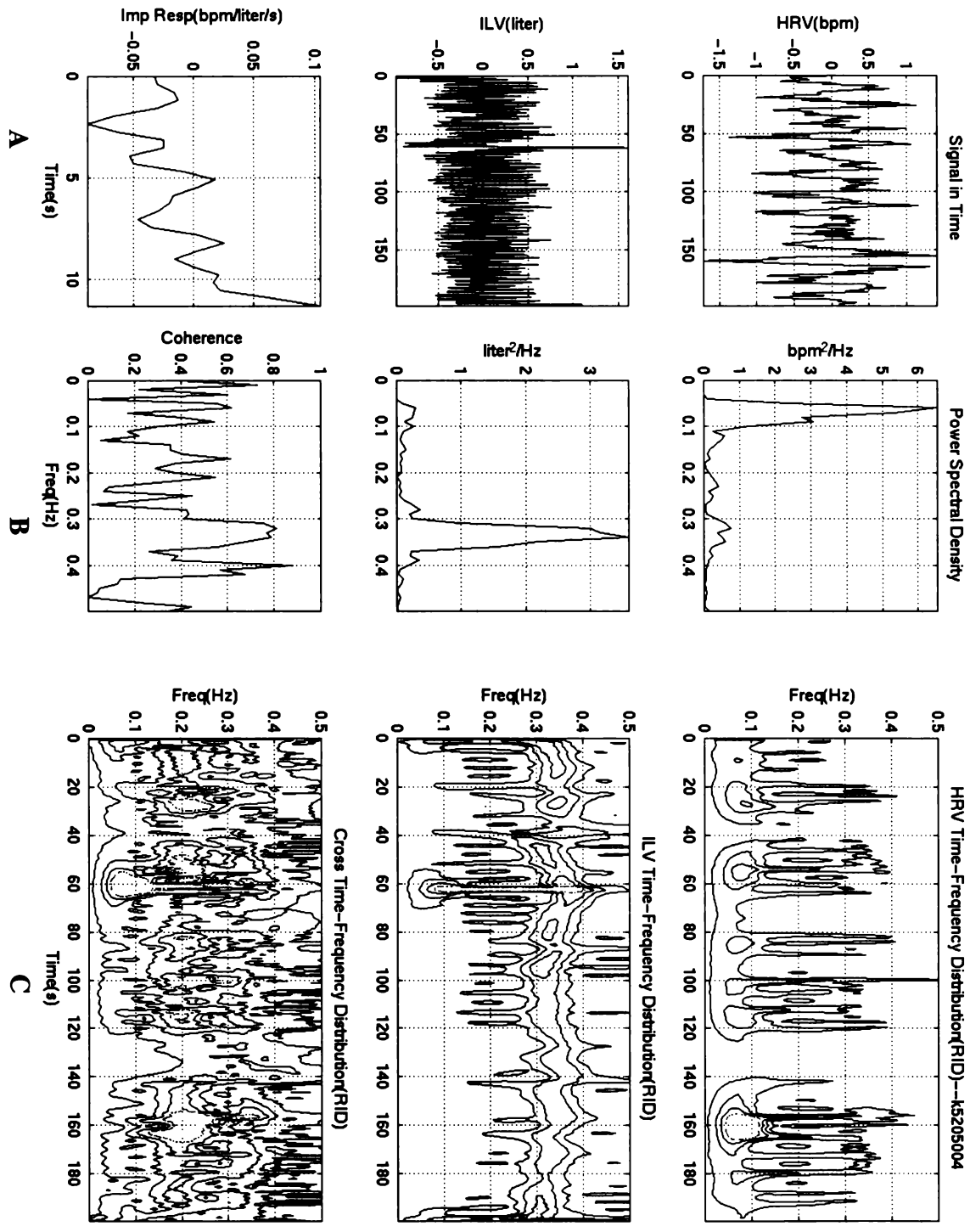

Figure 9- 2 An example of a patient subject in GP4 in spontaneous breathing pattern. A. HRV, the spectrum of HRV and impulse response. B. ILV, the spectrum of ILV and coherence function. C. HRV auto RID, ILV auto RID and cross RID of HRV and ILV (All data from the subject presented in Fig. 9-1).

The results show that the amplitude of both components and the slow time constants change significantly ($p<0.05$) from random breathing to regular breathing which obviously reflects the change of breathing pattern. Whereas, the fast time constant does not change significantly with breathing pattern.

The coherence was higher during random breathing compared with regular breathing at every breathing frequency although both show a significant relationship (> 0.5 coherence) at breathing frequency.

NUMERIC VALUES	1 AMP1_R	2 AMP2_R	3 TC1_R	4 TC2_R	5 AMP1_5	6 AMP2_5	7 TC1_5	8 TC2_5
b1r5	4.312	4.467	2.345	.435	2.819	3.132	2.687	.423
b2r5	3.539	3.830	2.391	.392	1.141	.499	2.642	.473
b3r5	3.845	2.611	2.122	.404	2.418	2.553	2.461	.440
b4r5	1.850	1.701	2.885	.362	.857	.843	3.006	.482
b5r5	1.090	1.170	3.402	.454	.787	.853	4.518	.377
sr105	2.424	2.550	2.658	.416	.766	.847	2.535	.426
sr25	.893	1.024	2.655	.383	1.055	1.178	2.752	.386
sr35	3.019	2.891	2.420	.441	1.589	1.761	2.783	.431
sr45	1.440	1.602	2.959	.464	1.147	1.251	3.080	.501

Table 9- 1 The parameters of impulse response in healthy subject group GH1. Parameters of impulse response for healthy subjects in supine posture during random and regular breathing. Data in 1~4 columns are for subjects in random breathing and 5~8 columns are for subjects in regular breathing.

Valid Number = 9	Random Supine		Regular Supine		T-test	
	Mean	Std.Dv	Mean	Std.Dv	t	P
Slow Time Constant(Sec)	2.6486	0.389	2.940	0.6245	-2.5289	0.03512
Fast Time Constant (Sec)	0.4168	0.0344	0.4377	0.0418	-1.099	0.30347
Slow Amplitude(bmp/liter)	2.4902	1.2531	1.3977	0.7423	4.0435	0.00372
Fast Amplitude(bmp/liter)	2.4273	1.1806	1.4352	0.8837	2.7780	0.02400

* Marked differences are significant at $P < 0.05$

Table 9- 2 Result of T-test for Dependent Samples to compare random breathing with regular breathing in supine posture in healthy subject group GH1.

9.3.3 The effect of change in posture in random breathing for healthy subjects

The sensitivity of the parameters of the low order ARX model to change in posture is demonstrated by a comparison of the results obtained from each subject of group

GH1 in supine state and standing state depicted in Figs. 9-3 and 9-5. Table 9-3 shows the parameters of the decomposed impulse response for each one in healthy subject group GH1.

NUMERIC VALUES	1 AMP1_S	2 AMP2_S	3 TC1_S	4 TC2_S	5 AMP1_U	6 AMP2_U	7 TC1_U	8 TC2_U
b1r00000	4.312	4.467	2.345	.435	3.408	3.766	3.891	.455
b2r00000	3.539	3.939	2.391	.392	1.943	2.145	4.091	.358
b3r00000	3.845	2.661	2.122	.404	2.771	3.039	3.261	.371
b4r00000	1.950	1.701	2.995	.362	.653	.737	8.187	.336
b5r00000	1.090	1.170	3.402	.454	.824	.413	4.536	.350
sr10	1.817	2.058	3.042	.437	.992	1.119	3.652	.420
sr11	1.464	1.584	2.845	.483	1.967	1.449	4.769	.485
sr2	.893	1.024	2.955	.383	.677	.755	4.555	.392
sr3	3.019	2.891	2.420	.441	1.462	.751	4.917	.402
sr4	1.440	1.602	2.959	.464	.487	.518	6.035	.408
sr6	.451	.427	4.093	.379	.433	.345	6.106	.335
sr7	.610	.505	5.472	.520	.574	.454	6.343	.565
sr8	1.069	.671	3.014	.368	.748	.720	5.632	.506
sr9	.795	.927	2.630	.352	.322	.289	6.655	.456

Table 9- 3 Parameters of impulse response for healthy subjects (GH1) in supine and standing posture during random breathing. Data in 1~4 columns are for subjects in supine posture and 5~8 columns are for subjects in standing posture.

Valid Number = 14	Random Supine		Random Upright		T-test	
	Mean	Std.Dv	Mean	Std.Dv	t	P
Slow Time Constant(Sec)	3.048	0.855	5.188	1.366	-6.3019	.000027
Fast Time Constant (Sec)	0.4196	0.050	0.417	0.069	0.1466	.885669
Slow Amplitude(bmp/liter)	1.8781	1.280	1.232	0.8510	3.8605	.001968
Fast Amplitude(bmp/liter)	1.8305	1.2517	1.1786	1.0730	3.4363	.004423

* Marked differences are significant at P < 0.05

Table 9- 4 Result of T-test for Dependent Samples to compare different posture from supine to standing in random breathing in healthy subject group GH1.

T-test for Dependent Samples was performed for parameters of the decomposed impulse response to evaluate the effects of posture between supine and upright in group GH1 and these statistical comparisons are summarized in Table 9-4. The results showed that the amplitude of both components were significantly decreased ($p< 0.001$, $n=14$) in upright posture compared with the supine posture and the slow

time constant changes significantly in posture from supine state to standing state. Whereas, the fast time constant does not change significantly with posture.

9.3.4 The effect of change in posture in regular breathing for healthy subjects

T-test for Dependent Samples was performed in the healthy subject group GH1 (only 5 subjects did this test) for parameters of the decomposed impulse response to evaluate the differences of change in posture from supine to standing in regular breathing rate 15 breaths/min, as may be seen more clearly from the Fig. 9-6 and Fig. 9-7.

The results in Table 9-4 showed that the amplitude of the slow component was significantly decreased ($p< 0.001$, $n=15$) in upright posture compared with the supine posture and slow time constant changes significantly in posture from standing state to supine state. Whereas the fast time constant and the amplitude of the fast component does not change significantly with posture.

NUMERIC VALUES	1 AMP1_U	2 AMP2_U	3 TC1_U	4 TC2_U	5 AMP1_5	6 AMP2_5	7 TC1_5	8 TC2_5
sr105	1.265	1.364	3.664	.453	.766	.847	2.535	.426
sr115	.822	.379	5.331	.547	1.894	2.005	2.612	.404
sr25	1.659	.961	3.470	.448	1.055	1.178	2.752	.386
sr35	2.221	1.510	3.578	.391	1.589	1.761	2.783	.431
sr45	1.350	.910	5.638	.382	1.147	1.251	3.080	.501

Table 9- 5 Parameters of impulse response for healthy subjects (GH1) in supine and standing posture during regular breathing. Data in 1~4 columns are for subjects in supine posture and 5~8 columns are for subjects in standing posture.

Valid Number = 5	Regular Supine		Regular Upright		T-test	
	Mean	Std.Dv	Mean	Std.Dv	t	P
Slow Time Constant(Sec)	2.7524	0.20903	4.3362	1.0562	3.6257	0.002224
Fast Time Constant (Sec)	0.4296	0.04379	0.4296	0.04378	0.3276	0.75963
Slow Amplitude(bmp/liter)	1.0758	0.32759	1.6778	0.3937	4.30212	0.012624
Fast Amplitude(bmp/liter)	1.0832	0.5119	1.3600	.44711	0.7154	0.51390

* Marked differences are significant at $P < 0.05$

Table 9- 6 Result of T-test for Dependent Samples to compare different posture from supine to standing in regular breathing for healthy subjects (GH1)

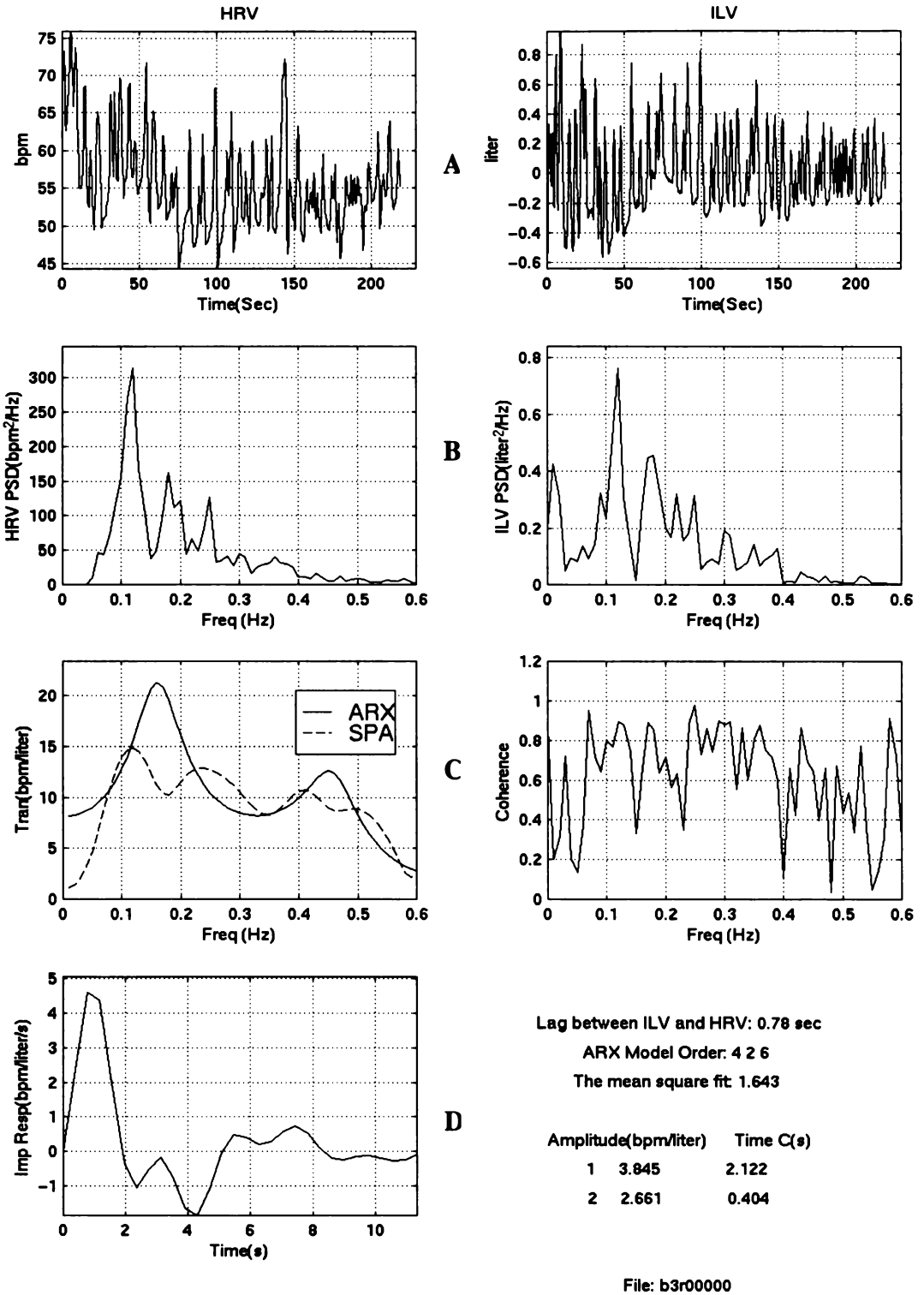

Figure 9- 3 An example result for a healthy subject (GH1) during random breathing pattern in supine posture. HRV and ILV signals (A), Spectrum of HRV and ILV (B). Transfer function from ARX model and spectral method (C). The impulse response synthesized from high and low frequency components determined by the model parameter (D).

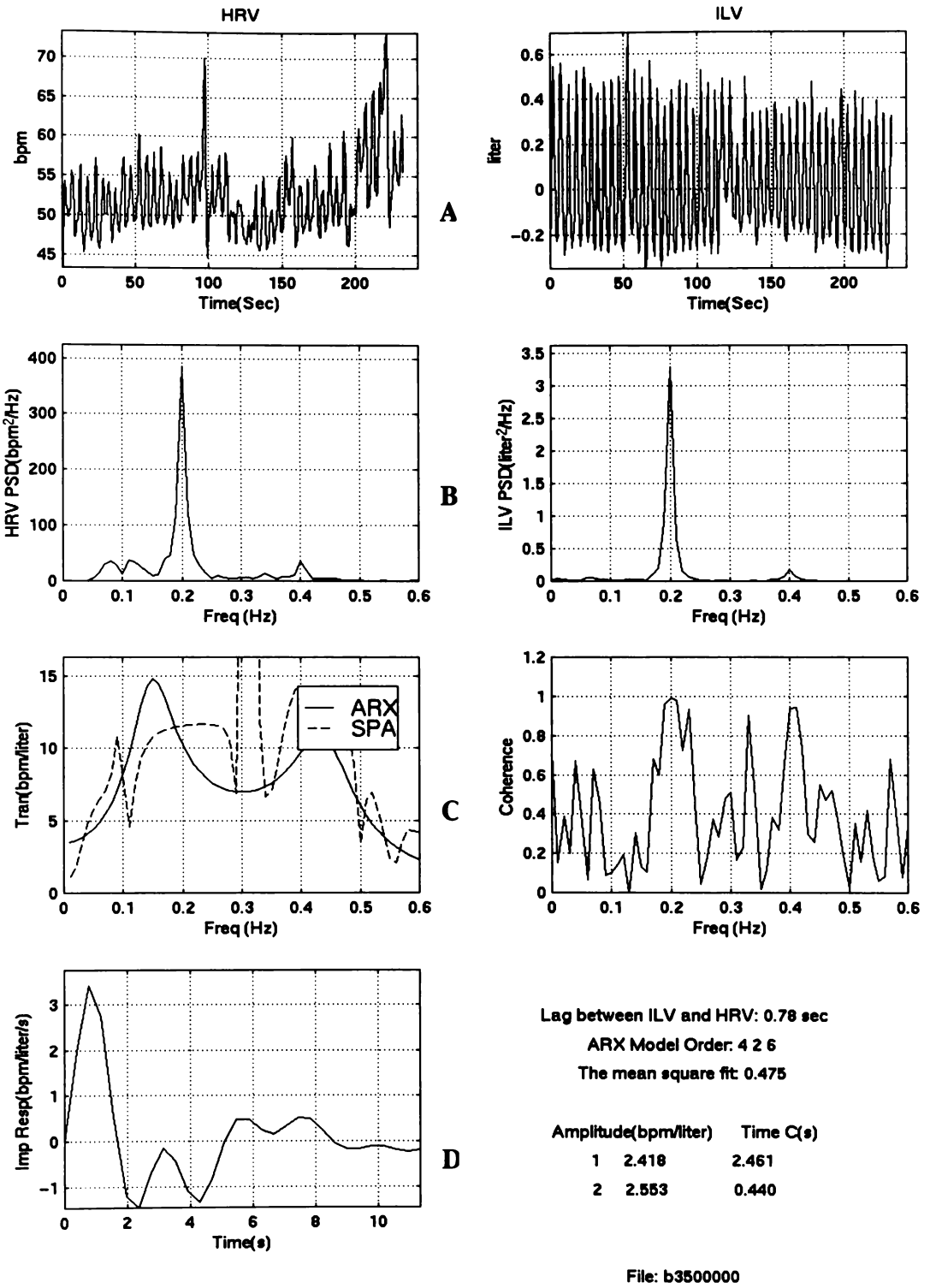

Figure 9- 4 An example of healthy subject group GH1 (same one as one in Fig. 9-3) during regular breathing pattern in supine posture. HRV and ILV signals (A). Spectrum of HRV and ILV (B). Transfer function from ARX model and spectral method (C). The impulse response synthesized from high and low frequency components determined by the model parameter (D).

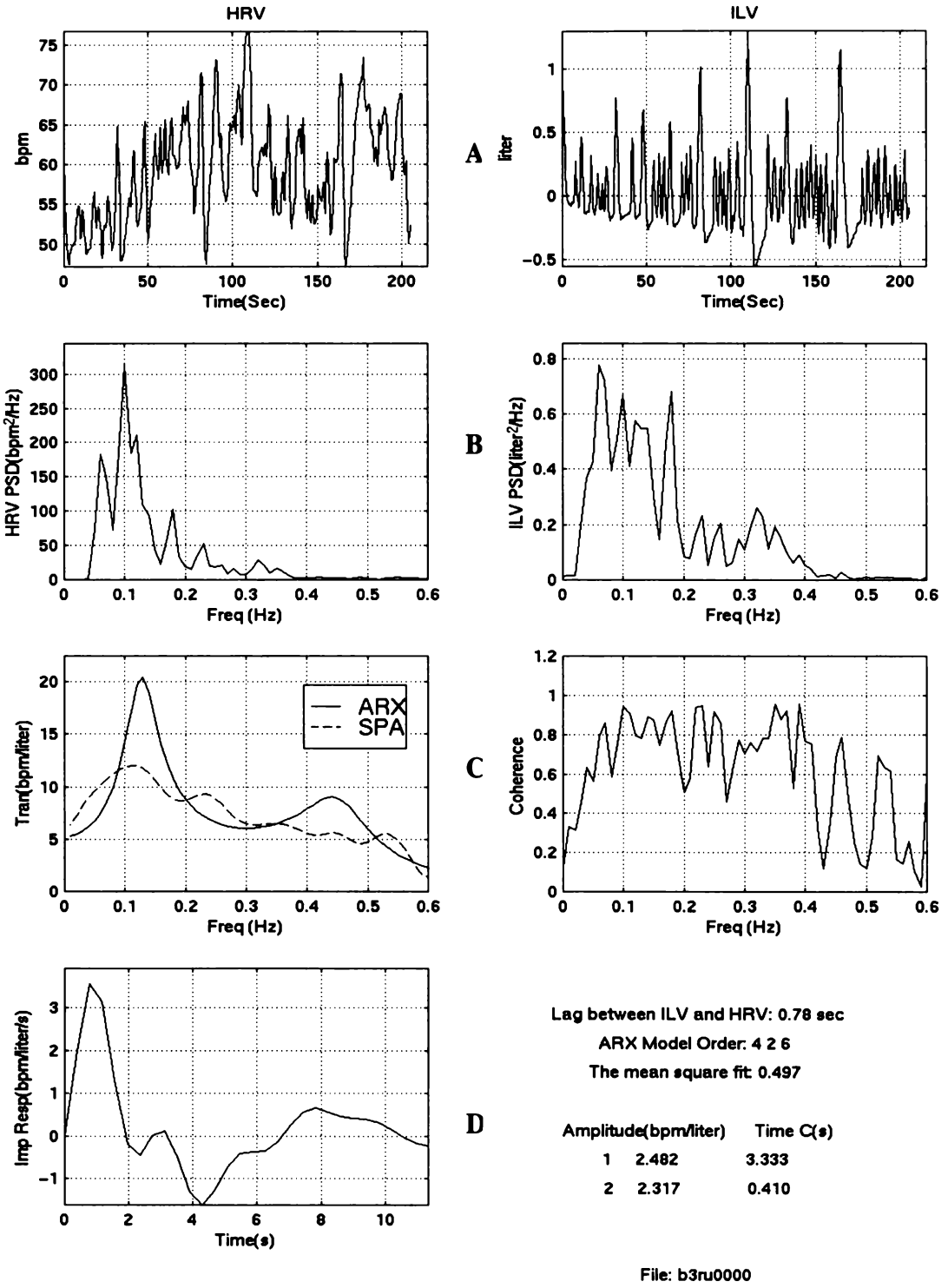

Figure 9- 5 An example of healthy subject group GH1 (same one as in Fig. 9-3) during random breathing pattern in standing posture. HRV and ILV signals (A), Spectrum of HRV and ILV (B), transfer function from ARX model and spectral method (C). The impulse response synthesized from high and low frequency components determined by the model parameters. (D).

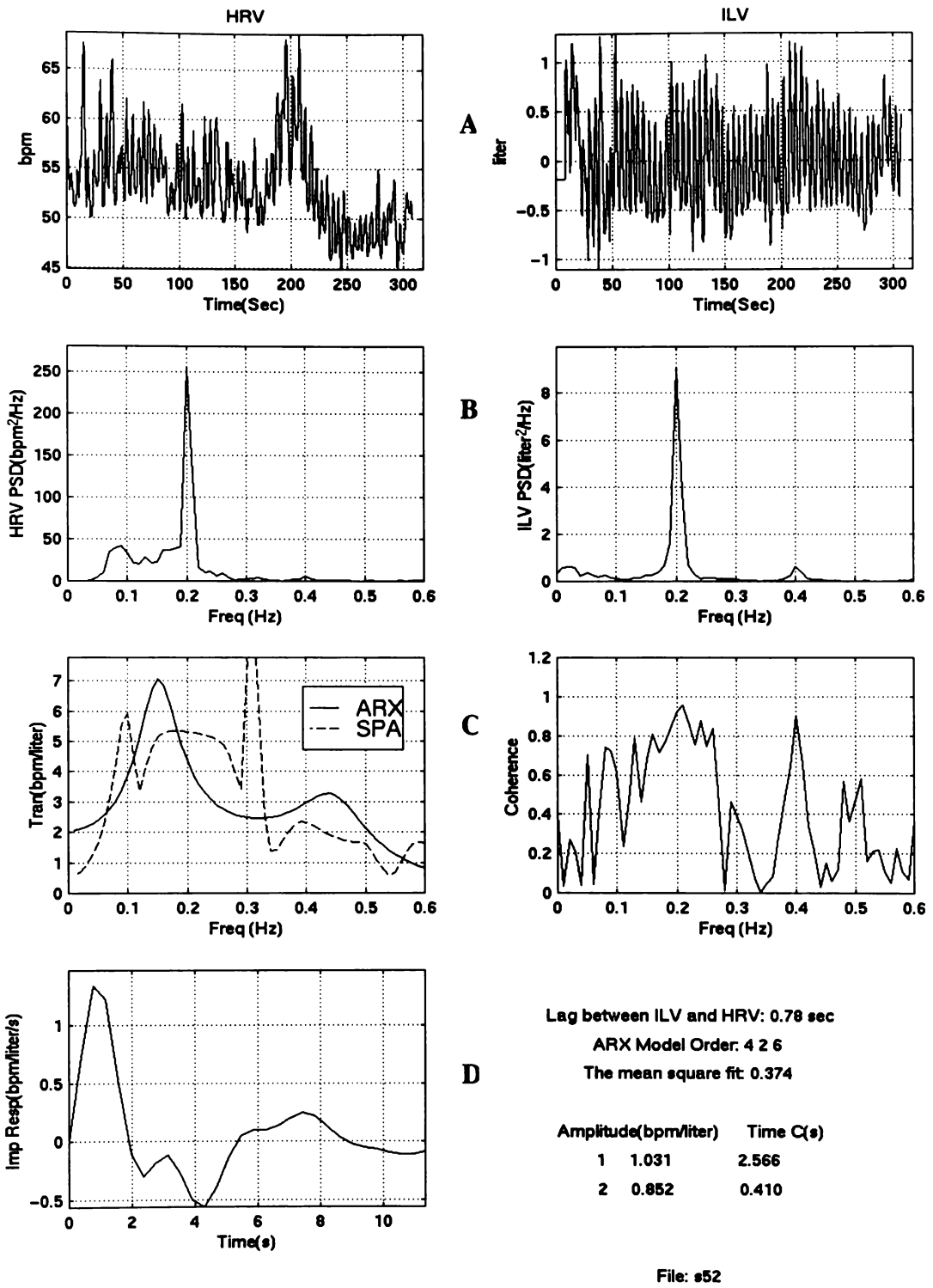

Figure 9- 6 An example of a healthy subject group GH1 during regular breathing pattern in supine posture. HRV and ILV signals (A). Spectrum of HRV and ILV (B). Transfer function from ARX model and spectral method (C). The impulse response synthesized from high and low frequency components determined by the model parameter (D).

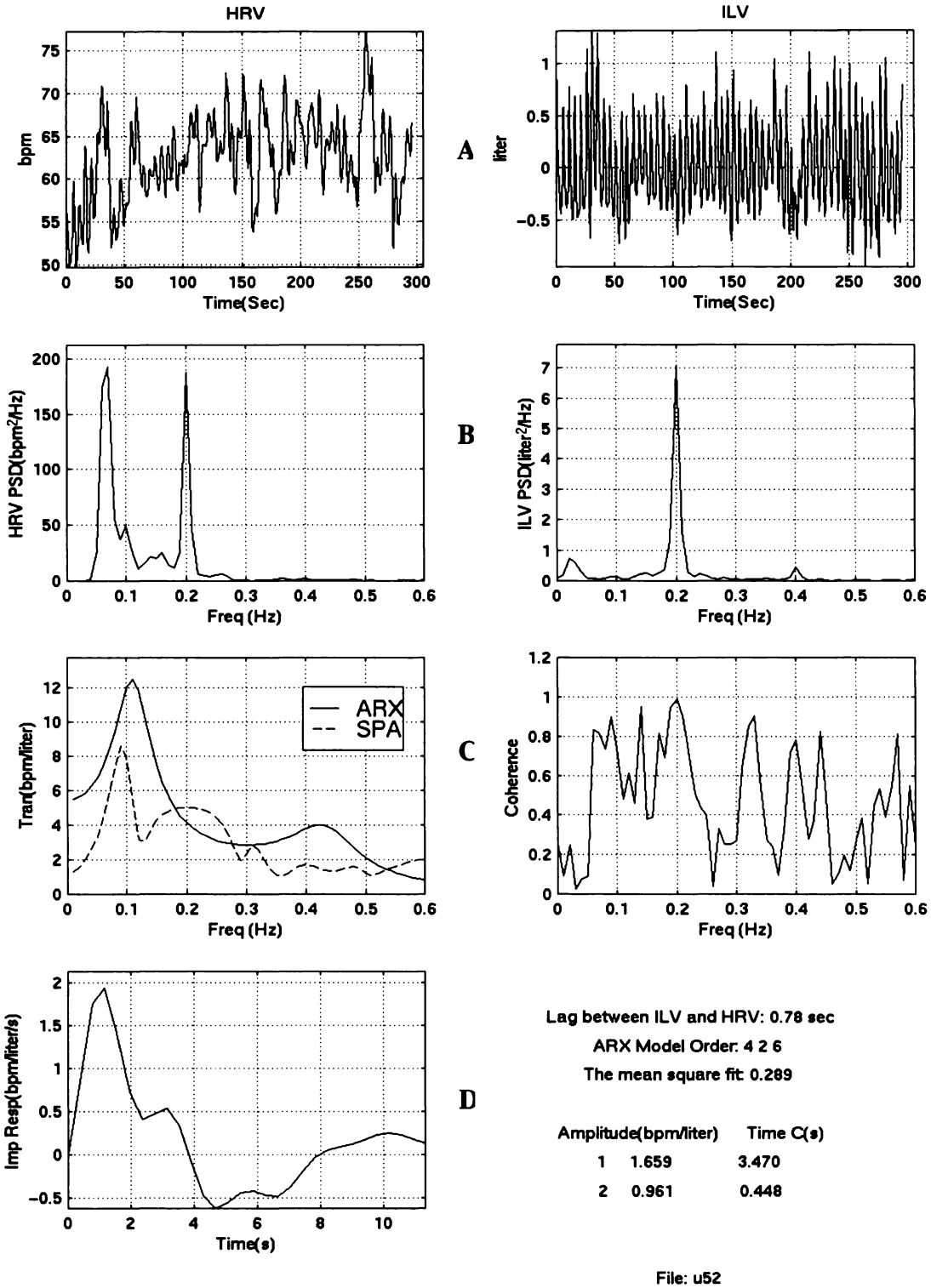

Figure 9- 7 An example of healthy subject group GH1 (same subject as one in Fig. 9-6 during regular breathing patterns in standing posture. HRV and ILV signals (A). Spectrum of HRV and ILV (B) Transfer function from ARX model and spectral method (C). The impulse response synthesized from high and low frequency components determined by the model parameter (D).

9.3.5 Modeling the patient subjects

Fig. 9-8 shows an example of a patient in subject group GP1 during spontaneous breathing pattern in supine posture. For comparison, Fig. 9-9 shows an example of a patient in subject group GP2 with a large sympathetic input. These figures show good modeling results of a low order ARX model applied for patient subjects in both groups GP1 and GP2. The T-test for Independent Samples was performed for parameters of the decomposed impulse response to evaluate the following paired differences between the three groups: (i) Patient subject group GP1 and healthy subject group GH1. (ii) Patient subject group GP1 and the patient subject with a large sympathetic input GP2. (iii) Healthy subject group GH1 and the patient subject group with a large sympathetic input GP2.

VALUES	1 AMP1	2 AMP2	3 TC1	4 TC2	5 G
a1805000	.791	.427	3.055	.388	1
a3105000	.355	.370	3.512	.427	1
b2305002	.822	.775	3.007	.450	1
c3810000	.043	.048	2.703	.503	1
d1105000	.264	.225	1.868	.386	1
f2205000	.383	.423	3.331	.428	1
g1540000	.195	.216	2.381	.383	1
h0705000	1.530	.442	2.038	.438	1
h0740000	1.094	.381	3.108	.348	1
h4905000	.185	.123	2.663	.427	1
l1305000	.374	.162	2.105	.484	1
l3615000	.307	.173	3.192	.421	1
l4605000	.164	.153	2.764	.534	1
m0925000	.121	.038	3.326	.388	1
r0605000	.061	.063	3.219	.465	1
r2105000	.100	.103	2.316	.454	1
r2110000	.732	.738	2.475	.412	1
s5630000	.256	.284	1.901	.445	1
t5530000	.109	.118	3.415	.457	1
w0505000	.273	.217	3.227	.437	1
w1905000	.300	.295	2.670	.410	1
w1915004	.374	.151	2.472	.386	1
w3305007	.223	.104	1.891	.394	1
w4805000	.037	.041	3.072	.396	1
b1r	4.312	4.467	2.345	.435	2
b2r	3.539	3.939	2.391	.392	2
b3r	3.845	2.661	2.122	.404	2
b4r	1.950	1.701	2.995	.362	2
b5r	1.090	1.170	3.402	.454	2
sr10	1.817	2.058	3.042	.437	2
sr11	1.464	1.584	2.845	.483	2
sr2	.893	1.024	2.955	.383	2
sr3	3.019	2.891	2.420	.441	2
sr4	1.440	1.602	2.959	.464	2
sr8	1.069	.671	3.014	.368	2
sr9	.795	.927	2.630	.352	2
b15	2.819	3.132	2.687	.423	2
b25	1.141	.499	2.642	.473	2
b35	2.418	2.553	2.461	.440	2
b45	.857	.843	3.006	.482	2
s510	.766	.847	2.535	.426	2
s511	1.894	2.005	2.612	.404	2
s52	1.055	1.178	2.752	.386	2
s53	1.589	1.761	2.783	.431	2
s54	1.147	1.251	3.080	.501	2
finca00	.278	.072	5.073	.566	3
hdinnj001	1.220	.666	3.832	.598	3
13615003	.196	.137	4.362	.414	3
maxwe00	.035	.035	3.734	.415	3
rpomw000	.421	.443	4.243	.473	3
sr270500	.610	.505	5.472	.520	3
b500600	.787	.853	4.518	.377	3
d420000	.451	.427	4.093	.379	3

Table 9- 7 Parameters of impulse response for all the subjects of group GH1, GP1 and GP2 in supine posture. The column marked G on the right identifies the group. Data in rows with 1 in G column are patient subjects (GP1) in spontaneous breathing, data in rows with 2 in G column are healthy subject (GH1) in either random or regular breathing and data in rows with 3 in G column are patient subject with a large sympathetic input (GP2).

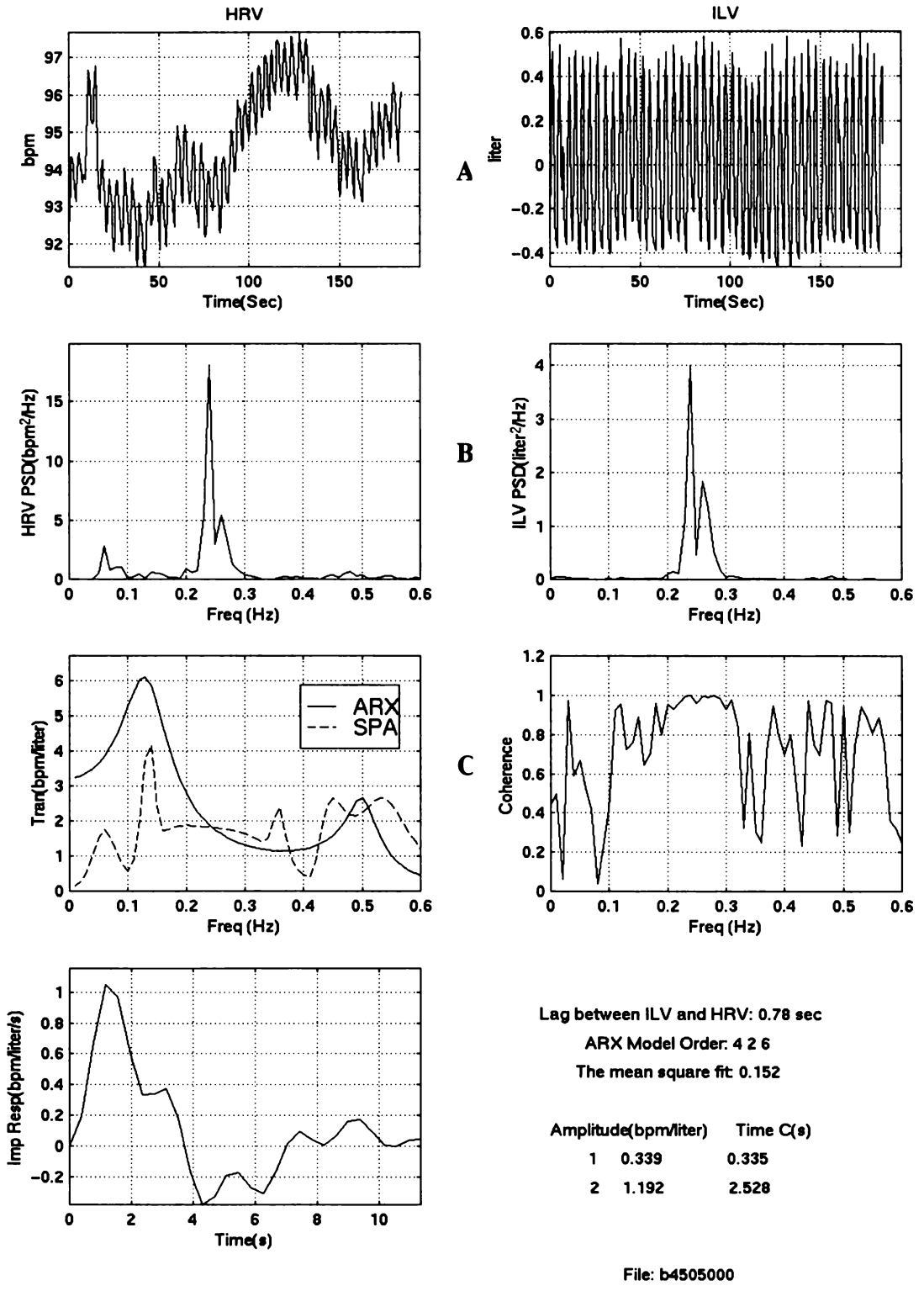

Figure 9- 8 An example of patient subject group GP1 during spontaneous breathing pattern in supine posture. HRV and ILV signals (A). Spectrum of HRV and ILV (B). Transfer function from ARX model and spectral method (C). The impulse response synthesized from high and low frequency components determined by the model parameter (D).

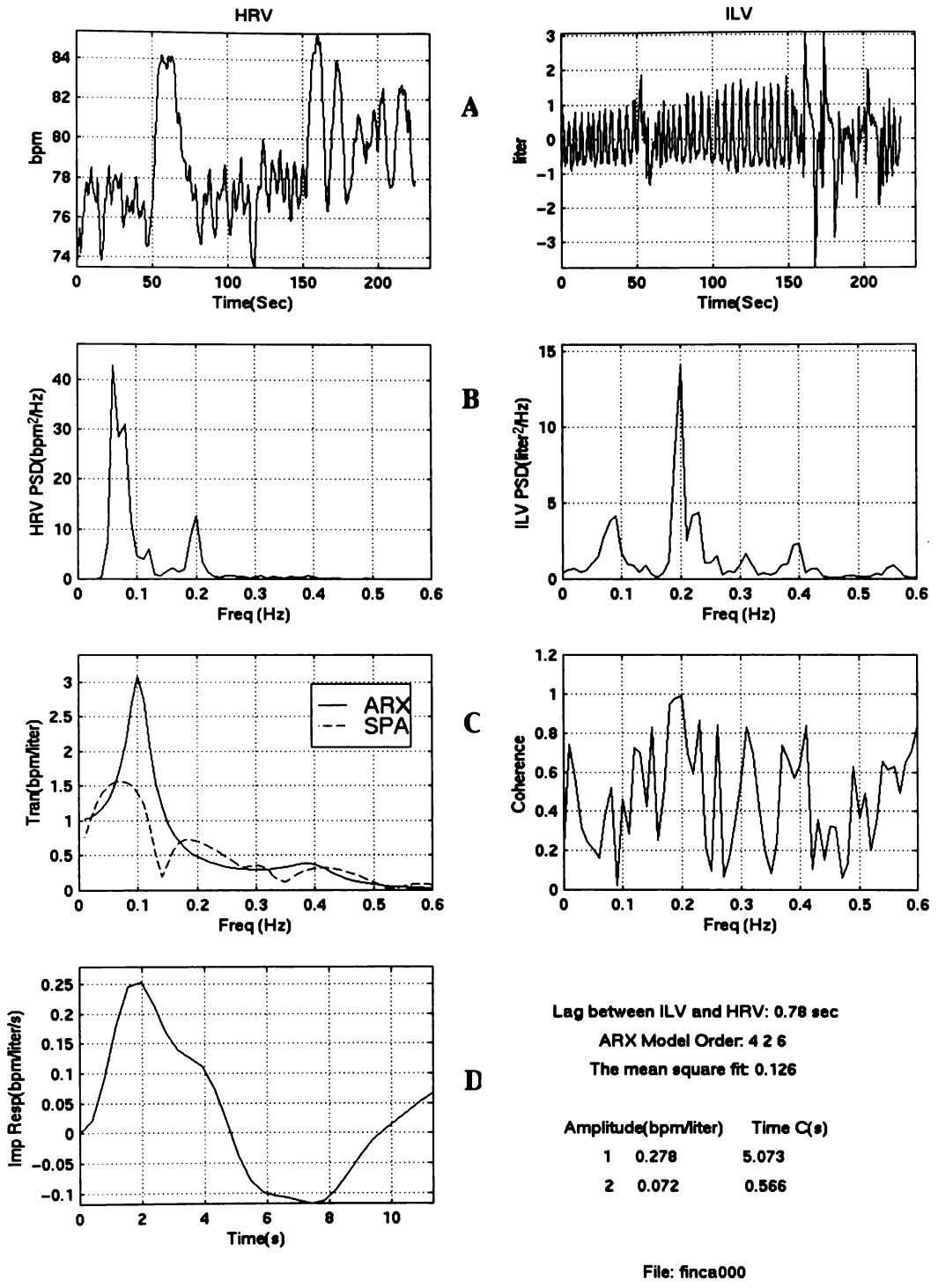

Figure 9- 9 An example of patient subjects with a large sympathetic input during (GP2) spontaneous breathing pattern in supine posture. HRV and ILV signals (A). Spectrum of HRV and ILV (B). Transfer function from ARX model and spectral method (C). The impulse response synthesized from high and low frequency components determined by the model parameter (D).

Valid Number of subject = 45	Patients (24)		Healthy (21)		T-test	
	Mean	Std.Dv	Mean	Std.Dv	t	p
Slow Time Constant(Sec)	2.73795	.526509	2.74657	.307011	-0.06576	.947871
Fast Time Constant (Sec)	.427543	.042629	.425762	.004220	0.14038	.889013
Slow Amplitude(bmp/liter)	.378875	.365265	1.8532	1.07067	-6.34619	.000000
Fast Amplitude(bmp/liter)	.252917	.200332	1.8459	1.00808	-7.09372	.000000

Marked differences are significant at P < 0.05

Table 9- 8 Result of T-test for Independent Samples to compare difference between patient group GP1 and healthy subject GH1

Valid Number of subject = 32	Patients (24)		Patients with high sympathetic input (8)		T-test	
	Mean	Std.Dv	Mean	Std.Dv	T	p
Slow Time Constant(Sec)	2.73795	.526509	4.41588	.597679	-7.55595	0.00000
Fast Time Constant (Sec)	.427543	.042629	.467750	.008549	.1.76935	0.0870
Slow Amplitude(bmp/liter)	.378875	.365265	.49975	.374050	-.80603	.436571
Fast Amplitude(bmp/liter)	.252917	.200332	.39225	.292542	-1.51519	.140191

Marked differences are significant at P < 0.05

Table 9- 9 Result of T-test for Independent Samples to compare difference between patient subject group GP1 and patient subject with a large sympathetic input subject GP2

Valid Number of subject = 29	Healthy subjects (21)		Patients with high sympathetic input(8)		T-test	
	Mean	Std.Dv	Mean	Std.Dv	T	p
Slow Time Constant(Sec)	2.74657	.307011	4.41588	.597679	-9.96909	.000000
Fast Time Constant (Sec)	.425762	.004220	.467750	.008549	-1.78269	.085886
Slow Amplitude(bmp/liter)	1.8532	1.07067	.49975	.374050	2.46220	.001800
Fast Amplitude(bmp/liter)	1.8459	1.00808	.39225	.292542	3.71393	.000939

Marked differences are significant at P < 0.05

Table 9- 10 Result of T-test for Independent Samples to compare the difference between healthy subject GH1 and patient subject with a large sympathetic input GP2

Table 9-8 shows that the amplitude of both components for patient subjects group GP1 was significantly small ($p< 0.001$) compared with healthy subject group GH1 and both time constants have no significant difference between healthy subjects and patients.

Comparing the general patient subjects with the patients with a large sympathetic input GP2, only the fast time constant in GP2 is significantly larger than the one in patient subjects GP1 (Table 9-9).

Excepting that the fast time constant has no significant difference between healthy subject GH1 and patients with a large sympathetic input GP2, other components have significant differences (Table 9-10).

9.3.6 The patient subject in nonlinear cardiorespiratory coupling

Fig. 9-10 shows a typical example of the eight patient subjects in GP3 with low coherence function, which indicate no significant relation existed between HRV and ILV. The coherence in high frequency range (0.15~0.5 Hz) is 0.1889 and in low frequency range (0.5~0.15 Hz) it is 0.05.

Table 9-11 lists coherence HF and coherence LF for all eight patient subjects.

Subjects (GP3)	*c44200*	*b50060*	*b57050*	*c47050*	*g16155*	*o14050*	*s27300*	*w34050*
Coh HF	0.1889	0.1725	0.3106	0.1744	0.2509	0.2868	0.1435	0.2808
Coh LF	0.0505	0.1853	0.3648	0.2134	0.1636	0.3427	0.3821	0.1654

Table 9- 11 Coherence function in high and low frequency range for patient subject group GP3 in low coherence

Subjects (GP4)	*h07051*	*m09301*	*m09450*	*p25050*	*r06057*	*r21102*	*r30054*	*rpom0*	*w34054*
Coh HF	0.5398	0.5151	0.5187	0.6840	0.4326	0.5279	0.7021	0.6036	0.5678
Coh LF	0.4902	0.4809	0.5613	0.3271	0.6588	0.4349	0.4833	0.5816	0.6221

Table 9- 12 Coherence function in high and low frequency range for patient subject group GP4 in around 0.5 coherence

Table 9-12 lists coherence function in high and low frequency ranges for all patient subjects in group GP4, where the coherences have averages above the 0.5 threshold. However, for GP4 patients nonlinear cardiorespiratory coupling existed when the

time-frequency distribution was used to test. One example has been demonstrated in the previous section and is shown in Figs. 9-1 and 9-2.

To investigate why patients in GP3 and GP4 were modeled poorly they were compared with the patients that modeled well, i.e., GP1. 22 patients from GP1 and whose medical history was known were compared with 14 patients whose medical history was known in GP3 and GP4. Fishers Exact Test [Neil and Matthew 1991] showed there was no significant difference between the groups as to age, sex, or operation type in this small and uncontrolled study. However, the poor group had a significantly larger pre-operation history of vascular disease, smoking, or thyroid disease (p=0.002).

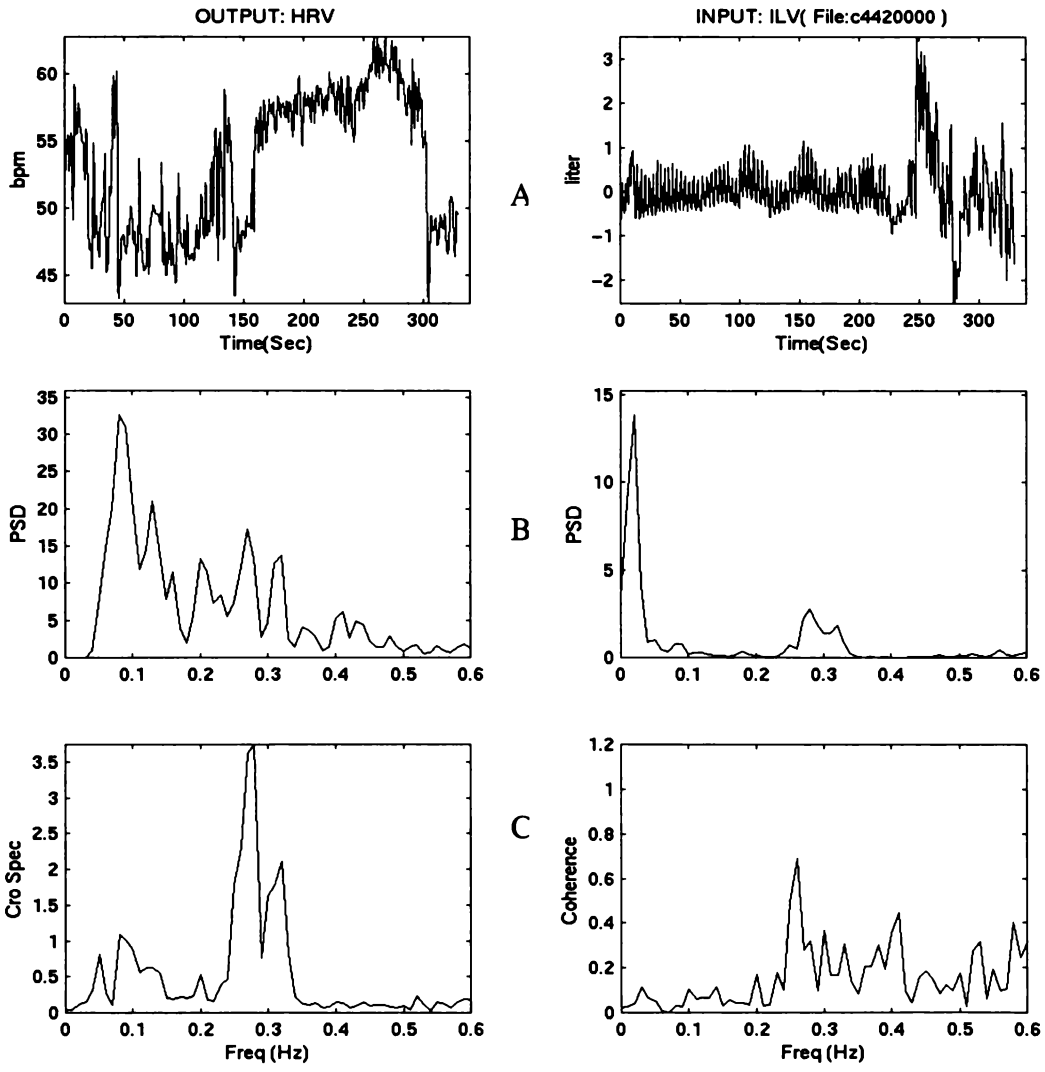

Figure 9- 10 Low coherence in patient subject group GP3. A. Time series of HRV and ILV. B. The power spectral of HRV and ILB. C. Cross-spectral and coherence function of HRV and ILV.

9.4 Discussion

Our results demonstrate that the amplitude and time constant of impulse response components of the system that generates RSA in humans can be efficiently determined during random breathing patterns and regular breathing patterns for healthy subjects and during spontaneous breathing pattern for 65% of general patient subjects or patient subjects with a large sympathetic activity. The results further show that model parameter analysis, in terms of the amplitude and time constant of impulse response components, by using the low order ARX model can identify differences in system response that are due to the shifts in autonomic balance produced by the changing posture and can distinguish patients with a large sympathetic input.

9.4.1 Data test preliminary to system identification

In studying respiratory sinus arrhythmia, one is faced with a dilemma. The mechanisms regulating the cardiovascular system are known theoretically to contain many nonlinearities, and the system as a whole is known to be nonstationary. Yet, the dominant techniques for system identification – for example ARX model - are based on the assumption of linear dynamics and stationarity. This is why in certain cases application of the ARX model to RSA would produce poor results, especially for patients. Therefore, it is desirable to have a simple tool to detect nonlinearities and non-stationarities in cardiorespiratory interaction. This detection allows us to have an indication of how complex the system is and how the ARX model is and is not capturing all of the information in RSA in each particular case.

The stationarity of a system must be established before the ARX model can be used for its identification and analysis. The recurrence plot is known as a detector of non-stationarity and was described in section 4.4.1. Prefiltering is used to remove the trends in output data which reflect the non-stationarity of the system. In addition, we need to check any nonlinear effects in the output resulting from the change in the input, like different responses at different levels, or different responses to a step up and a step down. We must determine if there are nonlinear effects in the system before proceeding with identification using the ARX model.

In any case, whenever coherence is less than 0.5 in most frequency ranges, either the system is nonlinear, the signals do not have a completely causal relationship (i.e., the signal are contaminated by noise), or both. According to previous work Berger *et al*

[1989] and Yana *et al* [1993] in both the frequency and time domain, the coherence function relating ILV and HRV is large enough (especially in the frequency range 0.04~0.5 Hz) to assume the system is primarily linear.

The strength of cardiorespiratory coupling is usually estimated by coherence analysis, which is suited for describing only the linear aspect of the interrelations. However, coherence as a frequency description of linear coupling between signals alone is not sufficient in the problems of nonlinear or nonstationary coupling between the input and output. Hence, cross time-frequency analysis can be used to analyze the relation between HRV, ILV in their t-f representation. This provides a tool to check any nonlinearity or nonstationarity in the system before setting up the linear ARX model. Figs. 9-1 and 9-2 show a typical example of one patient subject in group GP4 with close nonlinear coupling between HRV and ILV. This is the case where we are not able to do system identification through the low order ARX model.

9.4.2 Autonomic mediation of RSA

System identification using the low order ARX model was evaluated in terms of its capability to differentiate between altered autonomic states, because it is important in assessing the success of the system-identification procedure to determine whether the results are consistent with accepted physiological findings.

It is well know that the posture change is accompanied by a shift in the balance between sympathetic and parasympathetic activity [Burke *et al* 1977]. The change in posture from supine to standing results in a relative shift from parasympathetic to sympathetic cardiovascular control. The components of the ARX model should reflect the posture-induced change in the system. We found a statistically significant change occurs in the related components of impulse response, in both random and regular breathing, summarized in Tables 9-4 and 9-6. The most substantial changes we observed are the slow components of time constant and amplitude which are both markedly increased in the upright posture, presumably due to change in a relative shift from parasympathetic to sympathetic cardiovascular control. It is important to point out that the peak in the low frequency range of the transfer function moves toward low frequency with change of posture from supine to upright. The slow component of impulse response reflects this change quantitatively.

The ratio between the low and high frequency power spectrum of HRV is widely accepted as an index of balance between the sympathetic and parasympathetic system, to quantify autonomic function. However, one should take into account that

low frequency power is also affected by respiratory or tidal volume. Novak's study has clearly demonstrated by continuous slowing of respiration frequency that the nonrespiratory frequency content can pace the hemodynamic fluctuation in this range [Novak *et al* 1993]. If the respiratory spectral content in the frequency range, 0.05- to 0.1- Hz, is not extracted, or if respiration is not considered, the indexes based on the ratio of low to high frequency can be artificially elevated. In contrast, our slow components of impulse response are more informative in quantifying the balance in the sympathetic and parasympathetic system due to respiration.

Furthermore, our result for the supine and standing posture (Tables 9-3 and 9-4) is consistent with and validates the observation of Mullen *et al* [1997] who used a high order ARX model. They found that the statistically significant changes occur in decreasing peak amplitude, but with no statistically significant change in increasing area and characteristic time from supine to standing. Corresponding to a decrease in peak amplitude, our results also show a significant decrease in the amplitude of both components which in term show a weaker response mainly to parasympathetic input. Mullen *et al.* [1997] also found a slightly increased characteristic time. However, the slow time constant in our model increased significantly, this is consistent with the well-accepted finding that posture changes are accompanied by a shift in the balance between sympathetic and parasympathetic activity.

Using this slow component, we then tested further the hypothesis that the slow component in impulse response can be an index of balance between cardiac sympathetic and parasympathetic modulation on the evidence of HRV response to ILV in patient subjects with a large sympathetic input. The sensitivity of our model components to the change of sympathetic modulation due to respiration is well demonstrated by a statistical comparison among healthy subjects, patients and patients with a large sympathetic input (Tables 9-9 and 9-10). The slow time constant is significantly larger in patients with a large sympathetic input than in the others while parasympathetic components are not significantly different. These finding are consistent with the fact that the sympathetic system can only mediate low-frequency fluctuations in HRV [Saul *et al* 1989,1991]. These observations also give further support to the proposition that an assessment of the relative sympathetic–parasympathetic balance can be derived by analysis of slow components of impulse response from the low order ARX model.

9.4.3 The cardiorespiratory coupling for patient subjects

The influence of voluntary control of breathing on human autonomic activity is small [Cooke *et al.* 1998] confirming the efficacy of the random breathing control technique to maintain a relatively constant respiratory stimulus over a variety of conditions (in both of the relevant frequency bands, HF and LF). However, the need for voluntary control of respiration limits the scope of applicability of the random breathing method to patient subjects, especially for those subjects who are not able to cooperate with the investigator. For this reason, it would be useful to have an ARX model to assess RSA in uncontrolled situations.

To our knowledge, this is the first attempt to use an ARX model to quantify RSA for patients in uncontrolled situations where the spontaneous breathing pattern can take on a variety of forms. Our study shows that the results of this system identification for patients are reliable quantitative indexes of RSA if one can ensure that cardiorespiratory interaction is linear and stationary. This is achieved by checking if the values of the coherence function are above the 0.5 threshold, and the recurrence plot and RID time frequency distribution are used to test for nonstationarity and nonlinearity, i.e., selecting records suitable for further system identification.

Fig. 9-10 and Table 9-11 present the results of the coherence analysis showing that 8 subjects (GP3) of 41 patient subjects have very low coherence function in both the high and low frequency range. As well, results from 9 subjects in patient group GP4 having poor linear cardiorespiratory interaction although around 0.5 coherence in both high and low frequency range, are presented (Table 9-11, Figs. 9-1 and 9-2). Taken all together, 42% of patient subjects (17 subjects from a total of 41 patient subjects) can not be modeled by our linear low order ARX model, as opposed to healthy subjects where 100% could be modeled.

The present study was performed to determine the accuracy and reliability of estimating the RSA impulse response from healthy subjects, the general patient subjects and the patient subjects with a large sympathetic input in which the breathing pattern in some subjects is spontaneous. Table 9-7 lists the components of impulse responses of healthy subjects, patients and patients with a large sympathetic input. From the comparison between healthy and patient subjects shown in Table 9-8, the amplitude of both slow and fast components for patient subjects are significantly smaller than those for healthy subjects. This result demonstrated that HRV has a weaker response to both sympathetic and parasympathetic changes due to respiration in patient subjects than in healthy subjects whereas both time constants

are not much different. The most plausible explanation for this phenomenon is that the balance between sympathetic and parasympathetic is little changed when we compare generally healthy subjects with patients. This explanation also can be proved by the significant change of time constants due to more sympathetic input in patients.

Comparison of patients whose medical records were known, 22 patients with good models and 14 patients with poor models, shows the poor group had a significantly greater pre-operative history of vascular disease, smoking, or thyroid disease ($p=0.002$). This may be one major explanation for nonlinear cardiorespiratory coupling for patient subjects with poor ARX models. In addition, the results of this comparison also show that there was no significant difference between the groups as to age, sex, or operation type. However, these speculations need to be tested more rigorously in further study.

Chapter 10

Conclusions and Future Research

The goal of this thesis can be summarized in the following question, that has underlain the whole research: "Can the low order ILV-HRV ARX model be used for cardiovascular system identification in order to assess the respiratory sinus arrhythmia in healthy subjects and patients?" While RSA has been widely used as an indicator of impaired autonomic regulation of the heart, i.e. as a noninvasive measure of vagal cardiac input, the exact causative mechanism of RSA is unclear. Classical signal processing, such as transfer function analysis has been performed on the relation between ILV and HRV signal and shown its value both in extending the understanding of RSA and in suggesting a noninvasive measure for clinical practice. However, this type of analysis has shown limitations, so recent work has turned to more innovative techniques such as system identification based on the ARX model, time-frequency analysis and neural networks.

10.1 System Identification Using the Low Order ARX Model

Recently, the application of system identification methods to the analysis of the fluctuations in cardiovascular variables, based on the ARX model has been widely used to represent the dynamics of the cardiovascular system. It provides useful information about the dynamic behavior of the autonomic nervous system. While ARX models with high model order in previous research agree well with the

observed data in random breathing, a question remains concerning the number of model parameters. Does the model with a high order describe the 'true system', and can the high order of the model be physiologically interpreted in accordance with *a priori* knowledge of the dynamic relationship between ILV and HRV?

After an introduction to the ARX model, a low order ARX model, based on both mathematical theory and the relationship between ILV and HRV, was proposed in this thesis. Regarding the applicability of the low order ARX model to the cardiovascular system, the need for signal processing and selection was suggested to ensure the system was linear and stationary.

Linear detrending before modeling and prefiltering of the output signal were shown to be efficient in removing the nonstationary components and cutting away the noise or unwanted part of output signal. The effects of different filters on the stationarity of the output signal HRV were explored by using the recurrence plot.

In addition to nonstationarity of the system, we still found it necessary to check any nonlinear effects in the output resulting from the input. RID cross time-frequency analysis provides a tool to check any nonlinearity and nonstationarity in the system before setting up the linear ARX model.

An obvious improvement regarding system identification is to achieve a low order ARX model. Based on prefiltering data, both the false nearest neighbors (FNN) algorithm and visual inspection of the loss function are reliable for determining model order. In addition, the dead time was estimated accurately by both correlation and ARX model estimation method. As a result, good model qualities obtained by low order ARX models were proved by model validations, and agreed well with the results of previous research.

The simplicity of our ARX model has contributed to the explanation of qualitative properties of the system. As one of this model's contributions, the low order ARX model makes it possible for the impulse response to be analytically decomposed into two combinations of exponential decays, i.e., the fast and slow response components. Applying the low order model parameter analysis in respiratory sinus arrhythmia, these low order ARX model parameters are demonstrated to be able to characterize quantitatively the system and evaluate how the respiratory sinus arrhythmia adapts in response to varying physiopathological conditions.

Furthermore, to identify the different inputs (ILV and SBP) contribution to the system response (HRV), NNARX model sensitivity analysis was performed, which provided a good support for our cardiovascular system model.

From a technical point of view, one of the main achievements of this work has been to show that the low order ARX model performed well in system identification of RSA after the ILV and HRV signal was prefiltered. However, such a single input low ARX model is unable to account for the effects of ILV on HRV mediated by blood pressure fluctuations. Therefore a dual-input low order ARX model was used for the cardiovascular system with input ILV and SPB, but both model order and dead time had to be well qualified because of low frequency of effects on HRV from SPB. Moreover, the baroreflex acts as a nonlinear negative-feedback which tends to stabilize arterial pressure. Significant nonlinearities have been found in heart and blood pressure [Eckberg 1980]. Therefore, the nonlinear interrelations between HRV and SPB affect the linear system identification.

In addition to coherence analysis, RID cross time-frequency analysis was proposed to visually check the nonlinear cardiorespiratory coupling. However, we found the strength of cardiorespiratory coupling can not be estimated by this method. We failed to develop a time-frequency distribution coherence which would give us the coherence distribution in the t-f plane. Certainly, a time-frequency distribution coherence would not only enable more sensitive nonlinear cardiorespiratory coupling classification of patient subjects than conventional linear coherence and cross time-frequency distribution, but could also improve the understanding of cardiorespiratory coupling in medical diagnosis. Alternatively a new approach to estimate nonlinear cardiorespiratory couplings involving independent measures of complexity and predictability, were proposed recently by Hoyer *et al.* [1998], which enabled a quantitative evaluation of the different coupling strengths during sleep and active state. Further applications to cardiorespiratory coupling in healthy subjects and patients would be of interest.

10.2 Analysis of the Model Parameters in Respiratory Sinus Arrhythmia

Once the cardiovascular system model had been established, the schemes proposed and studied in the low order ARX model technical section of this thesis have been applied to ILV and HRV signals for analysis of RSA,. Their usefulness for such system identification has been addressed. Five groups of data recording were taken, coming from healthy subjects, general patients and patients characterized by features

such as a large sympathetic input, patients having a history of vascular disease or thyroid disease, or heavy smoking.

The human cardiovascular system model has been proposed to represent relationships between HRV, ILV and SBP and gives physiologically reasonable explanations of the origin of RSA in humans in normal condition. The model demonstrated that the central linkage of respiratory rhythm-generating neurons with cardiovagal motor neurons in the medulla would form the major contribution to RSA. The sensitivity analysis of HRV to changes in ILV and SBP was performed by using a neural network. The results showed good agreement with our cardiovascular system model.

The success of the cardiovascular system identification using the low order ARX model has been shown by the fact that the results are consistent with accepted physiological findings. We have been able to get equivalent results with a low order model in healthy subjects – much more physiologically meaningful. Moreover, for both random and regular breathing patterns, the quality of the low order ARX model proved to be good.

The simplicity of our ARX model has contributed to the explanation of qualitative properties of RSA. The two components of impulse response of HRV reflect autonomic nervous cardiorespiratory modulation. Based on the physiological meaning of the two components of impulse response, model parameter analysis of RSA allows us to evaluate the differences found in the assessment of autonomic control variations in breathing pattern and in posture in healthy subjects and in variations due to sympathetic input in patients.

As one of main results, compared with the ratio HF:LF, the slow components of the impulse response have been proved to be more informative to quantify the balance in the sympathetic and parasympathetic system due to respiration. The model parameter analysis on the basis of a low order ARX model appears to be a desirable means of evaluating the effects of physiological alterations associated with pharmacological interventions, changes in the environment, physiological stresses and disease processes.

The use of an ARX model to quantify RSA for patients in uncontrolled situations seems to yield more information. On the one hand, 24 of 41 patient subjects were modeled well by a low order ARX model, although this rate is significantly lower than in the healthy subjects where all were modeled well. A possible extension of this work would then consist of analysis of the impulse components for different patients and assessing the possibility of getting alternative classification parameters.

On the other hand, the bad model group had significantly more pre-operation history of vascular disease, smoking, or thyroid disease. However, it remains to verify if this really is a feature of this group, or if it is possibly due to the low quality of the recording.

The ambitious question raised at the beginning of this work has only been partially answered here. While indications have been given on the possible use of a low order ARX model in healthy subjects and patients, many questions remain open. The model parameter analysis provides a new way of studying and monitoring RSA, and may bring something to clinical practice. However, it is by no means proven that the linear low order ARX model can reliably be used in medical practice. The problem discussed above, such as its poor applicability to a number of patients, (the bad model group), must be solved before this question can be answered.

Appendix A

Heart Rate Band-limited Interpolation

Henderson, J. D., H. Bo, J. P. Meagher, and J. W. Sleigh

Abstract

The heart rate signal and its power spectral density have been widely employed in studies of the autonomic system. Inherently the heart rate signal can only be sampled irregularly, at discrete time intervals determined by the heart rate, and therefore ambiguity arises over its frequency content. A new method for estimating a set of uniform samples from the non-uniformly sampled heart rate data, Iterative Band Limited Interpolation (IBLI), has been developed and results are presented demonstrating its application to the estimation of heart rate power spectra. In the first instance results are derived from data generated by the theoretical Integral Pulse Frequency Modulation (IPFM) heart pacemaker model. These results show that spectra recovered by the new method do not display the undesirable high frequency roll off, harmonic content and intermodulation products which are characteristic of previous methods of heart rate estimation. A second set of results derived from clinically measured ECGs by means of the new method shows increased high frequency content in heart rate spectra thereby demonstrating other methods of heart rate measurement may well underestimate the high frequency power present in the heart rate spectrum.

Introduction

An efficient method for determining the heart rate signal from the ECG was reported and evaluated by Berger *et al* [1986], and has subsequently been used by this group in studies of autonomic heart rate control, [1989]. They showed that power spectra recovered by means of their method almost exactly match the ``true" heart rate spectrum as indicated by the Integral Pulse Frequency Modulation model, (IPFM), of heart rate control. The IPFM model has been widely used in heart rate studies, [Berger *et al* 1986, DeBoer *et al* 1987, Hyndman *et al* 1975, Rempelman *et al* 1977]. We will show in our analysis that the method proposed by Berger et al, which we will subsequently refer to as the Berger method, is based on linear interpolation of the integrated heart rate signal and that despite its many useful properties, eg., simplicity and speed, it underestimates high frequency content relative to more sophisticated interpolation procedures. In this paper, we analyze three methods for recovering the heart rate signal. The first is based on linear interpolation, of which the Berger method is a principal representative. The second is based on interpolation by means of the cubic spline, see Brown *et al* [1993] and the third is the new method we are proposing, Iterative Band Limited Interpolation (IBLI).

The heart rate signal, as determined from the ECG, is postulated to be a continuous signal for which samples are available only at irregular intervals in time, see figure A-1. Thus to obtain its spectrum assumptions must be made about values taken by the signal between sample points. Commonly, interpolation is based on the assumption that mathematical functions have a polynomial nature between samples and as we shall show, the Berger method assumes a first order polynomial while other procedures such as the Lomb Transform [1976] for determining power spectra of non-uniformly sampled data use Lagrangian interpolation, i.e., higher order polynomials. While recognizing that in the absence of greater physiological information than afforded by the IPFM model, e.g., details of cardiac pacemaker activity, there is a degree of arbitrariness in the form of the heart rate signal, we feel that a more appropriate assumption than polynomial smoothness is that the signal be band-limited, i.e., contains no frequency content above half the *average* sample rate. The reason for this assumption is that the signal is the output of a physical process - the autonomic system which is generally slow acting and therefore band-limited. We shall show that the band-limited assumption is sufficient to determine the signal and its power spectrum. This result is similar to that given by the Shannon sampling

theorem [Jerri 1977], with the difference that here we are dealing with a non-uniformly sampled signal.

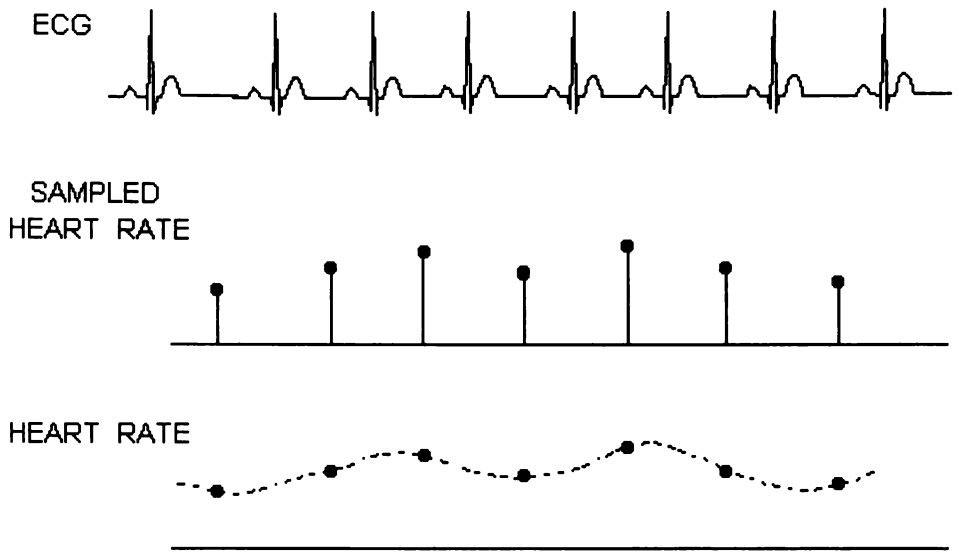

Figure A- 1 The Heart Rate Signal. The heart rate samples equal the inverse R-R intervals of the ECG. The dotted heart rate signal signifies that values in between samples are unknown.

The heart rate signal is of particular interest in studies of cardiovascular dynamics, [Appel *et al* 1989, Bianchi *et al* 1993, Muzi *et al* 1993, Galletly *et al* 1992], but it is not the only example of a non-uniformly sampled signal for which the spectrum is required. Other instances include astronomical observation [Lomb *et al* 1976], x-ray computed tomography [Bates *et al* 1983], and machine vision [Knutsson *et al* 1993]. We therefore note that while we are using spectral analysis for investigating autonomic control in anaesthetized patients [Henderson *et al* 1993, Ireland *et al* 1996], the method of band-limited interpolation based on non-uniform samples we are proposing may have wider application than for heart rate alone.

The Heart Rate Signal

When analyzing the dynamics of the autonomic system the various physiological variables such as arterial blood pressure and instantaneous lung volume are available as continuous analogue functions of time. However, as demonstrated above, heart rate as determined from the ECG can only be measured on a point by point basis. This leads us, along with other workers in the field, Berger *et al* [1986], DeBoer *et al* [1987], Rempelman *et al* [1977], to postulate an underlying continuous signal

which in the dynamics of cardiac control is representative of heart rate. Following these workers such a signal may be considered as the input controlling the IPFM cardiac pacemaker model.

Unfortunately, there is no universal agreement in the literature as to whether heart rate should be expressed in terms of the R-R interval or its inverse. Along with Berger et al we have used the reciprocal R-R interval as the measure of heart rate because we believe with them that as hemodynamic variables such as blood pressure and flow have a direct rather than inverse relation to heart rate then the inverse R-R interval, i.e. beats per unit time is more appropriate as a state variable, especially in system models of autonomic control.

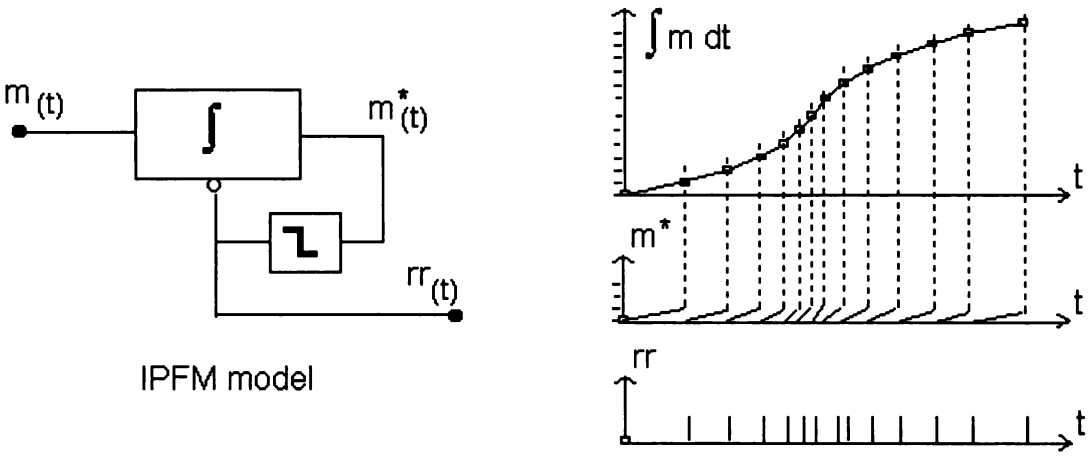

Figure A- 2 The IPFM model. (b) Associated signal waveforms. Note: sample points of $\int m\,dt$ are equally spaced on the vertical axis.

The IPFM model is shown in figure A-2(a). The input $m_{(t)}$ is integrated until the integrator output reaches a threshold whereupon it resets and emits a pulse. Shown in figure A-2(b) are waveforms associated with the IPFM model and also shown because of its importance is the unrest integral of m(t). The output pulse train rr(t) simulates the R-R interval sequence of the ECG and each RR interval is a measure of the average input during that interval. Thus, it can be seen that the input signal controls the frequency of the oscillator and it may therefore be considered to be the continuous heart rate signal. The purpose of any heart rate recovery algorithm should be to recover the complete signal m(t), not just its average over each beat, and moreover this recovery should be obtained solely by means of knowledge of the pulse train rr(t).

As m(t) is the derivative of $\int m\,dt$, the problem of recovering the heart rate signal m(t) can be solved by first determining and then differentiating $\int m\,dt$. Referring to the figure A-3, it is $\int m\,dt$ apparent that is a function which, to within a multiplicative constant, (the integrator threshold h), passes through the points:

$$(0, 0),(t_1, 1),(t_2, 2)\ldots (t_n, n)$$

Thus $\int m\,dt$ is a continuous function which is non-uniformly sampled along the time axis. The various methods of determining heart rate make different assumption about the nature of between sample points.

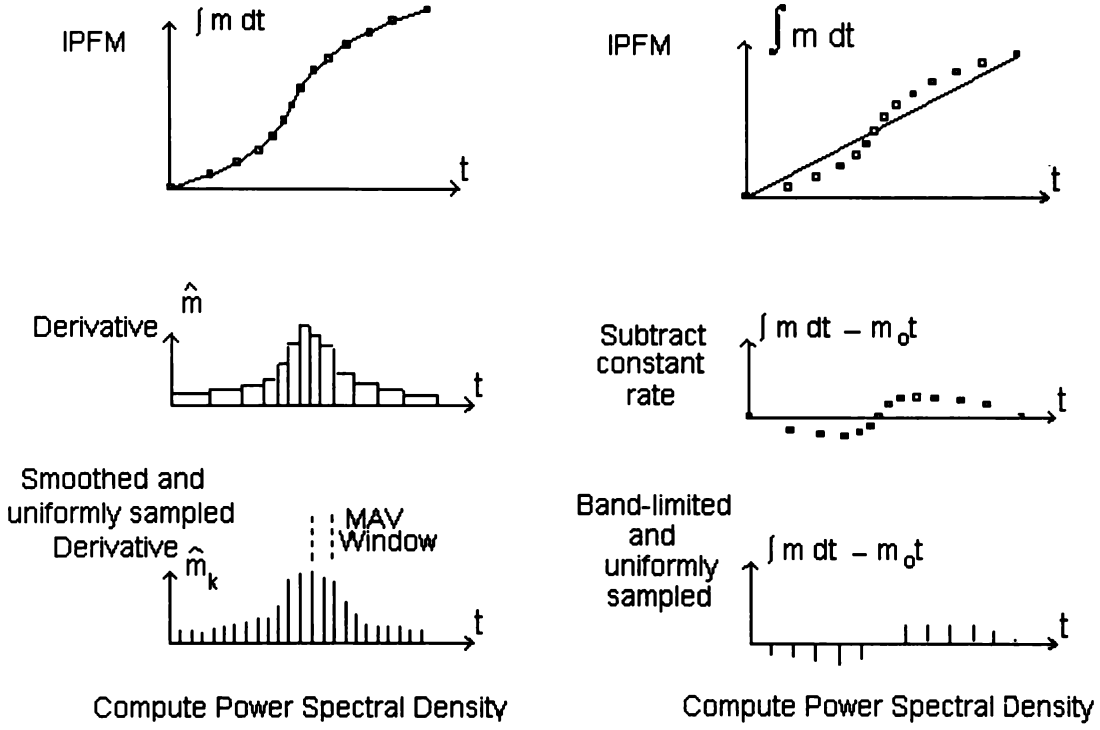

Figure A- 3 Illustration of methods for finding Heart Rate Spectral Density by, (a) the Berger method, (b) the Iterative band-limited interpolation method.

Methods for Recovering Heart Rate

The Berger Method

The Berger method as given in [1986] can be shown to involve the following procedure. Referring to figure A-3 (a), $\int m\,dt$ the function is linearly interpolated between sample points and the derivative of this piecewise continuous function is determined, in the time domain, resulting in a discontinuous function which is constant between sample points. Its spectral density is then found, first applying a moving average digital filter with a sample rate several times greater than the average heart rate and with a window width of twice the sample period. This procedure serves to provide a set of uniform samples for spectral analysis and also provides an anti-aliasing filter to remove the higher frequencies introduced by the discontinuities. Lastly, the effect of the moving average filter is compensated for by applying its inverse to the spectral density in the frequency domain. Thus it can be seen that the Berger heart rate is the time derivative of the linearly interpolated.

Cubic Spline

The cubic spline being continuous in its first denvative $\int m\,dt$ is widely used to produce smooth interpolation of sampled data see Brown *et al* [1993]. In this particular application, the only difference from the Berger (linear) method described in section A is that the uniformly sampled heart rate signal is recovered by applying a cubic spline to $\int m\,dt$.

Iterative Band-Limited Interpolation, (IBLI)

Any signal containing frequencies no higher than W is uniquely specified by a set of samples, $\{f_n\}$, uniformly spaced in time by $\Delta T=1/2w$ - the Nyquist sampling rate. The value of the signal at any time t may then be recovered by the band-limited interpolation, [Jerri 1977]:

$$f_{(t)} = \sum f_n \frac{\sin(\pi(t - t_n/\Delta T)}{(\pi(t - t_n)\Delta T)} \qquad \text{(A-1)}$$

Therefore if over a period T, 2TW arbitrarily spaced samples of the signal, $\{f_p\}$ are taken at times $\{t_p\}$, it is possible to write down the set of 2TW equations:

$$f_p = \sum f_n \frac{\sin(\pi(t - t_n/\Delta T)}{(\pi(t - t_n)\Delta T)}, \qquad p = 1....2TW \qquad \text{(A-2)}$$

Then in principle it is possible to recover the unknowns, i.e., the uniformly sampled set $\{f_n\}$, by solving these equations. However this involves inverting a large matrix and the process may also be susceptible to noise and numerical error.

The algorithm we have developed solves these equation iteratively by first estimating the unknown coefficients $\{f_n\}$ by means of a cubic spline interpolation from the known $\{f_p\}$, and then substituting these in equation (A-2) to determine a set of residuals, i.e., differences between actual and computed $\{f_p\}$. The residuals are then interpolated, again by means of the cubic spline, to find corrections to the set $\{f_n\}$ and so the process continues until the residuals are negligible. It must be noted that the cubic spline in this procedure acts only as an *estimator* in the iterative process, not as in last section where it provides the actual interpolation. The essential property of the cubic spline in the iterative process is that residuals at samples far from a particular point will have an influence on corrections applied at that point. This is important because the uniformly sampled points which are being estimated also have a wide range influence through the sin(x)/x function. A second useful property of the Cubic spline is that its coefficients are found by solving an almost diagonal matrix and so large computer storage is not required.

Our method of recovering heart rate is illustrated in figure A-2(b). First $\int m\,dt$ is divided into two components: m_0t due to the average heart rate and the variable component, $\int m\,dt - m_0t$. As the first of these contributes only dc power to the heart rate spectrum, spectral analysis need be applied only to the second component. IBLI as described in the previous paragraph is applied to the variable component of $\int m\,dt$, yielding a set of samples uniformly spaced along the time axis at intervals equal to the average heart rate. Differentiation is then required to find the variable component of m(t). This is achieved by performing an FFT, multiplying by $j\omega$ and doing the inverse FFT. We then find the power spectrum using Welch's method as described in following section.

Methods for testing and applying the algorithms

IPFM test inputs

Following de Boer *et al* [1987] and Berger *et al* [1986], we test the algorithms using the IPFM model. Sinusoidal inputs m(t) of different frequencies and harmonic

content generate sequences of r-r intervals characteristic of heart rate as seen in the ECG.

First, a dc term plus a single harmonic component with varying frequency *f*, varied over the range 0-0.4Hz, is used to test the capability of the algorithms to recover the amplitude of the variable component irrespective of its frequency and to test for the generation of spurious harmonics. Thus

$$m(t) = 1.0 + 0.3\cos(2\pi ft) \qquad \text{(A-3)}$$

Second, a dc term plus two harmonics is used to test whether any of the algorithms will (incorrectly) indicate the show the presence of Intermodulation products. Thus

$$m(t) = 1.0 + 0.3\cos(2\pi ft) + 0.3\cos(2\pi f2\, t) \qquad \text{(A-4)}$$

In both cases the reset threshold of the integrator is set at h=1.05s.

For purposes of comparison, the choice of the input signals equations (A-3) & (A-4) and the IPFM parameter h is the same as used by DeBoer *et al* [1987] and Burger [1986]. Note that the dc component of m(t) acting alone would result in a sequence of output beats with a frequency of 1/h or 57.14 bpm. Similarly, the harmonic components have peak amplitude 0.3 as large, i.e., 17.14 bpm. Thus the power in each of the harmonics is: $0.5x(peak)^2$, i.e., 146.9 bpm^2. These signals provide a severe test of the algorithms because they represent heart rates varying by plus and minus thirty percent, resulting in very irregularly sampled signals - at the upper end of cardiac variability.

The r-r sequences formed by the IPFM model are processed using the three different methods of interpolation, (i) iterative bandlimited interpolation, (ii) cubic spline interpolation and (iii) the Berger (linear interpolation) method. We again emphasize that cubic spline interpolation should not be confused with IBLI in which the cubic spline is used merely as an estimator.

The recovered heart rate signals are processed to produce power spectra using Welch's method [1967]. We divide the signal resample at 2.56 sample/s into half-overlapping segments each 100s in length, apply a Bartlett data window and compute and add the periodograms of each segment. Again, for purposes of comparison with results of previous workers the Bartlett window was chosen.

Clinical ECG test inputs

After testing the algorithms with IPFM generated data, the algorithms were applied to clinical data obtained from patients' ECGs by means of a 12-bit ADC at 200 samples/s. RR intervals were determined to +1/ms accuracy using quadratic interpolation between samples at the top of R wave to estimate the exact peak position. The RR sequences were then processed exactly as described above for the IPFM model outputs.

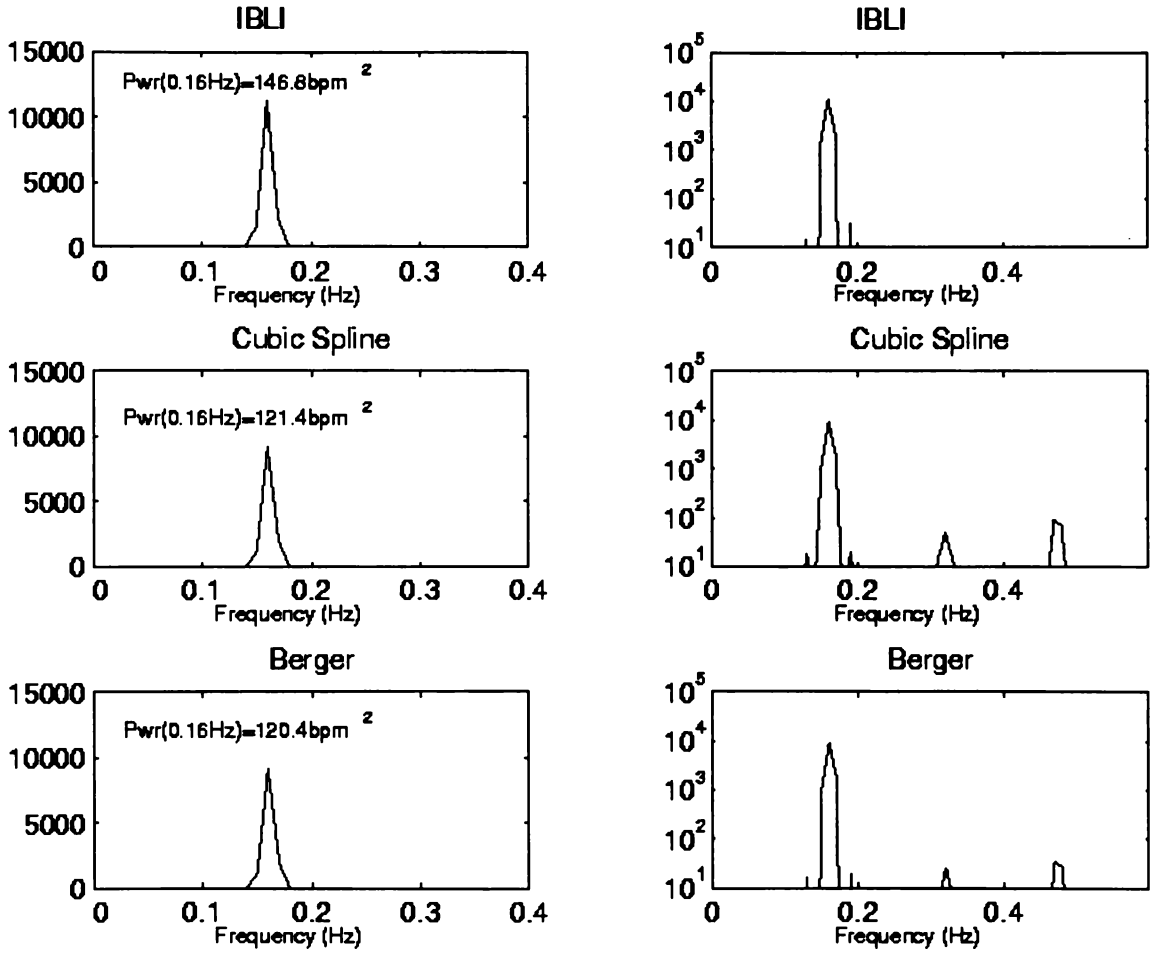

Figure A- 4 Spectral density of heart rate signal estimated by the three methods. Single harmonic component: f = 0.16Hz present in input. Linear plot shows power in main peak and log plot shows harmonics generated by the interpolation process. (Vertical axes bpm^2/Hz)}

Results

Frequency Response and harmonics

Typical power spectra recovered by the three algorithms when tested using the IPFM model with dc plus a single harmonic (f=0.16Hz) input, equation (A-3), are shown in figure A-7. The figures on the left have linear scales so that areas represent power whereas the scales of those on the right are logarithmic so that the harmonics generated (at 0.32HZ and 0.48Hz) are more clearly visible. Computation of areas under the graphs shows that the IBLI algorithm alone recovers the true harmonic power of 146.9 bpm^2. Both the cubic spline and the IBLI algorithm is the only one not showing spurious harmonic generation.

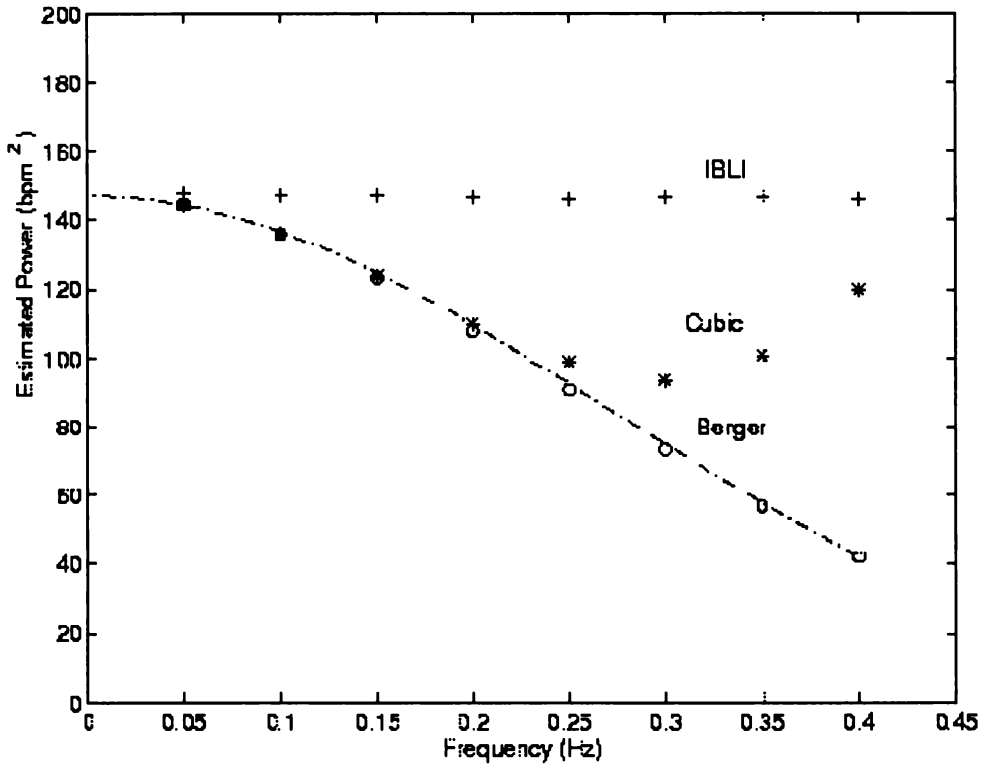

Figure A- 5 Estimated power of single harmonic component of the heart rate signal: m = 1 + 0.3 cos ($2\pi ft$) based on rr(t) output sequence of IPFM model with threshold h=1.05 (i) IBLI.(ii) Cubic spline(iii) Berger method.

Similar spectra were generated for input frequencies ranging between 0.05Hz and 0.40Hz at 0.05Hz intervals. The powers estimated by the three algorithms were found and are graphed in figure A-8. It is apparent that the IBLI method estimates the correct power across the complete frequency range whereas the other two methods both show rolloff, severely underestimating higher frequencies. The line shown on this graph is a theoretical curve associated with the Berger method and is discussed later.

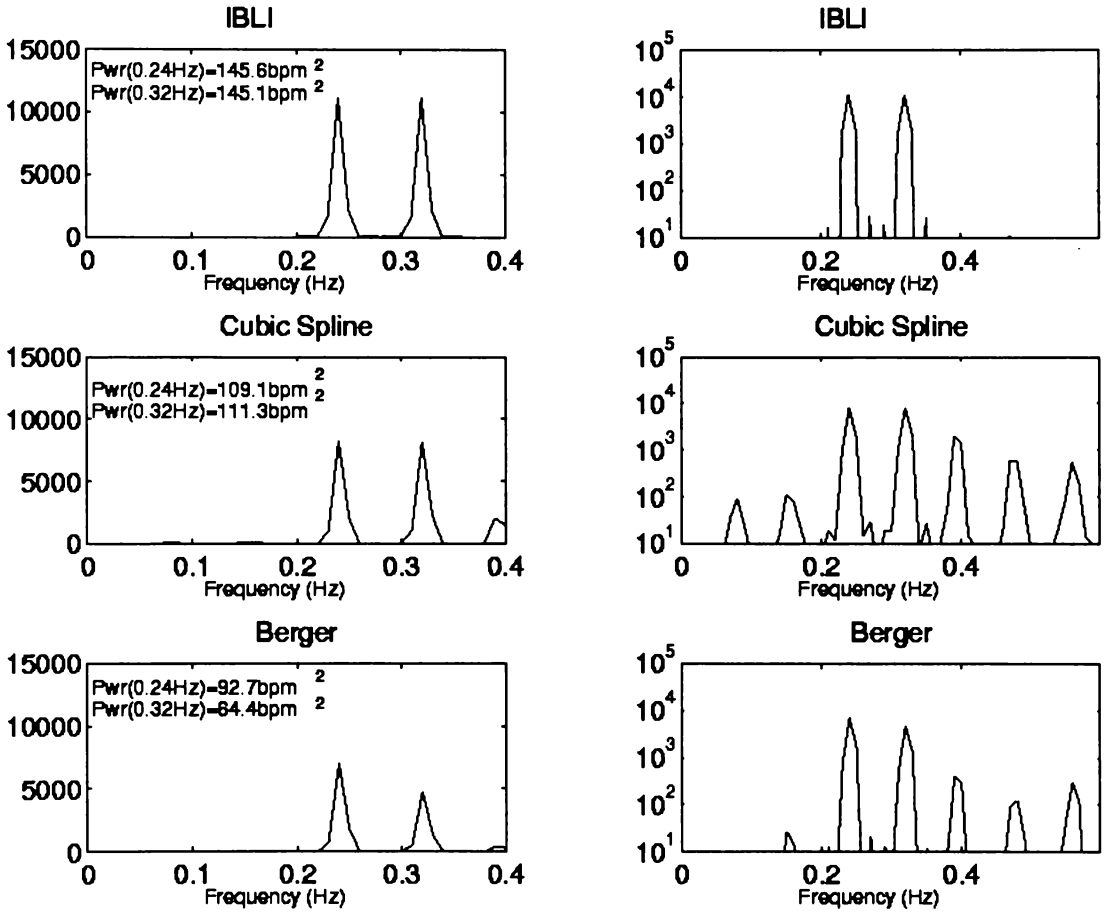

Figure A- 6 Spectral density of heart rate signal estimated by the three methods. Two harmonic components: f = 0.24Hz, 0.32Hz present in input. Linear plot shows power in main peaks and log plot shows harmonics and intermodulation products, (generated by the interpolation process) (Vertical axes bpm^2/Hz)}

Intermodulation products

Typical power spectra recovered by the algorithms when tested by an input having two harmonic components (f=0.24Hz, f=0.32Hz), equation A-4, are shown in figure A-6. The figures on the left with linear scales again show that the IBLI has no high frequency roll off which however is clearly seen is the response of the other two methods. The figures with log scales clearly demonstrate Intermodulation products in spectra obtained by the Berger and cubic spline methods. The small spike apparent in the IBLI spectra is sidebands due to the finite width of the data window.

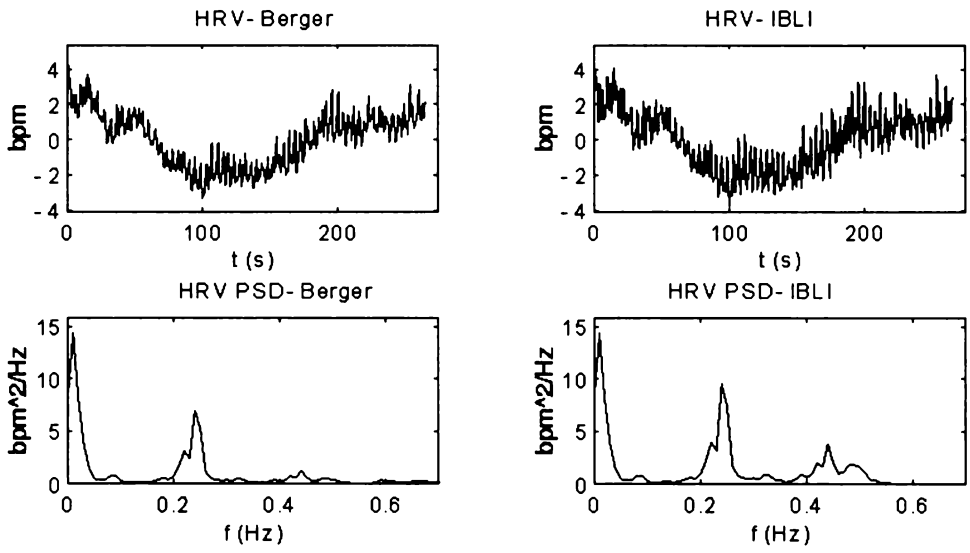

Figure A- 7 HRV plotted as departure from the mean and its spectra as determined by Berger and IBLI methods notice how the IBLI methods recover greater high frequency components

Clinical heart rate spectra

A patient heart rate signal, selected because of its strong respiratory component at 0.25Hz, corresponding to 15 breath/min, is shown in figure A-7. Its spectra computed by the Berger and the IBLI method are similar. However, the higher

frequencies are attenuated in the former as would be expected from the IPFM model results above. When the areas are calculated, the ratios of power in the three bands: 0--.05 Hz, 0.05-0.15Hz, 0.15-0.5Hz are found to be: 101%, 100%, 168%, thus demonstrating the Berger method underestimated high frequency power. Notice also, as is to be expected, that there is no power in the IBLI spectra above 0.58Hz, corresponding to 34.8 cycle/min which is half the average sample rate, ie, the average heart rate of 69.6bpm.

Discussion

The results of our analysis show that the IBLI method gives improved estimates of power spectral density in several respects: no roll off with frequency, figure A-8, negligible generation of harmonics figure A-7, and no intermodulation products, figure A-6. Furthermore, the clinical spectra computed using IBLI show substantially increased power in the higher frequency 'respiratory' band.

Frequency roll off

The Berger and Cubic spline, (both polynomial type), interpolations provide uniformly sampled heart rate signal but lead to power spectra with underestimation of harmonic components as frequency increases, figure A-8. Some appreciation for the cause of this behavior can be gained in the case of linear interpolation, ie., the Berger method by means of the following argument. If the integrated $\int m\,dt$ heart rate signal was accessible for uniform sampling at a rate equal to the average heart rate, then it could be differenced, (i.e., differentiation of a sampled signal), and passed through a zero order sample and hold. The power spectrum of the resulting signal $S^*_{M(f)}$ would be given in terms of the unsampled spectrum by:

$$S^*_{M(f)} = S_{M(f)}\left[\frac{\sin(\pi h f)}{\pi h f}\right]^4$$

where h is the IPFM threshold. See the Appendix B for the derivation of this equation. This response describes a process of linear interpolation with uniform sampling and is plotted in figure A-8 where its low pass characteristic is apparent. Despite the fact that the Berger method involves non-uniform sampling, its high frequency roll off closely matches that of linear interpolation with uniform sampling

thereby suggesting that the frequency roll off is due to linear interpolation. It can be seen that linear interpolation with uniform sampling almost identically matches the Berger response.

Harmonics and intermodulation products

Both the Berger and Cubic spline interpolation show characteristics of non-linear processing. Both result in a power spectrum having frequencies not present in the original heart rate signal. This appears to be a characteristic of polynomial type interpolation but is not present in the spectra estimated by IBLI.

Processing complexity

It must be acknowledged that the Berger method is particularly simple to implement and is very fast. The IBLI method on other hand involves considerable processing requiring up to one minute, (i486™ processor), to process five hundred seconds of heart rate data. It is for this reason, we decided to continue to its use receiving the possibility of using IBLT at a later stage.

Conclusions

1. Power spectra of band-limited signals can be accurately estimated by IBLI from a set of non-uniform samples of the type generated by the IPFM model - which is a good model for the production of rr (t) intervals of the ECG. The principal property of such signals is that sample intervals do not deviate too much, (less than +/-30\%), from the average sample rate throughout the record.
2. Band-limited estimates of power spectra produced by IBLI do not suffer frequency dependent distortion and do not generate harmonic and intermodulation products typical of the polynomial interpolation methods.
3. The Berger method which has a number of attractive features, notably speed, underestimates higher frequency power spectrum components.
4. The IBLI power spectra method is computationally far more demanding than the linear, (Berger), method which therefore remains the preferred method in practical situations. However, it does provide a means for assessing the accuracy of the latter

in problematic situations, in particular where underestimation of high frequencies is a suspected. This is currently being investigated.

Appendix

Suppose that $p(t)=\int md$, i.e., the integrated heart rate signal shown in figure (2), is available for measurement. Then a signal *q(t)* formed by the difference between p(t) advanced by △T/2 and *p(t)* delayed by △T/2 will represent $\int mdt$ over the interval (t+△T/2, t-.△T/2). If this signal is then sampled regularly by means of a sample and hold circuit with sample period △T the output will be a set of constant values representing the $\int mdt$ over successive sample intervals. It is therefore, when multiplied by 1/△T, identical to the heart rate signal b(t) which would be produced by the linear interpolation algorithm, (Berger method), when $\int mdt$ is uniformly sampled. This process is shown in figure (A-8).
Therefore, in the frequency range f < 1/2△T and with the Fourier transform of m(t) given by M(j):

$$B(j\omega) = \left(\exp^{j\omega\Delta T/2} - \exp^{-j\omega\Delta T/2}\right) \times \left(\frac{\exp^{j\omega\Delta T/2} - \exp^{-j\omega\Delta T/2}}{j\omega\Delta T}\right) \frac{M}{j\omega\Delta T}$$

$$= \left(\frac{\exp^{j\omega\Delta T/2} - \exp^{-j\omega\Delta T/2}}{j\omega\Delta T}\right)^2 M$$

$$= \left(\frac{\sin(\tau/\Delta T}{\tau/\Delta T}\right)^2 M$$

Now the sample rate is not constant, but over a long period P, the number of integrator resets in the IPFM model will be given:

$$n = \frac{1}{h}\int_0^P mdt = \frac{Pm_{av}}{h}$$

Therefore the average sample period will be:

$$\Delta T_{av} = \frac{P}{n} = \frac{h}{m_{av}}$$

As the input has the form:

$$m(t) = 1.0 + 0.3\cos(2\tau / t), \qquad then \quad \Delta T_{av} = h$$

Letting the power spectral density of m be given by SM(f) and that of b be $S^*M(f)$ we can substitute $\Delta T_{av} = h$ for ΔT in the result for the Fourier amplitude ratio above, to obtain the approximation:

$$S^*_{M(f)} = S_{M(f)}\left[\frac{\sin(\pi hf)}{\pi hf}\right]^4$$

This expression becomes more exact as heart rate and hence sample rate becomes more constant.

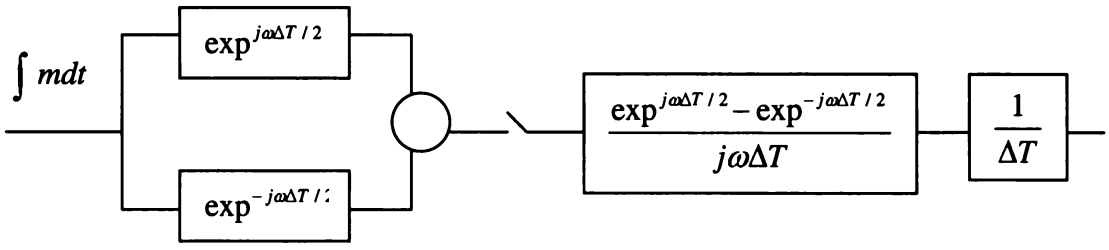

Figure A- 8 Processing of $\int mdt$ to produce the uniformly sampled Berger Heart Rate signal.

Appendix B

Variability of R-R, P-R and R-T Intervals

Forester, J., H. Bo, J. W. Sleigh and J. D. Henderson

Abstract:

We analyzed the effect of changing from supine to standing on the variability of R-to-R(RR), P-to-R(PR) and R-to-T(RT) intervals in 10 healthy volunteers using power spectral analysis. An ECG and respiratory trace were recorded before and after postural change. Variability in the PR and RT intervals was much less than in the RR interval and demonstrated a lower low frequency(LF) to high frequency(HF) ratio. Changing from a supine to standing position showed no change in indices of vagal influence on the PR and RT variability; in contrast to the well documented decrease in the indices of vagal influence on the RR variability; (HF power decreased from 2.33 to 0.41msec^2, p=0.003; the amplitude of the respiration-to-heart rate impulse response decreased from 31.6 to 14.4msec/ml/sec, p=0.03; and the LF:HF ratio increased from 1.96 to 5.22, p=0.005). We concluded from this study that the effects of standing were an observed reduction in vagal influence on the HRV of the RR interval whilst maintaining lung-volume related vagal modulation of the PR and RT intervals.

Introduction

Heart rate variability (HRV) is influenced by a variety of physiological stimuli and has been used to try to understand some aspects of the cardiovascular control mechanisms. Almost all attention has been focussed on various ways of analyzing the RR interval or heart rate. However, there is evidence that specific branches of the autonomic nervous system may influence different parts of the cardiac cycle to differing degrees. For example, the QT interval is prolonged in sleep, independent of heart rate [Browne *et al* 1982], suggesting cardiac cycle length (RR interval) and repolarization (QT interval) are independently controlled by the autonomic system. Power spectral analysis (PSA) has been commonly used to quantify the relative dominance of vagal and sympathetic influence on the heart [Malliani *et al* 1991, Pomeranz *et al* 1985]. Whilst the interpretation of PSA of HRV in various clinical situations is not fully understood, it is widely agreed that the area under the high frequency (HF) peak (0.15-0.4Hz) is predominantly related to respiratory modulation of the cardiac vagal input (Van 1993); and the relative low frequency (LF)(0.04 - 0.15Hz) to high frequency ratio (LF: HF) is a reasonable measure of the relative effects of the sympathetic and parasympathetic outflows to the SA node in healthy volunteers [Malliani *et al* 1994]. In the supine position, there is a vagal predominance, whereas the upright position results in vagal inhibition and sympathetic predominance. To our knowledge, the PSA of the PR and RT variability has not been studied previously in healthy volunteers. Therefore, this study investigates the feasibility of determining the PSA of RR, RT, and PR intervals, and reports on the effect of change in posture.

Methods

The study was approved by the regional ethics committee and full informed consent obtained from all participants. Ten healthy volunteers (4 male and 6 female) aged between 26 and 35 years (mean age 29.7) participated in the study. A three lead ECG was recorded from the subject at the same time a respiratory trace was recorded. This was achieved with inductance plethysmograph (Respitrace -Studely Data Systems, Oxford). Each data record was 300 seconds in duration. The subjects were initially supine and were cued by a computer bleep to breathe regularly at 5-second intervals. In order to determine the broad band response in terms of an impulse response, a second recording was then done after the computer program had

been changed to cue irregular breathing having a random Poisson distribution as described by Berger (2)(mean 5 sec, range 1 to 15 sec). A further two similar recordings were then repeated with the subject in an upright position. Sampling frequency was 200 Hz. Data was collected with an analog to digital converter (Strobes APC, Wellington), and stored on a personal computer for further analysis.

Waveform and Spectral analysis

The data were analyzed off-line using purpose written software written in C++ language and Matlab (Matlab 4.2, The Mathworks Inc.) The QRS complex was detected (7) and then the peak of the R wave precisely located using local quadratic interpolation of the surrounding five data points. On the basis of previous data collected at a sampling frequency of 1000Hz, this method of interpolation gave an estimated accuracy of +/-1msec. To estimate the PR and RT intervals, the peak of P wave and T wave were identified as those two peaks each side of the R peaks within a certain time window. The width of the window for the P peak was one third of the RR interval and for the T peak, the width was one fourth of the RR interval. For ease of data acquisition, we followed Sarma *et al* [1994] in using the peaks of the ECG waves to define the PR and RT intervals. Thus our usage of PR and RT interval is not identical to the commonly used definitions; which define the PR interval as being are from the start of the P wave to the start of the Q wave, and the QT interval as being from the start of the Q wave until the end of the T wave.

Cursors on the screen visually identified the R, P and T peaks being measured and allowed semi-manual editing of artifacts. The resultant RR, PR and RT intervals were then linearly interpolated by Berger's method [1986] and decimated to 2.56 Hz for further processing. This is a commonly accepted method of deriving a function that can be sampled at regular time intervals from a signal that is sampled at irregular times (i.e. when each heart beat occurs).

The signal was then transformed via Fast Fourier analysis using the Bartlett window to derive the spectral power. We followed the recommendations of the Task Force of the European Society of Cardiology and the North American Society of Pacing and Electrophysiology [1996] in the nomenclature of the various power spectral wavebands. High frequency (HF) band was 0.15 to 0.4 Hz, low frequency (LF) band was 0.04 to 0.15Hz, and very low frequency (VLF) band from 0.01 to 0.04 Hz.

Statistical analysis

To provide some internal validation of our results we used three different methods to estimate the effect of vagal modulation of heart rate. Firstly, when the subjects were breathing regularly, the power in the HF waveband was used as a measure of vagal tone. Secondly, the lung-volume to heart rate impulse response was derived from the random breathing part of the study, using the method of Yana *et al* [1993]. By 'impulse response', it is meant that a short pulse of respiratory 'energy' is introduced in order to observe the system's return to equilibrium. The impulse response function is used to describe the relationship between input (lung volume) and output (heart rate) in the time domain. Its equivalent in the frequency domain is the transfer function. The impulse response is commonly modeled using one (or two) exponential functions, thus enabling the total effect of breathing on the heart rate to be understood intuitively in terms of a certain amplitude of heart rate response per unit change in lung volume; and a corresponding time-constant to describe the time for the heart rate to return to a homeostatic steady state.

Thirdly, the HRV was normalized by using the ratio of LF: HF power as an estimate of relative sympathetic to vagal balance [Malliani *et al* 1994]. The Wilcoxon test was used to compare-paired supine and standing results, and to compare PR, RR, and RT spectra. NCSS software (NCSS 6.0.21, Kaysville, Utah) was used for statistical analysis. Data was presented as mean +/-SEM, and $p<0.05$ was considered statistically significant.

Results

Overall, the amount of power in the PR and RT spectra was two to three orders of magnitude less than that in the RR spectrum ($p<0.001$). The impulse response of breathing on the RR interval (23.0 +/-4.9 msec/ml/sec) was twenty times the PR (0.94 +/-0.29 msec/ml/sec) or RT (1.19+/-0.09 msec/ml/sec) intervals ($p<0.001$).

In the PR and RT spectra the proportion of low frequency power (LF:HF) was approximately one third of that in RR spectrum ($p<0.001$). When the subjects were breathing regularly, we were able to show a clear respiratory peak in the power spectra of all three intervals (see figure B-1).

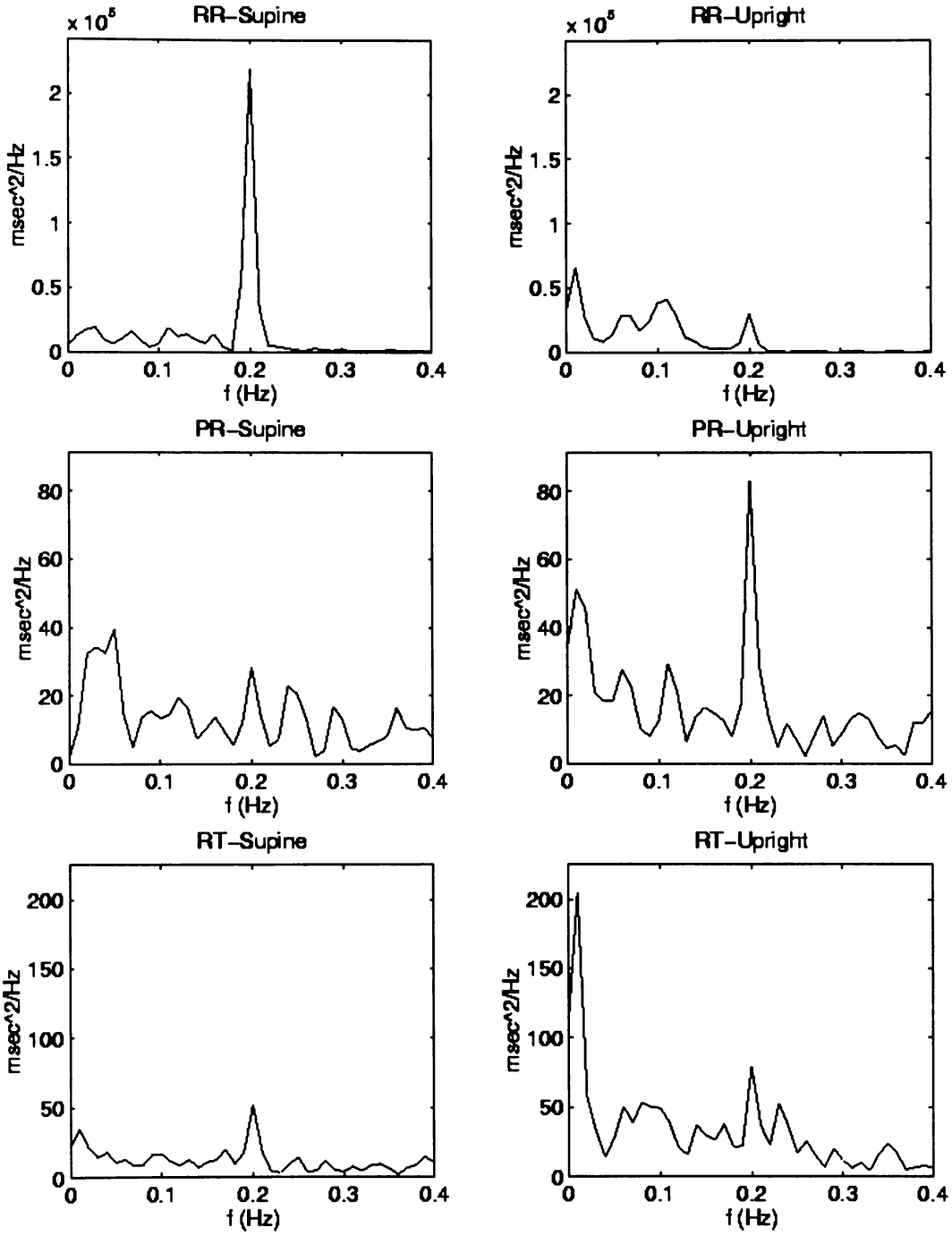

Figure B- 1 Typical power spectra of the RR, PR, RT intervals showing clear respiration-related high frequency peaks at 0.2 Hz. The vertical axis is the spectral power ($msec^2/Hz$), and the horizontal axis is frequency (Hz). The figures on the left are for an individual in a supine posture, and those on the right for the same individual when upright.

		Supine	Upright	p value
RR	VLF	1.87(0.77)	1.14(0.29)	0.55
	LF	3.23(1.11)	1.67(0.28)	0.69
	HF	2.33(0.86)	0.41(0.08)	0.003
	impulse	31.6(7.4)	14.4(2.4)	0.03
	LF:HF	1.96(0.39)	5.22(0.85)	0.005
PR	VLF	4.23(1.21)	7.18(2.31)	0.27
	LF	5.54(1.51)	8.27(2.04)	0.19
	HF	6.97(1.54)	9.49(2.57)	0.11
	Impulse	1.07(0.35)	0.81(0.23)	0.56
	LF:HF	0.77(0.07)	0.78(0.09)	0.96
RT	VLF	5.20(2.21)	7.49(3.24)	0.32
	LF	9.39(5.06)	8.83(2.98)	0.62
	HF	13.36(7.91)	13.42(4.52)	0.49
	Impulse	1.28(0.32)	1.10(0.15)	0.64
	LF:HF	0.81(0.10)	0.78(0.08)	0.62

Table B- 1 Comparison of HRV indices between the supine and upright groups. Data are presented as mean(SEM). The units of the spectral power are $msec^2$, and of the impulse responses are msec/ml/sec. Spectral power of the PR and RT indices (VLF, LF, and HF) are multiplied by a factor of 10^{-3}. The power spectral wavebands were defined as per international convention - high frequency (HF) band was 0.15 to 0.4 Hz, low frequency (LF) band was 0.04 to 0.15Hz, and very low frequency (VLF) band from 0.01 to 0.04 Hz.

The effects of posture

The mean duration of all three intervals were significantly reduced when changing to the upright position. The RR interval decreased the most (932 to 787 msec, $p < 0.001$); as compared with the PR (139 to 130 msec, p=0.002), and RT intervals (268 to 251 msec, p=0.007).

The HRV effects of change in posture from supine to standing (causing a reduction in parasympathetic activity) are summarized in Table A-1. As has been previously shown (Malliani,1994), the most striking feature is the very significant and consistent decrease in all measures of vagal activity on the SA node. There was a

decrease in R-to-R HF power, a decrease in R-to-R impulse response, and an increase in LF: HF ratio. In contrast, there was no change in any of the indices of vagal tone to the AV node, or ventricular repolarization. For the PR and RT intervals, neither the HF power, nor the impulse response, nor the LF: HF ratios changed significantly with standing.

Thus, in summary, the effects of standing were an observed reduction in vagal influence on the HRV of the RR interval whilst maintaining lung-volume related vagal modulation of the PR and RT intervals. Standing did not produce a significant change in the LF and VLF spectral power of any interval.

Discussion

This study demonstrated that it is possible to use power spectral techniques to analyze autonomic influences on the PR interval and ventricular repolarization. It must be acknowledged that, by measuring the PR interval from the peak of the P wave to the peak of the R wave, we are not accurately measuring the pure atrioventricular conduction time but are including effects of variation in P wave morphology and early bundle of His depolarization. Nevertheless AV conduction is generally considered to be the most important determinant of the PR interval (Berne and Levy. 1992), and we clearly demonstrated a respiratory related pattern, rather than random noise; even though the PR variability lay in the range of approximately 2 to 20 msec, which is at the limits of our resolution of the waveforms.

The second aspect of our study demonstrated the functional specificity in indices of activity of different branches of the autonomic supply to the heart. This complements the work by Randall and co-workers [1988] who have previously demonstrated anatomically discrete parasympathetic and sympathetic pathways to the SA and AV nodes in dogs. In addition to observing the effects of localized pharmacological blockade of sympathetic and parasympathetic influence, they also showed phasic cardiorespiratory electrical activity in the vagal ganglia leading to the SA node.

In agreement with previous studies, the effect of standing caused shortening of all three intervals, and a marked decrease in indices of respiration-induced vagal influence on the SA node (as shown by the R-to-R interval heart rate variability in the HF band, the LF: HF ratio, and the impulse-response function). In contrast, there was little change, or even an increase, in respiratory modulation on the AV

node as estimated by the PR interval HRV indices and ventricular repolarization (RT interval HRV indices). Whilst further work needs to be done to separate effects due to the local cardiac responses from those caused by the changes in autonomic neural outflow, our observations suggest that standing results in: 1) an inhibition of respiratory vagal modulation of the SA node and, possibly, an increase in sympathetic tone, which shortens all three intervals, and increases the heart rate. 2) relative preservation of the respiratory modulation of the AV node conduction time and ventricular repolarization time.

Recent work by Piepoli *et al.* [1997] suggests that respiration-induced discharges from the arterial baroreceptors form the afferent loop of a reflex arc that acts via the cardiac vagus on the SA node to cause most of the observed respiratory sinus arrhythmia. From our study, because the respiration-related variability of the PR and RT intervals did not change with standing, one may speculate that vagal activity to the AV node and ventricular myocardium may be relatively independent of baroreceptor input.

Also of interest was the strong vagal influence on the RT variability. Using beta blockade Sarma *et al* [1994] suggested that the QT interval was relatively insensitive to vagal activity - however, we found clear respiratory-related PSA peaks in most subjects. The differences in results may be due to the fact that we studied healthy volunteers whereas Sarma was studying patients who were suffering from angina which is known to be associated with a sympathetic predominance as well as inhibited cardiac end-organ sensitivity to neural influences.

Thus, in summary, the effects of standing were an observed reduction in vagal influence on the HRV of the RR interval whilst maintaining lung-volume related vagal modulation of the PR and RT intervals. Standing did not produce a significant change in the LF and VLF spectral power of any interval.

Appendix C

Diagram of Program for HRV, ILV and ABP Signal Acquisition and Standardization

ACQUIRE (V1.0) 29 April 1996

(The C Program for Heart Rate, ILV and ABP Signal Acquisition and Processing)

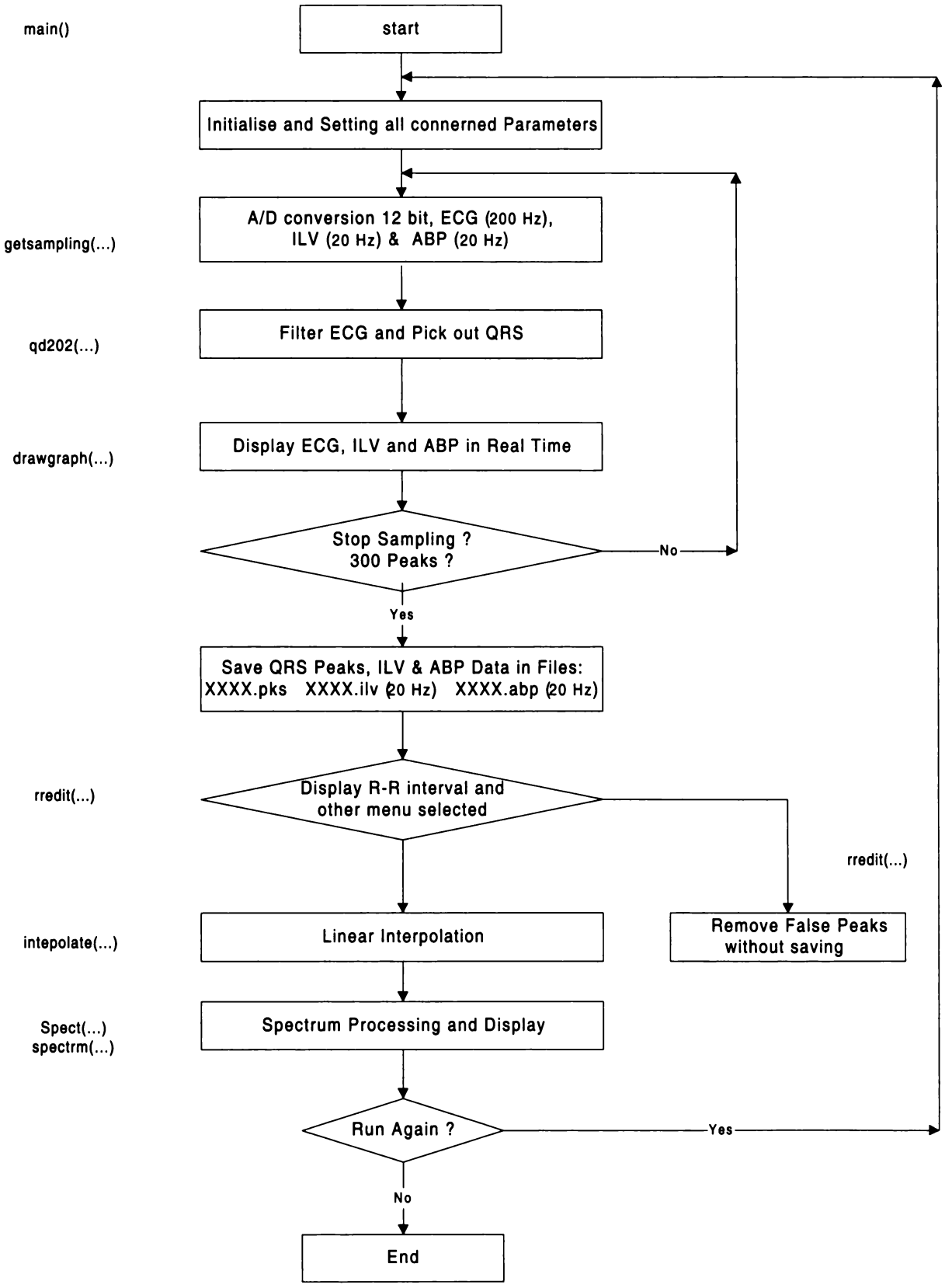

Data Standardisation (Matlab program)

28th April 1996

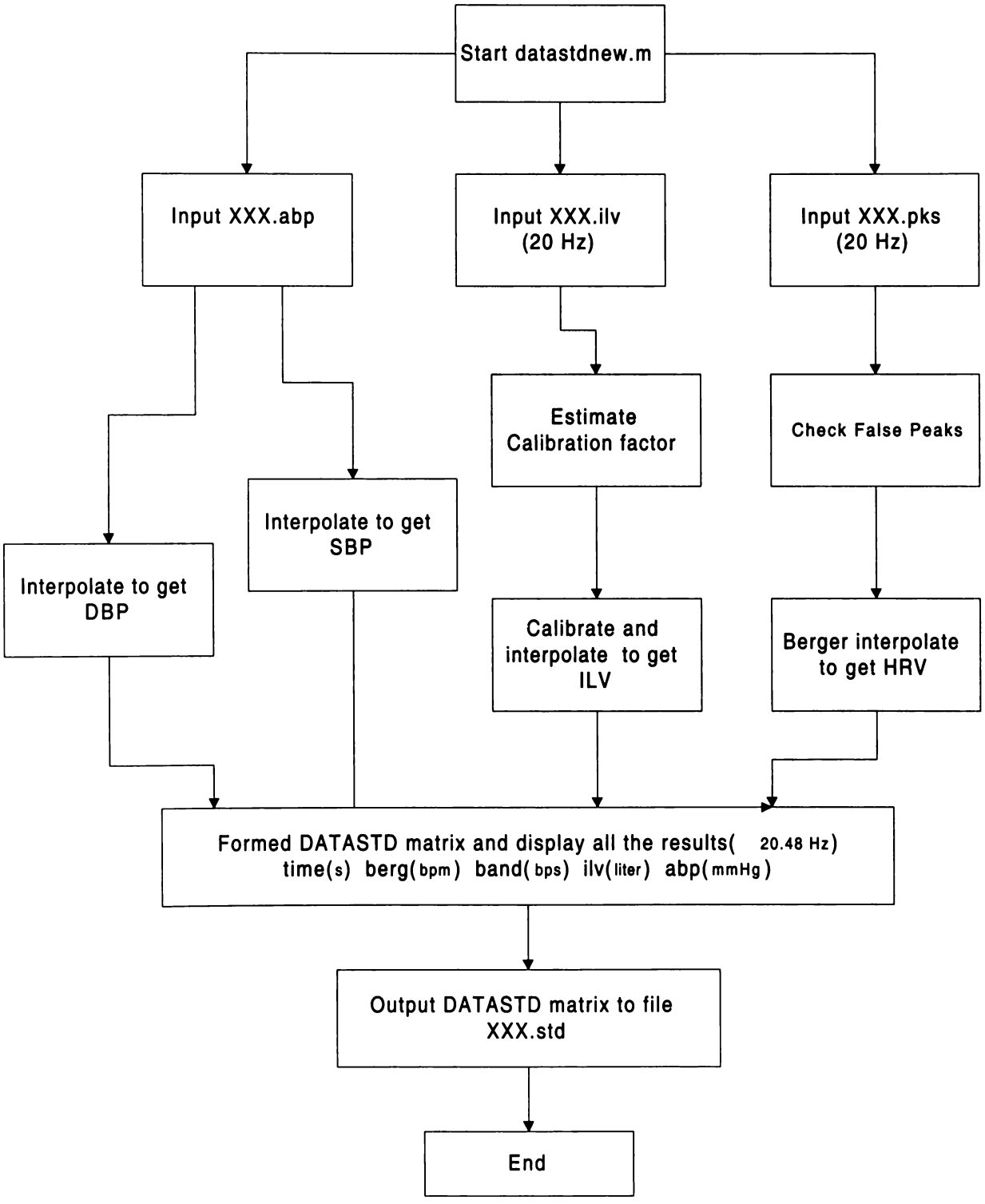

Appendix D

A summary of the parameters used in BEP networks to control the training behavior

Max Hidden Neurons: This parameter has two modes of operation. In standard BEP learning it is the number of hidden neurons created during the initialization of the network. The number remains constant for the life of the network. When Automatic Increment mode of training is selected, then Max Hid Neurons means the maximum number of hidden neurons that can be added to the model during the training session.

Learning Rate: The learning rate for the hidden layer to output layer connections. In standard BEP training, this number is used for the entire training session. If any of the incremental learning options are selected then this number represents the initial learning rate and it is reduced on the older neurons as newer neurons are added.

Error Tolerance: This parameter is used to stop training if the Stop Training On - Error The error tolerance is the maximum value of the Sum Square error that would be considered acceptable.

Good RSQ: This parameter is used to stop training should an acceptable R square statistic develop during the training and the Stop Training On - Good R Square radio button is selected. This parameter should be set to what the user considers a good R square.

References

Ahlstrom, M. L., and W. J. Tompkins. Automated high-speed analysis of Holter tapes with microcomputers. *IEEE Trans. Biomed. Eng.* 30: 651-657, 1983.

Akselrod, S., D. Gordon, J. B. Madwed, N. C. Snidman, D. C. Shannon, and R. J. Cohen. Hemodynamic regulation: investigation by spectral analysis. *Am. J. Physiol.* 18: H867-H875, 1985.

Appel, M. L., R. D. Berger, J. P. Saul, J. M. Smith, and R. J. Cohen. Beat to beat variability in cardiovascular variables: Noise or Music? *J. Amer. Col. Cardiology.* 14: 5, 1139-1148, 1989.

Auger, F., P. Flandrin, P. Goncalvès, and O. Lemoine. Time-Frequency Toolbox. CNRS (France) and Rice University (USA). *http://www-isis.enst.fr/Applications/tftb /iutsn.univ-nantes.fr/auger/tftb.html.* 1995.

Barbieri, B., V. Di Virgilio, J. K. Triedman, A. M. Bianchi, S. Cerutti, J. P. Saul. Multivariate autoregressive spectral analysis: heart rate baroreflex and respiratory influence under administration of atropine and propanolol. *Computers in Cardiology*, 1997.

Bates, R. H. T., K L Garden, and T M Peters. Overview of computerized tomography with emphasis on future developments. *Proc IEEE* 71: 356-372, 1983.

Baselli, G., S. Cerutti, F. Badilini, L. Biacardi, A. Porta Model for assessment of heart period and arterial pressure variability interactions and of respiration influences. *Med. Biol. Eng. Comput.* 32: 143-152, 1994.

Berne, R. M., and M. N. Levy. Electrical activity of the heart: in cardiovascular physiology (eds) *6th ed, Mosby Year Book, St Louis.* p40, 1992.

Berger, R. D., S. Akselrod, D. Gordon, and R. J. Cohen. An efficient algorithm for spectral analysis of heart rate variability. *IEEE Trans. Biomed. Eng.* 33: 900-904, 1986.

Berger, R. D., J. P. Saul, and R. J. Cohen. Assessment of autonomic response by broad-band respiration. *IEEE Trans. Biomed. Eng.* 36: 529-543, 1989.

Bianchi, A. M., L. Mainardi, E. Pettrucci, M. G. Signorini, M. Mainardi, and S. Cerutti. Time-variant power spectrum analysis for the detection of transient episodes in HRV signal. *IEEE Trans BME. 40:* 136-144, 1993.

Blaber, A. P., and R. L. Hughson. Cardiorespiratory interactions during fixed-pace resistive breathing. *J. Appl. Physiol.* 80: 1618-1626, 1996.

Bosch, P. P. J. van den, and A. C. van der Klauw. Modeling, identification, and simulation of dynamical systems. CRC Press, 1994.

Brown, T., L. A. Beightol, J. Kon, and D. L. Eckley. Important influence of respiration on human R-R interval power spectra is largely ignored. *J. Appl. Physiol.* 75: 310-2317, 1993.

Browne, K. F., D. P. Zipes, J. J. Heger, and E. N. Prystowsky. Influence of the autonomic nervous system on the QT interval in males. *Am. J. Cardiolo.* 50: 1099-1033, 1982.

Burke, D., G. Sundlof, and B. G. Wallin. Posture effects on muscle sympathetic activity in man. *J. Physiol. Lond.* 272: 399-414, 1977.

Chon, Ki. H., T. J. Mullen, and R. J. Cohen. A dual-input nonlinear system analysis of autonomic modulation of heart rate. *IEEE Trans. Biomed. Eng.* 43: 529-543, 1996.

Chon, Ki. H., and R. J. Cohen. Linear and nonlinear ARMA model parameter estimation using an artificial neural network *IEEE Trans. Biomed. Eng.* 44: 168-173, 1997.

Choi, H. I., and W. J. Williams. Improved time-varying filtering and signal estimation of multicomponent signals using exponential kernels. *IEEE Trans. Acoust. Speech, signal processing.* 37: 862-871, 1989.

Classen, TCM, and WFC Mecklenbrauker. The Wigner distribution- A tool for time-frequency signal analysis. *Phylips J. Res.* 35: 217-389, 1980.

Cohen, L. Generalized phase-space distribution function. *J. of Math. Phys.* 7: 781-871, 1966.

Cooke, W. H., J, F. Cox, A. M. Diederich, J. A. Taylor, L. A. Taylor, J. E. Ames IV, J. B, Hoag, H. Seidel, and D. L. Eckberg. Control breathing protocols probe human autonomic cardiovascular rhythms. *Am. J. Physiol.* 274 (*Heart Circ. Physiol.* 22): H708-H718, 1998.

DeBoer, J., M. Karemaker, and J. Strackee. Hemodynamic fluctuations and baroreflex sensitivity in humans: a beat-beat model. *Am. J. Physiol.* 253 (*Heart Circ. Physiol.* 22): H680-H689, 1987.

Eckberg, D. l. Nonlinearities of the human carotid baroreceptor-cardiac reflex. *Circ. Res.* 47: 208-216. 1980.

Eckberg, D. l. Human sinus arrhythmia is an index of vagal cardiac outflow. *J. Appl Physiol.* 54: 961-966, 1983.

Eckberg, D. l., and P. Sleight. Human baroreflexes in health and disease. Oxford University Press: New York, NY 276-278, 1992.

Eckmann, J. P.,, S. O. Kamphors, D. Ruelle. Recurrence plot of dynamical system. *Europhys. Lett.*4: 973-977, 1987.

Franklin, G. F., J. D. Powell, and A. Emami-Naeini. Feedback control of dynamic systems. *Addison-Wesley publishing company.* 540-547, 1988.

Gabor, D., Theory of communication. J. Inst. Elec. Eng., 93: 429-457, 1946.

Galletly, D. J., T. Corfiatis, A. M. Westernberg, and B. J. Robinson. Heart rate periodiocities during induction of Propofol - Nitrous Oxide - Isoflurane anaesthesia. *Brit.J.of Anaesthesia* 68: 360-364, 1992.

Goovaerts, H. G., H. H. Ros. T. J. vabden Akker, and H. Schneider. A digital QRS detector based on the principle of contour limiting. *IEEE Trans. Biomed. Eng.* 23: 154-163, 1976.

Guyton, A. C. Function of the human body. 3rd. Philadelphia, Saunders. 1969.

Guyton, A. C. Physiology of the human body. 6th ed. Philadelphia. Saunders College Pub. 1984.

Henderson, J. D., and J. W. Sleigh. Power spectral density estimation of patient heart rate. *National Physics Conference. Uni of Waikato, Hamilton.* 1993.

Hiroyuki, S., M. Noshiro, Y. Makoto, Y. Fukuoka, M. Ishikawa, and H, Minamitani. A new method for parameter estimation in the NARMAX model using neural computation. *Computers in Cardiology*, 1994.

Hirsch, J. A., and A. C. Bishop. Respiratory sinus arrhythmia in human: how breathing patterns modulate heart rate. *Am. J. Physiol.* 241 (*Heart Circ. Physiol.* 10): H620-H629, 1981.

Hoyer, D., R. Bayer, B. Walter, and U. Zwiener. Estimation of nonlinear couplings on the basis of complexity and predictability—a new method applied to cardiorespiratory coordination. *IEEE Trans. Biomed. Eng.* 45: 545-552, 1998.

Hyndman, B. W., and R. K. Mohn. A model of the cardiac pacemaker and its use in decoding the information content of cardiac intervals. *Automedica* 1: 239-252, 1975.

Ireland, N., J. Meagher, J. W. Sleigh, and J. D. Henderson. Heart rate variability in patients recovering from general anesthesia. *British J of Anesthesia* 76: 657-662, 1996.

Jeong J., and W. J. Williams. Kernel design for reduced interference distribution. *IEEE Trans. Signal processing.*, 40: 402-412, 1992.

Jennings, J. R., J. D. McKnight, and M. V. D. Molen. Phase-sensitive interaction of cardiac and respiratory timing in humans. *Psychophysiology.* 33: 514-521, 1996.

Jerri A. B. The Shannon Sampling Theorem - its various extensions and applications: a tutorial review. *Proc. IEEE.* 65: 1565-1596, 1977.

Kanters, J. K., M. V. Hojgaard, E. Agner, and N. Holstein-Rathlou. Influence of forced respiration on nonlinear dynamics in heart rate variability. *Am. J. Physiol.* 268 (*Regulatory Integrative Comp. Physiol.* 41): 1149-1154, 1997.

Kennel, M. B., R. Brown, and H. D. I. Abarbanel. Determining embedding dimension for phase space reconstruction using a geometrical reconstruction. *Phys. Rev. A.* 45: 3403-3411, 1992.

Kim, Tae-Sun., and M. C. K. Khoo. Estimation of cardiorespiratory transfer under spontaneous breathing conditions: a theoretical study. *Am. J. Physiol.* 273 (*Heart Circ. Physiol.* 41): H1012-H1023, 1997

Knutsson, K., and C. F. Westin. Normalised and differential convolution: methods for interpolation and filtering of incomplete and uncertain data. *IEEE Computer Soc. Conf. on computer vision and pattern recognition.* 515-523, 1993.

Krauss, T. P., L. Shure, and J. N. Little. Signal processing toolbox for use with Matlab. The MathWorks, Inc., 1994.

Ligtenberg, A., and M. Kunt. A robust-digital QRS-detection algorithm for arrhythmia. *monotoring. Comput. Biomed.* Res. 16: 273-286. 1983.

Ljung, L. System Identification: Theory for the user. Englewood Cliffs, NJ: Prentice-Hall, 1987.

Ljung, L. System identification toolbox for use with Matlab. The MathWorks, Inc., 1995.

Lutes, S. GeometryID toolbox for Matlab. http://www.bcm.tmc.edu/cfbd/geometryID. 1996.

Lomb, N. R. Least-squares frequency analysis of unequally spaced data. *Astrophysics & Space Science.* 39: 447-462, 1976.

Lynn, P. A. Online digital filter for biological signals: some fast designs for a small computer. *Comput.* 15: 534-540. 1977.

Malliani, A., F. Lombardi, and M. Pagani. Power spectral analysis of heart rate variability: a tool to explore neural regulatory mechanisms. *British Heart Journal.* 71: 1-2, 1994.

Malliani, A., M. Pagani, F. Lombardi, and S. Cerutti. Research advance series; cardiovascular neural regulation explored in the frequency domain. *Circulation.* 84: 482-492, 1991.

Marmarelis, P. Z., and V. Z. Marmarelis. Analysis of physiological systems: the white-noise approach. Plenum Press. 11-178, 1978.

Middleton, G. V. Nonlinear dynamics and fractals, new numerical techniques for sedimentary data. Tulsa, Okla.: SEPM. 1995

Mullen, T. J., L. Marvin, R. M. Appel, J. M. Mathias and R. J. Cohen. System identification of closed-loop cardiovascular control: effects of posture and autonomic blockade *Am. J. Physiol.* 272 (*Heart Circ. Physiol.* 41): H448-H461, 1997.

Murray, S. Neural networks for statistical modeling. International Thomson Computer Press. 1996.

Muzi, M., and T. E. Ebert, Quantification of heart rate variability with power spectral analysis. *Curr. Opin. Anaes.* 6: 3-17, 1993.

Neil A. W., and J. H. Matthew. Introductory statistics. Addison-Wesley Publishing Company. 539:580, 1991.

Neural Fusion. Neural network based multivariable statistical modeling program *http://www.neuralfusion.com/* 1997.

Novak, V., P. Novak, J. De Chaplain, A. R. Le Blanc, R. Martin, and R. Nadeau. Influence of respiration on heart rate and blood pressure fluctuations. *J. Appl. Physiol.* 74(2): 617-626, 1993.

Nøgaard, M., O. Ravn, L.K. Hansen, N.K. Poulsen: The NNSYSID toolbox - A MATLAB toolbox for system identification with neural networks. *Proceedings of the 1996 IEEE International Symposium on Computer-Aided Control System Design, Dearborn, Michigan, USA, Sep. 15-18,* 374-379,1996.

Nygards, M., and L. Sornmo. A QRS delineation algorithm with low sensitivity to noise and morphology changes. *Comput. Cardio.*. 347-350, 1981.

Panerai, R. B., M. A. James and J. F. Potter. Impulse response analysis of baroreceptor sensitivity. *Am. J. Physiol* 270: H1866-H1875, 1997.

Patton, D. J., J. K. Triedman, M. H. Perrot, A. A. Vidian, and J. P. Saul. Baroreflex gain: characterization using autoregressive moving average analysis. *Am. J. Physiol* 270: H1240-H1249, 1996.

Pahlm, O., and L. Sornmo. Software QRS detection in ambulatory monitoring – A review. *Med. Biol. Eng. Comput.* 22: 289-297, 1984.

Patwardhan, A. R., J. M. Evans, E. N. Bruce, D. L. Eckberg, and C.F. Knapp. Voluntary control of breathing does not alter vagal modulation of heart rate. *J. Appl. Physiol.* 78: 2087-2094, 1995.

Pan, J., and W. J. Tompkins. A real-time QRS detection algorithm. *IEEE Trans. Biomed. Eng.* 32: 230-235, 1985.

Piepoli, M., P. Sleight, S. Leuzzi, F. Valle, G. Spadicini, C. Passino, J. Johnston, and L. Bernardi. Origin of respiratory sinus arrhythmia in conscious humans: An important role for arterial carotid baroreceptors. *Circulation.* 95: 1813-1821, 1997.

Perrott, M. H., and R. J. Cohen. An efficient approach to ARMA modeling of biological systems with multiple inputs and delays. *IEEE Trans. Biomed. Eng.* 43: 1-13, 1996.

Pomeranz, B., R. J. B. Macaulay, and M. A. Caudill. Assessment of autonomic function in humans by heart rate spectral analysis. *Am. J. Physiol* 248: H151-H153, 1985.

Randall, W. C., J. L. Ardell, M. F. O'Toole, and R.D. Wurster. Differential autonomic control of SAN and AVN regions of the canine heart: structure and function. *Progress in Clinical & Biological research.* 275: 15-31, 1988.

Rempelman, R., A. Loenen, and R. Kitrey. Measurement of heart rate variability - Part 1". *Med & Biol. Eng & Comput* v15: 233-239, 1977.

Rhodes, C., and M. Morari, Determining the model order of nonlinear input/output systems, *AIChE Journal.* 44: 151-163, 1998.

Rhodes, C., and M. Morari. False nearest neighbor algorithm and noise corrupted time series, *Physical Review E.* 55: 6162-6170, 1997.

Rihaczek, W. Signals energy distribution in time and frequency. *IEEE Trans, Inform. Theory.* IT-14: 369:374, 1968.

Saul, J. P., R. D. Berger, M. H. Chen, and R. D. Cohen. Transfer function analysis of autonomic regulation. II. Respiratory sinus arrhythmia. *Am. J. Physiol.* 256 (*Heart Circ. Physiol.* 25): H153-H161, 1989.

Saul, J. P., R. D. Berger, P. Albrecht, S. P. Stein, M. H. Chen, and R. D. Cohen. Transfer function analysis of circulation: unique insights into cardiovascular regulation. *Am. J. Physiol.* 261 (*Heart Circ. Physiol.* 30): H1231-H1245, 1991.

Sarma, J. S., N. Singh, M. P. Schoenbaum, K. Venkataaraman, and B. N. Singh. Circadian and power spectral changes of RR and QT intervals during treatment of patients with angina pectoris with nadolol providing evidence of differential autonomic modulation of heart rate and ventricular repolarization. American Journal of Cardiology. 74: 131-136, 1994.

Starr, C. and B. McMillan. Human biology, 2nd Ed. Wadsworth Publishing Co., 1996.

Task Force of the European Society of Cardiology and the North American Society of Pacing and Electrophysiology. Heart rate variability. Standards of measurement, physiological interpretation, and clinical use. *Circulation.* 93: 1043-1065, 1996.

Taha, B. H., P. M. Simon, J. A. Dempsey, J. B. Skatrud, and C. Iber. Respiratory sinus arrhythmia in humans: an obligatory role for vagal feedback from the lungs. *J. Appl. Physiol.* 78: 638-645,1995.

Takens, F. Detecting strange attractors in turbulence. In D.A.B and and L.S. Young, editor, D*ynamical systems and turbulence,* Warwick. 366-391, Springer-Verlag, 1981.

Thakor, N. V., J. G. Webster, and W. J. Tompkins. Optimal QRS detector. *Med. Biol. Emg. Comput.,* 21: 343-350, 1983.

Thibodeau, G. A.. Anatomy and physiology. 2nd ed. St. Louis: Mosby. 1992.

Thibodeau, G. A.. Structure & function of the body. 9th ed. St. Louis: Mosby Year Book. 1992.

Tortora, G. J. Principles of anatomy and physiology. 5th ed. Harper international ed. New York: Harper & Row. 1987.

Triedman, J. K., M. H. Perrott, R. J. Cohen, and P. Saul. Respiratory sinus arrhythmia: domain characterization using autoregressive moving average analysis. Am. J. Physiol. 268 (*Heart Circ. Physiol.* 37): H2232-H2238, 1995.

Van Ravenswaaij-Arts C. M., L. A. Kollee, J. C. Hopman , G. B. Stoelinga ,and H. P. Van Geign. Heart rate variability. *Annals of Internal Medicine.* 118: 436-447, 1993.

Ville, J. Theorie at applications dela notion de signal analytique. *Cables Transmiss.,* 20A: 61-74, 1948.

Welch, P. D. The use of FFT for the estimation of power spectra. *IEEE Trans. Audio. Electrocoust.* AU-15(2): 70-73, 1967.

Webber, C. L. J. and J. P. Zbilut. Dynamical assessment of physiological system and states using recurrence plot strategies. *J. Appl. Physiol.* 76(2): 965-973, 1994.

William, H. P., A. T. Saul, H. V. William and F. P. Brian. Numerical recipes in C: the art of scientific computing. 2nd ed. Cambridge University Press. 1992.

Williams, W. J. and J. Jeong. New time-frequency distributions for the analysis of multicomponent signals. *Proc. SPIE Int. Soc. Opt. Eng.*, 1152: 483-495, 1989.

Williams, W. J., H. P. Zaveri and J. C. Sackellares. Time-Frequency analysis of electrophysiology signals in epilepsy. *IEEE Eng. In Med. and Bio.* 133-143, 1995.

Yana, K., J. P. Saul, R. D. Berger, M. H. Perrott, and R. J. Cohen. A time domain approach for the fluctuation analysis of heart rate related to instantaneous lung volume. *IEEE Trans. Biomed. Eng.* 40: 73-81, 1993.

Zhang, P. Z., N. T. Walter, S. R. Stanley, and H. N. Benjamin. Respiration response curve analysis of heart rate variability. *IEEE Trans. Biomed. Eng., 44*: 321-325, 1997.